by B.L. EMMINK

COLORECTAL CANCER STEM CELLS

Regulation of the phenotype and implications for therapy resistance

COLORECTAL CANCER STEM CELLS
Regulation of the phenotype and implications for therapy resistance

Thesis, Faculty of Medicine, University Utrecht, the Netherlands, with summary in Dutch.
Proefschrift, Medische faculteit, Universiteit Utrecht, Nederland, met een samenvatting in het Nederlands.

The work described in this thesis was supported by a personal grant from the Dutch Cancer Society.

Publication of this thesis was financially supported by: Afdeling Heelkunde UMC Utrecht, Dutch Cancer Society, Chipsoft BV, Pfizer Oncology, Thermo Fisher Scientific, Olympus Nederland BV, Abbott Nederland, Bayer Healthcare, Panasonic biomedical.

© B.L. Emmink 2014

All rights reserved. No part of this publication may be reproduced, stored in a retrieval system of any nature or transmitted in any form or by any means, electronic, mechanical, photocopying, recording or otherwise, without prior permission of the author, or when appropriate, the publishers of the papers.

ISBN/EAN: 978-94-6108-812-3
Cover design: Nicole Nijhuis - Gildeprint, Benjamin L. Emmink
Lay out: Gildeprint, Enschede
Printed by: Gildeprint, Enschede

COLORECTAL CANCER STEM CELLS

Regulation of the phenotype and implications for therapy resistance

(met een samenvatting in het Nederlands)

PROEFSCHRIFT

ter verkrijging van de graad van doctor
aan de Universiteit Utrecht
op gezag van de rector magnificus, prof. dr. G.J. van der Zwaan,
ingevolge het besluit van het college voor promoties
in het openbaar te verdedigen op
donderdag 6 november 2014 des middags te 2.30 uur

door

Benjamin Lucas Emmink
geboren op 12 november 1981 te Utrecht

Promotor:	**Prof. dr. I.H.M. Borel Rinkes**
Copromotoren:	**Dr. O. Kranenburg**
	Dr. C.R. Jimenez

Aan Laura en Benjamin

CONTENT

CHAPTER 1:	Introduction and outline of the thesis	9
CHAPTER 2:	Differentiated human colorectal cancer cells protect tumor-initiating cells from irinotecan. *Gastroenterology. 2011 Jul;141(1):269-78*	17
CHAPTER 3:	Proteomics in studying cancer stem cell biology *Expert Review of Proteomics. 2012 Jun;9(3):325-36*	51
CHAPTER 4:	Comparative proteomics of colon cancer stem cells and differentiated tumor cells identifies BIRC6 as a potential therapeutic target. *Molecular & Cellular Proteomics. 2011 Dec;10(12):M111.*	69
CHAPTER 5:	The secretome of colon cancer stem cells contains drug-metabolizing enzymes *Journal of Proteomics. 2013 Jul 5;91C:84-96*	89
CHAPTER 6:	GPx2 suppression of H2O2 stress links the formation of differentiated tumor mass to metastatic capacity in colorectal cancer. *Cancer Research. 2014 Sep; in press*	117
CHAPTER 7:	Hypoxia after liver surgery imposes an aggressive cancer stem cell phenotype on residual tumor cells. *Annals of Surgery. 2014 Apr;259(4):750-9*	157
CHAPTER 8:	Maspin is a marker for early recurrence in primary stage III and IV colorectal cancer. *British Journal of Cancer. 2013 Sep 17;109(6):1636-47*	175
CHAPTER 9:	General discussion	203
CHAPTER 10:	Summary in Dutch – Nederlandse samenvatting	211
CHAPTER 11:	Appendices:	
	Authors and affiliations	218
	Review committee	219
	Dankwoord	220
	List of publications	225
	Curriculum vitae auctoris	228

1

INTRODUCTION AND OUTLINE OF THE THESIS

The cancer stem cell concept

Central to the cancer stem cell (CSC) concept is the notion that not all cells in tumors are equal[1]. According to the CSC concept the growth of tumors, similar to the growth of normal intestinal tissue, is fuelled by limited numbers of (cancer) stem cells that generate daughter stem cells but also proliferating and differentiated cells that make up the bulk of the tumor but have lost the capacity for self-renewal and long-term sustenance of tumor growth.

CSCs are usually defined operationally: First, as cells with a high clonogenic and tumor-initiating potential. Second, as cells that form tumors which recapitulate the heterogeneity of cell types in the original tumor. Third, as cells that, when isolated from tumor tissue, can regenerate the original tumor in serial transplantations, demonstrating self-renewal and differentiation capacity. The first evidence for the existence of CSC was obtained in the context of acute myeloid leukemia, where only a small portion of harvested leukemic cells from patients could recapitulate the same cancer in immune-deficient mice[2]. Later on, CSC were also demonstrated to exist in solid tumors[3-5].

CSCs may arise from normal tissue stem cells by the accumulation of cancer-causing mutations[6-8]. However, non-stem cells may also acquire self-renewal capacity and immortality though mutagenic events. Indeed, the origin of CSCs is still an active area of research and is likely to be cancer-specific[9]. In the following chapters we will frequently use the term 'tumor-initiating cells', as this reflects a key functional property that can be readily tested.

In the last decade, the CSC concept, has created great excitement in the research community. As a result of their self-renewal capacity, longevity and resistance to (geno-)toxic insults, CSCs could be responsible for therapy resistance and metastasis formation. The CSC concept could, for example, explain local tumor recurrence in patients that were initially treated 'successfully' with chemotherapy and/or radiotherapy, but in which a small percentage of therapy-resistant CSCs survive and subsequently regenerate the original tumor. This implies that the CSC concept not only forms a framework for describing and understanding the pathophysiology of cancer, but could also have a profound impact on the development of prognostic and predictive tools and on the design of alternative (CSC-directed) therapies.

Cancer stem cells in colorectal cancer

Colorectal tumors display a hierarchical organization and adhere to the CSC concept: First, colorectal tumors contain small identifiable subpopulations of tumor cells that can serially transplant the tumor, produce differentiated offspring, and generate phenocopies of the original tumor in immune-deficient mice[4, 10]. Second, genetic lineage tracing experiments have recently demonstrated that the growth of intestinal adenomas is fuelled by stem-like tumor cells[11]. Third, high Wnt pathway activity is essential for normal stem cell (SC) maintenance[12] and identifies colorectal tumor cells with high tumor- and clone-forming potential[13, 14]. Finally, gene expression signatures derived from normal intestinal SCs and CSCs identify recurrence-prone CRC tumors[13, 15, 16].

Colorectal CSCs can be identified based on the expression of (combinations of) various cell surface markers[4, 10, 15, 17-19]. In addition, colorectal CSCs are characterized by high aldehyde dehydrogenase (ALDH) activity[20-22] and by high Wnt pathway activity[14]. Serial transplantation experiments based on high ALDH activity[22, 23] have further demonstrated the stem cell-like nature of these tumor cells as opposed to marker-negative cells. These data firmly establish Aldefluor® as a reliable marker for purifying the CSC fraction from many different colorectal tumors.

Isolation and propagating of colorectal CSCs

Initial studies detecting CSC in colorectal cancer follow a common scenario: a marker or marker combination is found to be expressed in a heterogeneous fashion. On the basis of this marker heterogeneity, subpopulations of cells are sorted from primary tumors and transplanted into immunodeficient mice by limiting dilution, after which tumor growth is scored in the following weeks or months. We and others have used a novel culture method to propagate CSCs from resected tumor specimens as CSC-enriched three-dimensional 'colonosphere' cultures[10, 24]. In brief, single cells are isolated from resected colorectal cancer specimens and are cultured in serum-free stem cell medium which maintains undifferentiated CSCs. Single cells capable of self-renewal grow out into tumor-derived three-dimensional 'colonosphere' cultures, expressing various validated CSC cell surface markers[4, 10, 15, 17-19]. Xenografting these cultures in mice generates close phenocopies of the original patients' tumors, similar to direct CSC transplantation[10]. In chapter 2 we also show that these colonosphere cultures are highly enriched in CSCs but also contain 15-30% differentiated tumor cells which fail to form clones and tumors. Tumor-derived colonosphere cultures are currently one of the best in vitro culture systems for human colorectal tumors.

Cancer stem cells and drug resistance

It is often suggested that CSCs are resistant to therapy in the same way that normal stem cells are protected against toxic insults, due to increased DNA repair activity, an increased ability to neutralize radical oxygen species (ROS), a slow proliferation rate, and/or high expression of anti-apoptotic proteins[25]. Several reports have shown that chemotherapy causes an enrichment of the CSC population in xenografts of colorectal tumors in mice[21, 26, 27]. This may be due to a relative resistance of the CSC population to chemotherapy[28]. Consequently, drug-resistant CSCs may be the driving force behind tumor recurrence[29-32]. Which of these mechanisms indeed operate in colorectal CSCs is only beginning to be studied. Nevertheless, the phenomenon of intrinsically therapy-resistant CSCs cannot be generalized, as, for instance, the undifferentiated cells that drive testicular germ cell tumors are more sensitive to radiation or cisplatin therapy than their differentiated cellular progeny[33].

Chemotherapy of colorectal tumors is based primarily on 5-fluorouracil, oxaliplatin, and irinotecan[34]. However, in general 40-50% of colorectal tumors fail to respond to chemotherapy altogether, leaving the majority of tumor cells to survive treatment[34]. It is presently unknown how these clinical observations fit a model in which chemoresistance is mediated by a population of rare CSCs. In **chapter 2**, we study the relationship between CSCs and irinotecan (topoisomerase I inhibitor) resistance using tumor-derived colonosphere cultures, which are enriched for tumorigenic CSCs with differentiated cells on the fringes. We show that non-tumorigenic differentiated cells protect the CSC from which they originated from irinotecan through ABCB1-mediated drug-efflux.

Proteome and secretome of cancer stem cells

'Omics'-type analysis of tumors is now widely used to elucidate molecular perturbations in cancer cells. However genome-wide DNA and RNA analysis does not always reflect the functional activities of the encoded proteins[35, 36]. Proteomics is a large-scale comprehensive approach to study the protein composition of a cell population or tissue. Proteomics could therefore provide in-depth information about the dysregulation of pathways resulting from alterations in expression and/or activities of proteins in CSCs. Identifying proteins specifically expressed in CSCs could help to clarify mechanisms that support CSC proliferation, differentiation, motility, invasion, drug

resistance, and tumor recurrence. In addition, proteomics is an ideal tool to analyze cell states, and it has frequently been applied to studying the biology of embryonic stem cells (ESCs)[37]. In **chapter 3**, we review the emerging roll of proteomics as a tool to identify the signalling complexes and pathways that control multi- and pluri-potency and SC differentiation and present a comprehensive strategy for the use of proteomics in studying CSC biology.

Colonosphere cultures can be used to establish isogenic cultures of stably differentiated non-tumorigenic cells. This allows for a comparative analysis of the proteome of tumorigenic CSC and their non-tumorigenic differentiated cells. In **chapter 4**, we have used proteomics to show that proteins governing cell survival are overrepresented in colon CSC cultures and that differentiation of CSCs is accompanied by an altered regulation of cell death pathways. In this chapter we focus on the most prominently overexpressed survival protein, BIRC6/BRUCE/Apollon, an Inhibitor of Apoptosis Protein (IAP). We show that BIRC6 helps protecting colon CSCs against platinum drugs.

In addition to the proteome, analysis of secreted factors also provides insight into intracellular processes, as many tumor cells shed intracellular and even nuclear proteins into the extracellular space[38]. Factors secreted by cancer cells in multiple tumor types have been shown to modulate drug resistance[27, 39-41]. Given the central role that CSCs are thought to play in mediating drug resistance it is important to identify the plethora of factors that are secreted by them. In **chapter 5,** we show, with use of paired cultures of highly tumorigenic CSCs and their isogenic non-tumorigenic differentiated progeny, that the secretome of CSCs is enriched with cell protection pathways. In addition, we have identified several CSC-secreted drug-modifying enzymes that are shown to modulate drug responsiveness of nearby non-CSCs.

Effects of reactive oxygen species and hypoxia on phenotype of cancer stem cells

Reactive oxygen species (ROS) are by-products of aerobic metabolism, but can also be generated as second messengers in signalling pathways. ROS are increased in many types of cancer cells[42] and modulate cancer initiation, promotion, and progression[43, 44]. The increase in intracellular ROS in cancer cells may involve a diversity of mechanisms. ROS generation in tumor cells may result from the activation of oncogenes, inactivation of tumor suppressor genes, high metabolism, and/or mitochondrial dysfunction[43]. In addition, an abnormal microenvironment and anti-cancer therapy can also influence ROS levels in tumor cells. Cancer cells have adapted to deal with persistently high ROS levels by (i) activating redox-sensitive transcription factors that upregulate ROS scavenging enzymes, (ii) activating expression of survival factors, and (iii) inhibiting cell death factors. These adaptive changes prevent ROS-induced cell-death[43].

Normal stem cells and early progenitors contain lower levels of ROS than their more mature progeny. Low ROS levels are critical for maintaining stem cell function[45, 46]. In comparison with normal stem cells and cancer cells as a whole population, relatively little is known about ROS levels in CSCs. ROS and its effects on CSCs have so far only been studied in breast cancer. Breast CSCs have lower intracellular ROS levels than non-CSCs, due to an increased expression of free radical scavenging systems[47, 48]. These breast CSCs develop less DNA damage, due to low ROS levels, and are preferentially spared after irradiation compared to non CSCs[47, 48].

How redox homeostasis is achieved and may affect the colon CSCs phenotype and whether this influences differentiation is unknown. Elucidation of these mechanisms is essential for understanding CSC-driven colon tumor growth, differentiation and therapy resistance. In **chapter 6**, we identify intestinal glutathione peroxidase (GPx2), a major H2O2-neutralizing enzyme, as an important determinant of the fate of colon CSCs: Firstly, GPx2 protects colon CSCs against apoptosis induced by a variety of stress-inducing conditions, and, as such, is essential for

their clone- and metastasis-forming capacity. Secondly, and more surprisingly, GPx2-mediated ROS neutralization is absolutely essential for CSCs to produce proliferating and differentiated offspring forming the tumor mass. We conclude that redox control links metastatic capacity to the generation of proliferative differentiated tumor mass.

ROS production is paradoxically increased under hypoxia[49]. Hypoxia, defined as insufficient oxygenation to meet the metabolic demands of viable tumor cells, is one of the most commonly recognized features of the tumor microenvironment. A distinctive feature of insufficient oxygenation is decreased tissue perfusion, induced by tissue injury. Previous work by our group demonstrated that micrometastases in the liver adopt a highly aggressive phenotype after liver injury induced by ischemia-reperfusion[50-52] or local ablation[53]. These areas of cells with an aggressive phenotype were characterized by hypoxia[51, 53]. Previous reports, have shown that tumor cells exposed to hypoxia are poorly differentiated and express stem cell markers[54, 55], and that hypoxia inhibits differentiation of embryonic stem cells and progenitor cells[56]. In **chapter 7**, we set out to investigate how surgery-generated hypoxia affects the CSC phenotype. For this purpose mice bearing patient-derived liver metastases were used. Surgery-generated hypoxia in the liver resulted in rapid de-differentiation of tumor cells into immature CSCs with high clone- and metastasis-forming capacity. Additionally we show that these aggressive CSCs can be targeted by hypoxia-activated pro-drugs. These results are clinically relevant as they help explain the phenomenon of aggressive local tumor recurrence after liver surgery and offer a potential strategy to kill aggressive CSCs by hypoxia-activated pro-drugs.

Identification of genes/proteins associated with tumor progression in colorectal cancer

Several biomarkers are associated with a poor clinical outcome in colon cancer but few of them are being used in the clinic[57]. The discovery of novel biomarkers for predicting tumour behaviour is not only valuable from a prognostic viewpoint, but can also help to gain insight into the mechanisms that cause disease progression and metastasis formation. Recent advances in genomic and proteomic platforms make it possible to study the expression of thousands of genes or proteins at the same time in patient material. In primary colorectal tumors, gene expression profiling can distinguish colorectal tumors with different aggressiveness and metastatic potential[58, 59]. Gene expression signatures associated with survival in *metastasized* CRC have not yet been identified. In **chapter 8**, we set out to obtain insight into the mechanisms causing tumour progression and metastasis formation by identifying genes and proteins that correlate with early disease recurrence in patients with colorectal liver metastases. Such factors may also predict a propensity for metastasis in earlier stages of CRC. With the use of gene expression profiling and proteomics we identified a serine protease inhibitor, Maspin (Serpin B5), to be highly expressed in recurrence-prone stage IV (metastasized) CRC tumors. Subsequently, we showed that high Maspin expression was correlated with spread to local lymph nodes in stage III tumors as well, but had no predictive power in stage II tumors. We conclude that Maspin may have a stage-specific function that is possibly related to tumour cell dissemination and/or metastatic outgrowth.

REFERENCE LIST

1. Dick,J.E. Stem cell concepts renew cancer research. *Blood* 112, 4793-4807 (2008).
2. Bonnet,D. & Dick,J.E. Human acute myeloid leukemia is organized as a hierarchy that originates from a primitive hematopoietic cell. *Nat. Med.* 3, 730-737 (1997).
3. Dontu,G. *et al.* Role of Notch signaling in cell-fate determination of human mammary stem/progenitor cells. *Breast Cancer Res.* 6, R605-R615 (2004).
4. O'Brien,C.A. *et al.* A human colon cancer cell capable of initiating tumour growth in immunodeficient mice. *Nature* 445, 106-110 (2007).
5. Singh,S.K. *et al.* Identification of human brain tumour initiating cells. *Nature* 432, 396-401 (2004).
6. Barker,N. *et al.* Crypt stem cells as the cells-of-origin of intestinal cancer. *Nature* 457, 608-611 (2009).
7. Kim,C.F. *et al.* Identification of bronchioalveolar stem cells in normal lung and lung cancer. *Cell* 121, 823-835 (2005).
8. Le,L.Q. *et al.* Cell of origin and microenvironment contribution for NF1-associated dermal neurofibromas. *Cell Stem Cell* 4, 453-463 (2009).
9. Clarke,M.F. *et al.* Cancer stem cells--perspectives on current status and future directions: AACR Workshop on cancer stem cells. *Cancer Res.* 66, 9339-9344 (2006).
10. Ricci-Vitiani,L. *et al.* Identification and expansion of human colon-cancer-initiating cells. *Nature* 445, 111-115 (2007).
11. Schepers,A.G. *et al.* Lineage tracing reveals Lgr5+ stem cell activity in mouse intestinal adenomas. *Science* 337, 730-735 (2012).
12. van de Wetering,M. *et al.* The beta-catenin/TCF-4 complex imposes a crypt progenitor phenotype on colorectal cancer cells. *Cell* 111, 241-250 (2002).
13. Shenoy,A.K. *et al.* Transition from colitis to cancer: high Wnt activity sustains the tumor-initiating potential of colon cancer stem cell precursors. *Cancer Res.* 72, 5091-5100 (2012).
14. Vermeulen,L. *et al.* Wnt activity defines colon cancer stem cells and is regulated by the microenvironment. *Nat. Cell Biol.* 12, 468-476 (2010).
15. Merlos-Suarez,A. *et al.* The intestinal stem cell signature identifies colorectal cancer stem cells and predicts disease relapse. *Cell Stem Cell* 8, 511-524 (2011).
16. De Sousa E Melo *et al.* Methylation of cancer-stem-cell-associated Wnt target genes predicts poor prognosis in colorectal cancer patients. *Cell Stem Cell* 9, 476-485 (2011).
17. Dalerba,P. *et al.* Phenotypic characterization of human colorectal cancer stem cells. *Proc. Natl. Acad. Sci. U. S. A* 104, 10158-10163 (2007).
18. Kemper,K. *et al.* Monoclonal antibodies against Lgr5 identify human colorectal cancer stem cells. *Stem Cells* 30, 2378-2386 (2012).
19. Vermeulen,L. *et al.* Single-cell cloning of colon cancer stem cells reveals a multi-lineage differentiation capacity. *Proc. Natl. Acad. Sci. U. S. A* 105, 13427-13432 (2008).
20. Carpentino,J.E. *et al.* Aldehyde dehydrogenase-expressing colon stem cells contribute to tumorigenesis in the transition from colitis to cancer. *Cancer Res.* 69, 8208-8215 (2009).
21. Dylla,S.J. *et al.* Colorectal cancer stem cells are enriched in xenogeneic tumors following chemotherapy. *PLoS. One.* 3, e2428 (2008).
22. Huang,E.H. *et al.* Aldehyde dehydrogenase 1 is a marker for normal and malignant human colonic stem cells (SC) and tracks SC overpopulation during colon tumorigenesis. *Cancer Res.* 69, 3382-3389 (2009).
23. Shenoy,A., Butterworth,E., & Huang,E.H. ALDH as a marker for enriching tumorigenic human colonic stem cells. *Methods Mol. Biol.* 916, 373-385 (2012).
24. Sato,T. *et al.* Long-term expansion of epithelial organoids from human colon, adenoma, adenocarcinoma, and Barrett's epithelium. *Gastroenterology* 141, 1762-1772 (2011).
25. Zhou,B.B. *et al.* Tumour-initiating cells: challenges and opportunities for anticancer drug discovery. *Nat. Rev. Drug Discov.* 8, 806-823 (2009).
26. Pang,R. *et al.* A subpopulation of CD26+ cancer stem cells with metastatic capacity in human colorectal cancer. *Cell Stem Cell* 6, 603-615 (2010).
27. Todaro,M. *et al.* Colon cancer stem cells dictate tumor growth and resist cell death by production of interleukin-4. *Cell Stem Cell* 1, 389-402 (2007).
28. Dean,M. ABC transporters, drug resistance, and cancer stem cells. *J. Mammary. Gland. Biol. Neoplasia.* 14, 3-9 (2009).

29. Dean,M. *et al.* Tumour stem cells and drug resistance. *Nat. Rev. Cancer* 5, 275-284 (2005).
30. Donnenberg,V.S. & Donnenberg,A.D. Multiple drug resistance in cancer revisited: the cancer stem cell hypothesis. *J. Clin. Pharmacol.* 45, 872-877 (2005).
31. Eyler,C.E. & Rich,J.N. Survival of the fittest: cancer stem cells in therapeutic resistance and angiogenesis. *J. Clin. Oncol.* 26, 2839-2845 (2008).
32. O'Brien,C.A. *et al.* ID1 and ID3 regulate the self-renewal capacity of human colon cancer-initiating cells through p21. *Cancer Cell* 21, 777-792 (2012).
33. Masters,J.R. & Koberle,B. Curing metastatic cancer: lessons from testicular germ-cell tumours. *Nat. Rev. Cancer* 3, 517-525 (2003).
34. Chau,I. & Cunningham,D. Treatment in advanced colorectal cancer: what, when and how? *Br. J. Cancer* 100, 1704-1719 (2009).
35. Tian,Q. *et al.* Integrated genomic and proteomic analyses of gene expression in Mammalian cells. *Mol. Cell Proteomics.* 3, 960-969 (2004).
36. Huber,K.V. *et al.* Stereospecific targeting of MTH1 by (S)-crizotinib as an anticancer strategy. *Nature* 508, 222-227 (2014).
37. Mallanna,S.K. & Rizzino,A. Systems biology provides new insights into the molecular mechanisms that control the fate of embryonic stem cells. *J. Cell Physiol* 227, 27-34 (2012).
38. Karagiannis,G.S. *et al.* Cancer secretomics reveal pathophysiological pathways in cancer molecular oncology. *Mol. Oncol.* 4, 496-510 (2010).
39. Arlt,A. *et al.* Autocrine production of interleukin 1beta confers constitutive nuclear factor kappaB activity and chemoresistance in pancreatic carcinoma cell lines. *Cancer Res.* 62, 910-916 (2002).
40. Conze,D. *et al.* Autocrine production of interleukin 6 causes multidrug resistance in breast cancer cells. *Cancer Res.* 61, 8851-8858 (2001).
41. Yao,L. *et al.* Discovery of IL-18 as a novel secreted protein contributing to doxorubicin resistance by comparative secretome analysis of MCF-7 and MCF-7/Dox. *PLoS. One.* 6, e24684 (2011).
42. Szatrowski,T.P. & Nathan,C.F. Production of large amounts of hydrogen peroxide by human tumor cells. *Cancer Res.* 51, 794-798 (1991).
43. Trachootham,D. *et al.* Targeting cancer cells by ROS-mediated mechanisms: a radical therapeutic approach? *Nat. Rev. Drug Discov.* 8, 579-591 (2009).
44. Pani,G. *et al.*Metastasis: cancer cell's escape from oxidative stress. *Cancer Metastasis Rev.* 29, 351-378 (2010).
45. Miyamoto,K. *et al.* Foxo3a is essential for maintenance of the hematopoietic stem cell pool. *Cell Stem Cell* 1, 101-112 (2007).
46. Tsatmali,M. *et al.* Newborn neurons acquire high levels of reactive oxygen species and increased mitochondrial proteins upon differentiation from progenitors. *Brain Res.* 1040, 137-150 (2005).
47. Diehn,M. *et al.* Association of reactive oxygen species levels and radioresistance in cancer stem cells. *Nature* 458, 780-783 (2009).
48. Phillips,T.M. *et al.* The response of CD24(-/low)/CD44+ breast cancer-initiating cells to radiation. *J. Natl. Cancer Inst.* 98, 1777-1785 (2006).
49. Bell,E.L. *et al.* The Qo site of the mitochondrial complex III is required for the transduction of hypoxic signaling via reactive oxygen species production. *J. Cell Biol.* 177, 1029-1036 (2007).
50. van der Bilt,J.D. *et al.* Ischemia/reperfusion accelerates the outgrowth of hepatic micrometastases in a highly standardized murine model. *Hepatology* 42, 165-175 (2005).
51. van der Bilt,J.D. *et al.* Perinecrotic hypoxia contributes to ischemia/reperfusion-accelerated outgrowth of colorectal micrometastases. *Am. J. Pathol.* 170, 1379-1388 (2007).
52. Nijkamp,M.W. *et al.* Prolonged portal triad clamping during liver surgery for colorectal liver metastases is associated with decreased time to hepatic tumour recurrence. *Eur. J. Surg. Oncol.* 36, 182-188 (2010).
53. Nijkamp,M.W. *et al.* Accelerated perinecrotic outgrowth of colorectal liver metastases following radiofrequency ablation is a hypoxia-driven phenomenon. *Ann. Surg.* 249, 814-823 (2009).
54. Das,B. *et al.* Hypoxia enhances tumor stemness by increasing the invasive and tumorigenic side population fraction. *Stem Cells* 26, 1818-1830 (2008).
55. Jogi,A. *et al.* Hypoxia alters gene expression in human neuroblastoma cells toward an immature and neural crest-like phenotype. *Proc. Natl. Acad. Sci. U. S. A* 99, 7021-7026 (2002).
56. Ezashi,T. *et al.* Low O2 tensions and the prevention of differentiation of hES cells. *Proc. Natl. Acad. Sci. U. S. A* 102, 4783-4788 (2005).

57. Locker,G.Y. *et al.* ASCO 2006 update of recommendations for the use of tumor markers in gastrointestinal cancer. *J. Clin. Oncol.* 24, 5313-5327 (2006).
58. Frederiksen,C.M. *et al.* Classification of Dukes' B and C colorectal cancers using expression arrays. *J. Cancer Res. Clin. Oncol.* 129, 263-271 (2003).
59. Salazar,R. *et al.* Gene expression signature to improve prognosis prediction of stage II and III colorectal cancer. *J. Clin. Oncol.* 29, 17-24 (2011).

2

DIFFERENTIATED HUMAN COLORECTAL CANCER CELLS PROTECT TUMOR-INITIATING CELLS FROM IRINOTECAN

Benjamin L. Emmink[1]*, Winan J. Van Houdt[1]*, Robert G. Vries [2],
Frederik J.H. Hoogwater[1], Klaas M. Govaert[1], Andre Verheem[1],
Maarten W. Nijkamp[1], Ernst J.A. Steller[1], Connie R. Jimenez[3], Hans Clevers[2],
Inne H.M. Borel Rinkes[1] and Onno Kranenburg[1]

[1] Department of Surgery University Medical Center Utrecht, The Netherlands
[2]Hubrecht Institute KNAW & University Medical Center Utrecht, The Netherlands
[3]OncoProteomics Laboratory, VU University Medical Center Amsterdam, The Netherlands

* Equal contribution

Gastroenterology. 2011 Jul;141(1):269-78

ABSTRACT

BACKGROUND: Normal tissue stem cells possess resistance mechanisms that allow them to endure a lifetime of genotoxic insults. By inheriting these traits, tumor-initiating cells are thought to be endowed with an intrinsic resistance to chemotherapy. However, the relationship between chemoresistance and tumor-initiating potential is poorly understood. Here we studied how resistance to the topoisomerase I inhibitor irinotecan is related to tumor-initiating potential in colorectal cancer. **METHODS:** Colonosphere cultures were established from resected primary tumors and liver metastases. Stem cell and differentiation markers were analyzed by Western blotting and FACS. Clone- and tumor-initiating capacity was assessed by single cell cloning and subcutaneous injections into immunodeficient mice. Sensitivity to irinotecan was assessed *in vitro* and in tumor-bearing immune-deficient mice. The relationship between drug resistance and tumor-initiating capacity was tested by FACS-sorting colonosphere cells on the basis of ABCB1 expression and aldehyde dehydrogenase (ALDH) activity. **RESULTS:** Colonosphere cultures displayed high tumor-initiating capacity and resistance to irinotecan. Inhibition of the drug-efflux pump ABCB1 by PSC-833 allowed irinotecan to ablate tumor-initiating potential. However, ABCB1 was only expressed on a small subpopulation of differentiated tumor cells that was unable to initiate the formation of clones or tumors. Conversely, tumor-initiating cells were ABCB1-negative and were identified by high aldehyde dehydrogenase (ALDH)-activity. Tumorigenic $ALDH^{high}/ABCB1^{negative}$ cells generated non-tumorigenic $ALDH^{low}/ABCB1^{positive}$ offspring *in vitro* and in tumor xenografts. Finally, PSC-833 strongly enhanced the therapeutic efficacy of irinotecan in tumor-bearing mice. **CONCLUSION:** The resistance of colorectal tumors to irinotecan requires the cooperative action of tumor-initiating $ALDH^{high}/ABCB1^{negative}$ cells and their differentiated drug-expelling $ALDH^{low}/ABCB1^{positive}$ offspring.

INTRODUCTION

Intestinal stem cells drive normal tissue turnover by generating daughter stem cells and a rapidly proliferating pool of progenitor cells that give rise to differentiated cell types with specialized functions[1]. This functional hierarchy is preserved in colon tumors in which a small tumor-initiating cell compartment drives the formation of proliferating and differentiated cell types with reduced tumorigenic potential[2-5]. Normal tissue stem cells have recently been identified as the cells of origin of several tumor types, including those of intestinal origin[6-10]. Preservation of the resistance mechanisms that characterise normal tissue stem cells during oncogenic transformation would provide the resulting tumor-initiating cells with an innate resistance to genotoxic agents. Therefore, tumor-initiating cells may not only drive tumor progression, but may also be responsible for resistance to chemotherapy and for subsequent tumor recurrence[11-13]. Indeed, tumor-initiating cells from a diverse range of tumors were found to display intrinsic chemo-resistance[13-18].

Chemotherapy of colorectal tumors is primarily based on 5-fluorouracil (5-FU), oxaliplatin and irinotecan[19]. However, colorectal tumors frequently fail to respond to chemotherapy, leaving the majority of tumor cells to survive treatment. Response rates are limited to 40-50%[19]. It is presently unknown how these clinical observations fit a model in which chemo-resistance is mediated by the small fraction of tumor cells with tumor-initiating capacity. Furthermore, drug efflux capacity does not appear to mark intestinal or colorectal tumor-initiating cells[20, 21]. Nevertheless, chemotherapy does enrich the population of clonogenic cancer cells in colorectal xenograft models, suggesting that these cells do display some form of selective drug resistance[4, 22].

Here, we studied the relationship between tumor-initiating potential and irinotecan resistance by using a series of highly clonogenic and tumorigenic colonosphere cultures isolated from freshly resected primary colorectal tumors and liver metastases.

MATERIALS AND METHODS

Collection of Tumor Specimens

Human colorectal tumor specimens were obtained from 28 patients undergoing a colon or liver resection for primary or metastatic adenocarcinoma, in accordance with the ethical committee on human experimentation. Informed consent was obtained from all patients. Diagnosis of tumor type and grade was based on histological examination.

Isolation and Expansion of Colorectal Tumor-Initiating Cell Cultures

A detailed procedure describing the isolation and expansion of colorectal tumor-initiating cell cultures is given in the supplementary material.

Colonosphere-Forming Efficiency (CFE)

Single cell suspensions derived from colonospheres and differentiated tumor cell cultures were counted, suspended in Matrigel (100 cells in 100µl) and allowed to set in 48-well plates. After setting, stem cell medium with fresh growth factors was added. Clone formation was analyzed after three weeks of culture. Colonies were counted using a Leica DM IRBE microscope and the colonosphere-forming efficiency (CFE) was calculated as the percentage of seeded cells that formed colonospheres.

Irinotecan Sensitivity Assay
Both colonosphere cultures and their differentiated derivatives were cultured in stem cell medium in the presence of irinotecan (Campo,Pfizer) at the indicated concentrations for five days. In addition colonosphere cultures were cultured in the presence of the ABCB1 inhibitor PSC833 (2 μM; Novartis, Basel Switzerland), the ABCG2 inhibitor Ko143 (200 nM; kindly provided by Dr. Alfred Schinkel, NKI, the Netherlands) and the ABCC1 inhibitor MK571 (30 μM; Sigma) either alone, or in combination with 50 μg/ml irinotecan for three consecutive days. Mitochondrial activity was evaluated using CellTiter 96 Aqueous One Solution Cell Proliferation Assay (MTS) (Promega). All absorbance values are expressed as percentages of vehicle-treated control wells.

Immunofluorescence and immunohistochemistry
Immunofluorescence were performed according to standard procedures, as specified in the supplementary material.

Statistical Analysis
The student's t test (unpaired, two-tailed) was performed to analyze statistically significant differences between groups. Outcome variables are depicted as point estimates, with a 95% confidence interval. In vivo tumor formation and drug treatment experiments were analyzed by one-way ANOVA followed by a Bonferroni multiple comparison test using GraphPad Prism software (GraphPad San Diego, CA). Differences with a p value of <0.05 were considered to be statistically significant.

RESULTS

A novel series of undifferentiated colonosphere cultures from primary colorectal tumors and liver metastases
To study the relationship between tumor-initiating capacity and irinotecan resistance, we established a series of colonosphere cultures isolated from freshly resected primary colorectal tumors and liver metastases. Immediately following surgery, biopsies were obtained from the resection specimens. Single cell cultures were prepared from the biopsies and these were cultured in serum-free stem cell medium in low-adherence flasks. Colonospheres formed in 8/20 of these cultures, four originating from primary CRC tumors and four originating from liver metastases (supplementary Table 1). Single cell suspensions of all eight colonosphere cultures displayed high colonosphere-forming efficiency (CFE) ranging from 20-62% (supplementary Table 1). Furthermore, these cells were highly tumorigenic when injected into immune deficient mice (supplementary Table 1). Flow cytometry and Western blot analysis for the expression of published markers for tumor-initiating cells[2, 3, 5, 22-24] showed that all colonospheres were positive for CD44 (50-100% of the cells) and ALDH1, while expression of CD133 and CD166 was more variable, ranging from 0-100% CD133-positive cells, and from 15-100% CD166-positive cells (supplementary Table 1). Colonosphere-initiated xenografts displayed extensive differentiation and were histologically similar to the tumors from which they were derived (Supplementary Figure 1).

When exposed to serum-containing medium the colonospheres attached to the culture dish and grew out to form adherent cultures with heterogeneous morphology (Figure 1A). A subpopulation of cells was positive in the periodic acid-Schiff (PAS) stain for mucin-producing

Goblet cells (Figure 1*A*) and all adherent cultures expressed the differentiation marker cytokeratin 20 (CK20) (Figure 1*B*). Distinct subpopulations of the adherent tumor cell populations expressed CK20 and the enterocyte brush border marker phospho-ezrin (Figure 1*C*).

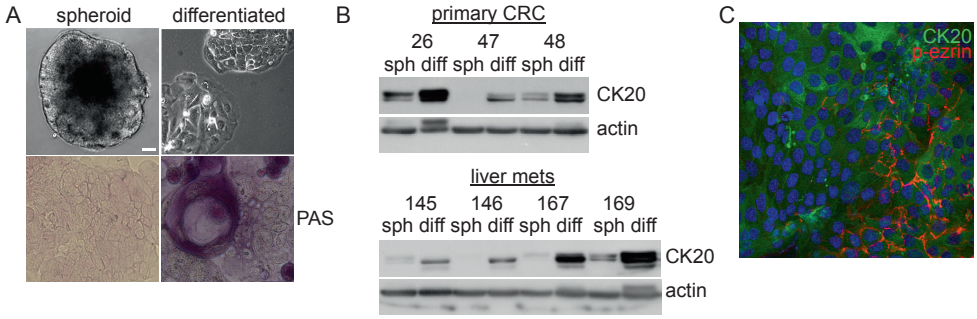

Figure 1. Differentiation of colonosphere-forming cells from human colorectal tumors. *(A)* Light microscopic images of a representative colonosphere and a population of colonosphere-derived adherent tumor cells. Bar 20 μm. The lower panel shows Periodic Acid Schiff-stained cultures. *(B)* Western blot analysis of the expression of cytokeratin 20 (CK20) and actin in isogenic colonosphere and adherent tumor cell cultures. *(C)* Adherent tumor cells were grown on glass coverslips and were analyzed by immunofluorescence to detect the differentiation markers CK20 (in green) and phospho-ezrin (in red). Bar 20 μm.

An unbiased proteomics screen of the tumorigenic and non-tumorigenic differentiated tumor cell populations revealed that aldehyde dehydrogenase 1 (ALDH1) was strongly expressed in all tumor-initiating cell-enriched cultures, but not in the differentiated cultures. Western blot analysis confirmed the selective expression of ALDH1 in the colonosphere cultures (Figure 2*A*). Colonosphere-derived single cell populations displayed heterogeneous ALDH activity as measured by Aldefluor® (Supplementary Figure 2), and cells with high ALDH activity displayed a significantly higher clone-forming potential when compared to cells with low ALDH activity (56% versus 14%, difference = 42%; 95% CI = 34% to 49%, $p<0.0001$) (Figure 2*B*). Co-staining with Aldefluor® and CD44 showed that the vast majority (>96%) of Aldefluor®-positive colonosphere cells were also positive for CD44 (Supplementary Figure 2). Importantly, serial transplantation of $ALDH^{high}$ cells into immune-deficient mice revealed their capacity to self-renew and to form tumors (Figure 2*C*, Supplementary Figure 3). Upon *in vitro* differentiation, ALDH1-expression dropped, and this was accompanied by a drastic reduction in clone- and tumor-forming potential (supplementary Table 1, Figure 2 *D-E*) (For statistics see supplementary Table 2). ALDH1 expression in spheroid-initiated xenografts dropped to similarly low levels as those obtained following *in vitro* differentiation (Supplementary Figure 1). These results are in line with recent reports identifying ALDH1 as a marker for colorectal tumor-initiating cells[22, 23]. Taken together, we have established an *in vitro* culture system for the maintenance of ALDH1-positive, differentiation-competent colorectal tumor-initiating cells.

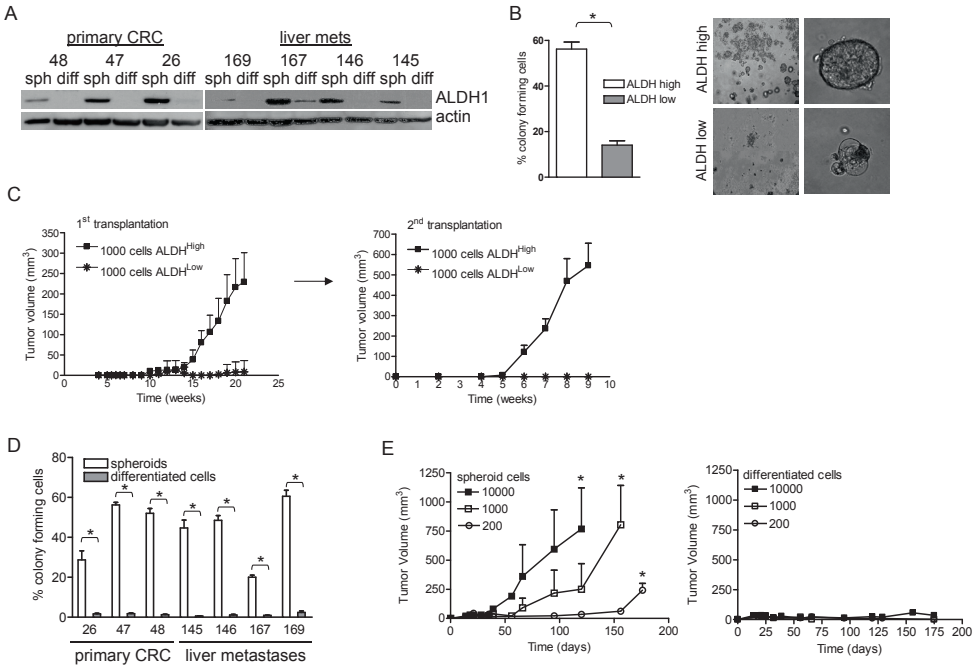

Figure 2. ALDH1 marks tumor-initiating cells in colonospheres. *(A)* Lysates of paired colonosphere and differentiated cultures derived from primary colorectal tumors and liver metastases were analyzed for the expression of ALDH1 by Western blotting. *(B)* Cultures enriched for tumor-initiating cells were analyzed for ALDH activity. Clone forming potential of cells with high and low ALDH activity was determined after 3 weeks. Representative examples of clones formed in ALDH-high and ALDH-low cultures are shown. *(C)* $ALDH^{high}$ and $ALDH^{low}$ cell populations within the spheroids were separated by making use of the fluorescent ALDH substrate Aldefluor®. $ALDH^{high}$ and $ALDH^{low}$ cells (1000) were injected into the flanks of nude mice (n=8). Tumors generated by $ALDH^{high}$ cells were harvested and processed to generate single cell suspensions. Again $ALDH^{high}$ and $ALDH^{low}$ cell populations were separated by FACS sorting and these were injected into the flanks of nude mice (1000 cells). Tumor growth was analyzed by caliper measurements. The mean tumor volume of all tumors is shown. *(D)* Single cell populations were generated from the indicated colonosphere lines and from adherent tumor cell cultures and these were suspended in Matrigel at 1000 cells/ml. Equal numbers of Matrigel-embedded cells (n=100 in 100 µl) were allowed to set in 48-well plates and clone formation was analyzed after three weeks of culture. *(E)* Single cell populations were generated from L145 colonospheres and from adherent tumor cell cultures and these were suspended in Matrigel. Mice were injected with 10.000 (n=3), 1000 (n=3), or 200 (n=3) tumor cells as indicated and tumor growth was followed over time by calliper measurements. *denotes statistical significance (Unpaired, 2-tailed t test: $p<0.05$).

Colonosphere cultures display resistance to irinotecan

We next used the metastasis-derived pairs of tumorigenic colonosphere and non-tumorigenic differentiated tumor cell populations to assess their relative sensitivity to irinotecan, a frequently used chemotherapeutic agent in the treatment of metastasized colorectal cancer[19]. Mitochondrial activity assays revealed that all colonosphere cultures were significantly more resistant to irinotecan than differentiated tumor cells (Figure 3*A*) (For statistics see supplementary Table 3). Irinotecan treatment of differentiated tumor cells caused loss of BrdU incorporation (Figure 3*B*), rapid stabilization of p53 and processing of caspase 3 (Figure 3*C*), reflecting cell cycle arrest and apoptosis. In colonosphere cultures irinotecan reduced BrdU incorporation by ~50% (Figure 3*B*; For statistics see supplementary Table 3), similar to the reduction in mitochondrial activity (Figure 3*A*), but p53 stabilization or caspase 3 processing were not observed (Figure 3*C*).

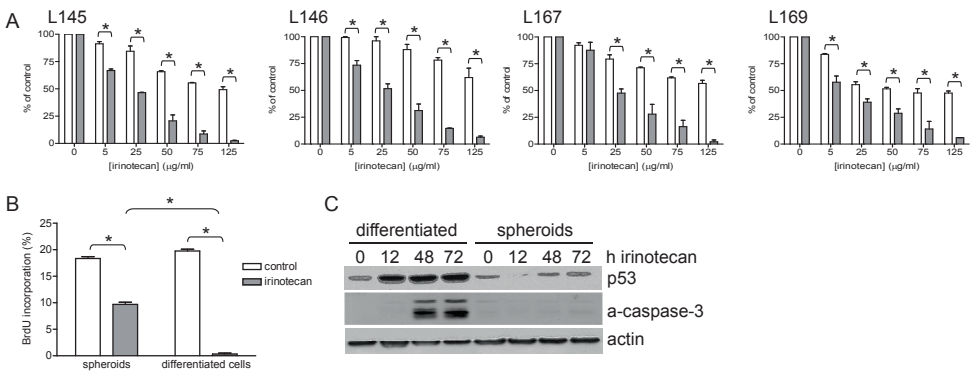

Figure 3. Colonosphere resistance to irinotecan. *(A)* Colonospheres (open bars) and isogenic differentiated tumor cells (closed bars) were seeded in 48-well plates in triplicate and were exposed to the indicated concentrations of irinotecan for five days. Mitochondrial activity was then tested by standard MTS assays. Absorbance values are expressed as percentages of vehicle-treated control wells. *(B)* L145 colonospheres and differentiated tumor cells were treated either with vehicle (open bars) or with 125 µg/ml irinotecan (closed bars) for 72 hours. The cells were then pulse-labelled with BrdU for 30 minutes and the percentage of BrdU-positive cells was determined by FACS analysis. *(C)* L145 colonospheres and differentiated tumor cells were treated with irinotecan for the indicated periods of time. Cell lysates were prepared and were analyzed for the presence of p53 and activated (cleaved) capsase-3 (a-caspase-3). *denotes statistical significance (Unpaired, 2-tailed t test: $p<0.05$).

Irinotecan resistance is mediated by ABCB1

An important mechanism of resistance to irinotecan is the expression of drug efflux pumps of the ABC transporter family [25]. The fluorescent DNA-binding dye Hoechst-33342 is a good substrate for the ABC pumps, offering a convenient assay for relevant ABC transporter activity. Hoechst-33342 readily stained the differentiated cell populations, but colonospheres failed to retain the dye (supplementary Figure 4). Verapamil, a relatively non-selective inhibitor of ABCB1, ABCG2, and to a lesser extent ABCC1, allowed Hoechst retention throughout the colonospheres, without affecting cell viability (supplementary Figure 4). To assess whether irinotecan resistance is caused by ABC transporter activity, the colonosphere cultures were exposed to irinotecan in combination with selective inhibitors of ABCB1 (PSC833), ABCG2 (Ko143) and ABCC1 (MK-571). Only PSC833 sensitized the colonosphere cultures to irinotecan (Figure 4*A* and supplementary Figure 8) (For statistics see supplementary Table 4), which was accompanied by capase 3 cleavage and apoptosis induction (Figure 4*B*). Only the combination treatment, but neither irinotecan alone nor PSC833 alone, caused caspase-3 processing (Figure 4*B*). The irinotecan-related fluorescent drug topotecan was also excluded from colonospheres, but PSC833 allowed its uptake and retention (Supplementary Figure 5). These results suggest that co-treatment of colonospheres with PSC-833 and irinotecan suffices to kill tumor-initiating cells. To test this directly, colonospheres were treated with vehicle, PSC-833 alone, irinotecan alone or with the drug combination. The resulting cell populations were then injected into nude mice to assess tumor-initiating potential. PSC833-treatment did not affect tumor formation or latency time, when compared to treatment with vehicle. Irinotecan treatment did not affect tumor incidence, although latency time was ~1 week longer. However, co-treatment with PSC-833 and irinotecan completely abolished tumor-initiating potential.

The PSC833-target ABCB1 was highly expressed in colonosphere cultures, but not in differentiated tumor cells (Figure 4*D*). Irinotecan treatment further increased ABCB1 expression (Figure 4*D*). Strikingly, FACS analysis showed that only ~12% of the colonosphere cell population expressed ABCB1 (supplementary Figure 6), even though the entire population displayed irinotecan resistance. FACS analysis of colonospheres and colonosphere-initiated tumors for ABCB1 and ALDH activity showed that these markers were expressed in a mutually exclusive fashion, with less than 0.3% double positive cells (Figure 4*E*). Exposure to irinotecan did not cause an increase in the percentage of ABCB1/ALDH^{high} double-positive cells, although ABCB1 single-positive cells were somewhat increased (Figure 4*F,* supplementary Figure 6).

Figure 4. Irinotecan resistance is mediated by a subpopulation of tumor cells expressing ABCB1. *(A)* L145 and L167 colonospheres were cultured in the presence of irinotecan (50 μg/ml) the ABCB1 inhibitor PSC833 (2 μM), the ABCG2 inhibitor Ko143 (200 nM), or the ABCC1 inhibitor MK571 (30 μM), either alone or in combination as indicated. Mitochondrial activity was then assessed by MTS assays for three consecutive days. Absorbance values are expressed as percentages of vehicle-treated control wells. *denotes statistical significance (Unpaired, 2-tailed t test: $p<0.05$). *(B)* L145 colonospheres were cultured in the presence of irinotecan either in the absence or presence of the ABCB1 inhibitor PSC833. Cell lysates were prepared at the indicated periods of time and these were analyzed for the presence of activated (cleaved) caspase-3 (a-caspase-3). *(C)* L145 colonospheres were treated with vehicle, PSC833 alone (2 μM), irinotecan alone (75 μg/ml) or with the combination. The resulting cell populations were injected into the flanks of nude mice to assess tumor-initiating potential. Tumor growth was measured by calliper measurements. *(D)* Cell lysates of colonosphere cultures and differentiated tumor cells of the indicated tumors were lysed and analyzed for the presence of ABCB1 by Western blotting. L145 colonospheres were treated with vehicle or with irinotecan for 72 hours and lysates were prepared for analysis of ABCB1 expression by Western blotting. *(E)* FACS analysis of ABCB1 and Aldefluor® in three different colonosphere lines and in two spheroid-initiated tumors. (*F*) FACS analysis of ABCB1 and Aldefluor® in irinotecan-treated L145 colonosphere cultures (75 μg/ml; 24 h).

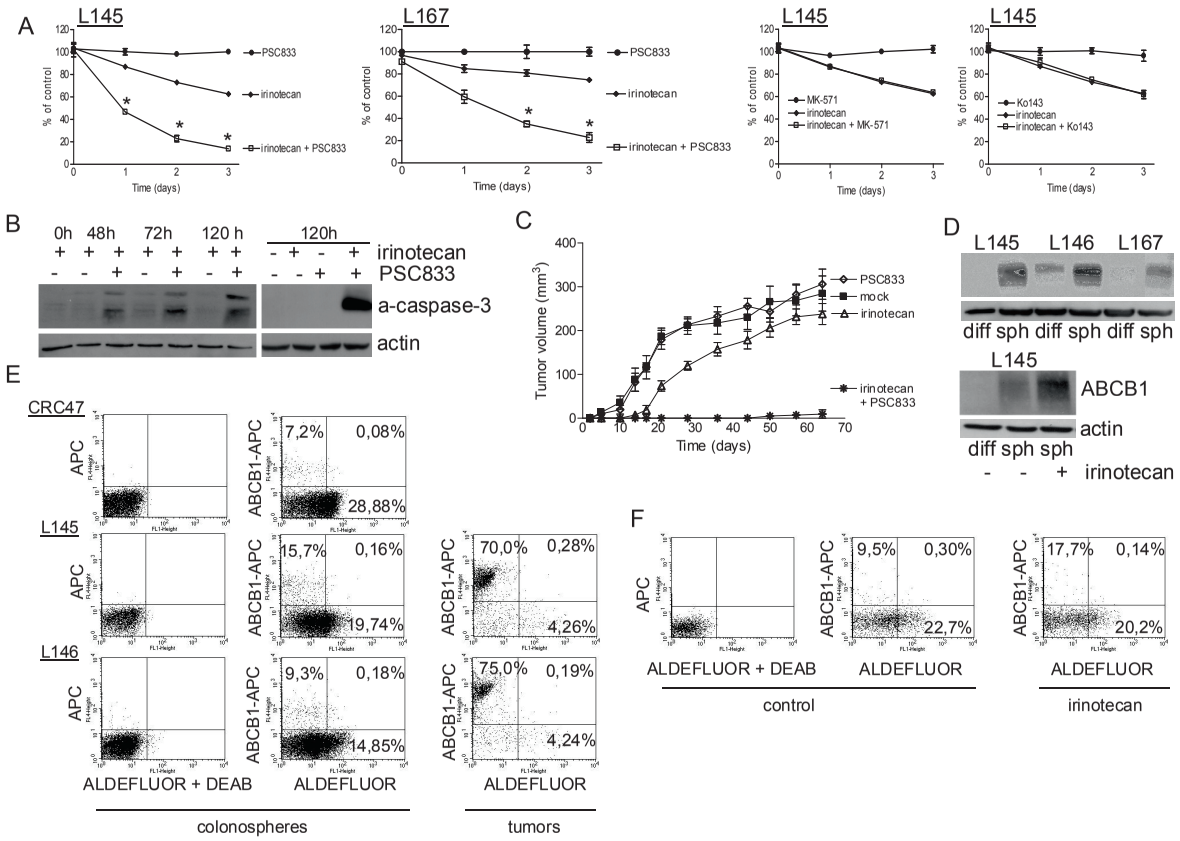
A
L145
L167
L145
L145
% of control
Time (days)
PSC833
irinotecan
irinotecan + PSC833
MK-571
irinotecan + MK-571
Ko143
irinotecan + Ko143
B
0h 48h 72h 120 h 120h
irinotecan
PSC833
a-caspase-3
actin
C
Tumor volume (mm3)
Time (days)
PSC833
mock
irinotecan
irinotecan + PSC833
D
L145 L146 L167
diff sph diff sph diff sph
L145
ABCB1
actin
diff sph sph
- - + irinotecan
E
CRC47
L145
L146
APC
ABCB1-APC
7,2%
0,08%
28,88%
15,7%
0,16%
19,74%
9,3%
0,18%
14,85%
70,0%
0,28%
4,26%
75,0%
0,19%
4,24%
ALDEFLUOR + DEAB
ALDEFLUOR
colonospheres
tumors
F
9,5%
0,30%
22,7%
17,7%
0,14%
20,2%
ALDEFLUOR + DEAB
ALDEFLUOR
control
irinotecan

ABCB1 marks a differentiated non-tumorigenic minor subpopulation of colonosphere cells

Immunofluorescence analysis showed that ABCB1 expression was restricted to the apical membrane of the single outer cell layer of L145 and CRC26 colonospheres, whereas CD44 and EpCAM showed a homogeneous staining pattern (Figure 5*A* and supplementary Figure 8). Similar results were obtained for L146, L167 and L169. Furthermore, ABCB1 was also strongly expressed on cells forming tubules inside large colonospheres (Figure 5*B*). These cells co-expressed the brush border marker phospho-ezrin. Irinotecan exposure did not alter the pattern of expression throughout the colonosphere (Figure 5A, lower panel). In human colorectal liver metastases ABCB1 predominantly localized to the luminal side of differentiated tubule-forming cells (Figure 5*C,D*). ALDH1-positive cells were predominantly localized in undifferentiated areas of the tumor and were generally not a part of the ABCB1-positive tubules (Figure 5*C*). In L145 colonospheres the ABCB1-positive cells also expressed cytokeratin-20 and the enterocyte brush border marker phospho-ezrin (Figure 5*E*), but were negative in the PAS stain (Figure 1*A*). Similar results were obtained for L146, L167 and L169. While normal intestinal enterocytes are post-mitotic, approximately 30% of the enterocyte-like colonosphere cells expressed the proliferation marker Ki67 (Figure 5*F*). Similarly, ABCB1-positive tubule-forming cells in human colorectal liver metastases express Ki67. Cell proliferation in the inner cell mass of the colonospheres was significantly lower (27% versus 7%, difference=20%; 95% CI=10 to 29, p=0.002) (Figure 5*F*). ABCB1 therefore marks a population of differentiated, yet proliferation-competent tumor cells. These cells are clearly distinct from the stably differentiated adherent cultures that were obtained after serum stimulation and that lack expression of ABCB1.

Figure 5. ABCB1 marks a population of proliferating tubule-forming cells displaying enterocyte-like differentiation. *(A)* L145 colonospheres were fixed in formalin and processed for immunofluorescence using validated antibodies directed at ABCB1, CD44 and EpCAM. Irinotecan-treated cultures (75 μg/ml; 72h) were also analyzed for ABCB1 localization (lower panel). *(B)* Large colonospheres with signs of intra-sphere tubule formation were fixed and stained for ABCB1 and phospho-ezrin as in A. *(C)* Paraffin-embedded (left panels) and frozen (right panels) tissue sections of the same region in human colorectal tumor tissue (L150) were stained for expression of ABCB1 and ALDH1. Representative images are shown. ABCB1 is mainly found on the apical membrane of tubule forming cells. ALDH1 is expressed by non-tubule-forming cells in poorly differentiated tumor areas which lie between the tubule-forming cells. Bar 50 μm. *(D)* Colonospheres were fixed in formalin and processed for immunofluorescence using validated antibodies directed at cytokeratin 20 (CK20) and phospho-ezrin (p-ezrin). A representative L145 sphere is shown. *(E)* Expression of the proliferation marker Ki67 in the CK20/ABCB1/p-ezrin-positive outer cell layer relative to inner sphere cells was assessed by immunofluorescence as in A. Quantification was performed by counting the number of outer and inner cells displaying Ki67 expression. A representative example is shown in the left panel, quantification of Ki67 in the two cell compartments was based on analysis of 16 spheres from L145, L146 and L150 each. *denotes statistical significance (p=0.0002). All bars 20 μm.

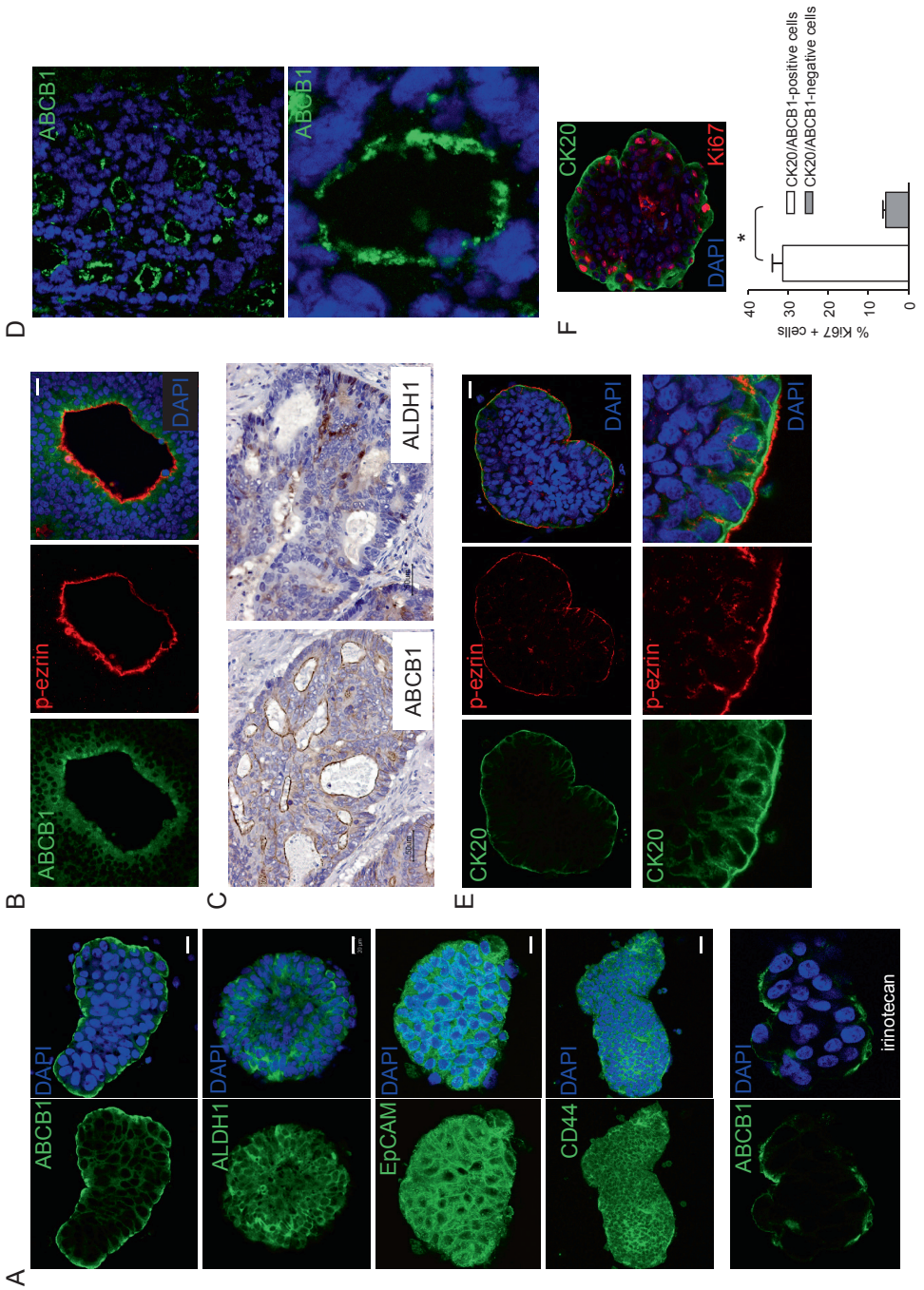
A
ABCB1
DAPI
ALDH1
EpCAM
CD44
irinotecan
B
p-ezrin
C
ALDH1
ABCB1
D
E
CK20
F
Ki67
% Ki67 + cells
CK20/ABCB1-positive cells
CK20/ABCB1-negative cells
*

Differentiated ABCB1-positive cells protect ALDH1-positive tumor-initiating cells from irinotecan

To test whether the ABCB1-expressing outer cell layer protects the inner cell mass from irinotecan, colonospheres were dissociated and single cell suspensions were exposed to irinotecan in the presence or absence of PSC-833. The vast majority of colonosphere-derived single cells (~90%) were killed by irinotecan, while intact colonospheres displayed resistance (Figure 6*A;* see also Figure 3*A*) (For statistics see supplementary Table 6). The remaining live cells following single cell treatment were unable to form new clones (Figure 6*B*). By contrast, irinotecan-treated colonospheres retained their clone-forming potential (Figure 6*B*). PSC-833 treatment allowed irinotecan to kill colonospheres with similar efficiency as single cell cultures (Figure 6*A*). This suggests that ABCB1-mediated drug efflux is the major determinant of colonosphere resistance to irinotecan. To further assess the relationship between drug resistance (ABCB1 expression) and tumor-initiating potential, the ABCB1-positive and ABCB1-negative cells were separated by FACS sorting using two independent antibodies (MM-4.17 and F4). ABCB1-negative cells were highly clonogenic, but ABCB1-positive cells failed to form clones (Figure 6*C*, supplementary Figures 7 & 8) (64% versus 2%, difference 62%; 95% CI = 55.18% to 68.83%, p<0.0001). Furthermore, ABCB1-negative cells induced tumor formation in immunodeficient mice (3/4), but ABCB1-positive cells failed to do so (0/4). FACS analysis of the clones generated by ABCB1-negative cells revealed that they were composed of subpopulations of ABCB1-positive and ABCB1-negative cells with a distribution similar to the colonospheres from which they were derived (Figure 6*D*). Thus, ABCB1-negative cells were able to generate ABCB1-positive cells, but not *vice versa*. Interestingly, ABCB1-negative tumor cells were characterized by expression of the cancer stem cell marker ALDH1, while non-tumorigenic ABCB1-positive cells expressed the differentiation marker CK20 (Figure 6*E*).

Figure 6. Separation of irinotecan-resistance and tumor-initiating potential on the basis of ABCB1 expression. *(A)* L145 colonospheres and sphere-derived single cell populations were treated either with vehicle or with irinotecan in the presence or absence of PSC-833 for five days at the indicated concentrations. Mitochondrial activity was then assessed by MTS assays for three consecutive days. Absorbance values are expressed as percentages of vehicle-treated control wells. *(B)* L145 colonospheres were either left as spheres or were processed to generate single cell populations. Colonospheres and single cell populations were then treated with irinotecan. All cultures were washed and the spheres were processed to generate single cell populations. All single cell populations were resuspended in Matrigel at 1000 live cells/ml. Equal numbers of Matrigel-embedded cells (n=100 in 100 μl) were allowed to set in 48-well plates and clone formation was analyzed after two weeks (left panel) 4 weeks (middle panel) or 8 weeks (right panel) of cell culture. *(C)* Single cell cultures were derived from L145 colonospheres and these cells were stained for expression of ABCB1 by using 2 independent antibodies (MM4.17 and F4; see also Supplementary Figure 7). The ABCB1-positive and ABCB1-negative subpopulations were separated by FACS sorting and analyzed for clone-forming and tumor-initiating capacity as above. Part of the cells was re-sorted to assess their proper separation. *(D)* The clones generated by the ABCB1-negative cells were recovered from the Matrigel and single cell populations were prepared and analyzed for ABCB1 expression by FACS analysis. *(E)* Tumors were excised and processed to generate single cell suspensions. ABCB1-positive and -negative epithelial (EpCAM+) cells were separated by FACS sorting and analyzed for expression of ALDH1 and CK20 by Western blotting. *(F)* Intestinal organoid cultures from *Lgr5-EGFP-ires-CreERT2* mice [27] (n=3, each containing 25-50 organoids) were treated for 24 hours with the indicated concentrations of irinotecan. The number of GFP-positive organoids was assessed by fluorescence microscopy using DAPI as counterstain for healthy cells. *denotes statistical significance (Unpaired, 2-tailed t test: p<0.05).

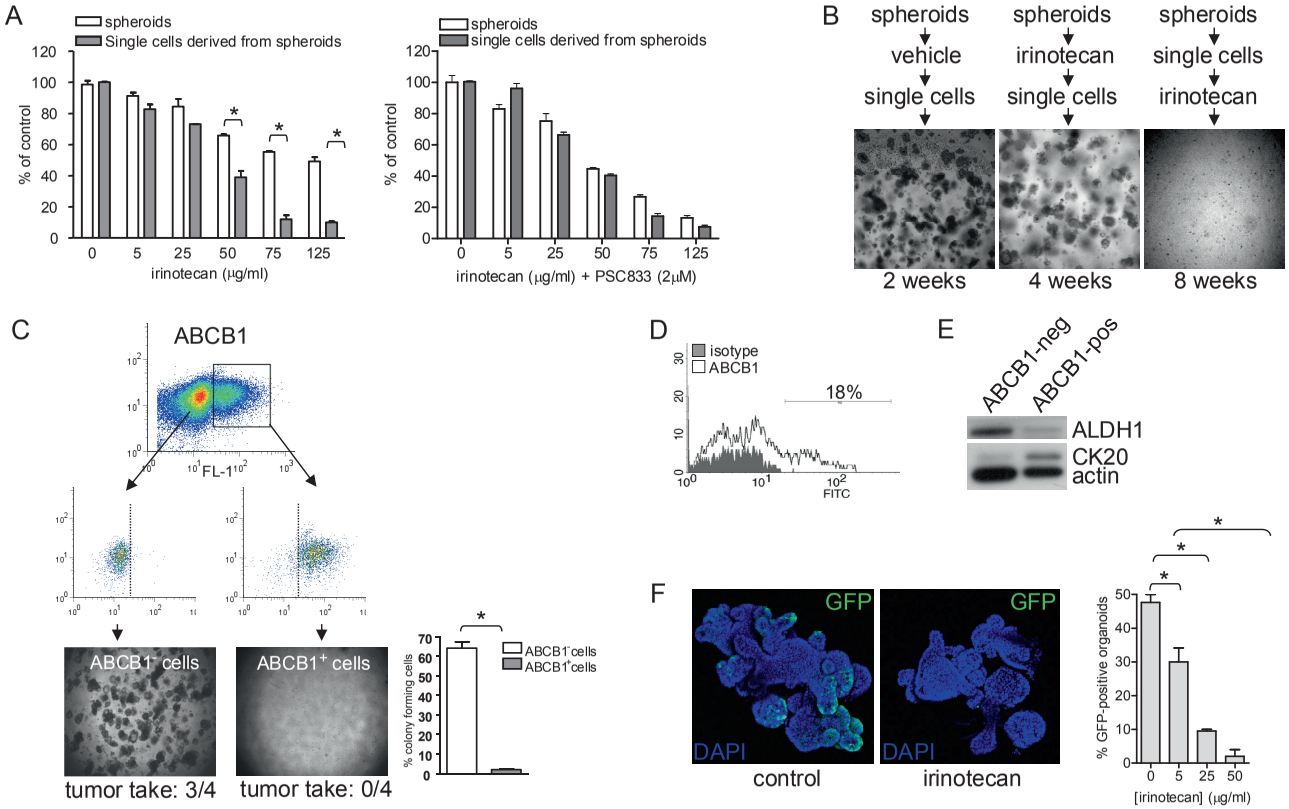
A
spheroids
Single cells derived from spheroids
% of control
irinotecan (μg/ml)
spheroids
single cells derived from spheroids
irinotecan (μg/ml) + PSC833 (2μM)
B
spheroids
vehicle
single cells
spheroids
irinotecan
single cells
spheroids
single cells
irinotecan
2 weeks
4 weeks
8 weeks
C
ABCB1
FL-1
ABCB1⁻ cells
ABCB1⁺ cells
tumor take: 3/4
tumor take: 0/4
% colony forming cells
ABCB1⁻cells
ABCB1⁺cells
D
isotype
ABCB1
18%
FITC
E
ABCB1-neg
ABCB1-pos
ALDH1
CK20
actin
F
GFP
DAPI
control
irinotecan
% GFP-positive organoids
[irinotecan] (μg/ml)

Normal intestinal stem cells are the cells of origin of intestinal tumors[6, 10] and express low levels of ABC transporters[26]. This predicts that intestinal stem cells could also be sensitive to irinotecan. To test this we employed the recently described organoid culture system in which intestinal stem cells are marked by *Lgr5* promoter-driven expression of green fluorescent protein (GFP)[27]. Fluorescence microscopy showed that irinotecan treatment caused a rapid depletion of GFP-positive stem cells from the organoid cultures (Figure 6*E*) (For statistics see supplementary Table 6). Washed and re-plated populations of irinotecan-treated organoids failed to form new organoids, demonstrating the loss of tissue stem cells with regenerative potential.

Finally, we evaluated whether PSC833 could enhance the therapeutic efficacy of irinotecan against human colorectal tumor xenografts initiated by injection of either colonospheres or of unsegregated human tumor tissue. Tumor growth was observed in all injected animals. Tumor-bearing mice were treated with vehicle, irinotecan alone, PSC-833 alone, or the combination. Only the combination treatment had a robust anti-tumor effect against both types of xenograft (Figure 7*A*). Combination treatment was not associated with overt morbidity. In complete accordance with the *in vitro* findings, tumor cell apoptosis (active caspase-3) was only observed in tumors treated with the combination therapy (Figure 7*B*). FACS analysis of the treated xenografts further showed that irinotecan treatment alone enhanced the percentage of Aldefluor^{high} cells, but that co-treatment with PSC-833 caused a marked reduction in the percentage of Aldefluor^{high} cells (Figure 7*C*). The percentage of Aldefluor^{high} cells in xenografts treated with irinotecan and PSC-833 does not differ from that in mock-treated tumors. However, the absolute number of Aldefluor^{high} cells is reduced 3-6 fold when compared to single compound or mock-treated tumors (Supplementary Table 7). This is due to the lower tumor volume selectively in combination-treated animals.

Figure 7. PSC-833 enhances the anti-tumor efficacy of irinotecan. *(A)* Subcutaneous tumor xenografts were generated by injection of colonospheres (n=8) or by transplantation of unsegregated biopsies from a freshly resected human colorectal liver metastasis (n=8). Tumor growth was observed in all injected animals. Treatment (vehicle, irinotecan, PSC-833, or the combination) was started (day 0) after tumors reached a volume of 250-350 mm^3. Tumor volume was analyzed by calliper measurements. Tumors were harvested and pooled samples of each group were analyzed *(B)* for active caspase-3 by Western blotting, or *(C)* for ALDH activity by FACS analysis, using Aldefluor®.

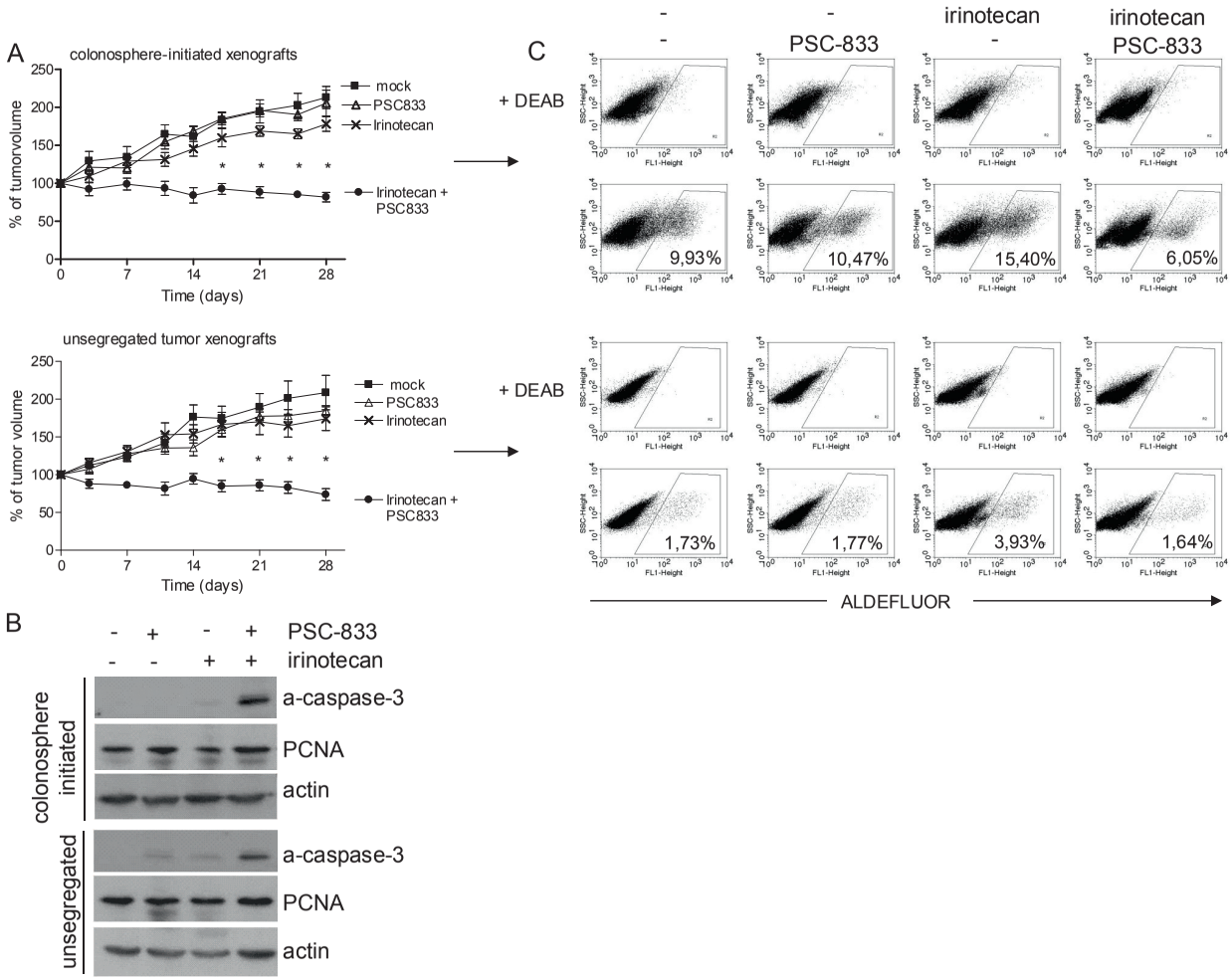
A
colonosphere-initiated xenografts
% of tumorvolume
Time (days)
mock
PSC833
Irinotecan
Irinotecan + PSC833
unsegregated tumor xenografts
% of tumor volume
Time (days)
B
PSC-833
irinotecan
colonosphere initiated
unsegregated
a-caspase-3
PCNA
actin
C
+ DEAB
PSC-833
irinotecan
9,93%
10,47%
15,40%
6,05%
1,73%
1,77%
3,93%
1,64%
ALDEFLUOR

DISCUSSION

The generation of colonosphere cultures from resection specimens is currently believed to be the most relevant cell culture system for colorectal tumors available. In this report we provide evidence that the maintenance of tumorigenic colonosphere cells following irinotecan exposure requires two types of tumor cells: First, a cell population with intrinsic tumor-initiating capacity and second, a drug-expelling non-tumorigenic differentiated cell population that provides protection to the tumor-initiating cells from which they originated. To our knowledge this is the first example of how differentiated tumor cells and tumor-initiating cells display functional cooperation.

Differentiated ABCB1^{high} cells are the lumen-forming cells in colon carcinomas and may keep the intra-tumor drug concentration low by expelling irinotecan into this lumen. In doing so, ABCB1^{positive}/ALDH^{low} cells may provide *in-trans* protection to tumor-initiating ABCB1^{negative}/ALDH^{high} cells that lack drug-expelling capacity. Our study does not address whether ABCB1^{negative} and ABCB1^{positive} cells display different *intrinsic* sensitivities to the drug. Current models of chemoresistance have implicated intrinsically drug-resistant tumor-initiating cells as the driving force behind tumor recurrence following chemotherapy[11, 12, 28]. This is based on the fact that normal tissue stem cells generally express high levels of ABC transporters and DNA repair enzymes and are relatively resistant to apoptosis, and on more recent reports showing that tissue stem cells are the cells of origin of a number of different tumor types[6-10].

Recently, it has been shown that treatment of colon cancer xenografts with irinotecan caused a minor increase in the percentage of cells co-expressing the 'cancer stem cell' markers CD44 and CD166[22]. However, the vast majority of tumor cells surviving treatment (>90%) were negative for these markers[22]. This suggests that mechanisms other than intrinsically drug-resistant tumor-initiating cells must play a major role in determining the resistance of colorectal tumors to irinotecan. Furthermore, the clinical observation that colorectal tumors frequently fail to respond to cytotoxic chemotherapeutics at all[29-31] is hard to reconcile with the idea that a small fraction of drug-resistant tumor-initiating cells is the primary cause of chemoresistance. The relationship between drug resistance and tumor-initiating potential is most likely dependent on the specific drug and on the mechanism(s) of resistance to that drug. For instance, ALDH^{high} tumor-initiating cells are intrinsically resistant to cyclophosphamide due to direct detoxification of this drug by ALDH1[22], but they are not capable of expelling irinotecan due to low level ABCB1 expression (this report). These relationships need to be clarified for all relevant chemotherapeutic drugs.

Irinotecan is a good substrate for the ABC transporters ABCB1 and ABCG2[25]. The contribution of the various ABC transporters to primary and acquired irinotecan resistance in colon cancer patients is currently unknown. The expression of ABCG2 increases following irinotecan exposure[32], but whether this represents a major resistance mechanism has not been tested. 'Reversal trials' using ABC transporter inhibitors in combination with chemotherapeutics have generated disappointing results. This is possibly due to the fact that mechanisms other than ABC transporter-mediated drug clearance also play an important role in determining drug resistance. These include inadequate drug delivery to tumor cells within a tumor mass, metabolic drug conversion and cell intrinsic properties such as increased levels of DNA repair enzymes[33]. Several reversal trials have been performed in colorectal cancer patients, but none of these involved irinotecan[33, 34]. Future work should clarify whether inhibition of ABCB1 activity is sufficient to kill tumor-initiating cells by irinotecan in the context of human colorectal tumor tissue. Irinotecan/PSC-833 combination therapy greatly reduced the total number of residual Aldefluor^{high} cells and also the percentage of these cells when compared to tumors treated with irinotecan alone. This may have clinical relevance

as it is most likely the total number of residual tumor-initiating cells which determines the time-to-progression in chemotherapy-treated cancer patients. Since not all residual tumor-initiating cells are eliminated by irinotecan/PSC-833 combination treatment, ABC transporter-unrelated resistance mechanisms, such as those discussed above, must play a role as well.

In normal intestinal tissue, expression of ABC transporters is restricted to the top compartment of differentiated cells facing the lumen[26]. This not only prevents the entry of toxic substances across the intestinal barrier, but also expels intravenously delivered drugs, such as irinotecan, into the gastrointestinal lumen. In contrast, ABC transporter expression in the crypt stem cell compartment is very low[26]. In line with this, we find that Lgr5-positive intestinal stem cells are readily eradicated by irinotecan. One of the major dose-limiting toxicities associated with irinotecan-based chemotherapy is severe diarrhea. This is observed in up to 82% of the patients, and is associated with morphological and functional changes in the intestinal mucosa[19, 35-37]. While acute diarrhea is short-lasting and manageable, delayed onset diarrhea (from three days onwards) is more difficult to treat, and its causes are obscure[36]. Our results suggest that depletion of the ABCB1-negative intestinal stem cell population by irinotecan and a consequent disturbance of intestinal homeostasis may contribute to delayed onset intestinal toxicity.

Taken together, we have shown that tumor-initiating potential and irinotecan-expelling activity are separable traits in colonosphere cultures. In recent years the identification of tumor-initiating cells and the pathways on which they depend has received an enormous amount of attention. Our work suggests that the conventional anti-cancer drug irinotecan can reduce the total number of colorectal tumor-initiating cells, as long as the non-tumorigenic ABCB1-expressing cells are targeted simultaneously.

Acknowledgements
The authors thank the surgeons and pathologists in our hospital for their help in obtaining the patient samples.

REFERENCE LIST

1. van der Flier,L.G. & Clevers,H. Stem cells, self-renewal, and differentiation in the intestinal epithelium. *Annu. Rev. Physiol* 71, 241-260 (2009).
2. O'Brien,C.A. *et al.* A human colon cancer cell capable of initiating tumour growth in immunodeficient mice. *Nature* 445, 106-110 (2007).
3. Ricci-Vitiani,L. *et al.* Identification and expansion of human colon-cancer-initiating cells. *Nature* 445, 111-115 (2007).
4. Todaro,M. *et al.* Colon cancer stem cells dictate tumor growth and resist cell death by production of interleukin-4. *Cell Stem Cell* 1, 389-402 (2007).
5. Vermeulen,L. *et al.* Single-cell cloning of colon cancer stem cells reveals a multi-lineage differentiation capacity. *Proc. Natl. Acad. Sci. U. S. A* 105, 13427-13432 (2008).
6. Barker,N. *et al.* Crypt stem cells as the cells-of-origin of intestinal cancer. *Nature* 457, 608-611 (2009).
7. Kim,C.F. *et al.* Identification of bronchioalveolar stem cells in normal lung and lung cancer. *Cell* 121, 823-835 (2005).
8. Le,L.Q. *et al.* Cell of origin and microenvironment contribution for NF1-associated dermal neurofibromas. *Cell Stem Cell* 4, 453-463 (2009).
9. Perez-Caro,M. *et al.* Cancer induction by restriction of oncogene expression to the stem cell compartment. *EMBO J.* 28, 8-20 (2009).
10. Zhu,L. *et al.* Prominin 1 marks intestinal stem cells that are susceptible to neoplastic transformation. *Nature* 457, 603-607 (2009).
11. Dean,M. *et al.* Tumour stem cells and drug resistance. *Nat. Rev. Cancer* 5, 275-284 (2005).
12. Donnenberg,V.S. & Donnenberg,A.D. Multiple drug resistance in cancer revisited: the cancer stem cell hypothesis. *J. Clin. Pharmacol.* 45, 872-877 (2005).
13. Eyler,C.E. & Rich,J.N. Survival of the fittest: cancer stem cells in therapeutic resistance and angiogenesis. *J. Clin. Oncol.* 26, 2839-2845 (2008).
14. Hermann,P.C. *et al.* Distinct populations of cancer stem cells determine tumor growth and metastatic activity in human pancreatic cancer. *Cell Stem Cell* 1, 313-323 (2007).
15. Hirschmann-Jax,C. *et al.* A distinct "side population" of cells with high drug efflux capacity in human tumor cells. *Proc. Natl. Acad. Sci. U. S. A* 101, 14228-14233 (2004).
16. Li,X. *et al.* Intrinsic resistance of tumorigenic breast cancer cells to chemotherapy. *J. Natl. Cancer Inst.* 100, 672-679 (2008).
17. Liu,G. *et al.* Analysis of gene expression and chemoresistance of CD133+ cancer stem cells in glioblastoma. *Mol. Cancer* 5, 67 (2006).
18. Ma,S. *et al.* CD133+ HCC cancer stem cells confer chemoresistance by preferential expression of the Akt/PKB survival pathway. *Oncogene* 27, 1749-1758 (2008).
19. Chau,I. & Cunningham,D. Treatment in advanced colorectal cancer: what, when and how? *Br. J. Cancer*(2009).
20. Alison,M.R. *et al.* Isolation of gut SP cells does not automatically enrich for stem cells. *Gastroenterology* 130, 1012-1013 (2006).
21. Burkert,J., Otto,W.R., & Wright,N.A. Side populations of gastrointestinal cancers are not in stem cells. *J. Pathol.* 214, 564-573 (2008).
22. Dylla,S.J. *et al.* Colorectal cancer stem cells are enriched in xenogeneic tumors following chemotherapy. *PLoS. ONE.* 3, e2428 (2008).
23. Huang,E.H. *et al.* Aldehyde dehydrogenase 1 is a marker for normal and malignant human colonic stem cells (SC) and tracks SC overpopulation during colon tumorigenesis. *Cancer Res.* 69, 3382-3389 (2009).
24. Dalerba,P. *et al.* Phenotypic characterization of human colorectal cancer stem cells. *Proc. Natl. Acad. Sci. U. S. A* 104, 10158-10163 (2007).
25. Smith,N.F. *et al.* Pharmacogenetics of irinotecan metabolism and transport: an update. *Toxicol. In Vitro* 20, 163-175 (2006).
26. Kosinski,C. *et al.* Gene expression patterns of human colon tops and basal crypts and BMP antagonists as intestinal stem cell niche factors. *Proc. Natl. Acad. Sci. U. S. A* 104, 15418-15423 (2007).
27. Sato,T. *et al.* Single Lgr5 stem cells build crypt-villus structures in vitro without a mesenchymal niche. *Nature* 459, 262-265 (2009).

28. Dean,M. ABC transporters, drug resistance, and cancer stem cells. *J. Mammary. Gland. Biol. Neoplasia.* 14, 3-9 (2009).
29. Alberts,S.R. & Wagman,L.D. Chemotherapy for colorectal cancer liver metastases. *Oncologist.* 13, 1063-1073 (2008).
30. Mitry,E. *et al.* Predictive factors of survival in patients with advanced colorectal cancer: an individual data analysis of 602 patients included in irinotecan phase III trials. *Ann. Oncol.* 15, 1013-1017 (2004).
31. Douillard,J.Y. *et al.* Irinotecan combined with fluorouracil compared with fluorouracil alone as first-line treatment for metastatic colorectal cancer: a multicentre randomised trial. *Lancet* 355, 1041-1047 (2000).
32. Candeil,L. *et al.* ABCG2 overexpression in colon cancer cells resistant to SN38 and in irinotecan-treated metastases. *Int. J. Cancer* 109, 848-854 (2004).
33. Bradshaw,D.M. & Arceci,R.J. Clinical relevance of transmembrane drug efflux as a mechanism of multidrug resistance. *J. Clin. Oncol.* 16, 3674-3690 (1998).
34. Linn,S.C. & Giaccone,G. MDR1/P-glycoprotein expression in colorectal cancer. *Eur. J. Cancer* 31A, 1291-1294 (1995).
35. Ikuno,N. *et al.* Irinotecan (CPT-11) and characteristic mucosal changes in the mouse ileum and cecum. *J. Natl. Cancer Inst.* 87, 1876-1883 (1995).
36. Saliba,F. *et al.* Pathophysiology and therapy of irinotecan-induced delayed-onset diarrhea in patients with advanced colorectal cancer: a prospective assessment. *J. Clin. Oncol.* 16, 2745-2751 (1998).
37. Di,F.F. & Van,C.E. Acute and long-term gastrointestinal consequences of chemotherapy. *Best. Pract. Res. Clin. Gastroenterol.* 23, 113-124 (2009).

SUPPLEMENTARY TABLES

Supplementary Table 1

Case	Tumor site	Tumor type	Tumor stage	Differentiation
CRC26	Sigmoid	Adenocarcinoma	T3N2M1	Moderate
CRC29	Right colon	Adenocarcinoma	T3N0Mx	Poor
CRC47	Sigmoid	Adenocarcinoma	T3N1MX	Poor
CRC48	Right colon	Adenocarcinoma	T3N1M1	Moderate
L145	Liver segment VII	Adenocarcinoma		ND
L146	Liver segment IV	Adenocarcinoma		ND
L167	Liver segment II-IV	Adenocarcinoma		ND
L169	Liver segment	Adenocarcinoma		ND

	Stem Cell Markers			Clone formation	Tumor formation colonosphere cells			diff. cells
Tumor	*CD133*	*CD44*	*CD166*	*%*	*200*	*1.000*	*10.000*	*10.000*
CRC26	++++	+++	++	30	0/3	1/3	3/3	0/3
CRC29	++++	++++	+	59	3/3	3/3	3/3	#
CRC47	++	++++	++++	59	1/3	2/3	3/3	1/3*
CRC48	+++	+++	++	58	3/3	3/3	3/3	0/3
L145	-	++++	++++	46	3/3	3/3	3/3	0/3
L146	+++	++++	++++	50	2/3	2/3	2/3	0/3
L167	++	++	++	20	0/3	1/3	2/3	0/3
L169	-	++++	+++	62	1/3	2/3	3/3	ND

Table 1. Expression of stem cell markers and clone- and tumor-forming potential of human colorectal colonosphere cultures. Upper part: Tumor characteristics. Lower part: Expression of stem cell markers is depicted as % positive cells, based on FACS analysis. -: 0%; +: 1-25%; ++: 26-50%; +++: 51-75%; ++++: 76-100%. ND: not determined. # CRC29 cells were unable to form differentiated progeny under these experimental conditions. * Histological examination revealed that this was a cyst-like fluid-filled structure, rather than a tumor.

Supplementary Table 2 – Statistics for Figure 2

Fig 2B

L145	% of colony forming cells	
	Aldh high	Aldh low
N	9	9
Mean	56.16	14.04
Diff	42.12	
95% CI	34.30 to 49.88	
P value	<0.0001	

Fig 2C

Cell line	C26		C47		C48		L145	
	spheroids	diff. cells	spheroids	diff. cells	spheroids	diff. cells	spheroids	diff. cells
N	7	6	8	6	7	6	16	6
Mean	28.71	1.63	56.25	1.25	52.00	1.28	44.71	0.57
Diff	27.08		54.48		50.78		44.14	
95% CI	16,28 to 37.88		51.24 to 57.73		44.95 to 56.60		30.58 to 57.71	
P value	0,0002		<0.0001		<0.0001		<0.0001	

Cell line	L146		L167		L169	
	spheroids	diff. cells	spheroids	diff. cells	spheroids	diff. cells
N	15	6	12	6	17	6
Mean	48.47	1.08	20.04	0.92	66.92	2.40
Diff	47.39		19.13		64.52	
95% CI	39.30 to 55.47		16.09 to 22.17		39.73 to 89.32	
P value	<0.0001		<0.0001		<0.0001	

Fig 2D

L145	200 cells (day 176)		1000 cells (day 156)		10000 cells (day 125)	
	spheroids	diff. cells	spheroids	diff. cells	spheroids	diff. cells
N	3	3	3	3	3	3
Mean	241.7	0	803.3	0	835.3	15.67
Diff	241.7		803.3		819.7	
95% CI	79.73 to 403.6		16.85 to 1590		16.17 to 1623	
P value	0,0143		0,0471		0,0473	

Supplementary Table 3 – Statistics for Figure 3

Fig 3A

L145	5 µg/ml irino		25 µg/ml irino		50 µg/ml irino		75 µg/ml irino		125 µg/ml irino	
	spheroids	diff. cells	spheroids	diff. cells	spheroids	diff. cells	spheroids	diff. cells	spheroids	diff. cells
N	2	2	2	2	2	2	2	2	2	2
Mean	91.30	66.75	84.42	46.54	65.70	20.71	55.39	8.737	49.25	2.427
Diff	27.08		54.48		50.78		44.14		46.83	
95% CI	13.92 to 35.17		16.87 to 58.88		21.29 to 68.69		34.76 to 58.54		34.89 to 58.76	
P value	0,01		0,0162		0,0147		0,0035		0,0035	

L146	5 µg/ml irino		25 µg/ml irino		50 µg/ml irino		75 µg/ml irino		125 µg/ml irino	
	spheroids	diff. cells	spheroids	diff. cells	spheroids	diff. cells	spheroids	diff. cells	spheroids	diff. cells
N	2	2	2	2	2	2	2	2	2	2
Mean	99.30	73.52	96.10	51.59	88.03	31.22	78.23	14.61	61.95	6.398
Diff	25.79		44.51		56.81		63.63		55.55	
95% CI	7.028 to 44.54		18.67 to 70.35		23.25 to 90.37		53.52 to 73.74		17.65 to 93.45	
P value	0,0274		0,0177		0,0183		0,0014		0,0242	

L167	5 µg/ml irino		25 µg/ml irino		50 µg/ml irino		75 µg/ml irino		125 µg/ml irino	
	spheroids	diff. cells	spheroids	diff. cells	spheroids	diff. cells	spheroids	diff. cells	spheroids	diff. cells
N	2	2	2	2	2	2	2	2	2	2
Mean	92.18	87.63	79.41	47.61	71.22	27.96	61.79	16.32	56.61	2.10
Diff	4.543		31.80		43.26		45.47		54.52	
95% CI	-28.83 to 37.92		8.246 to 55.36		3.806 to 82.72		19.97 to 70.97		39.84 to 69.19	
P value	0,6173		0,0284		0,0421		0,0166		0,0039	

L169	5 µg/ml irino		25 µg/ml irino		50 µg/ml irino		75 µg/ml irino		125 µg/ml irino	
	spheroids	diff. cells	spheroids	diff. cells	spheroids	diff. cells	spheroids	diff. cells	spheroids	diff. cells
N	2	2	2	2	2	2	2	2	2	2
Mean	83.72	57.82	55.42	39.10	51.54	28.82	47.74	13.14	47.61	5.945
Diff	25.90		16.32		22.72		34.60		41.67	
95% CI	0.8770 to 50.93		-1.655 to 34.30		4.196 to 41.24		3.383 to 65.82		33.43 to 49.91	
P value	0,0469		0,0597		0,0341		0,0413		0,0021	

Fig 3B

	Spheroids		Differentiated cells		Irinotecan treated	
	control	irinotecan	control	irinotecan	Spheroids	Diff cells
N	2	2	2	2	2	2
Mean	18.35	9.7	19.75	0.35	9.7	0.35
Diff	8.650		19.40		9.35	
95% CI	6.363 to 10.94		17.76 to 21.04		7.512 to 11.19	
P value	0,0038		0,0004		0.0021	

Supplementary Table 4 – Statistics for Figure 4

L145	Day 0		Day 1		Day 2		Day 3	
	irinotecan	Irinotec + PSC	irinotecan	Irinotec + PSC	irinotecan	Irinotec + PSC	irinotecan	Irinotec + PSC
N	2	2	2	2	2	2	2	2
Mean	103.6	102.1	86.99	46.65	72.91	22.90	62.67	13.87
Diff	1.495		40.33		50.01		48.80	
95% CI	-30.92 to 33.91		30.95 to 49.72		36.87 to 63.15		44.00 to 53.60	
P value	0,861		0,0029		0,0037		0,0005	

L145	Day 0		Day 1		Day 2		Day 3	
	irinotecan	Irinotec + MK	irinotecan	Irinotec + MK	irinotecan	Irinotec + MK	irinotecan	Irinotec + MK
N	2	2	2	2	2	2	2	2
Mean	103.6	103.0	86.99	86.37	72.91	74.18	62.67	63.62
Diff	0.6067		0.6155		-1.276		-9506	
95% CI	-22.68 to 23.89		-6.080 to 7.311		-6.856 to 4.303		-6.433 to 4.532	
P value	0,921		0,7306		0,4287		0,5334	

L145	Day 0		Day 1		Day 2		Day 3	
	irinotecan	Irinotec + KO	irinotecan	Irinotec + KO	irinotecan	Irinotec + KO	irinotecan	Irinotec + KO
N	2	2	2	2	2	2	2	2
Mean	103.6	102.5	86.99	90.31	72.91	75.04	62.67	61.85
Diff	1.169		-3.322		-2.133		0.8215	
95% CI	-21.27 to 23.61		-21.73 to 15.08		-10.16 to 5.893		-15.80 to 17.44	
P value	0,8434		0,5186		0,3712		0,8513	

L167	Day 0		Day 1		Day 2		Day 3	
	irinotecan	Irinotec + PSC	irinotecan	Irinotec + PSC	irinotecan	Irinotec + PSC	irinotecan	Irinotec + PSC
N	2	2	2	2	2	2	2	2
Mean	96.85	91.13	84.82	59.45	80.85	35.10	74.66	22.88
Diff	5.717		25.37		45.76		51.78	
95% CI	-2.952 to 14.39		-4.115 to 54.86		29.58 to 61.93		32.03 to 71.53	
P value	0,105		0,0658		0,0067		0,0078	

Supplementary Table 5 – Statistics for Figure 5

Fig 5E

L145	% Ki67-positive cells	
	Outer ring	Inner ring
N	9	9
Mean	27.57	7.30
Diff	20.27	
95% CI	10.76 to 29.79	
P value	0.0002	

Supplementary Table 6 – Statistics for Figure 6

Fig 6A

L145	5 µg/ml irino		25 µg/ml irino		50 µg/ml irino		75 µg/ml irino		125 µg/ml irino	
	spheroids	Sph. cells	spheroids	sph. cells	spheroids	sph. cells	spheroids	sph. cells	spheroids	sph. cells
N	2	2	2	2	2	2	2	2	2	2
Mean	98.50	100.0	91.30	82.67	84.42	73.05	65.70	39.03	55.39	12.06
Diff	-1.500 ± 2.595		8.626 ± 3.704		11.37 ± 4.873		26.67 ± 4.127		43.33 ± 2.625	
95% CI	-12.66 to 9.665		-7.314 to 24.57		-9.601 to 32.34		8.913 to 44.43		32.03 to 54.62	
P value	0,6216		0,1453		0,1449		0,0231		0,0037	

Fig 6C

L145	% of colony forming cells	
	ABCB1+	ABCB1-
N	9	9
Mean	64,06	2,056
Diff	62.01	
95% CI	55.18 to 68.83	
P value	P<0.0001	

Fig 6F

	5 µg/ml irino		25 µg/ml irino		50 µg/ml irino	
	0 µg/ml	5 µg/ml	0 µg/ml	25 µg/ml	0 µg/ml	50 µg/ml
N	3	3	3	2	3	2
Mean	47.67	30.0	47.67	9.5	47.67	2.0
Diff	17.67		38.17		45.67	
95% CI	4.418 to 30.92		28.51 to 47.82		34.97 to 56.36	
P value	0,0208		0,0011		0,0009	

Supplementary Table 7 – Influence of PSC833 and irinotecan on tumor volume and total number of Aldefluor^{high} cells

	Spheroid-initiated xenografts	
	Tumor volume (fold change)	Total # Aldefluor^{high} cells (fold change)
Mock *vs.* PSC (P)	-1,04	1,09
Mock *vs.* irinotecan (I)	-1,2	1,86
Mock *vs.* I+P	**-2,63**	**-4,32**
PSC *vs.* irinotecan	-1,16	1,71
PSC *vs.* I+P	**-2,53**	**-4,37**
Irinotecan *vs.* I+P	**-2,19**	**-5,57**

	Unsegregated xenografts	
	Tumor volume (fold change)	Total # Aldefluor^{high} cells (fold change)
Mock *vs.* PSC (P)	-1,12	1,15
Mock *vs.* irinotecan (I)	-1,19	2,7
Mock *vs.* I+P	**-2,86**	**-3,02**
PSC *vs.* irinotecan	-1,06	2,35
PSC *vs.* I+P	**-2,55**	**-2,75**
Irinotecan *vs.* I+P	**-2,41**	**-5,78**

From the data presented in Figure 7 the fold change in tumor volume and the change in total numbers of Aldefluor^{high} cells was calculated for each treatment group. In both types of xenograft the combination treatment reduced tumor volume as well as the total number of Aldefluor^{high} cells.

SUPPLEMENTARY FIGURES

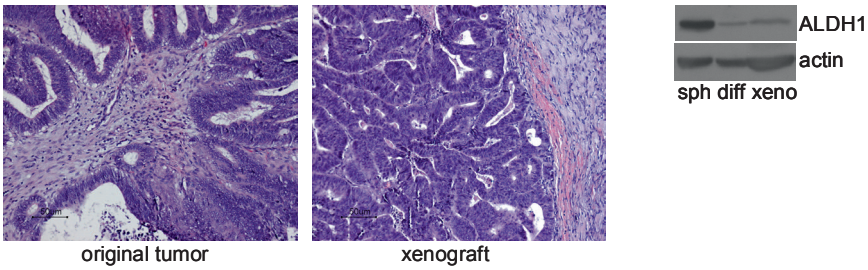

Supplementary Figure 1. Spheroid-initiated tumors display a differentiated phenotype and loose ALDH1 expression. Tumors generated by 200 colonosphere-derived cells (Table 1) were fixed in formalin and embedded in paraffin. Tissue sections were stained with Haematoxylin and Eosin (H&E) to reveal general tissue architecture. A representative example is shown. Colonosphere-initiated tumors show extensive differentiation and tubule-formation in the xenograft. Western blot analysis shows strongly reduced ALDH1 expression in the xenograft (xeno) when compared to the colonospheres (sph). FACS analysis of these tumors shows that the percentage of ALDH^{high} cells in the tumors is reduced 3-5 fold when compared to colonospheres (Figure 4*E*). Differentiated tumor cells (diff) are shown for comparison.

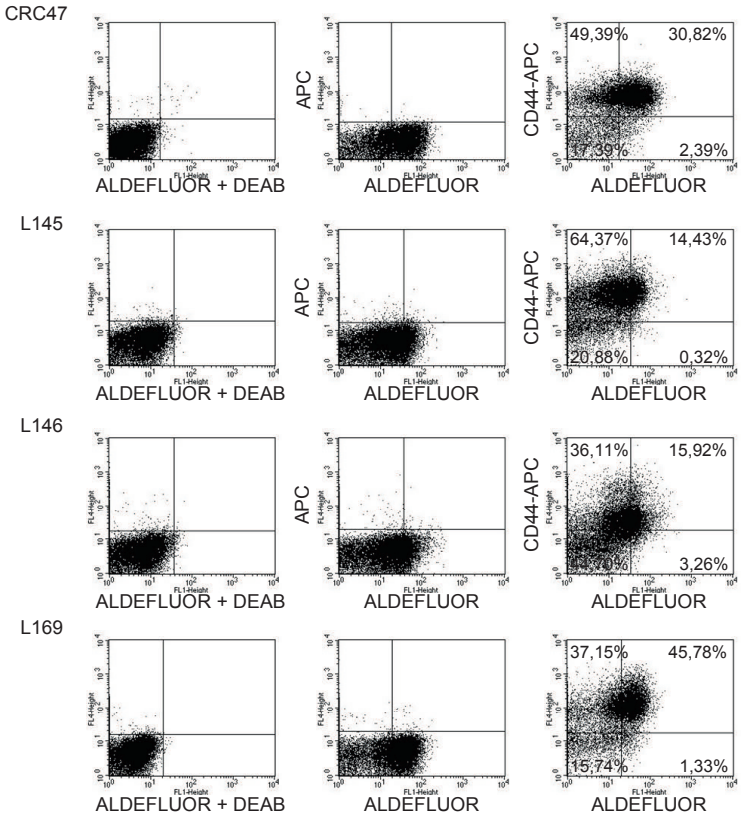

Supplementary Figure 2. The vast majortiy of Aldefluor®-positive cells are also positive for CD44. Colonosphere cells derived of 4 different tumors were analyzed for co-expression of CD44 and high Aldefluor® activity. Diethylaminobenzaldehyde (DEAB) was used to identify the negative cell population.

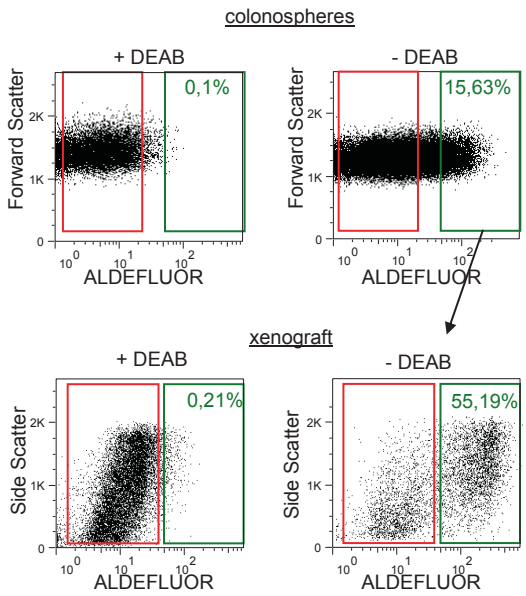

Supplementary Figure 3. ALDH activity marks tumor-initiating cells. Spheroid ALDH activity was assessed by Aldefluor®, using DEAB to identify the negative cell population (upper panel). ALDH^{high} and ALDH^{low} cells were then separated by FACS sorting and injected into nude mice. Only ALDH^{high} cells were capable of forming tumors (Figure 2*C*). Single cell suspensions of these tumors were generated and evaluated for ALDH activity (lower panel). ALDH^{high}-initiated tumors existed of both ALDH^{high} and ALDH^{low} cells. ALDH^{high} and ALDH^{low} cells were again separated by FACS sorting and evaluated for their tumor-initiating potential (Figure 2*C*).

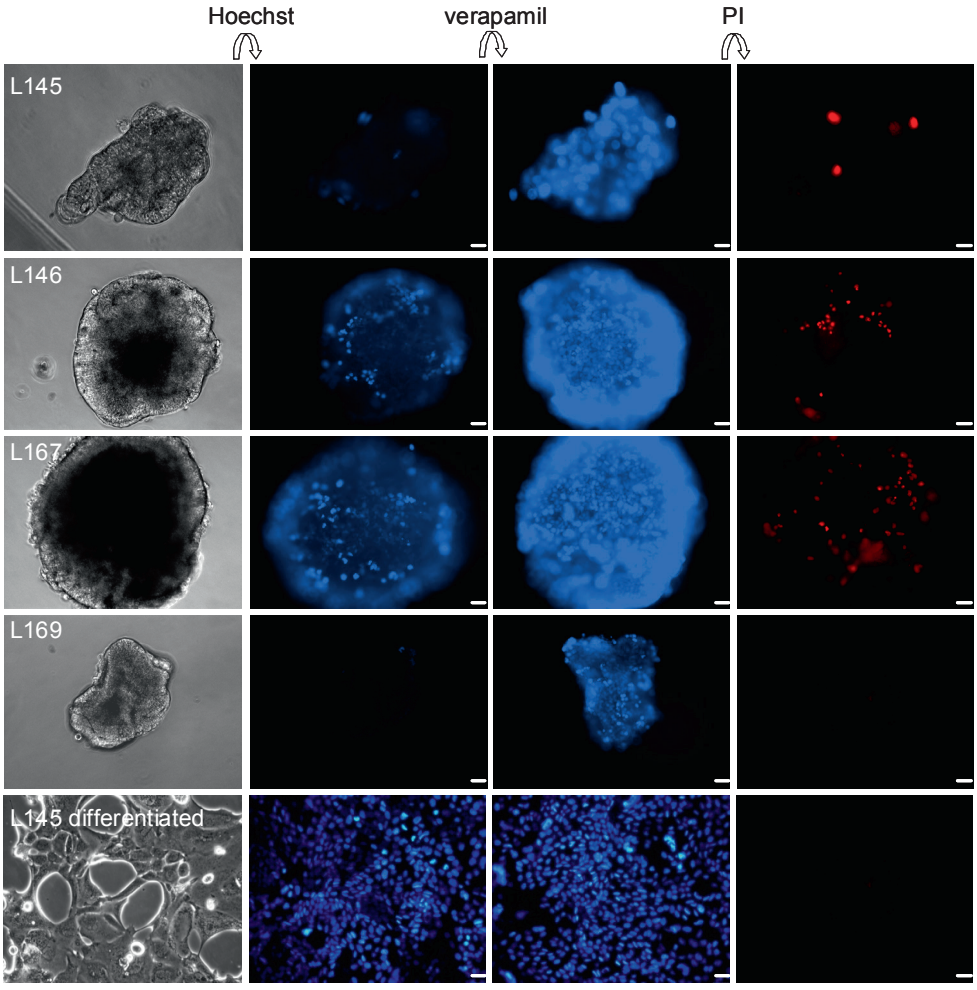

Supplementary Figure 4. Hoechst 33342 retention by colorectal spheroid cultures requires inhibition of ABC transporter activity. Spheroids and differentiated tumor cells were photographed after which Hoechst 33342 (5 µg/ml) was added to the medium. Hoechst uptake was assessed by fluorescence microscopy. Next, verapamil (50 µM) was added to the medium and the same spheroids were analyzed by fluorescence microscopy. To assess cell viability propidium iodide (PI) was added to the culture and PI uptake (dead cells) was assessed by fluorescence microscopy. The figure shows that Hoechst is taken up in spheroids only after verapamil treatment and that this is not due to extensive cell death. Differentiated tumor cells do not require verapamil to take up Hoechst. Bars 40 µm.

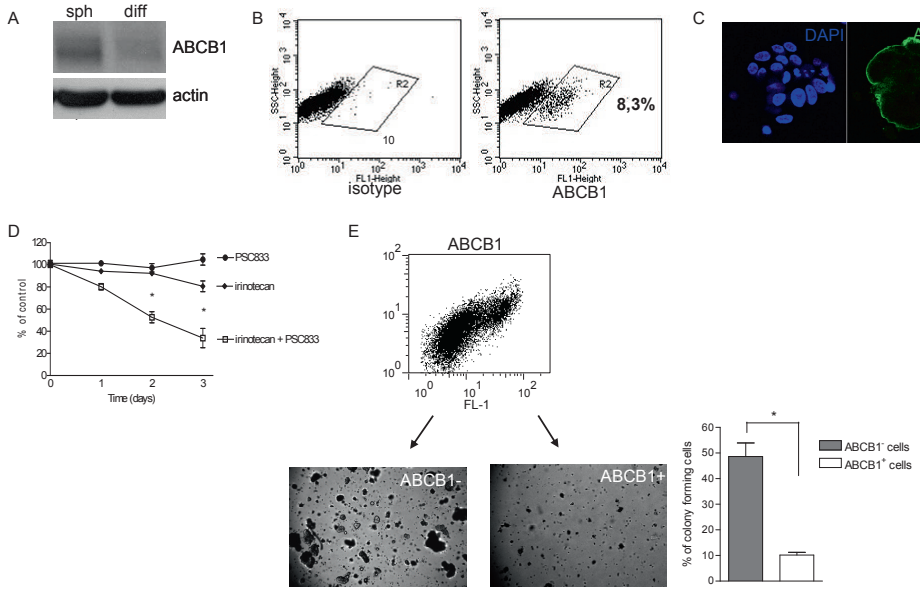

Supplementary Figure 5. ABCB1 marks non-clonogenic cells in colonospheres derived from a primary colorectal tumor (CRC26). A. Western blot analysis of ABCB1 in spheroid cultures and isogenic stably differentiated derivatives. B. FACS analysis identifies 8% of the colonosphere cells to be ABCB1 positive. C. Immunofluorescence analysis shows that ABCB1-positve cells represent the single outer cell layer of the colonospheres. D. MTS assays of colonosphere cells exposed to vehicle, irinotecan, PSC-833, or the combination, for 0-3 days. E. Single cell cultures from colonospheres were used to separate the ABCB1-positive from the ABCB1-negative population. Both populations were analyzed for clone-forming potential. A minor population of ABCB1-positive cells also formed colonies but these remained small, were morphologically clearly distinct from true spheroids, and consisted of highly vacuolarized cells that could not be further established. Most likely the latter colonies were initiated by cells with residual proliferative capacity but lacking self-renewal capacity.

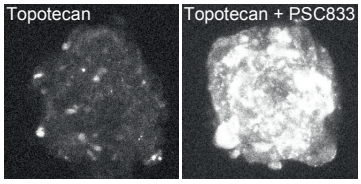

Supplementary Figure 6. PSC-833 allows uptake of topotecan. L145 colonospheres were treated with topetecan (20 μM) either alone or together with the ABCB1 inhibitor PSC833 (2 μM). The uptake of fluorescent topotecan was analyzed by confocal microscopy. A z-stack projection of a representative colonosphere is shown.

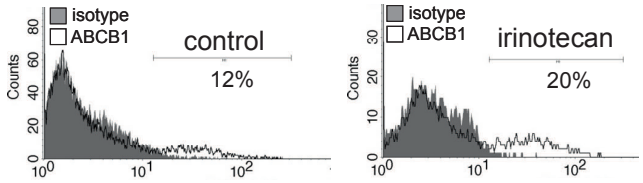

Supplementary Figure 7. Irinotecan exposure increases the percentage of ABCB1-positive cells. L145 colonospheres were treated with vehicle or with irinotecan for 72 hours. Single cell cultures were prepared and analyzed for the presence of cell surface ABCB1 by FACS analysis. An isotype control antibody was used as a negative control.

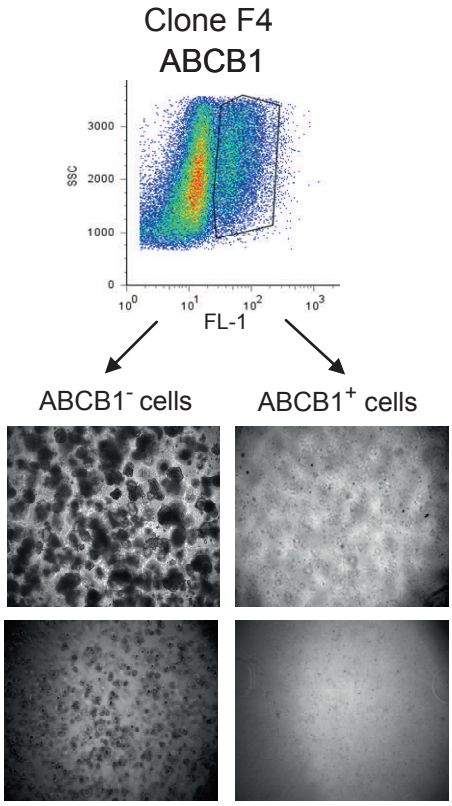

Supplementary Figure 8. Anti-ABCB1 (clone F4) identifies the non-clonogenic population of L145 colonosphere cells. Single cell populations were generated from colonospheres and were stained with anti-ABCB1 clone F4. After FACS sorting, ABCB1-positive and ABCB1-negative cells were re-suspended in Matrigel and allowed to form clones for three weeks. ABCB1(F4)-negative, but not ABCB1(F4)-positive cells were clonogenic.

SUPPLEMENTARY MATERIALS AND METHODS

Isolation and Expansion of Colorectal Tumor-Initiating Cell Cultures

The obtained tissue fragments were washed extensively with PBS and were mechanically dissociated using scalpels and vigorous trituration to yield small fragments (<1mm^3) and single cells. Enzymatic digestion was performed using thermolysin 0.05% (Sigma, Type X) in DMEM/F12 containing 5 mM Hepes (Gibco) for 2hr at 37°C. The suspension was then filtered through a 40-µm-pore size nylon cell strainer (BD Falcon) to separate the tissue fragments from the single cells. The single cell suspension was cultured in advanced DMEM/F12 (Gibco) supplemented with 0,6% glucose (BDH Lab. Supplies), 2 mM L-glutamine (Biowhittaker), 9.6 µg/ml putrescin (Sigma), 6.3 ng/ml progesterone (Sigma), 5.2 ng/ml sodium selenite (Sigma), 25 µg/ml insulin (Sigma), 100 µg/ml apotransferrin (Sigma), 5 mM hepes (Gibco), 0,005 µg/ml trace element A (Cellgro), 0,01 µg/ml trace element B (Cellgro), 0,01 µg/ml trace element C (Cellgro), 100 µM β-mercapto ethanol (Merck), 10 ml antibiotic-antimycotic (Gibco), 4 µg/ml gentamicine (Invitrogen), 0.002% lipid mixture (Sigma), 5 µg/ml glutathione (Roche) and 4 µg/ml Heparin (Sigma). Growth factors (20 ng/ml EGF (Invitrogen) and 10 ng/ml b-FGF (Abcam)) were added to the cell culture medium freshly each week. All cell culture was carried out in non-tissue culture treated flasks (BD Falcon) at 37° C in a 5% CO_2 humidified incubator. In vitro differentiation was induced by culturing colon colonospheres for 3 weeks on collagen-coated dishes in DMEM-F12 (GIBCO) supplemented with 20% fetal bovine serum.

Antibodies

The antibodies used in this study are anti human epithelial antigen (Ep-CAM, clone BER-EP4; Dako), anti human CD133/1 - APC (clone AC133; Miltenyi Biotec), anti human CD44 – APC (clone G44-26; BD Pharmingen), anti human CD166 – PE (clone 3A6; BD Pharmingen), anti human MDR-1 (Ab2, clone F4; Neomarkers). Anti-human MDR-1 (clone MM4.17; Chemicon), anti-MRP1 (MRPm6; Alexis Biochemicals), anti-ABCG2 (BXP-21; Abcam), anti-cleaved-caspase-3 (Cell Signaling), anti-p53 (DO-1; Santa Cruz), anti-ALDH1 (#44; BD Biosciences), anti-cytokeratin 20 (Ks20.8; Dako), anti-β-actin (AC-15; Novis Biologicals), anti-phospho-ezrin (Thr567) (Cell Signaling), and Ki67 (SP6, Neomarkers). The Aldefluor™ reagent was purchased form StemCell Technologies and used according to the manufacturer's instruction.

Hoechst and Topotecan Uptake Assay

Colonospheres and differentiated progeny were stained with Hoechst 33342 (5 µg/ml; 90 min) (Cambrex) and were visualized using a Leica DM IRBE microscope. Images were captured using a QImaging Retiga EXi CCD digital camera. Verapamil (Fluka) (50 µM) was added for 30 min and Hoechst uptake by the same colonospheres was assessed by fluorescence microscopy. Cell viability was assessed by adding 10µg/ml propidium iodide (PI) to the medium. PI-excluding cells were considered viable. Colonosphere cultures were incubated with 20 µM topotecan (Hycamtin, GlaxoSmithKline) with or without 2 µM PSC833 for 90 minutes at 37°C. After incubation, the colonospheres were gently washed twice with medium before analysis of fluorescence uptake by confocal microscopy at 405 nm (Zeiss LSM 510 Meta).

Immunofluorescence

Immunofluorescence staining was performed on colonospheres and their differentiated derivatives. Colonospheres growing in suspension were attached to coverslips by cytospin (800

rpm, 5 minutes). Cells were fixed in 3.7% formaldehyde and permeabilized with ice-cold (-20°C) methanol. After blocking with PBS-1%BSA, cells were incubated overnight at 4°C with primary antibodies. Secondary antibodies (incubated overnight at 4°C) goat anti-rabbit Alexa fluor 568 (Invitrogen) or chicken anti-mouse Alexa fluor 488 (Invitrogen), mixed with 0.5 μg/mL DAPI were used. Confocal microscopy was performed using the Zeiss LSM510 META microscope and Zeiss LSM5 Software.

Immunohistochemistry

Immunohistochemistry was performed using anti-ABCB1 Ab-5 (clone C494; Neomarkers, Lab Vision Corp, Fremont, CA, USA) and anti-ALDH1 (BD Transduction Laboratories). For detection goat anti Ms/Rb/Rt-poly-HRP (Powervision, Immunologic, Immunovision Technologies, Brisbane, USA) was used. All slides were developed with diaminobenzidine followed by heamatoxylin couterstaining. Frozen tissue sections were fixed with acetone for 20 minutes at room temperature, followed by a permeabilization and blocking step. Slides were incubated overnight at 4°C with anti-ABCB1 (clone 494; Neomarkers, Lab Vision Corp, Fremont, CA, USA) and chicken anti-mouse Alexa fluor 488 (Invitrogen), mixed with 0.5 μg/mL DAPI. Confocal microscopy was performed using the Zeiss LSM510 META microscope and Zeiss LSM5 Software.

Tumor formation and drug treatment

Single cell populations were diluted to 200, 1000 and 10.000 live spheroid-derived cells, mixed with BD Matrigel (BD Biosciences) at a 1:1 ratio (total volume 100 μl) and injected subcutaneous into the flanks of 6 weeks old BALB/$c^{nu/nu}$ mice. The same procedure was followed after FACS sorting experiments in which ABCB1-positive and -negative or Aldefluor® (Stemcell Technologies, Grenoble, France) -positive and -negative cell populations were mixed with Matrigel (BD Biosciences) at 1000 cells/50 μl and injected into the flanks of BALB/$c^{nu/nu}$ mice.

For drug treatment experiments mice were inoculated either with colonospheres mixed with Matrigel (1:1) or with 4x4 mm fragments of unsegregated colorectal tumors. Treatment was started (day 0) after tumors reached a volume ($V=AxB^2x0.5263$) of 250-350 mm^3. Valspodar (PSC833 (100 mg/kg oral gavage); Novartis, Basel Switzerland) and irinotecan (Campo, Pfizer; 50 mg/kg intraperitoneal (colonosphere-initiated tumors) or 15 mg/kg (biopsy-initiated tumors)) were given once weekly. Valspodar was given two hours prior to irinotecan. Control mice received vehicle only.

Tumor growth in all treated and untreated mice was followed for up to 5 months or when tumors reached a maximum of 1 cm^3. Mice were sacrificed by cervical dislocation. All experiments involving the use of animals were performed in accordance with University of Utrecht institutional animal welfare guidelines.

Isolation of single cells from xenografts and colonospheres

Tumor xenografts were mechanically dissociated to yield small fragments that were further dissociated using dispaseII (Roche)/collagenaseXI (Sigma; 30 min 37C). The cells were washed once with PBS and were subsequently incubated with TrypLE express (Invitrogen) including 2,000 U/ml DNase (Sigma; 30 min 37C). To obtain single cell suspensions from colonospheres, they were incubated with Accumax (Innovative Cell Technologies) plus 2 U/ml DNAse1 (Sigma) for 10 minutes in a rotary incubator at 37°C. Both types of cell suspensions were then filtered though a 40-μm-pore size nylon cell strainer (BD Falcon) to obtain single cells.

Flow Cytometry and Cell Sorting

The expression of a panel of cell surface markers was analyzed using a FACScalibur (BD Biosciences, San Diego, USA). All antibody incubation steps were carried out at 4°C. Dead cells were excluded using viability marker 7-aminoactinomycin D (7-AAD) and cell doublets and clumps were excluded using doublet discrimination gating. For analysis of xenografts, anti-EpCAM (1/1000) was always included as a marker for epithelial cells. Aldefluor®-positive cells were analyzed according to the manusfacturer's protocol by using the ALDH substrate BAAA (1 µmol/l per 1×10^6 cells). Negative control samples were co-incubated with diethylaminobenzaldehyde (DEAB; 50 mM). The cell sorting experiments were conducted with DAKO-Cytomation MoFlo High Speed Sorter.

For FACS-based cell cycle analysis, cells were incubated for 30 minutes with 1µM BrdU at 37°C. BrdU-positive cells were detected with an anti-BrdU-FITC antibody (BD Bioscience) according to the manufacturer's protocol. For determination of DNA content 10µg/ml propidium iodide (PI) was added in the presence of 250 µg/ml RNase.

3

PROTEOMICS IN STUDYING CANCER STEM CELL BIOLOGY

Benjamin L Emmink[1]*, Onno Kranenburg[1]*, Jaco Knol[2], Winan J van Houdt[1], Inne H M Borel Rinkes[1] and Connie R Jimenez[2]

[1] Department of Surgery, University Medical Center Utrecht, The Netherlands
[2] OncoProteomics Laboratory, VU University Medical Center Amsterdam, The Netherlands

*Equal contribution

Expert Review of Proteomics. 2012 Jun;9(3):325-36

SUMMARY

Normal multipotent tissue stem cells (SCs) are the driving force behind tissue turnover and repair. The cancer stem cell (CSC) theory holds that tumors also contain stem-like cells that drive tumor growth and metastasis formation. However, very little is known about the regulation of SC maintenance pathways in cancer and how these are affected by cancer-specific genetic alterations and by treatment. Proteomics is emerging as a powerful tool to identify the signaling complexes and pathways that control multi- and pluripotency and SC differentiation. Here, we review the novel insights that these studies have provided and present a comprehensive strategy for the use of proteomics in studying CSC biology.

INTRODUCTION

Normal proliferative tissues contain multipotent stem cells that drive tissue turnover. Stem cells are capable of maintaining themselves (self-renewal) but also give rise to a proliferative 'transit amplifying' (TA) compartment, and ultimately to post-mitotic differentiated cells with specialized functions. In case of tissue damage, stem cells also drive regeneration of the lost tissue. By contrast, TA cells and differentiated cells are incapable of self-renewal and tissue regeneration.

According to the cancer stem cell (CSC) concept, the cellular hierarchy in normal tissues is preserved in a number of hematological and solid malignancies. Tumors, like the tissues from which they originate, contain a unique stem cell population that is capable of self-renewal and of sustaining tumor growth indefinitely. Furthermore, pathways controlling the self-renewal capacity of normal tissue stem cells are frequently deregulated in human cancer[1].

The CSC is defined as a cancer cell with self-renewing capacity that can re-generate the original tumor in all its differentiated heterogeneity. The CSC theory is attractive because it offers an explanation for tumor heterogeneity, for the inefficiency of metastasis formation and for tumor re-growth after an apparently complete remission. However, the CSC theory also contains a number of critical assumptions that require experimental testing[2]. In addition, some tumor types do not appear to adhere to the CSC concept at all[3, 4], or may have multiple independent tumor-initiating cell populations[5]. Obviously, the study of CSCs in any given tumor type, by proteomics or other approaches, requires prior validation of their actual existence.

THE CHALLENGE

A complicating matter is that the 'CSC state' may not be stable over time and that gain or loss of this trait may occur relatively frequently[4, 6, 7]. Such transitions may occur spontaneously but may also be influenced by the tumor microenvironment[8] (Figure 1). The pathways governing the transition from an undifferentiated tumorigenic state to a differentiated non-tumorigenic state and *vice versa* are poorly understood. Such pathways may vary between tumor types and even between tumors of the same tissue type. Indeed, the 'differentiation status' as assessed by simple histology or by expression or absence of specific differentiation markers, is widely divergent between tumors of a given tumor type. By inference, the extent to which the normal cellular hierarchy from stem cells to differentiated tumor cells is maintained is probably equally diverse.

Proteomics is an ideal tool to analyze cell states and it has frequently been applied to studying the biology of embryonic stem cells (ESC's)[9]. Studying *cancer* stem cells faces at least two extra layers of complexity. First, each individual tumor has its own specific set of tumor-driving mutations, which generates *inter*-tumor genetic heterogeneity. Second, tumors often consist of more than one genetic subclone, generating an additional level of *intra*-tumor genetic heterogeneity (Figure 2). The set of mutations in tumor-driving genes is unique to every single tumor[10]. It follows that the impact of genetic alterations on the regulation of CSC behavior and on tumor cell differentiation are probably also unique to each individual tumor. An intriguing link between tumor genetics and stem cell biology was shown in a recent report, demonstrating that the commonly mutated p53 tumor suppressor gene not only controls cell cycle and apoptosis pathways, but is also a master regulator of stem cell division[11, 12]. Other examples are c-Myc, a powerful oncogenic transcription factor with stem cell-inducing properties[13], and the *APC* tumor suppressor gene which prevents expansion of the intestinal stem cell pool[14]. Interestingly, it is

not uncommon for colorectal tumors to have inactivating mutations in both p53 *and* APC *and* to contain an amplification of c-Myc. Therefore, proteomics approaches aimed at studying CSC biology should ideally be accompanied by careful genetic analysis of the tumors or cell lines that are being studied.

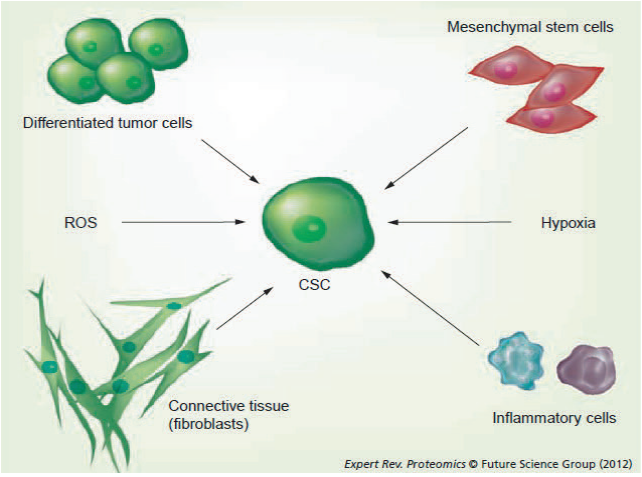

Figure 1. Factors influencing the Cancer Stem Cell phenotype.
The CSC phenotype is most likely not a stable state, but dependent on and influenced by multiple factors within the tumor microenvironment. These include several cell types (differentiated tumor cells, mesenchymal stem cells, inflammatory cells, and connective tissue), but also conditions such as oxygen tension, reactive oxygen species and extracellular matrix composition. All of these potential CSC-modulating cells and conditions are lost during isolation and purification of CSCs for analysis.

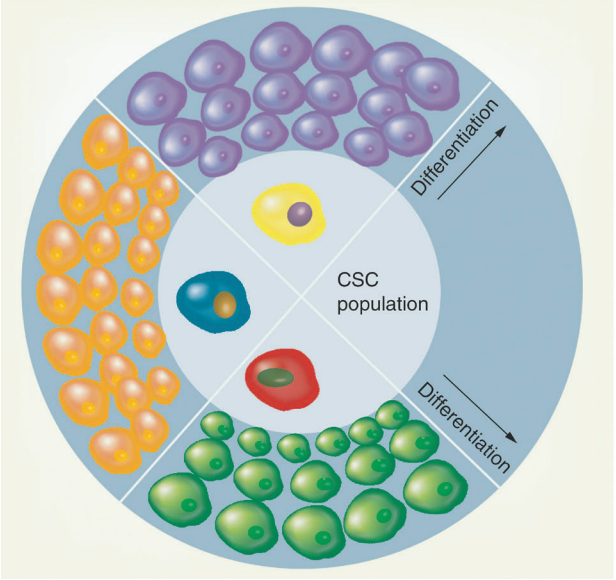

Figure 2. Genetic heterogeneity complicates the study of Cancer Stem Cells.
Tumors often consist of multiple genetic subclones. Growth of each of these subclones is fuelled by genetically distinct CSC populations producing their own differentiated offspring. Intra-tumor heterogeneity within the CSC pool therefore complicates the interpretation of proteomics data.

THE SOURCE

A critical issue in any proteomics study aiming to analyze CSC's is the source of starting material. There are a number of different options. The best way to study the CSC proteome probably is to capture them in their normal microenvironment, i.e. from within the patient tumor. This requires markers that can discriminate between CSC's and non-CSC's. Although many such markers have been published, most of them have also been disputed, and their relevance to CSC biology is mostly unclear[2]. In a typical experiment the resection specimen would be immediately snap-frozen following surgical resection. Tissue sections would then be stained for the CSC marker and positive cells would be collected by tissue microdissection (Figure 3). Current state-of-the-art proteomics indeed allow analysis of laser microdissected tumor material from formalin-fixed paraffin-embedded (FFPE) tumor tissue[15]. However, even this approach requires the input of (ten-) thousands of cells[15, 16]. These reports make the important claim that proteomics on micro-dissected patient material from FFPE tissue is feasible. Whether this method is applicable to CSC research will depend on the percentage of identifiable CSC's within the tumor and probably also on their position in relation to each other (i.e. clustered versus sparse distribution). FFPE would also allow capturing of the stromal compartment surrounding the CSCs. Proteomics analysis of such cells may identify essential 'niche' components.

Alternatively, CSC's may be FACS-sorted from the resected patient tumor, based on the presence of specific cell surface markers (such as CD133) and/or enzyme activities (such as Aldehyde dehydrogenase) (Figure 3). In a proof of principle study it was shown that as little as 5.000 FACS-sorted stem cells from the mouse intestine yielded sufficient starting material for proteome analysis[17]. In this case, FACS sorting was based on GFP expression in intestinal stem cells driven by the Lgr5-promoter. A major limitation for most major human tumor types is that no definitive cell surface markers have been identified that can prospectively identify the CSC population in large series of patient-derived tumors[2]. In addition, FACS sorting involves tissue processing into single cells. This generates non-physiological stress resulting in the activation of cell death pathways. Obviously, this will influence the results of proteome analyses.

Finally, novel tissue culture protocols allow the isolation and propagation of tumor-derived 3D-spheroid/organoid cultures that are enriched in CSC's (Figure 3)[18-20]. Spheroid cultures are highly tumorigenic when transplanted into immunodeficient mice, and generate tumors that closely resemble the original patient tumor, at least when analyzed by histological methods. Furthermore, a study on brain tumor spheroids has shown that during prolonged in vitro culture proteome changes are minimal, suggesting that these cultures are indeed relatively genetically stable[21]. While spheroid cultures are enriched for CSC's, they also contain a considerable number of differentiated tumor cells that contribute to the culture's proteome. So even when using CSC-enriched spheroids as a source for CSC's the results will have to be validated using FACS-based separation of the tumorigenic (CSC) and non-tumorigenic (differentiated) cell populations[18, 22]. Finally, spheroid-generated xenografts may be used as a source for CSCs, providing an ex-patient in vivo experimental system in which CSCs are located within a 3D tumor environment, albeit of murine origin. The protocol for isolation of CSCs from xenografts would then be similar to that for their isolation directly from human tumors.

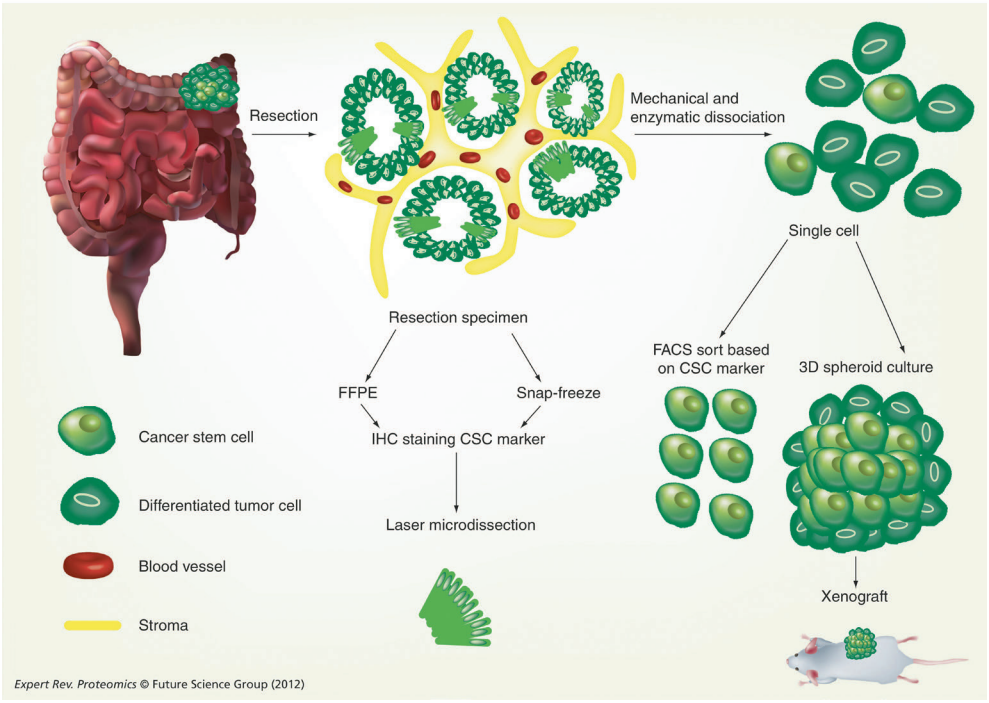

Figure 3. Potential Cancer Stem Cell sources as starting material for proteomics.
There are a number of different ways to isolate CSCs for analysis by proteomics. First, CSCs may be directly isolated from their normal microenvironment using either formalin-fixed paraffin-embedded (FFPE) or snap-frozen tissue. This requires staining of CSCs by immunohistochemistry (IHC) and subsequent laser microdissection of the positive cells. Second, the tumor tissue may be processed to generate single cell cultures, allowing purification of CSCs by FACS-sorting based on expression of CSC surface markers. Third, single cell cultures may be grown into spheroids or organoids using recently established culture techniques. Such cultures are enriched for tumor-initiating cells but also contain differentiated cells. Spheroids may also be used to generate xenografts in mice. These can then be used to isolate CSCs from the complex tumor micro-environment in an experimental setting.

MASS SPECTROMETRY PROCEDURES

Mass spectrometers are extremely sensitive instruments with limits-of-detection typically in the low attomole range when simple protein mixtures are analyzed[23-25]. In specialist labs, even higher sensitivities in the zeptomole range have been reported[26].

When complex biological samples are analyzed by mass spectrometry-based proteomics, the depth of proteome analysis depends on several factors. Since there is no amplification tool for proteins, the first important factor is the amount of starting material: generally the more sample (number of cells) is analyzed, the more proteins are identified[16, 27-29] (Figure 4). In these studies as little as 500-1000 cells were analyzed. However, the number of identified proteins varied from 70-1500 (Figure 4). These differences are most likely associated with the different proteomics procedures that were employed (See below).

The next important factor that determines the depth of proteome analysis is the extent of fractionation and instrument time spent on the sample: for a comprehensive proteome analysis

that includes low abundant proteins, fractionation is needed to increase the dynamic range of detection in the mass spectrometer. However, more sample fractionation also means more sample loss. Therefore, when a very limited number of cells is available, as is the case in CSC studies, a balance must be found between the extent of fractionation and the depth of proteome analysis.

Proteomics workflows may employ different combinations of fractionation methods, usually each with its own strengths and weaknesses[30, 31]. The oldest proteomics workflow is based on two-dimensional (2D) gel electrophoresis that separates proteins based on their isoelectric point and molecular weight. This method has been widely used and can resolve protein isoforms but is time-consuming and not suitable for the analysis of hydrophobic (membrane) proteins and large proteins. In recent years, nanoLC-MS/MS-based proteomics has emerged as a powerful alternative. Currently, three popular two dimensional separation strategies coupled to nanoLC-MS/MS are 1D GeL-nanoLC-MS/MS, Iso-electric focussing coupled to nanoLC-MS/MS and 2DLC-MS/MS often with strong cation exchange usually as the first dimension LC step. In two recent workflow comparison studies, the 1D GeL-nanoLC-MS/MS workflow was shown to outperform the other workflows[32, 33]. The GeLC-MS/MS workflow may be slightly lower throughput than 2DLC-MS/MS but has the advantage of providing molecular weight information which may reveal the presence of isoforms or cleaved forms. For example, in an elaborate study of 5000 human ESCs two-dimensional fractionation was used to identify ~400 proteins[28]. Increasing the gradient of a single dimension nanoLC-MS/MS run has proven to be a good strategy to improve the depth of analysis without including extra steps and potential sample loss[16], which occurs during second dimension separation.

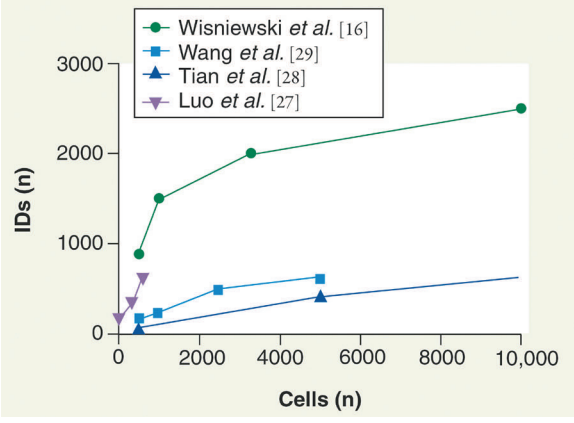

Figure 4. The balance between the amount of starting material and the depth of proteome analysis. The amount of identified proteins (IDs) in different proteomics studies varies greatly, due to differences in methodology. State-of-the-art mass spectrometry and sample preparation procedures now allow robust proteome analysis (thousands of proteins) by using 1.000-10.000 cells as starting material.

The third factor important for the depth of proteome analysis is the sample preparation protocol. Procedures that are robust, simple, fast and compatible with the use of detergents are usually the best. For example, the stream-lined filter-aided sample preparation (FASP) protocol employing SDS and glycol[16] outperformed the standard lysis and in-solution digest protocol[29] when similar numbers of cells are analyzed (Figure 4). Since both studies performed proteome analysis in a single dimension nanoLC-MS/MS run with comparable gradient length, the differences may

be largely attributed to the differences in sample preparation. Importantly, the FASP protocol is compatible with protein and post-translational modification analysis in fixed archival material[16, 34].

Last-but-not-least, the available instrument time in proteomics laboratories can be limited. Recently, an in-depth comprehensive proteome analysis was reported for as little as 5000 FACS-sorted colonic stem cells analyzed by HILIC-reversed phase nanoLC-MS/MS[17]. However, it is not (yet) feasible to use this protocol for analysis of large series of samples, given the extent of fractionation and the extremely long instrument time (80 hrs) required.

THE RESULTS SO FAR

The studies that have used proteomics to analyze stem cell biology can roughly be divided into two categories: those documenting global differences/changes in the proteomes between two or more groups of cells or tissues, and those analyzing the function of specific stem cell regulators[35-38] (Table 1, 2).

The interactomes of stem cell regulators

Proteomics studies in embryonic stem cells using tagged Oct4, Nanog, Sox2 and KLF4 showed that these pluripotency-inducing transcription factors interact with several multiprotein complexes with distinct intracellular functions[39-44]. For instance, all 4 factors bind chromatin-remodeling complexes known to be essential for ESC self-renewal[40, 42-45]. In addition, Oct4 binds a plethora of transcription factors and co-factors, components of the basal transcription machinery, and proteins involved in DNA replication and repair[40, 43]. Sox2 also binds proteins involved in multiple processes, including chromatin organization and assembly, DNA and RNA processing, and posttranslational modification[44, 46, 47]. Strikingly, Sox2, Nanog, KLF4 and Oct4 regulate many of the same genes and bind many of the same proteins, suggesting that they could function in large multiprotein complexes to regulate stem cell-specific gene expression programs and, possibly, other cellular processes[9].

Several other studies have used proteomics to study stem cell regulators. For instance, new binding partners for the Polycomb group (PcG) RING1B were identified in erythroleukemia cells. This has provided mechanistic insight into how a single PcG protein can regulate different types of chromatin modification by joining different protein complexes[48]. In addition, analysis of the cdk2 interactome in ESCs strongly suggests that the function of this kinase is not restricted to stimulating the G1/S transition, but also includes regulation of the DNA damage response, chromatin remodeling and transcription[49].

An in-depth review of stem cell maintenance pathways falls out of the scope of this review and the reader is referred to excellent reviews on this topic[9, 50]. Taken together, the above studies demonstrate the power of proteomic approaches in discovering novel aspects of stem cell biology (Table 2). They can serve as general blueprints for analyzing any factor that is suspected to govern tissue SC and CSC maintenance. The same approach can be used for analyzing how the interactomes of stem cell regulators change during differentiation and, in the case of CSC's, the accompanying loss of tumorigenic potential[51].

Table 1. Cancer stem cell-associated proteins revealed by proteomics.

Human Gene	Cancer Type	Cell type	Comparison	Validation	Reference
Targeted proteomics: Sox2 bait					
FUS (TLS)	Glioblastoma	LN229	Endogenous Sox2 IP *vs* control IP	co-IP	47
HNRNPU	Glioblastoma	LN229	Endogenous Sox2 IP *vs* control IP	co-IP, reciprocal co-IP	47
XRCC5	Glioblastoma	LN229	Endogenous Sox2 IP *vs* control IP	co-IP	47
XRCC6	Glioblastoma	LN229	Endogenous Sox2 IP *vs* control IP	co-IP	47
Global proteomics					
BIRC6	Colon cancer	colonospheres	colonospheres *vs* differentiated cells	WB, FACS	22
PTPRZ1	Glioblastoma	HSR-GBM1	gliospheres *vs* differentiated cells*	WB	51
TNC	Glioblastoma	HSR-GBM1	gliospheres *vs* differentiated cells*	WB	51
PODXL	Glioblastoma	HSR-GBM1 vs U373	gliospheres *vs* adherent cells*	WB	75
NG2	Glioblastoma	HSR-GBM1 vs U373	gliospheres *vs* adherent cells*	WB	75
TNC	Glioblastoma	HSR-GBM1 vs U373	gliospheres *vs* adherent cells*	WB	75
PTPRZ1	Glioblastoma	HSR-GBM1 vs U373	gliospheres *vs* adherent cells*	WB	75
CD90	Glioblastoma	HSR-GBM1 vs U373	gliospheres *vs* adherent cells*	WB	75
CD44	Glioblastoma	HSR-GBM1 vs U373	gliospheres *vs* adherent cells	WB	75
ALDH1A1	Liver cancer	Huh7	$CD133^+$ *vs* $CD133^-$	WB, qPCR, Aldefluor	52
ALDH1A1	Colon cancer	colonospheres	colonospheres *vs* differentiated cells	WB, FACS	18
TAGLN1	Liver cancer	Huh7	$CD133^+$ *vs* $CD133^-$	WB, RT-PCR	54
CATD	Glioblastoma	Neurospheres	γ-secretase inhibitor‡*	WB	58
GANAB	Glioblastoma	Neurospheres	γ-secretase inhibitor‡*	WB	58
GLB1	Glioblastoma	Neurospheres	γ-secretase inhibitor‡*	WB	58
P4HA1	Glioblastoma	Neurospheres	γ-secretase inhibitor‡*	WB	58
NES	Glioblastoma	Neurospheres	γ-secretase inhibitor‡	MRM	59
PCNA	Glioblastoma	Neurospheres	γ-secretase inhibitor‡	WB	59
SOD1 (SODC)	Glioblastoma	Neurospheres	γ-secretase inhibitor‡	WB	59
DPPA4	Teratocarcinoma	hECC vs hESC	hECC cells *vs* hESC cells	IF	57
GDF3	Teratocarcinoma	hECC vs hESC	hECC cells *vs* hESC cells	IF	57
HSPB1	Teratocarcinoma	hECC vs hESC	hECC cells *vs* hESC cells	IF	57
MFGE8	Teratocarcinoma	hECC vs hESC	hECC cells *vs* hESC cells	IF	57

‡inhibitor blocks Notch pathway, depleting CSC.
* glycoproteomics
CSC: cancer stem cell; hECC: human embryonal carcinoma cell; hESC: human embryonic stem cell; IP: immunoprecipitation; qPCR: quantitative polymerase chain reaction; MRM: multiple reaction monitoring; WB: western blot.

Table 2. Embryonic stem cell-associated proteins revealed by targeted proteomics.

Human Gene	Organism	Comparison	Validation	Reference
Pou5f1 (Oct4) bait				
HDAC2	Mouse	Endogenous Oct4 IP	co-IP, reciprocal co-IP, ChIP	39
MTA1	Mouse	Endogenous Oct4 IP	co-IP, ChIP	39
MTA2	Mouse	Endogenous Oct4 IP	co-IP	39
CHD4	Mouse	Tagged-Oct4-expressing ESCs *vs* control ESCs	co-IP, endogenous Oct4 co-IP	43
GATAD2B	Mouse	Tagged-Oct4-expressing ESCs *vs* control ESCs	co-IP, TAP, endogenous Oct4 co-IP	43
HDAC1	Mouse	Tagged-Oct4-expressing ESCs *vs* control ESCs	co-IP, endogenous Oct4 co-IP	43
KAT7 (Myst2)	Mouse	Tagged-Oct4-expressing ESCs *vs* control ESCs	co-IP	43
MTA2	Mouse	Tagged-Oct4-expressing ESCs *vs* control ESCs	co-IP, TAP, endogenous Oct4 co-IP	43
POU5F1 (Oct4)	Mouse	Tagged-Oct4-expressing ESCs *vs* control ESCs	co-IP, TAP, endogenous Oct4 co-IP	43
SALL1	Mouse	Tagged-Oct4-expressing ESCs *vs* control ESCs	co-IP, TAP, endogenous Oct4 co-IP	43
SALL4	Mouse	Tagged-Oct4-expressing ESCs *vs* control ESCs	co-IP, endogenous Oct4 co-IP	43
TFE3 (Tcfe3)	Mouse	Tagged-Oct4-expressing ESCs *vs* control ESCs	co-IP, TAP, endogenous Oct4 co-IP	43
TFEB	Mouse	Tagged-Oct4-expressing ESCs *vs* control ESCs	co-IP, TAP	43
PARP1	Mouse	Tagged-Oct4-expressing ESCs *vs* control ESCs	co-IP, endogenous Oct4 co-IP	43
CHD4 (Mi2beta)	Mouse	Tagged-Oct4-expressing ESCs *vs* control ESCs	co-IP	40
KDM1A (LSD1)	Mouse	Tagged-Oct4-expressing ESCs *vs* control ESCs	co-IP	40
MBD3	Mouse	Tagged-Oct4-expressing ESCs *vs* control ESCs	co-IP	40
MTA1	Mouse	Tagged-Oct4-expressing ESCs *vs* control ESCs	co-IP	40
MTA2	Mouse	Tagged-Oct4-expressing ESCs *vs* control ESCs	co-IP, reciprocal co-IP	40
SALL1	Mouse	Tagged-Oct4-expressing ESCs *vs* control ESCs	co-IP	40
SALL4	Mouse	Tagged-Oct4-expressing ESCs *vs* control ESCs	co-IP, reciprocal co-IP	40
WDR5	Mouse	Tagged-Oct4-expressing ESCs *vs* control ESCs	co-IP, reciprocal co-IP	40
Sall4 bait				
MTA2	Mouse	Tagged-Sall4-expressing ESCs vs control ESCs	co-IP, reciprocal co-IP	40
NACC1 (Nac1)	Mouse	Tagged-Sall4-expressing ESCs vs control ESCs	reciprocal co-IP	40
SALL1	Mouse	Tagged-Sall4-expressing ESCs vs control ESCs	co-IP	40
ZNF143 (Zfp143)	Mouse	Tagged-Sall4-expressing ESCs vs control ESCs	reciprocal co-IP	40
Nr0b1 (Dax1) bait				
ESRRB	Mouse	Tagged-Dax1-expressing ESCs *vs* control ESCs	pull down	40
POU5F1 (Oct4)	Mouse	Tagged-Dax1-expressing ESCs *vs* control ESCs	pull down	40
SALL1	Mouse	Tagged-Dax1-expressing ESCs *vs* control ESCs	pull down	40
SALL4	Mouse	Tagged-Dax1-expressing ESCs *vs* control ESCs	pull down	40
WDR5	Mouse	Tagged-Dax1-expressing ESCs *vs* control ESCs	pull down	40
Tcfcp2l1 bait				
ESRRB	Mouse	Tagged-Tcfcp2l1-expressing ESCs *vs* control ESCs	co-IP	40
MTA2	Mouse	Tagged-Tcfcp2l1-expressing ESCs *vs* control ESCs	co-IP	40
Esrrb bait				
EP400	Mouse	Tagged-Esrrb-expressing ESCs *vs* control ESCs	pull down	40
MTA2	Mouse	Tagged-Esrrb-expressing ESCs *vs* control ESCs	pull down	40
NR0B1 (Dax1)	Mouse	Tagged-Esrrb-expressing ESCs *vs* control ESCs	pull down	40
SALL4	Mouse	Tagged-Esrrb-expressing ESCs *vs* control ESCs	pull down	40
TCFCP2L1	Mouse	Tagged-Esrrb-expressing ESCs *vs* control ESCs	pull down	40
Nanog bait				
GATAD2A	Mouse	Endogenous Nanog IP	co-IP, reciprocal co-IP	39
HDAC1	Mouse	Endogenous Nanog IP	co-IP	39
HDAC2	Mouse	Endogenous Nanog IP	co-IP, reciprocal co-IP, co-elution (GF); ChIP	39
KDM1A (Lsd1)	Mouse	Endogenous Nanog IP	reciprocal co-IP	39
MTA1	Mouse	Endogenous Nanog IP	co-IP, co-elution (GF), ChIP, knockdown	39
MTA2	Mouse	Endogenous Nanog IP	co-IP, co-elution (GF)	39
PML	Mouse	Endogenous Nanog IP	co-IP, co-elution (GF)	39
POU5F1 (Oct4)	Mouse	Endogenous Nanog IP	co-IP, co-elution (GF), ChIP	39
SIN3A	Mouse	Endogenous Nanog IP	co-IP, reciprocal co-IP	39
SALL4	Mouse	Tagged-Nanog-expressing ES cell IP	co-IP, reciprocal co-IP, ChIP, knockdown	45

NACC1 (Nac1)	Mouse	Tagged†-Nanog-expressing ESCs *vs* control ESCs	co-IP, reciprocal pull down, knockdown, ChIP	[41]
NR0B1 (Dax1)	Mouse	Tagged†-Nanog-expressing ESCs *vs* control ESCs	co-IP, reciprocal pull down, knockdown	[41]
POU5F1 (Oct4)	Mouse	Tagged†-Nanog-expressing ESCs *vs* control ESCs	co-IP, reciprocal pull down	[41]
RIF1	Mouse	Tagged†-Nanog-expressing ESCs *vs* control ESCs	co-IP	[41]
SALL4	Mouse	Tagged†-Nanog-expressing ESCs *vs* control ESCs	knock down	[41]
ZNF281 (Zfp281)	Mouse	Tagged†-Nanog-expressing ESCs *vs* control ESCs	co-IP, reciprocal pull down, knockdown, ChIP	[41]
Sox2 bait				
HDAC1	Mouse	Tagged-Sox2-expressing ESCs vs control ESCs	co-IP	[44]
HDAC2	Mouse	Tagged-Sox2-expressing ESCs vs control ESCs	co-IP	[44]
LIN28A	Mouse	Tagged-Sox2-expressing ESCs vs control ESCs	co-IP	[44]
SALL4	Mouse	Tagged-Sox2-expressing ESCs vs control ESCs	co-IP	[44]
SOX21	Mouse	Tagged-Sox2-expressing ESCs vs control ESCs	co-IP	[44]
Klf4 bait				
SMARCA2	Mouse	Tagged-Klf4-expressing ESCs *vs* control ESCs	overexpression‡, knockdown‡	[42]
SMARCA4	Mouse	Tagged-Klf4-expressing ESCs *vs* control ESCs	co-IP, overexpression‡, knockdown‡	[42]

†*In vivo* biotinylation of peptide tag by co-expressed BirA biotin ligase.
‡Using induction of mouse embryonic fibroblast (MEF) pluripotency assay.
ChIP: chromatin immunoprecipitation; ESC: embryonic stem cell; GF: gel filtration; IP: immunoprecipitation; TAP: tandem immunopurification.

Differences between CSC and non-CSC

Proteomics has been used to identify global differences between CSC-enriched colonosphere cultures isolated from colorectal tumors, and their non-tumorigenic differentiated derivatives. Aldehyde dehydrogenase 1A1 (ALDH1A1) was identified as a CSC-enriched protein and its selective expression in CSCs was validated by Western blotting and FACS[18]. ALDH1A1 was also highly expressed in the $CD133^+$ fraction of hepatocellular carcinoma (HCC) cell lines. This study was based on comparative 2-D PAGE analysis of $CD133^+$ and $CD133^-$ cells followed by mass spec analysis of the 10 differentially expressed proteins[52]. Importantly, the tumorigenic and non-tumorigenic cells could be separated on the basis of ALDH activity in both studies, as measured by the fluorescent probe Aldefluor®[18, 52]. In another study, colorectal cancer cells were isolated directly from a resected tumor and compared to $CD133^+$-enriched spheroid cells from the same tumor. LC-MS analysis of glycosylated cell surface proteins on both cell populations identified known CSC markers (like CD44 and CD166) and novel ones including CEACAM5, biglycan, and cadherin 17[53]. CD133 is also expressed on the tumorigenic but not on the non-tumorigenic fraction of the hepatocellular carcinoma cell line Huh7[54]. 2D gel electrophoresis and mass spectrometry analysis of the differentially expressed proteins revealed that transgelin, an actin cross-linking protein, was highly expressed in $CD133^+$ cells and was essential for their invasive capacity[54]. Pancreatic tumor cells with a CSC phenotype can be isolated on the basis of cell surface $CD44^+CD24^+ESA^+$ expression. Comparison of these cells with the tumor bulk resulted in the identification of putative CSC-altered pathways, including resistance to apoptosis, dysregulation of cell proliferation, association with inflammation and metastasis[55]. Unfortunately, none of these were validated or tested in follow-up experiments.

Lectins can be used to purify cell surface proteins, which can subsequently be analyzed by LC-MS/MS. This approach was used to compare differences in cell surface protein expression between CSC-like neurospheres (HSR-GBM1) and traditional glioblastoma cell lines. This resulted in the identification of a small set of HSR-GBM1-enriched proteins, 5 of which (PODXL, NG2, TNC, PTPRZ1, CD90) were validated by Western blotting. Surprisingly, CD44 (often enriched in CSCs) was significantly lower in HSR-GBM1 stem-like cells.

Interestingly, paired colonopshere cultures and differentiated tumor cell cultures are more alike than CSC cultures from different tumors[22]. Analysis of multiple pairs of CSC and differentiated tumor cell cultures has yielded a set of CSC-enriched proteins, which was dominated by regulators of cell survival[22]. This is similar to the study in pancreatic CSCs[55]. The most prominent of these, BIRC6, is an inhibitor of apoptosis protein (IAP) and was identified as a chemo-resistance protein that is highly expressed in the Aldefluor®+ fraction of colorectal tumors. By applying this approach to large series of paired tumorigenic and non-tumorigenic culture samples novel robust CSC markers may be identified. Hopefully, such markers will be relevant to the CSC phenotype and may have value in predicting tumor behavior and/or response to therapy.

Human ESCs in culture may acquire chromosomal alterations that turn them into malignant embryonic carcinoma cells (ECC). A study in which the ESC and ECC membrane-proteomes were compared revealed that these cell types are highly similar, but also demonstrated altered expression of Hedgehog (HH) and Wnt pathway components[56]. Whether the changes in these stem cell pathways contribute to the benign versus malignant nature of ESCs and ECCs remains to be tested. In a similar quantitative proteomics study comparing ESCs and ECCs ~200 differentially expressed proteins were identified, including regulators of pluripotency and differentiation[57]. The comparison between normal and malignant stem cells from various other tissues is a major goal for future proteomics studies.

Treatment-induced changes in CSC's

Proteomics has also been used to document changes in the CSC proteome by using spheroid cultures established from glioblastoma[58, 59]. As maintenance of CSC in glioblastoma requires Notch signaling, it was not surprising that differentiation markers were induced while proliferation markers were reduced. However, this study also found that Notch inhibition results in a marked decrease in glycolytic enzymes and proteins that protect cells against oxidative stress[59]. The glioblastoma CSC line GSC11 was used in a phospho-proteomics study documenting the changes occurring in this cell line following treatment with a JAK/STAT inhibitor, stimulation with interleukin-6, and during growth in hypoxia[60]. This study demonstrates the power of phospho-proteomics in documenting treatment-induced changes of signaling pathways and interconnections between signaling pathways in an unbiased and robust manner. However, unfractionated cell lines as a source for CSCs, even when they are enriched for CSCs, contain spontaneously differentiated tumor cells which contribute to the mass spec data. Therefore, to ascertain that the results indeed apply to CSCs requires validation in purified CSC populations.

Biomarkers

Recently, gene expression profiling has shown that poor-prognosis in colorectal cancer patients can be predicted by a signature derived from normal intestinal SC's[61]. Likewise, a proteomics study identified a stem cell signature that could distinguish hyperplastic prostate tissue from prostate carcinoma[62]. In general, (C)SC-enriched proteins may serve as biomarkers for disease behavior and response to therapy. Orthogonal Partial Least Squares Discriminant Analysis (OPLS-DA) of the proteomics data may subsequently be used to generate models that can discriminate between survival groups[63]. It will be interesting to see whether proteomics-generated signatures that are based on (C)SC's, from whatever source, can match or outperform those that are generated by gene expression profiling[64, 65].

EXPERT COMMENTARY

State-of-the-art mass spectrometry

Modern High-resolution mass spectrometry-based proteomics has been greatly improved in recent years, with rapid developments in instrument designs[30, 66, 67]. In particular, the combination of a linear ion trap with an Orbitrap analyzer has been very successful and has become one of the standard mass spectrometers to characterize and quantify proteomes[68]. Improved versions of this instrument family have been introduced over the last few years, with every next generation instrument exhibiting increased sensitivities and scan speed[69, 70]. The latest family member, the QExactive, can achieve near proteome coverage of the yeast proteome in a single-shot nanoLC-MS/MS run employing a long column and a 4 hr gradient[71]. Cycle times for a top 10 methods (survey scans followed by up to 10 MS/MS scans) are about one second, more than twice as fast as on previous instruments of the Orbitrap family[69]. Importantly, the results demonstrate an unexpectedly large dynamic range of the MS signal and sensitivity for LC-MS/MS alone. Due to the absence of fractionation steps, only small amounts of sample (a microgram of peptide; a few thousand cells) are required.

The experimental design for future CSC proteomics studies will depend on many factors, including the specific research question and the available equipment. We suggest the following workflow:

1: A robust single step protein extraction protocol with detergents like SDS.
2: A robust sample clean-up step like FASP or short gel electrophoresis
3: A high pressure nanoLC system employing a long gradient in a long chromatography column, coupled on-line to
4: A fast-scanning high resolution tandem mass spectrometer.

Applying proteomics to study CSC biology

The spheroid culture system provides a unique model for spontaneous cancer stem cell differentiation. Proteomics can be applied to study the dynamic alterations that accompany spontaneous differentiation in developing spheroid cultures. In addition to studying global proteomic changes this may also include more careful analysis of activated and de-activated pathways by phosphoproteomic approaches, as well as analysis of other protein modifications, such as methylation or acetylation. This can either be done globally aiming to find altered patterns and pathways, or in a targeted fashion, by focusing on known SC regulators. Such analyses are expected to result in the identification of pathways/factors that drive CSC differentiation and loss of tumor-initiating capacity. In addition, by using the same experimental setup, drug-induced changes in CSCs and non-CSCs may be studied, which will undoubtedly provide novel insight into the mechanisms of action of many anticancer drugs. In addition, such studies will clarify the relationship between cancer stemness and drug resistance for each of those drugs.

Another important issue is how stem cell pathways are altered in CSCs when compared to normal SCs. Multiple mouse models have been developed that allow SC isolation from different tissues using SC-specific promoters driving the expression of fluorescent proteins[72]. Similar models in which cancer stem cells may be traced in the tumors of genetically modified mice are likely to follow. An important consideration here is that it is currently unknown whether the known markers for tissue stem cells (for instance Lgr5 and BMI1 in the gut) are also proper CSC markers[2]. The recent finding that Lgr5 and other Wnt target genes are repressed by methylation in an aggressive subgroup of colorectal tumors strongly suggests that this may not be the case[73].

The comparison of normal SCs with CSCs from cancer patients requires isolation of both cell types as starting material. Novel culture techniques have made it possible to isolate and grow normal human tissue stem cells in vitro, for instance those from the colon[74]. Ideally, such stem cell cultures are established from resection specimens containing tumor and normal tissue, as this would provide a source for both normal and cancer SCs from the same individual. Plasma membrane proteomics comparing human embryonic SCs to their cancerous counterparts, revealed differential regulation of the hedgehog (HH) and Wnt pathways, indicating that deregulation of these self-renewal pathways may play a role in the development of testicular cancer[56]. Alterations in stemness pathways during tumorigenesis are expected to be very heterogeneous and to be dependent on the genetic make-up of each single tumor (see above).

FIVE-YEAR VIEW

The novel SC culture techniques and state-of-the art mass spectrometry protocols now set the stage for a new phase in CSC research. The coming years we expect to see a rapid development in our understanding of how pathways that control stem cell maintenance and differentiation are affected by tumor-specific genetic alterations, by spontaneous or induced CSC differentiation, and during treatment with anti-cancer drugs. Hopefully, such information will help in the design of effective drug combination strategies to treat metastatic cancer.

KEY ISSUES

- CSCs may be the driving force behind tumor growth and recurrence
- Very little is known about the regulation of stem cell maintenance pathways in CSCs
- Novel mass spectrometry and sample preparation protocols allow proteomics of minute amounts of sample, making proteomics analysis of CSCs a realistic option
- Novel cell culture techniques allow culturing of normal and cancer stem cells
- Proteomics is an ideal technique to probe various aspects of the CSC concept

REFERENCE LIST

1. Lobo,N.A. *et al.* The biology of cancer stem cells. *Annu. Rev. Cell Dev. Biol.* 23, 675-699 (2007).
2. Clevers,H. The cancer stem cell: premises, promises and challenges. *Nat. Med.* 17, 313-319 (2011).
3. Kelly,P.N. *et al.* Tumor growth need not be driven by rare cancer stem cells. *Science* 317, 337 (2007).
4. Quintana,E. *et al.* Phenotypic heterogeneity among tumorigenic melanoma cells from patients that is reversible and not hierarchically organized. *Cancer Cell* 18, 510-523 (2010).
5. Goardon,N. *et al.* Coexistence of LMPP-like and GMP-like leukemia stem cells in acute myeloid leukemia. *Cancer Cell* 19, 138-152 (2011).
6. Gupta,P.B. *et al.* Stochastic state transitions give rise to phenotypic equilibrium in populations of cancer cells. *Cell* 146, 633-644 (2011).
7. Roesch,A. *et al.* A temporarily distinct subpopulation of slow-cycling melanoma cells is required for continuous tumor growth. *Cell* 141, 583-594 (2010).
8. Vermeulen,L. *et al.* Wnt activity defines colon cancer stem cells and is regulated by the microenvironment. *Nat. Cell Biol.* 12, 468-476 (2010).
9. Mallanna,S.K. & Rizzino,A. Systems biology provides new insights into the molecular mechanisms that control the fate of embryonic stem cells. *J. Cell Physiol* 227, 27-34 (2012).
10. Sjoblom,T. *et al.* The consensus coding sequences of human breast and colorectal cancers. *Science* 314, 268-274 (2006).
11. Bonizzi,G. *et al.* The emerging role of p53 in stem cells. *Trends Mol. Med.*(2011).
12. Cicalese,A. *et al.* The tumor suppressor p53 regulates polarity of self-renewing divisions in mammary stem cells. *Cell* 138, 1083-1095 (2009).
13. Laurenti,E. *et al.* Myc's other life: stem cells and beyond. *Curr. Opin. Cell Biol.* 21, 844-854 (2009).
14. Feng,Y. *et al.* Mutant kras promotes hyperplasia and alters differentiation in the colon epithelium but does not expand the presumptive stem cell pool. *Gastroenterology* 141, 1003-1013 (2011).
15. Braakman,R.B. *et al.* Laser capture microdissection applications in breast cancer proteomics. *Methods Mol. Biol.* 755, 143-154 (2011).
16. Wisniewski,J.R. *et al.* High recovery FASP applied to the proteomic analysis of microdissected formalin fixed paraffin embedded cancer tissues retrieves known colon cancer markers. *J. Proteome. Res.* 10, 3040-3049 (2011).
17. Di,P.S. *et al.* Highly sensitive proteome analysis of FACS-sorted adult colon stem cells. *J. Proteome. Res.* 10, 3814-3819 (2011).
18. Emmink,B.L. *et al.* Differentiated human colorectal cancer cells protect tumor-initiating cells from irinotecan. *Gastroenterology* 141, 269-278 (2011).
19. Ricci-Vitiani,L. *et al.* Identification and expansion of human colon-cancer-initiating cells. *Nature* 445, 111-115 (2007).
20. Sato,T. *et al.* Long-term expansion of epithelial organoids from human colon, adenoma, adenocarcinoma, and Barrett's epithelium. *Gastroenterology* 141, 1762-1772 (2011).
21. Patru,C. *et al.* CD133, CD15/SSEA-1, CD34 or side populations do not resume tumor-initiating properties of long-term cultured cancer stem cells from human malignant glio-neuronal tumors. *BMC. Cancer* 10, 66 (2010).
22. van Houdt,W.J. *et al.* Comparative proteomics of colon cancer stem cells and differentiated tumor cells identifies BIRC6 as a potential therapeutic target. *Mol. Cell Proteomics.*(2011).
23. Geiger,T. *et al.* Proteomics on an Orbitrap benchtop mass spectrometer using all-ion fragmentation. *Mol. Cell Proteomics.* 9, 2252-2261 (2010).
24. Roth,M.J. *et al.* Sensitive and reproducible intact mass analysis of complex protein mixtures with superficially porous capillary reversed-phase liquid chromatography mass spectrometry. *Anal. Chem.* 83, 9586-9592 (2011).
25. Wang,D. *et al.* Ultrasensitive characterization of site-specific glycosylation of affinity-purified haptoglobin from lung cancer patient plasma using 10 mum i.d. porous layer open tubular liquid chromatography-linear ion trap collision-induced dissociation/electron transfer dissociation mass spectrometry. *Anal. Chem.* 83, 2029-2037 (2011).
26. Shen,Y. *et al.* Ultrasensitive proteomics using high-efficiency on-line micro-SPE-nanoLC-nanoESI MS and MS/MS. *Anal. Chem.* 76, 144-154 (2004).
27. Luo,Q. *et al.* On-line 1D and 2D porous layer open tubular/LC-ESI-MS using 10-microm-i.d. poly(styrene-divinylbenzene) columns for ultrasensitive proteomic analysis. *Anal. Chem.* 79, 6174-6181 (2007).

28. Tian,R. *et al.* Rare cell proteomic reactor applied to stable isotope labeling by amino acids in cell culture (SILAC)-based quantitative proteomics study of human embryonic stem cell differentiation. *Mol. Cell Proteomics.* 10, M110 (2011).
29. Wang,N. *et al.*Development of mass spectrometry-based shotgun method for proteome analysis of 500 to 5000 cancer cells. *Anal. Chem.* 82, 2262-2271 (2010).
30. Cox,J. & Mann,M. Quantitative, high-resolution proteomics for data-driven systems biology. *Annu. Rev. Biochem.* 80, 273-299 (2011).
31. Jimenez,C.R. *et al.* High-throughput and targeted in-depth mass spectrometry-based approaches for biofluid profiling and biomarker discovery. *Biomark. Med.* 1, 541-565 (2007).
32. Piersma,S.R. *et al.* Workflow comparison for label-free, quantitative secretome proteomics for cancer biomarker discovery: method evaluation, differential analysis, and verification in serum. *J. Proteome. Res.* 9, 1913-1922 (2010).
33. Fang,Y. *et al.* Quantitative analysis of proteome coverage and recovery rates for upstream fractionation methods in proteomics. *J. Proteome. Res.* 9, 1902-1912 (2010).
34. Ostasiewicz,P. *et al.* Proteome, phosphoproteome, and N-glycoproteome are quantitatively preserved in formalin-fixed paraffin-embedded tissue and analyzable by high-resolution mass spectrometry. *J. Proteome. Res.* 9, 3688-3700 (2010).
35. Hughes,C.S. *et al.* Proteomics of human embryonic stem cells. *Proteomics.* 11, 675-690 (2011).
36. Whetton,A.D. *et al.* The time is right: proteome biology of stem cells. *Cell Stem Cell* 2, 215-217 (2008).
37. Williamson,A.J. & Whetton,A.D. Development of approaches for systematic analysis of protein networks in stem cells. *Adv. Enzyme Regul.* 50, 273-284 (2010).
38. Williamson,A.J. & Whetton,A.D. The requirement for proteomics to unravel stem cell regulatory mechanisms. *J. Cell Physiol* 226, 2478-2483 (2011).
39. Liang,J. *et al.* Nanog and Oct4 associate with unique transcriptional repression complexes in embryonic stem cells. *Nat. Cell Biol.* 10, 731-739 (2008).
40. van den Berg,D.L. *et al.* An Oct4-centered protein interaction network in embryonic stem cells. *Cell Stem Cell* 6, 369-381 (2010).
41. Wang,J. *et al.* A protein interaction network for pluripotency of embryonic stem cells. *Nature* 444, 364-368 (2006).
42. Mak,A.B. *et al.* A lentiviral functional proteomics approach identifies chromatin remodeling complexes important for the induction of pluripotency. *Mol. Cell Proteomics.* 9, 811-823 (2010).
43. Pardo,M. *et al.* An expanded Oct4 interaction network: implications for stem cell biology, development, and disease. *Cell Stem Cell* 6, 382-395 (2010).
44. Mallanna,S.K. *et al.* Proteomic analysis of Sox2-associated proteins during early stages of mouse embryonic stem cell differentiation identifies Sox21 as a novel regulator of stem cell fate. *Stem Cells* 28, 1715-1727 (2010).
45. Wu,Q. *et al.* Sall4 interacts with Nanog and co-occupies Nanog genomic sites in embryonic stem cells. *J. Biol. Chem.* 281, 24090-24094 (2006).
46. Cox,J.L. *et al.* Sox2 uses multiple domains to associate with proteins present in Sox2-protein complexes. *PLoS. ONE.* 5, e15486 (2010).
47. Fang,X. *et al.* Landscape of the SOX2 protein-protein interactome. *Proteomics.* 11, 921-934 (2011).
48. Sanchez,C. *et al.* Proteomics analysis of Ring1B/Rnf2 interactors identifies a novel complex with the Fbxl10/Jhdm1B histone demethylase and the Bcl6 interacting corepressor. *Mol. Cell Proteomics.* 6, 820-834 (2007).
49. Neganova,I. *et al.* An important role for CDK2 in G1 to S checkpoint activation and DNA damage response in human embryonic stem cells. *Stem Cells* 29, 651-659 (2011).
50. Heng,J.C. & Ng,H.H. Transcriptional regulation in embryonic stem cells. *Adv. Exp. Med. Biol.* 695, 76-91 (2010).
51. He,J. *et al.* Glycoproteomic analysis of glioblastoma stem cell differentiation. *J. Proteome. Res.* 10, 330-338 (2011).
52. Ma,S. *et al.* Aldehyde dehydrogenase discriminates the CD133 liver cancer stem cell populations. *Mol. Cancer Res.* 6, 1146-1153 (2008).
53. Fang,D.D. *et al.* Expansion of CD133(+) colon cancer cultures retaining stem cell properties to enable cancer stem cell target discovery. *Br. J. Cancer* 102, 1265-1275 (2010).
54. Lee,E.K. *et al.* Transgelin promotes migration and invasion of cancer stem cells. *J. Proteome. Res.* 9, 5108-5117 (2010).

55. Dai,L. *et al.* Quantitative proteomic profiling studies of pancreatic cancer stem cells. *J. Proteome. Res.* 9, 3394-3402 (2010).
56. Dormeyer,W. *et al.* Plasma membrane proteomics of human embryonic stem cells and human embryonal carcinoma cells. *J. Proteome. Res.* 7, 2936-2951 (2008).
57. Chaerkady,R. *et al.* Comparative proteomics of human embryonic stem cells and embryonal carcinoma cells. *Proteomics.* 10, 1359-1373 (2010).
58. Dai,L. *et al.* Differential profiling studies of N-linked glycoproteins in glioblastoma cancer stem cells upon treatment with gamma-secretase inhibitor. *Proteomics.* 11, 4021-4028 (2011).
59. Dai,L. *et al.* Dose-Dependent Proteomic Analysis of Glioblastoma Cancer Stem Cells upon Treatment with Gamma-Secretase Inhibitor. *Proteomics.*(2011).
60. Nilsson,C.L. *et al.* Quantitative phosphoproteomic analysis of the STAT3/IL-6/HIF1alpha signaling network: an initial study in GSC11 glioblastoma stem cells. *J. Proteome. Res.* 9, 430-443 (2010).
61. Merlos-Suarez,A. *et al.* The intestinal stem cell signature identifies colorectal cancer stem cells and predicts disease relapse. *Cell Stem Cell* 8, 511-524 (2011).
62. Alaiya,A.A. *et al.* Proteomics-based signature for human benign prostate hyperplasia and prostate adenocarcinoma. *Int. J. Oncol.* 38, 1047-1057 (2011).
63. Chan,E.C. *et al.* Metabolic profiling of human colorectal cancer using high-resolution magic angle spinning nuclear magnetic resonance (HR-MAS NMR) spectroscopy and gas chromatography mass spectrometry (GC/MS). *J. Proteome. Res.* 8, 352-361 (2009).
64. Oakman,C. *et al.*Breast cancer assessment tools and optimizing adjuvant therapy. *Nat. Rev. Clin. Oncol.* 7, 725-732 (2010).
65. Kelley,R.K. & Venook,A.P. Prognostic and predictive markers in stage II colon cancer: is there a role for gene expression profiling? *Clin. Colorectal Cancer* 10, 73-80 (2011).
66. Aebersold,R. & Mann,M. Mass spectrometry-based proteomics. *Nature* 422, 198-207 (2003).
67. Nilsson,T. *et al.* Mass spectrometry in high-throughput proteomics: ready for the big time. *Nat. Methods* 7, 681-685 (2010).
68. Yates,J.R. *et al.*Proteomics by mass spectrometry: approaches, advances, and applications. *Annu. Rev. Biomed. Eng* 11, 49-79 (2009).
69. Michalski,A. *et al.* Mass spectrometry-based proteomics using Q Exactive, a high-performance benchtop quadrupole Orbitrap mass spectrometer. *Mol. Cell Proteomics.* 10, M111 (2011).
70. Thakur,S.S. *et al.* Deep and highly sensitive proteome coverage by LC-MS/MS without prefractionation. *Mol. Cell Proteomics.* 10, M110 (2011).
71. Nagaraj,N. *et al.* Systems-wide perturbation analysis with near complete coverage of the yeast proteome by single-shot UHPLC runs on a bench-top Orbitrap. *Mol. Cell Proteomics*.(2011).
72. Snippert,H.J. & Clevers,H. Tracking adult stem cells. *EMBO Rep.* 12, 113-122 (2011).
73. De Sousa E Melo *et al.* Methylation of cancer-stem-cell-associated Wnt target genes predicts poor prognosis in colorectal cancer patients. *Cell Stem Cell* 9, 476-485 (2011).
74. Jung,P. *et al.* Isolation and in vitro expansion of human colonic stem cells. *Nat. Med.* 17, 1225-1227 (2011).
75. He,J. *et al.* Identification of cell surface glycoprotein markers for glioblastoma-derived stem-like cells using a lectin microarray and LC-MS/MS approach. *J. Proteome. Res.* 9, 2565-2572 (2010).

4

COMPARATIVE PROTEOMICS OF COLON CANCER STEM CELLS AND DIFFERENTIATED TUMOR CELLS IDENTIFIES BIRC6 AS A POTENTIAL THERAPEUTIC TARGET

Benjamin L Emmink[1*], Winan J van Houdt[1*], Thang V Pham[2], Sander R Piersma[2], André Verheem[1], Rob Vries[3], Silvina A Fratantoni[2], Apollo Pronk[4], Hans Clevers[3], Inne HM Borel Rinkes[1], Connie R Jimenez[2], Onno Kranenburg[1]

[1] Department of Surgery, University Medical Center Utrecht, The Netherlands
[2] OncoProteomics Laboratory, VU University Medical Center Amsterdam, The Netherlands
[3] Hubrecht institute KNAW & University Medical Center Utrecht, The Netherlands
[4] Department of Surgery, Diakonessenhuis Utrecht, The Netherlands

* Equal contribution

Molecular & Cellular Proteomics. 2011 Dec; 10(12):M111.

SUMMARY

BACKGROUND: Patients with liver metastases from colon carcinoma show highly variable responses to chemotherapy and tumor recurrence is frequently observed. Therapy-resistant cancer stem cells have been implicated in drug resistance and tumor recurrence. However, the factors determining therapy resistance and tumor recurrence are poorly understood. The aim of this study was to gain insight into these mechanisms by comparing the proteomes of patient-derived cancer stem cell cultures and their differentiated isogenic offspring. **METHODS:** We established colonosphere cultures derived from resection specimens of liver metastases in patients with colon cancer. These colonospheres, enriched for colon cancer stem cells, were used to establish isogenic cultures of stably differentiated non-tumorigenic progeny. Proteomics based on 1D gel electrophoresis coupled to nanoLC-MS/MS was used to identify proteome differences between three of these paired cultures. The resulting data were analyzed using Ingenuity Pathway Software. **RESULTS:** Out of a total dataset of 3048 identified proteins, 32 proteins were at least 2 fold upregulated in the colon cancer stem cells when compared to the differentiated cells. Pathway analysis showed that 'cell death' regulation is strikingly different between the two cell types. Interestingly, one of the top-upregulated proteins was BIRC6, which belongs to the class of Inhibitor of Apoptosis Proteins. Knockdown of BIRC6 sensitized colon cancer stem cells against the chemotherapeutic drugs oxaliplatin and cisplatin. **CONCLUSION:** This study reveals that differentiation of colon cancer stem cells is accompanied by altered regulation of cell death pathways. We identified BIRC6 as an important mediator of cancer stem cell resistance against cisplatin and oxaliplatin. Targeting BIRC6, or other Inhibitors of Apoptosis Proteins, may help eradicating colon cancer stem cells.

INTRODUCTION

Treatment of colorectal cancer (CRC) patients with chemotherapy is characterized by highly divergent tumor responses, but tumor recurrence is almost always observed. Therefore, chemotherapy is not considered to be a curative modality in the treatment of CRC[1]. Tumor recurrence may be due to the presence of therapy-resistant, genetically distinct tumor subclones. These subclones may either be pre-existent or may be generated as a direct result of the chemotherapy itself. More recently, it has been suggested that therapy resistance and subsequent tumor recurrence could be mediated by the 'cancer stem cell' fraction of colorectal tumors. Cancer stem cells make up only a few percent of the total tumor cell mass, but are uniquely endowed with tumor-initiating capacity[2-5].

Interestingly, normal intestinal stem cells have been identified as the cell-of-origin of intestinal tumors[6, 7] Cancer stem cells may therefore be transformed descendants of normal tissue stem cells. While normal stem cells give rise to differentiated cells lacking tissue-regenerating capacity, cancer stem cells give rise to differentiated tumor cells lacking tumor-regenerating capacity [8, 9].

Normal colon stem cells are exposed to toxins and drugs for an entire lifetime. To cope with this continuous challenge, stem cells must possess intrinsic resistance mechanisms that protect their DNA from being mutated and that allow prolonged survival. Inheritance of these resistance mechanisms by cancer stem cells may protect them from the cytotoxic action of chemotherapeutic drugs. If cancer stem cells are indeed the major driving force behind tumor recurrence, novel strategies are required to target this subset of cancer cells. Indeed, several studies have shown that residual tumor tissue after chemotherapy is enriched for cancer stem cell-like cells[10, 11] However, the relationship between chemo-resistance and tumor-initiating potential and the mechanisms underlying cancer stem cell selective drug resistance are currently poorly understood [12-15].

Here we set out to address the relationship between colorectal cancer stem cells and drug resistance. To this end, we have generated cancer stem cell enriched human colonosphere cultures from colorectal liver metastases. In addition, we have generated colonosphere-derived stably differentiated progeny. These isogenic cell pairs were then used to identify proteome differences using mass spectrometry. Analysis of the data revealed that proteins governing cell survival are overrepresented in the cancer stem cell cultures. The most prominently overexpressed survival protein, BIRC6/BRUCE/Apollon, was identified as a key mediator of cancer stem cell resistance to cisplatin and oxaliplatin.

EXPERIMENTAL PROCEDURES

Colorectal cancer stem cells and differentiated tumor cell cultures

Collection of tumor specimens, isolation and expansion of colorectal cancer stem cell-and differentiated cell cultures was performed as described in Emmink et al[16]. Human colorectal tumor specimens were obtained from patients undergoing a liver resection for metastatic adenocarcinoma, in accordance with the ethical committee on human experimentation. Informed consent was obtained from all patients. All tumors were diagnosed as colorectal adenocarcinomas. Liver metastases were excised from segment VII (L145), segment IV (L146) and segment II-IV (L167). Differentiation status was not determined.

Isolation and expansion of colorectal cancer stem cell cultures

The obtained tissue fragments were washed extensively with PBS and were mechanically dissociated using scalpels and vigorous trituration to yield small fragments (<1mm3) and single cells. Enzymatic digestion was performed using thermolysin 0.05% (Sigma, Type X) in DMEM/F12 containing 5 mM Hepes (Gibco) for 2hr at 37ºC. The suspension was then filtered through a 40-µm-pore size nylon cell strainer (BD Falcon) to separate the tissue fragments from the single cells. The single cell suspension was cultured in advanced DMEM/F12 (Gibco) supplemented with 0.6% glucose (BDH Lab. Supplies), 2 mM L-glutamine (Biowhittaker), 9.6 µg/ml putrescin (Sigma), 6.3 ng/ml progesterone (Sigma), 5.2 ng/ml sodium selenite (Sigma), 25 µg/ml insulin (Sigma), 100 µg/ml apotransferrin (Sigma), 5 mM hepes (Gibco), 0,005 µg/ml trace element A (Cellgro), 0.01µg/ml trace element B (Cellgro), 0.01 µg/ml trace element C (Cellgro), 100 µM β-mercaptoethanol (Merck), 10 ml antibiotic-antimycotic (Gibco), 4 µg/ml gentamicine (Invitrogen), 0.002% lipid mixture (Sigma), 5 µg/ml glutathione (Roche) and 4 µg/ml Heparin (Sigma). Growth factors (20 ng/ml EGF (Invitrogen) and 10 ng/ml b-FGF (Abcam)) were added to the cell culture medium freshly each week. All cell culture was carried out in non-tissue culture treated flasks (BD Falcon) at 37° C in a 5% CO2 humidified incubator. In vitro differentiation was induced by culturing colon colonospheres for 3 weeks on collagen-coated dishes in DMEM-F12 (GIBCO) supplemented with 20% fetal bovine serum. Passage numbers of the clones used (n=3) spheroid cultures and the accompanying differentiated tumor cell cultures were all below 10.

Cell lysis and SDS-PAGE

Paired colonospheres and differentiated tumor cell cultures were seeded in 10 cm^2 diameter tissue culture plates and cultured for 24 hours in serum free stem cell medium. Cells were subsequently washed twice with PBS, centrifuged and washed with water to get rid of the excess salts. Lysisbuffer (20mM HEPES pH7.4, 1% NP40, 150mM NaCl, 5mM MgCl2, 10% glycerol) containing proteinase inhibitor was used to lyse cells. Equal amounts of protein (50 µg) were separated on NuPAGE Novex Bis-Tris Mini Gels (Invitrogen). Gels were stained with Coomassie brilliant blue G-250 (Pierce), washed and each lane was sliced into ten bands using a band pattern to guide the slicing. The gel slicing and in-gel digesting was performed in a laminar flow under keratin-free conditions.

In-gel digestion

Before MS analysis, separated proteins were in-gel digested as described[17]. Gel lanes corresponding to the different protein samples were sliced into ten bands. The bands were washed/dehydrated three times in 50 mM ammonium bicarbonate pH 7.9 + 50% acetonitrile. Subsequently, cysteine bonds were reduced with 10 mM dithiotreitol for 1 h at 56 °C and alkylated with 50 mM iodoacetamide for 45 min at RT in the dark. After two subsequent wash/dehydration cycles the bands were dried 10 min in a vacuum centrifuge and incubated overnight with 0.06 µg/µl trypsin at 25 °C. Peptides were extracted once in 1% formic acid and subsequently two times in 50% ACN in 5% formic acid. The volume was reduced to 50 µl in a vacuum centrifuge prior to LC-MS/MS analysis[187].

NanoLC - MS/MS analysis

Peptides were separated by an Ultimate 3000 nanoLC-MS/MS system (Dionex LC-Packings, Amsterdam, The Netherlands) equipped with a 20 cm × 75 µm ID fused silica column custom packed with 3 µm 120 Å ReproSil Pur C18 aqua (Dr Maisch GMBH, Ammerbuch-Entringen,

Germany). After injection, peptides were trapped at 30 µl/min on a 5 mm × 300 µm ID Pepmap C18 cartridge (Dionex LC-Packings, Amsterdam, The Netherlands) at 2% buffer B (buffer A: 0.05% formic acid in MQ; buffer B: 80% ACN + 0.05% formic acid in MQ) and separated at 300 nl/min in a 10–40% buffer B gradient in 60 min. Eluting peptides were ionized at 1.7 kV in a Nanomate Triversa Chip-based nanospray source using a Triversa LC coupler (Advion, Ithaca, NJ). Intact peptide mass spectra and fragmentation spectra were acquired on a LTQ-FT hybrid mass spectrometer (Thermo Fisher, Bremen, Germany). Intact masses were measured at resolution 50.000 in the ICR cell using a target value of 1×10^6 charges. In parallel, following an FT pre-scan, the top 5 peptide signals (charge-states 2^+ and higher) were submitted to MS/MS in the linear ion trap (3 amu isolation width, 30 ms activation, 35% normalized activation energy, *Q* value of 0.25 and a threshold of 5000 counts). Dynamic exclusion was applied with a repeat count of 1 and an exclusion time of 30s.

Label-free protein quantitation by spectral counting has emerged as a powerful alternative to labeling-based strategies, with each approach having its pros and cons. Notably, label-free analysis is less accurate than approaches in which proteins are labeled, in particular when small differences in protein levels across samples are quantified. However, with a good parallel workflow, label-free quantitation is simple, cheap, and allows for quantitation at a relative large dynamic range.

Database searching, statistics and Ingenuity Pathway Analysis

MS/MS spectra were searched against the human IPI database 3.31 (67511 entries) using Sequest (version 27, rev 12), which is part of the BioWorks 3.3 data analysis package (Thermo Fisher, San Jose, CA). MS/MS spectra were searched with a maximum allowed deviation of 10 ppm for the precursor mass and 1 amu for fragment masses. Methionine oxidation and cysteine carboxamidomethylation were allowed as variable modifications, two missed cleavages were allowed and the minimum number of tryptic termini was 1. After database searching the DTA and OUT files were imported into Scaffold 2.01.01 (Proteome software, Portland, OR). Scaffold was used to organize the gel-band data and to validate peptide identifications using the Peptide Prophet algorithm [18]. Only peptide identifications with a probability> 95% were retained. Subsequently, the ProteinProphet algorithm [19] was applied and protein identifications with a probability of >99% with 2 peptides or more in at least one of the samples were retained. Proteins that contained similar peptides and could not be differentiated based on MS/MS analysis alone were grouped. For each protein identified, the number of spectral counts (identified MS/MS spectra) in each sample (10 gel bands) was exported to Excel. The for each sample the spectral counts per protein were normalized on the sum of the spectral counts for that sample. The list of differentially expressed proteins, including fold changes was imported in the online software package Ingenuity (Ingenuity IPA, version 7.6) and pathway and network analysis was performed with only direct relationships. Furthermore the list of differentially expressed proteins was imported in the online STRING database of known and predicted protein interactions. The interactions include direct (physical) and indirect (functional) associations between proteins.

Lentiviral Constructs and Transduction

The lentiviral short-hairpin RNA (shRNA) constructs targeting BIRC6 were obtained from the TRC-Mm1.0 library (Sigma Aldrich). The target set used for BIRC6 (NM_016252) included TRCN0000004157, TRCN0000004158, TRCN00000059, TRCN0000004160, and TRCN0000004161. Of these constructs, transduction of cells with 58 and 59 produced the best

knock down. As the control vector, we used the same vector containing a sequence targeting luciferase, TGACCAGGCATTCACAGAAAT.

Western blotting and Antibodies
Lysates of colonospheres and their differentiated offspring were prepared in lysisbuffer (20mM HEPES pH7.4, 1% NP40, 150mM NaCl, 5mM MgCl2, 10% glycerol). Equal amounts of protein were run out on NuPAGE Novex Tris-Acetate Mini Gel (Invitrogen) and were analyzed by Western blotting using antibodies directed against BIRC6 (Ab19609, Abcam) and β-Actin (AC-15, Novus Biologicals, Littleton, CO, USA) was used.

Flow Cytometry and Cell Sorting
Dead cells were excluded using viability marker 7-aminoactinomycin D (7-AAD) (R&D) and cell doublets and clumps were excluded using doublet discrimination gating. Aldefluor®-positive cells were analyzed according to the manufacturer's protocol by using Aldefluor® and DEAB (STEMCELL Technologies). The cell sorting experiments were conducted with DAKO-Cytomation MoFlo High Speed Sorter.

Cisplatin and Oxaliplatin Sensitivity Assay.
Control and BIRC6 knockdown colonospheres and differentiated tumor cells were cultured in the presence of oxaliplatin (Pharmachemie BV, Haarlem) or cisplatin (Pharmachemie BV, Haarlem) at the indicated concentrations for five days. Mitochondrial activity was evaluated using CellTiter 96® AQ_{ueous} Non-Radioactive Cell Proliferation Assay (MTS) (Promega). All absorbance values are expressed as percentages of vehicle-treated control wells.

RESULTS

Proteome differences between colon cancer stem cells and their differentiated progeny
To compare the proteome of colon cancer stem cells to their differentiated progeny, we analyzed three isogenic pairs of colonospheres and differentiated tumor cells derived from freshly resected liver metastases. All colonosphere cultures were enriched for cancer stem cells based on their high clone- and tumor-forming potential[16]

The protein lysates of these cultures were fractionated on an SDS-PAGE gel (Figure 1A), followed by in-gel tryptic digestion. Analysis of the extracted peptides was performed by Nano-LC-MS/MS, followed by database searching. In total, 3048 proteins were identified in all sets of cells together, with an average of 2269 proteins per isogenic couple (Table 1). The number of proteins that was at least 2-fold upregulated in the colonospheres of each isogenic pair varied from 377 to 491. Of these >2-fold upregulated proteins, 32 proteins were upregulated in the colonospheres of all 3 isogenic pairs (Figure 1B). The unsupervised heat map of global clustering shows that the similarity between isogenic pairs of colonosphere cells and differentiated tumor cells is greater than the similarity among the different colonospheres cultures (Figure 2A). In contrast, supervised clustering including all significantly up- and downregulated proteins shows that all colonosphere cultures and differentiated cultures now cluster together (Figure 2B). This suggests that it may be possible to identify a cancer stem cell protein signature in colorectal cancer.

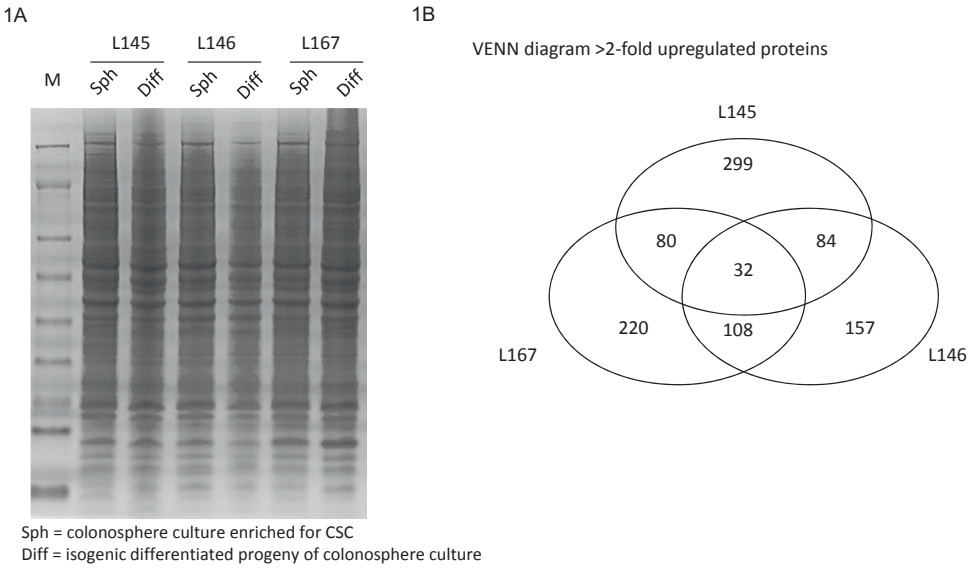

Sph = colonosphere culture enriched for CSC
Diff = isogenic differentiated progeny of colonosphere culture

Figure 1. NanoLC-MS/MS/based analysis of proteome differences between colonopspheres and isogenic differentiated tumor cells. A. Coomassie-stained protein gradient gel loaded with protein samples from colonospheres (Sph) and differentiated tumor cells (Diff) of the indicated tumors. This gel was used for mass-spec analysis. B. Venn diagram of all >2-fold upregulated proteins in colonospheres.

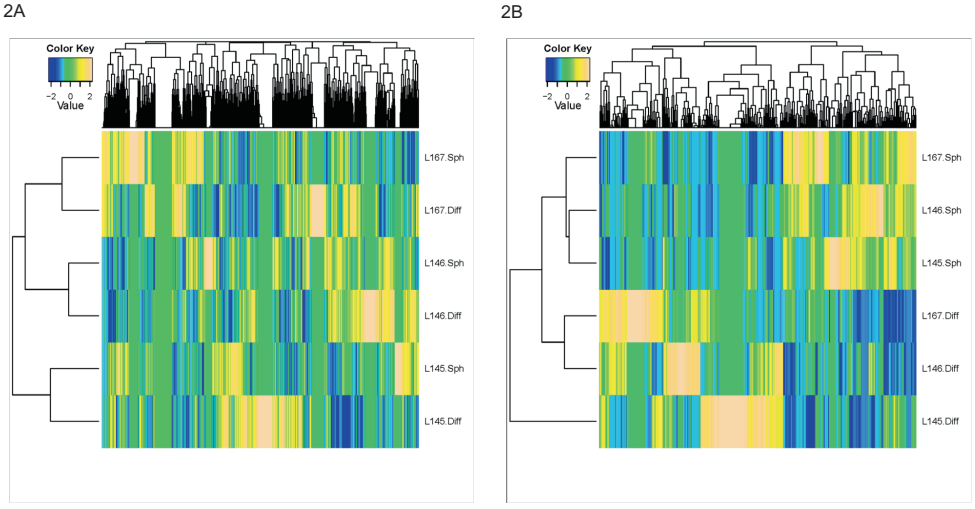

Figure 2. Separation of colonospheres from differentiated tumor cells by cluster analysis. A. Heat map of unsupervised cluster analysis of all identified proteins. B. Heat map of supervised cluster analysis of all significantly up- and downregulated proteins ($p<0.05$ according to the Fisher exact test per pair.) The selected list of regulated proteins separates colonospheres from differentiated tumor cells.

Table 1. Proteome differences between colonospheres and isogenic differentiated cells.

	L145	L146	L167	Overlap	
				2/3 pairs	3/3 pairs
all proteins	2242	2290	2376	1739	516
total upregulated proteins	1078	1001	1093	676	229
>2 fold upregulated	491	377	437	275	32

The numbers refer to all identified up-, down- and non-regulated proteins (top row), all upregulated proteins (middle row), and all >2 fold upregulated proteins. The number of proteins in all three categories that were identified in 2/3 and in 3/3 pairs are shown in the last 2 columns.

Proteins associated with survival are upregulated in colon cancer stem cells

Next, we divided the upregulated proteins in three categories: I) Top upregulated, ≥ 2 fold upregulated in 3 out of 3 isogenic pairs, II) Sub-top upregulated, ≥ 1.5 fold upregulated in 3 out of 3 isogenic pairs, and III) Rest upregulated, ≥ 1.5 fold upregulated in 2 out of 3 isogenic pairs. A total amount of 119 proteins was found to be enriched in colonospheres (32 in category I; 22 in category II, and 65 in category III) (Table 2, Supplementary Table 1). Interestingly, among the top upregulated proteins is ALDH1A1 (aldehyde dehydrogenase 1A1) which was recently identified by us and others as a bona fide colon (cancer) stem cell marker[19]. The identification of ALDH1A1 demonstrates the validity of our proteomics approach to identify upregulated factors in cancer stem cells.

Next, we used the Ingenuity Pathway Knowledge Base tool to identify biological functions and canonical pathways that distinguish colonospheres from differentiated cells. For this analysis all 119 colonosphere-enriched proteins (Table 2, Supplementary Table 1) were included. When classified according to function, proteins regulating 'Cell Death' (20) and proteins regulating 'Post-Translational Modification' (12) were most frequently identified. 'Cell cycle control of chromosomal replication', 'aryl hydrocarbon receptor signaling', 'estrogen receptor signaling', and 'mitochondrial dysfunction' were identified as the canonical pathways that are overrepresented in colonosphere cultures (Table 3).

Next, the STRING database was used to identify known and predicted protein interactions among the upregulated proteins. STRING analysis of all upregulated proteins showed five major clusters involved in redox regulation, transcription control, RNA splicing, DNA replication and regulation of translation initiation (Figure 3).

Given our interest in drug resistance we further focused on proteins regulating cell death and survival (Table 3). An extensive literature search revealed that the majority of overrepresented 'Cell Death' regulators (15/20) have anti-apoptotic activity (Table 4). Of these, Baculoviral IAP repeat-containing 6 (BIRC6; also known as BRUCE or Apollon), an Inhibitor of Apoptosis Protein (IAP), is a key regulator of the intrinsic apoptosis pathway and has previously been implicated in drug resistance[21, 22].

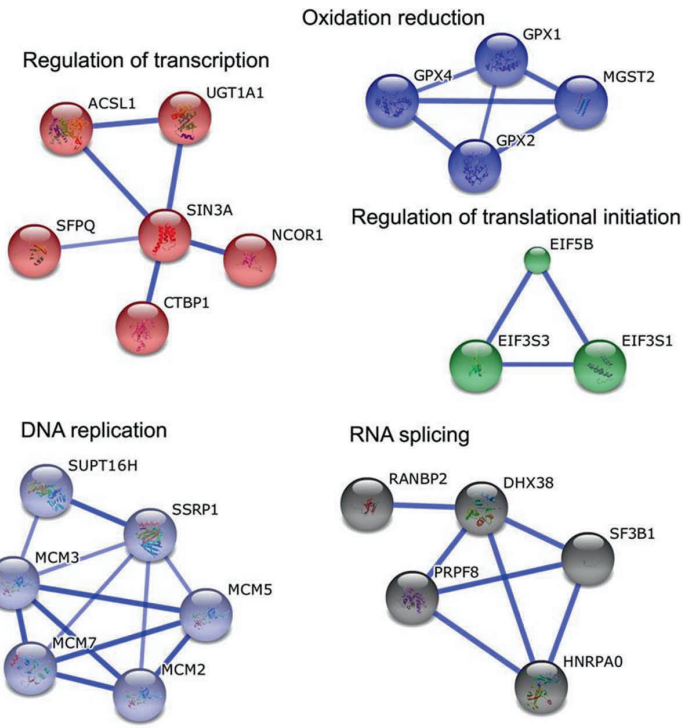

Figure 3. Colonopshere-enriched proteins display functional interactions. All colonosphere-enriched proteins (119) were analyzed against the STRING database for functional protein association networks. The strength of the associations is represented by line thickness. Networks with 3 or more protein interactions are shown. Required confidence (score) of protein association was 0.700 (high confidence).

Table 2. All proteins upregulated in colonospheres in comparison to differentiated tumor cells. The table shows all proteins that are upregulated in colonospheres when compared to differentiated tumor cells according to the following criteria: i) top upregulated, ≥ 2 fold upregulated in 3 out of 3 isogenic pairs (32) and ii) sub-top upregulated, ≥ 1.5 fold upregulated in 3 out of 3 isogenic pairs (22).

>2 fold upregulated proteins in 3/3 combinations											
			L145		**L146**		**L167**				
Protein	**Gene**	**Accession. Number**	**Diff**	**Sph**	**Diff**	**Sph**	**Diff**	**Sph**	**fold change**	**location**	**function**
glutathione peroxidase 2 (gastrointestinal)	GPX2	IPI00298176	0	13	0	23	0	12	∞	Cytoplasm	enzyme
glutathione peroxidase 1	GPX1	IPI00293975	0	10	0	8	0	12	∞	Cytoplasm	enzyme
ferritin, light polypeptide	FTL	IPI00852596	0	4	0	4	0	7	∞	Cytoplasm	other
neuroblastoma amplified sequence	NBAS	IPI00333913	0	5	0	6	0	3	∞	unknown	other
baculoviral IAP repeat-containing 6	BIRC6	IPI00299635	0	4	0	6	0	3	∞	Cytoplasm	enzyme
microsomal glutathione S-transferase 2	MGST2	IPI00017767	0	3	0	4	0	3	∞	Cytoplasm	enzyme
glutathione peroxidase 4 (phospholipid hydroperoxidase)	GPX4	IPI00304814	0	2	0	5	0	3	∞	Cytoplasm	enzyme
eukaryotic translation initiation factor 3, subunit H	EIF3H	IPI00647650	0	3	0	3	0	3	∞	Cytoplasm	translation regulator
CDGSH iron sulfur domain 3	CISD3	IPI00783359	0	2	0	4	0	3	∞	unknown	other
endosulfine alpha	ENSA	IPI00220797	0	3	0	3	0	2	∞	unknown	transporter
family with sequence similarity 98, member A	FAM98A	IPI00174442	0	2	0	2	0	3	∞	unknown	other
RAN binding protein 3	RANBP3	IPI00456728	0	2	0	2	0	3	∞	Nucleus	other
chromosome 11 open reading frame 31	C11ORF31	IPI00218054	0	2	0	2	0	3	∞	Nucleus	other
mitochondrial ribosomal protein S18B	MRPS18B	IPI00022316	0	2	0	3	0	2	∞	Cytoplasm	other
RRS1 ribosome biogenesis regulator homolog (S. cerevisiae)	RRS1	IPI00014253	0	2	0	3	0	2	∞	Nucleus	other
DEAH (Asp-Glu-Ala-His) box polypeptide 38	DHX38	IPI00294211	0	2	0	2	0	2	∞	Nucleus	enzyme
C-terminal binding protein 1	CTBP1	IPI00012835	0	2	0	2	0	2	∞	Nucleus	enzyme
SIN3 homolog A, transcription regulator (yeast)	SIN3A	IPI00170596	0	2	0	2	0	2	∞	Nucleus	transcription regulator
succinate dehydrogenase complex, subunit B, iron sulfur (Ip)	SDHB	IPI00294911	2	5	0	6	0	8	9.2	Cytoplasm	enzyme
RNA binding motif protein 25	RBM25	IPI00004273	0	6	0	5	2	7	8.7	Nucleus	other
E1A binding protein p400	EP400	IPI00064931	2	5	0	7	0	5	8.2	Nucleus	other
myosin, heavy chain 10, non-muscle	MYH10	IPI00397526	0	3	0	4	4	26	8.1	Cytoplasm	other
leucine rich repeat containing 16A	LRRC16A	IPI00014843	0	17	4	10	0	4	7.4	unknown	enzyme
CDC42 binding protein kinase beta (DMPK-like)	CDC42BPB	IPI00477763	2	6	0	4	0	3	6.2	Cytoplasm	kinase
eukaryotic translation initiation factor 3, subunit J	EIF3J	IPI00290461	2	6	0	2	0	3	5.2	Cytoplasm	translation regulator
TAF15 RNA polymerase II, TATA box binding protein (TBP)-associated factor, 68kDa	TAF15	IPI00020194	0	3	0	2	2	5	4.9	Nucleus	transcription regulator
PTK2 protein tyrosine kinase 2	PTK2	IPI00012885	0	3	0	3	2	4	4.8	Cytoplasm	kinase
protein arginine methyltransferase 5	PRMT5	IPI00441473	0	4	0	2	3	7	4.2	Cytoplasm	enzyme
activating signal cointegrator 1 complex subunit 3	ASCC3	IPI00430472	2	6	0	5	2	6	4.1	Nucleus	enzyme
aldehyde dehydrogenase 1 family, member A1	ALDH1A1	IPI00218914	11	76	26	102	45	113	3.4	Cytoplasm	enzyme
mitochondrial ribosomal protein S27	MRPS27	IPI00022002	0	2	2	6	2	6	3.4	Cytoplasm	other
vacuolar protein sorting 13 homolog C (S. cerevisiae)	VPS13C	IPI00465428	9	19	5	13	5	13	2.3	unknown	other

>1.5 fold upregulated proteins in 3/3 combinations											
			L145		L146		L167				
Protein	Gene	Accession. Number	Diff	Sph	Diff	Sph	Diff	Sph	fold change	location	function
adenylosuccinate lyase	ADSL	IPI00026904	0	5	3	5	0	5	4.8	Cytoplasm	enzyme
transmembrane protein 205	TMEM205	IPI00063130	0	5	0	3	3	5	4.2	unknown	other
transformation/transcription domain-associated protein	TRRAP	IPI00069084	5	8	0	7	0	6	4.0	Nucleus	transcription regulator
nuclear receptor co-repressor 1	NCOR1	IPI00289344	0	3	0	4	3	5	3.9	Nucleus	transcription regulator
ATP-binding cassette, sub-family B (MDR/TAP), member 1	ABCB1	IPI00027481	0	7	0	11	9	17	3.8	Plasma Membrane	transporter
CDGSH iron sulfur domain 1	CISD1	IPI00020510	0	3	0	8	6	10	3.4	Cytoplasm	other
methionine adenosyltransferase II, beta	MAT2B	IPI00002324	5	8	0	5	0	5	3.4	Cytoplasm	enzyme
NADH dehydrogenase (ubiquinone) 1 alpha subcomplex, 11, 14.7kDa	NDUFA11	IPI00329301	2	5	0	6	4	6	2.7	Cytoplasm	enzyme
succinate dehydrogenase complex, subunit A, flavoprotein (Fp)	SDHA	IPI00305166	5	18	12	21	6	23	2.6	Cytoplasm	enzyme
15 kDa selenoprotein	SEP15	IPI00030877	3	8	5	9	2	7	2.3	Cytoplasm	enzyme
aldehyde dehydrogenase 1 family, member B1	ALDH1B1	IPI00103467	8	17	15	46	14	22	2.2	Cytoplasm	enzyme
acetyl-CoA acyltransferase 1	ACAA1	IPI00012828	2	11	7	11	9	15	2.0	Cytoplasm	enzyme
eukaryotic translation initiation factor 5B	EIF5B	IPI00299254	6	12	6	11	3	8	2.0	Cytoplasm	translation regulator
heterogeneous nuclear ribonucleoprotein A0	HNRNPA0	IPI00011913	3	10	4	6	5	9	2.0	Nucleus	other
UDP-glucose 6-dehydrogenase	UGDH	IPI00031420	4	22	30	45	19	37	1.9	Nucleus	enzyme
valyl-tRNA synthetase	VARS	IPI00000873	9	24	15	22	14	23	1.8	Cytoplasm	enzyme
tubulin tyrosine ligase-like family, member 12	TTLL12	IPI00029048	6	10	12	27	8	12	1.8	unknown	other
interleukin enhancer binding factor 3, 90kDa	ILF3	IPI00298788	20	32	17	28	13	27	1.7	Nucleus	transcription regulator
carbamoyl-phosphate synthetase 2, aspartate transcarbamylase, and dihydroorotase	CAD	IPI00301263	24	36	33	58	19	33	1.6	Cytoplasm	enzyme
RAN binding protein 2	RANBP2	IPI00221325	28	45	22	35	28	42	1.5	Nucleus	enzyme

Sph = colonosphere culture enriched for cancer stem cells, Diff = isogenic differentiated progeny of colonosphere culture.

Table 3. Ingenuity analysis of colonosphere-enriched proteins. All 119 upregulated proteins were analyzed by Ingenuity. The main Molecular and Cellular functions represented by this protein group are 'Cell Death' (20) and 'Post Translational Modifications' (12). The main canonical pathways represented by this protein group are also shown.

Top functions	Associated molecules	Focus molecules
Molecular and cellular functions		
Cell Death	ABCB1, ALDH1A1, ARMC10, BAX, **BIRC6**, CTBP1, EIF3H, EP400, GPX2, HSPA4, HTT, MCM2, MDC1, PRKDC, PTK2, RBM25, SDHA, SDHB, TIMM50, TRAP1	20
Post-Translational Modification	BAX, CTBP1, FTL, HSPA4, HTT, NEDD8, PRKDC, PRMT5, SEP15, ST13, TIMM50, TTN, ABCB1, ACO2, ADSL, AKR1C3, ALDH1A1, BAX, BDH2, GPX4, HSPA4, HTT, MAT2B, SDHA, TST, UGDH	12

Top functions	Associated molecules	Number of identified molecules	Number of molecules in pathway
Canonical pathways			
Cell Cycle Control of Chromosomal Replication	MCM2, MCM3, MCM5, MCM7	4	30
Aryl Hydrocarbon Receptor Signaling	ALDH1A1, ALDH1B1, BAX, MCM7, MGST2, NEDD8	6	141
Estrogen Receptor Signaling	CTBP1, NCOR1, PRKDC, TAF15, TRRAP	5	134
Mitochondrial Dysfunction	GPX4, NDUFA11, NDUFB11, SDHA, SDHB	5	133

Table 4. Functional annotation of colonosphere-enriched 'Cell Death' proteins.

Protein	Gene	Accession. Number	fold change	anti-apoptotic	pre-apoptotic
glutathione peroxidase 2 (gastrointestinal)	GPX2	IPI00298176	∞	+	
baculoviral IAP repeat-containing 6	**BIRC6**	**IPI00299635**	**∞**	**+**	
eukaryotic translation initiation factor 3, subunit H	EIF3H	IPI00647650	∞	+	
C-terminal binding protein 1	CTBP1	IPI00012835	∞	+	
armadillo repeat containing 10	ARMC10	IPI00217968	∞	+	
succinate dehydrogenase complex, subunit B, iron sulfur	SDHB	IPI00294911	9.2	+	+
RNA binding motif protein 25	RBM25	IPI00004273	8.7	+	+
E1A binding protein p400	EP400	IPI00064931	8.2	+	
PTK2 protein tyrosine kinase 2	PTK2	IPI00012885	4.8	+	
aldehyde dehydrogenase 1 family, member A1	ALDH1A1	IPI00218914	3.4	+	
ATP-binding cassette, sub-family B (MDR), member 1	ABCB1	IPI00027481	3.8	+	
BCL2-associated X protein	BAX	IPI00071059	3.0		+
succinate dehydrogenase complex, subunit A	SDHA	IPI00305166	2.6	+	
Huntingtin	HTT	IPI00002335	∞	+	+
translocase of inner mitochondrial membrane 50	TIMM50	IPI00418497	3.1	+	
mediator of DNA-damage checkpoint 1	MDC1	IPI00470805	2.9	+	+
minichromosome maintenance complex component 2	MCM2	IPI00184330	1.7	+	
TNF receptor-associated protein 1	TRAP1	IPI00030275	1.6	+	
protein kinase, DNA-activated, catalytic polypeptide	PRKDC	IPI00296337	1.4	+	
heat shock 70kDa protein 4	HSPA4	IPI00002966	1.3	+	

The 20 colonosphere-enriched cell death regulators that were identified by Ingenuity were classified according to their pro-and anti-apoptotic function, based on literature.

BIRC6 mediates resistance of colorectal cancer stem cells to platinum compounds

Next, we tested whether BIRC6 plays a role in mediating chemotherapy resistance in colorectal cancer stem cells. First, we analyzed BIRC6 expression in the three sets of isogenic cell pairs by Western blotting. In line with the proteomics data, BIRC6 was highly upregulated in colonospheres when compared to differentiated cells (Figure 4A). Western blot analysis of other top upregulated proteins (GPX2, GPX1, ALDH1) also confirmed the proteomics data (data not shown, and see[16]). Our previous results have shown that ALDH activity (as measured by the fluorescent substrate Aldefluor®) defines the tumorigenic and clonogenic cancer stem cell population within colonospheres[16]. Therefore, we used FACS sorting to separate Aldefluor®^{high} from Aldefluor®^{low} cells (Figure 4B) and analyzed BIRC6 expression in both tumor cell fractions. Figure 4C shows that BIRC6 is highly expressed in tumorigenic Aldefluor®^{high} cells, but not in non-tumorigenic Aldefluor®^{low} cells.

Next, we assessed the importance of BIRC6 in mediating colonosphere resistance to oxaliplatin and cisplatin, two frequently used chemotherapeutic drugs. To this end, expression of BIRC6 was suppressed in colonospheres by using a set of lentiviral RNA interference (RNAi) vectors. Two vectors (58 en 59) were found to suppress BIRC6 expression very efficiently (Figure 5A).

Control and BIRC6 knockdown colonopsheres and differentiated tumor cells were treated with increasing concentrations of oxaliplatin or cisplatin and cell viability was measured by standard MTS assays. Knockdown of BIRC6 resulted in a significantly higher response of colonosphere cells to oxaliplatin and cisplatin (Figure 5B and 5C). The sensitivity of BIRC6 knockdown cells to both drugs was comparable to that of the differentiated tumor cells. These results identify BIRC6 as an important mediator of resistance to oxaliplatin and cisplatin and suggest that high BIRC6 expression may selectively protect the cancer stem cell fraction against these drugs.

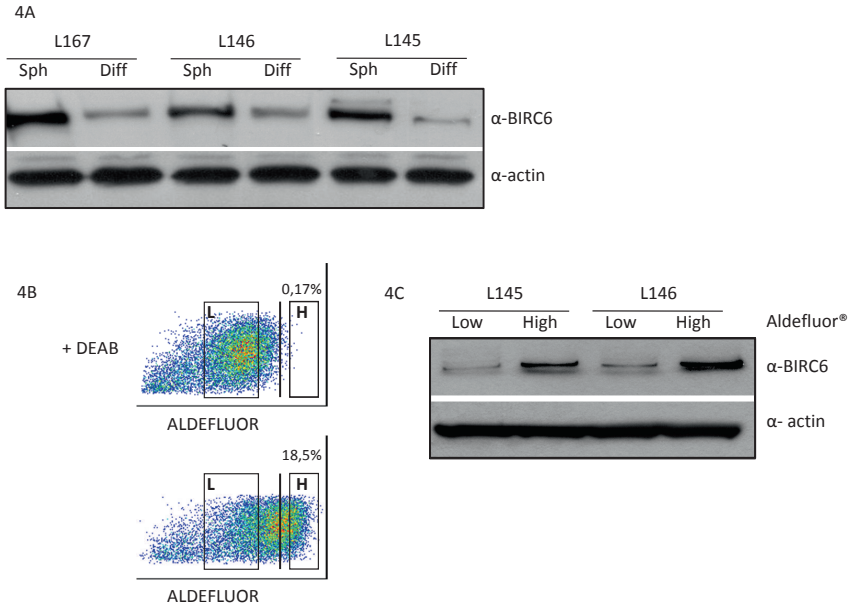

Figure 4. BIRC6 is expressed in the tumorigenic Aldefluor^{high} fraction of colonosphere cells. A. Western blot analysis of BIRC6 levels in colonospheres and differentiated tumor cells in all pairs. B. Single cell cultures of L145 colonospheres were separated into Aldefluor®^{high} and Aldefluor®^{low} cell populations by FACS sorting. C. Western blot analysis of Aldefluor®^{high} and Aldefluor®^{low} cell populations for expression of BIRC6.

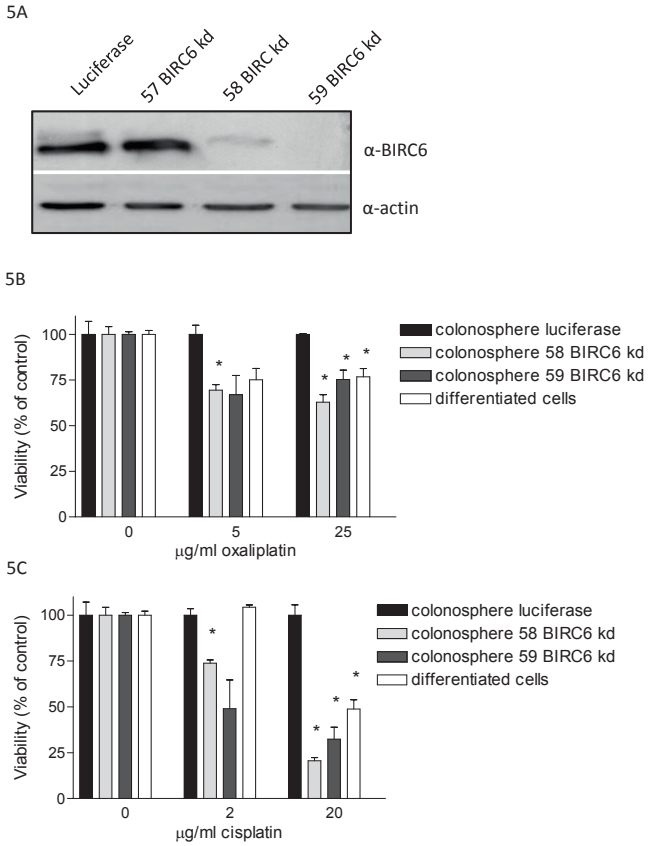

Figure 5. BIRC6 confers resistance against cisplatin and oxaliplatin. A. Western blot analysis of BIRC6 expression in L145 colonospheres transduced with control (luciferase, 57) and BIRC6 knockdown vectors (58, 59). B. Control and BIRC6 knockdown L145 colonospheres were treated with oxaliplatin or cisplatin for 3 days using the indicated concentrations. Cell viability was then assessed by MTS assays for mitochondrial activity. Absorbance values (in triplicate) are expressed as percentage of vehicle-treated control wells. *Statistical significance (unpaired, 2-tailed t test: $p < 0.05$).

DISCUSSION

In the present study we have used a proteomics approach to identify potential regulators of the cancer stem cell phenotype in colorectal tumors. We identified known (ALDH1A1) and novel factors enriched in cancer stem cell cultures (colonospheres) when compared to stably differentiated tumor cells. Interestingly, STRING analysis revealed that distinct protein complexes involved in transcriptional repression, DNA replication, RNA splicing, translation initiation and redox control are significantly enriched in colonospheres when compared to differentiated tumor cells. Future work should reveal the function of these complexes in the maintenance of colorectal cancer stem cells.

Importantly, cancer stem cells were also characterized by high expression of a set of survival proteins, the most prominent of which was BIRC6. BIRC6 deletion is associated with sensitization

to chemotherapy in *in vivo* and *in vitro studies* [20, 21]. Furthermore, BIRC6 deletion promotes p53 stabilization and caspase 3 activation [223].

Our data show that specifically colorectal cancer stem cell cultures display increased resistance to oxaliplatin and to cisplatin and that BIRC6 is an important mediator of resistance. Previously, it was shown by gene expression profiling that BIRC1 and BIRC6 are upregulated in colorectal tumors when compared to normal intestinal issue[23]. Our results suggest that it is predominantly the cancer stem cell-fraction in colorectal tumors that expresses this survival protein.

BIRC6, also known as Apollon or Bruce, belongs to the family of inhibitor of apoptosis (IAP) proteins. IAP's are major regulators of apoptosis due, at least in part, to their ability to inhibit caspase activation[24, 25]. Human IAP family members include X-chromosome–linked IAP (XIAP, also known as BIRC4), cellular IAP 1 (c-IAP1 also known as BIRC2), c-IAP2 (also known as BIRC3), neuronal apoptosis inhibitory protein (also known as BIRC1) and survivin (also known BIRC5). IAP proteins contain one to three baculovirus IAP repeat (BIR) domains that are required for their anti-apoptotic activity [245]. Our results are in line with previous studies showing that cancer stem cells express high levels of anti-apoptotic proteins and resist apoptotic stimuli[26, 27]. Recently it was demonstrated that IL4-stimulated expression of survivin (BIRC5) protects colorectal cancer stem cells against apoptosis[10, 27, 28]. The proteomics approach described here did not identify BIRC5 as a cancer stem cell-enriched protein. Possibly, different tumors resist apoptotic stimuli by increasing the expression of distinct IAP family members.

Since IAP's play an important role in tumor maintenance and therapy resistance they represent attractive targets for targeted therapy. Furthermore, IAP's are highly expressed in several cancer tissues [30]. Several small molecule IAP inhibitors have been developed, including Smac-based peptides and Smac mimetics targeting a broad spectrum of IAP's[29, 30]. Pre-clinical studies in mice carrying xenograft tumors have shown promising anti-tumor efficacy in the treatment of malignant glioma, breast cancer, non–small cell lung cancer, and multiple myeloma. However, most of these preclinical studies have focused on BIRC4 and surviving (BIRC5), rather than on BIRC6[31, 32]. Several IAP inhibitors are being tested for their safety and anti-tumor efficacy in clinical trials either in combination with irradiation or with chemotherapy[33, 34]. It is not yet established whether these compounds also target BIRC6. SMAC mimetics bind to and inhibit the BIR domains in IAP's. Since SMAC also binds to BIRC6[357], it is not unlikely that SMAC mimetics will inhibit BIRC6.

Based on the data presented here we propose that BIRC6 protects the cancer stem cell fraction of colorectal tumors against oxaliplatin and cisplatin. Targeting BIRC6 by SMAC mimetics or by novel specific BIRC6 inhibitors may therefore be effective in combination with platinum-based anticancer drugs. This may help eradicating the cancer stem cell fraction in colorectal tumors.

REFERENCE LIST

1. Chau,I. & Cunningham,D. Treatment in advanced colorectal cancer: what, when and how? *Br. J. Cancer*(2009).
2. Ricci-Vitiani,L. *et al.* Identification and expansion of human colon-cancer-initiating cells. *Nature* 445, 111-115 (2007).
3. O'Brien,C.A. *et al.* A human colon cancer cell capable of initiating tumour growth in immunodeficient mice. *Nature* 445, 106-110 (2007).
4. Todaro,M. *et al.* Colon cancer stem cells: promise of targeted therapy. *Gastroenterology* 138, 2151-2162 (2010).
5. Vermeulen,L. *et al.* Single-cell cloning of colon cancer stem cells reveals a multi-lineage differentiation capacity. *Proc. Natl. Acad. Sci. U. S. A* 105, 13427-13432 (2008).
6. Barker,N. *et al.* Crypt stem cells as the cells-of-origin of intestinal cancer. *Nature* 457, 608-611 (2009).
7. Zhu,L. *et al.* Prominin 1 marks intestinal stem cells that are susceptible to neoplastic transformation. *Nature* 457, 603-607 (2009).
8. Clarke,M.F. *et al.* Cancer stem cells--perspectives on current status and future directions: AACR Workshop on cancer stem cells. *Cancer Res.* 66, 9339-9344 (2006).
9. Hamburger,A.W. & Salmon,S.E. Primary bioassay of human tumor stem cells. *Science* 197, 461-463 (1977).
10. Todaro,M. *et al.* Colon cancer stem cells dictate tumor growth and resist cell death by production of interleukin-4. *Cell Stem Cell* 1, 389-402 (2007).
11. Dylla,S.J. *et al.* Colorectal cancer stem cells are enriched in xenogeneic tumors following chemotherapy. *PLoS. ONE.* 3, e2428 (2008).
12. Dean,M. *et al.* Tumour stem cells and drug resistance. *Nat. Rev. Cancer* 5, 275-284 (2005).
13. Dean,M. ABC transporters, drug resistance, and cancer stem cells. *J. Mammary. Gland. Biol. Neoplasia.* 14, 3-9 (2009).
14. Liu,G. *et al.* Analysis of gene expressio! and chemoresistance of CD133+ cancer stem cells in glioblastoma. *Mol. Cancer* 5, 67 (2006).
15. Hermann,P.C. *et al.* Distinct populations of cancer stem cells determine tumor growth and metastatic activity in human pancreatic cancer. *Cell Stem Cell* 1, 313-323 (2007).
16. Emmink BL *et al.* Differentiated colorectal cancer cells protect tumor-initiating cells from irinotecan. Gastroenterology in press. 2011.
17. Shevchenko,A. *et al.* Mass spectrometric sequencing of proteins silver-stained polyacrylamide gels. *Anal. Chem.* 68, 850-858 (1996).
18. Shevchenko,A. *et al.* Mass spectrometric sequencing of proteins silver-stained polyacrylamide gels. *Anal. Chem.* 68, 850-858 (1996).
19. Huang,E.H. *et al.* Aldehyde dehydrogenase 1 is a marker for normal and malignant human colonic stem cells (SC) and tracks SC overpopulation during colon tumorigenesis. *Cancer Res.* 69, 3382-3389 (2009).
20. Chu,L. *et al.* Oncolytic adenovirus-mediated shRNA against Apollon inhibits tumor cell growth and enhances antitumor effect of 5-fluorouracil. *Gene Ther.* 15, 484-494 (2008).
21. Chen,Z. *et al.* A human IAP-family gene, apollon, expressed in human brain cancer cells. *Biochem. Biophys. Res. Commun.* 264, 847-854 (1999).
22. Lopergolo,A. *et al.* Apollon gene silencing induces apoptosis in breast cancer cells through p53 stabilisation and caspase-3 activation. *Br. J. Cancer* 100, 739-746 (2009).
23. Bianchini,M. *et al.* Comparative study of gene expression by cDNA microarray in human colorectal cancer tissues and normal mucosa. *Int. J. Oncol.* 29, 83-94 (2006).
24. Salvesen,G.S. & Duckett,C.S. IAP proteins: blocking the road to death's door. *Nat. Rev. Mol. Cell Biol.* 3, 401-410 (2002).
25. Deveraux,Q.L. *et al.* Endogenous inhibitors of caspases. *J. Clin. Immunol.* 19, 388-398 (1999).
26. Eramo,A. *et al.* Chemotherapy resistance of glioblastoma stem cells. *Cell Death. Differ.* 13, 1238-1241 (2006).
27. Signore,M. *et al.* Targeting apoptosis pathways in cancer stem cells. *Cancer Lett.*(2011).
28. Di Stefano,A.B. *et al.* Survivin is regulated by interleukin-4 in colon cancer stem cells. *J. Cell Physiol* 225, 555-561 (2010).
29. Chen,D.J. & Huerta,S. Smac mimetics as new cancer therapeutics. *Anticancer Drugs* 20, 646-658 (2009).

30. Flygare,J.A. & Fairbrother,W.J. Small-molecule pan-IAP antagonists: a patent review. *Expert. Opin. Ther. Pat* 20, 251-267 (2010).
31. Oost,T.K. *et al.* Discovery of potent antagonists of the antiapoptotic protein XIAP for the treatment of cancer. *J. Med. Chem.* 47, 4417-4426 (2004).
32. Fulda,S. *et al.* Smac agonists sensitize for Apo2L/T. *Nat. Med.* 8, 808-815 (2002).
33. Gyrd-Hansen,M. & Meier,P. IAPs: from caspase inhibitors to modulators of NF-kappaB, inflammation and cancer. *Nat. Rev. Cancer* 10, 561-574 (2010).
34. Fulda,S. Targeting inhibitor of apoptosis proteins (IAPs) for cancer therapy. *Anticancer Agents Med. Chem.* 8, 533-539 (2008).
35. Chen,D.J. & Huerta,S. Smac mimetics as new cancer therapeutics. *Anticancer Drugs* 20, 646-658 (2009).

SUPPLEMENTARY TABLES

Supplementary Table 1. All proteins upregulated in colonospheres in comparison to differentiated tumor cells. The table shows all proteins (rest group) that are ≥ 1.5 fold upregulated in colonospheres when compared to differentiated tumor cells in 2 out of 3 isogenic pairs (65).

>1.5 fold upregulated proteins in 2/3 combinations											
			L145		**L146**		**L167**				
Protein		**Accession. Number**	**Diff**	**Sph**	**Diff**	**Sph**	**Diff**	**Sph**	**fold change**	**location**	**function**
3-hydroxybutyrate dehydrogenase, type 2	BDH2	IPI00607799	0	0	0	4	0	6	∞	Cytoplasm	enzyme
Huntingtin	HTT	IPI00002335	0	0	0	6	0	4	∞	Cytoplasm	transcription regulator
drebrin 1	DBN1	IPI00003406	0	0	0	4	0	5	∞	Cytoplasm	other
leucine zipper transcription factor-like 1	LZTFL1	IPI00299465	0	5	0	0	0	4	∞	unknown	other
DC2 protein	DC2	IPI00183603	0	0	0	4	0	4	∞	Cytoplasm	other
methyltransferase like 7B	METTL7B	IPI00090807	0	6	0	0	0	2	∞	unknown	enzyme
titin	TTN	IPI00023283	0	3	0	5	0	0	∞	Cytoplasm	peptidase
signal recognition particle 54kDa	SRP54	IPI00009822	0	0	0	4	0	3	∞	Cytoplasm	other
COP9 constitutive photomorphogenic homolog subunit 4 (Arabidopsis)	COPS4	IPI00171844	0	4	0	0	0	3	∞	Cytoplasm	other
mannosidase, alpha, class 2A, member 1	MAN2A1	IPI00003802	0	4	0	3	0	0	∞	Cytoplasm	enzyme
YLP motif containing 1	YLPM1	IPI00165434	0	2	0	0	0	5	∞	Nucleus	other
lysophosphatidylcholine acyltransferase 3	LPCAT3	IPI00306419	0	3	0	0	0	3	∞	Plasma Membrane	other
biorientation of chromosomes in cell division 1-like	BOD1L	IPI00386211	0	3	0	0	0	3	∞	unknown	other
NADH dehydrogenase (ubiquinone) 1 beta subcomplex, 11, 17.3kDa	NDUFB11	IPI00472058	0	3	0	3	0	0	∞	Cytoplasm	enzyme
hornerin	HRNR	IPI00398625	0	3	0	3	0	0	∞	Cytoplasm	other
chromobox homolog 1 (HP1 beta homolog Drosophila)	CBX1	IPI00010320	0	0	0	2	0	4	∞	Nucleus	other
thimet oligopeptidase 1	THOP1	IPI00549189	0	0	0	2	0	4	∞	Cytoplasm	peptidase
replication factor C (activator 1) 1, 145kDa	RFC1	IPI00375358	0	0	0	2	0	4	∞	Nucleus	transcription regulator
armadillo repeat containing 10	ARMC10	IPI00217968	0	2	0	4	0	0	∞	Cytoplasm	other
ER lipid raft associated 1	ERLIN1	IPI00007940	0	2	0	4	0	0	∞	Plasma Membrane	other
olfactomedin 4	OLFM4	IPI00022255	6	15	0	38	0	0	8.5	unknown	other
proteasome (prosome, macropain) 26S subunit, non-ATPase, 8	PSMD8	IPI00010201	3	4	0	4	0	7	4.8	Cytoplasm	other
adaptor-related protein complex 1, sigma 1 subunit	AP1S1	IPI00152898	2	2	0	3	0	5	4.8	Cytoplasm	transporter
MDN1, midasin homolog (yeast)	MDN1	IPI00167941	5	5	0	15	2	9	4.0	Nucleus	other
neural precursor cell expressed, developmentally down-regulated 8	NEDD8	IPI00020008	0	4	3	4	0	4	3.9	Nucleus	enzyme
adaptor-related protein complex 3, beta 1 subunit	AP3B1	IPI00021129	3	4	0	3	0	5	3.8	Cytoplasm	transporter
acyl-CoA binding domain containing 3	ACBD3	IPI00009315	3	7	0	5	0	0	3.8	Cytoplasm	other

>1.5 fold upregulated proteins in 2/3 combinations												
			L145		L146		L167					
Protein		Accession. Number	Diff	Sph	Diff	Sph	Diff	Sph	fold change	location	function
A kinase (PRKA) anchor protein (yotiao) 9	AKAP9	IPI00019223	6	8	0	7	0	7	3.5	Cytoplasm	other
ATPase type 13A1	ATP13A1	IPI00034277	0	4	0	6	4	4	3.4	Extracellular Space	transporter
acyl-CoA synthetase long-chain family member 1	ACSL1	IPI00012728	2	10	3	3	0	4	3.2	Cytoplasm	enzyme
translocase of inner mitochondrial membrane 50 homolog	TIMM50	IPI00418497	8	8	0	8	0	10	3.1	Cytoplasm	phosphatase
BCL2-associated X protein	BAX	IPI00071059	6	8	0	4	0	7	3.0	Cytoplasm	other
structure specific recognition protein 1	SSRP1	IPI00005154	8	6	2	10	0	15	3.0	Nucleus	other
mediator of DNA-damage checkpoint 1	MDC1	IPI00470805	4	2	2	7	0	9	2.9	Nucleus	other
minichromosome maintenance complex component 5	MCM5	IPI00018350	5	5	3	11	2	12	2.7	Nucleus	enzyme
phosphofructokinase, muscle	PFKM	IPI00465179	0	6	9	11	0	5	2.4	Cytoplasm	kinase
SON DNA binding protein	SON	IPI00000192	9	12	0	6	0	4	2.3	Nucleus	other
UDP glucuronosyltransferase 1 family, polypeptide A6	UGT1A6	IPI00451965	0	7	11	19	0	0	2.3	Cytoplasm	enzyme
LUC7-like 2 (S. cerevisiae)	LUC7L2	IPI00006932	0	8	5	5	4	8	2.3	unknown	other
thiosulfate sulfurtransferase (rhodanese)	TST	IPI00216293	0	12	7	15	10	12	2.2	Cytoplasm	enzyme
cytochrome P450, family 51, subfamily A, polypeptide 1	CYP51A1	IPI00295772	4	4	2	9	4	10	2.2	Cytoplasm	enzyme
aldo-keto reductase family 1, member C3	AKR1C3	IPI00291483	0	15	17	29	4	2	2.1	Cytoplasm	enzyme
aconitase 2, mitochondrial	ACO2	IPI00017855	7	18	18	43	14	17	1.9	Cytoplasm	enzyme
nipsnap homolog 1 (C. elegans)	NIPSNAP1	IPI00304435	2	6	6	16	9	11	1.9	Cytoplasm	enzyme
minichromosome maintenance complex component 3	MCM3	IPI00013214	8	8	8	15	3	14	1.9	Nucleus	enzyme
suppression of tumorigenicity 13 (colon carcinoma) (Hsp70 interacting protein)	ST13	IPI00032826	4	5	7	11	4	13	1.9	Cytoplasm	other
general transcription factor IIi	GTF2I	IPI00054042	12	20	12	16	7	24	1.9	Nucleus	transcription regulator
suppressor of Ty 16 homolog (S. cerevisiae)	SUPT16H	IPI00026970	18	26	12	28	15	32	1.8	Nucleus	transcription regulator
minichromosome maintenance complex component 7	MCM7	IPI00299904	14	7	6	17	2	17	1.8	Nucleus	enzyme
spectrin repeat containing, nuclear envelope 2	SYNE2	IPI00239405	22	43	3	20	22	24	1.8	Nucleus	other
minichromosome maintenance complex component 2	MCM2	IPI00184330	14	10	6	18	6	18	1.7	Nucleus	enzyme
PRP8 pre-mRNA processing factor 8 homolog (S. cerevisiae)	PRPF8	IPI00007928	32	46	26	48	28	50	1.6	Nucleus	other
solute carrier family 12 (sodium/ potassium/chloride transporters), member 2	SLC12A2	IPI00022649	22	55	16	41	39	33	1.6	Plasma Membrane	transporter
TNF receptor-associated protein 1	TRAP1	IPI00030275	22	20	17	34	16	35	1.6	Cytoplasm	enzyme

>1.5 fold upregulated proteins in 2/3 combinations												
			L145		L146		L167					
Protein		Accession. Number	Diff	Sph	Diff	Sph	Diff	Sph	fold change	location	function
ubiquitin specific peptidase 5 (isopeptidase T)	USP5	IPI00024664	17	32	14	17	7	13	1.6	Cytoplasm	peptidase
phosphoribosylglycinamide formyltransferase,	GART	IPI00025273	33	42	26	42	13	29	1.5	Cytoplasm	enzyme
carcinoembryonic antigen-related cell adhesion molecule 5	CEACAM5	IPI00027486	0	15	15	24	28	27	1.5	Plasma Membrane	other
methylenetetrahydrofolate dehydrogenase (NADP+ dependent) 1,	MTHFD1	IPI00218342	33	42	24	40	18	32	1.5	Cytoplasm	enzyme
protein disulfide isomerase family A, member 4	PDIA4	IPI00009904	50	75	88	119	62	107	1.5	Cytoplasm	enzyme
splicing factor proline/glutamine-rich	SFPQ	IPI00010740	16	32	25	30	16	24	1.5	Nucleus	other
protein kinase, DNA-activated, catalytic polypeptide	PRKDC	IPI00296337	187	198	110	199	178	303	1.4	Nucleus	kinase
splicing factor 3b, subunit 1, 155kDa	SF3B1	IPI00026089	22	36	23	30	19	27	1.4	Nucleus	other
dynein, cytoplasmic 1, heavy chain 1	DYNC1H1	IPI00456969	176	199	129	213	131	210	1.4	Cytoplasm	peptidase
heat shock 70kDa protein 4	HSPA4	IPI00002966	68	70	27	56	20	36	1.3	Cytoplasm	other
epiplakin 1	EPPK1	IPI00010951	35	89	82	43	58	102	1.3	Cytoplasm	other

Sph = colonosphere culture enriched for cancer stem cells, Diff = isogenic differentiated progeny of colonosphere culture.

5

THE SECRETOME OF COLON CANCER STEM CELLS CONTAINS DRUG-METABOLIZING ENZYMES

Benjamin L Emmink[1], André Verheem[1], Winan J van Houdt[1], Ernst JA Steller[1], Klaas M Govaert[1], Thang V Pham[2], Sander R Piersma[2], Inne HM Borel Rinkes[1], Connie R Jimenez[2] and Onno Kranenburg[1]

[1]Department of Surgery, University Medical Center Utrecht, The Netherlands
[2]OncoProteomics Laboratory, VU Medical Center Amsterdam, The Netherlands

Journal of Proteomics. 2013 Jul 5; 91C:84-96

ABSTRACT

Drug-resistant cancer stem cells (CSCs) have been implicated in tumor recurrence following chemotherapy. However, the contribution of CSCs to drug-resistance in colorectal cancer is unclear and CSC-intrinsic drug-resistance mechanisms are ill-defined. Here, we address these issues by proteomic analysis of the secretomes of CSCs and isogenic differentiated tumor cells (DTCs) isolated from three distinct metastasized colon tumors.

Mass spectrometry-based proteomics identified 1254 unique proteins in the conditioned media of the paired CSC and DTC cultures. Ingenuity Pathway Analysis revealed that proteins governing 'Cell Death' were most significantly enriched in the CSC secretome. The vast majority of these (37/43) promote cell survival. The CSC secretome is also characterized by a pro-survival Nrf2 antioxidant signature. Interestingly, proteome-maintenance networks are highly enriched in the CSC secretome. CSCs also secrete high levels of drug-metabolizing enzymes, including aldehyde dehydrogenase 1 (ALDH1A1) and bleomycin hydrolase (BLMH). We show that these enzymes cause extracellular detoxification of maphosphamide and bleomycin respectively.

We conclude that colorectal CSCs are characterized by extensive survival and anti-oxidant networks, which are likely to contribute to CSC-intrinsic drug-resistance. In addition, CSCs may modulate drug responses in nearby tumor cells by detoxifying chemotherapeutic drugs in the extracellular space.

BIOLOGICAL SIGNIFICANCE

Cancer stem cells are thought to play an important role in mediating drug resistance and tumor recurrence following chemotherapy. Therefore, it is important to identify the factors that are secreted by them. Our results provide novel insights into the pathways that govern the intrinsic resistance of CSCs to chemotherapy and, furthermore, demonstrate that they can also inactivate chemotherapeutic drugs in the extracellular space. A better understanding of the pathways that govern drug resistance in CSCs may help in developing effective CSC-targeting drugs.

HIGHLIGHTS

- Secretome analysis of cancer stem cells and differentiated tumor cells
- Survival proteins are enriched in the cancer stem cell secretome
- Cancer stem cells secrete high levels of drug-metabolizing enzymes
- Secreted drug-metabolizing enzymes detoxify drugs in the extracellular space
- Cancer stem cells may protect nearby non-CSCs from cytotoxic chemotherapy

INTRODUCTION

Colorectal cancer (CRC) is one of the leading causes of cancer-related deaths worldwide[1]. In recent years, the prognosis of patients with advanced disease has improved, mainly due to the addition of new targeted drugs to standard treatment regimens[2-5]. However, CRC is characterized by highly divergent tumor responses, and primary and acquired drug resistance is frequently observed.

Colorectal tumors are hierarchically organized with a minor cancer stem cell (CSC) pool driving the formation of more differentiated less malignant cells making up the bulk of the tumor[6-9]. CSCs have also been implicated in drug resistance and tumor recurrence although the nature of this relationship is only beginning to be clarified. Colorectal CSCs display relative resistance to oxaliplatin and 5-fluorouracil[10-12]. We recently identified BIRC6, an Inhibitor of Apoptosis Protein (IAP) as a CSC-intrinsic factor that contributes to resistance against platinum drugs[12]. Likewise, CSCs from other tumor types appear to be generally drug resistant[13]. Treatment of mice bearing colorectal tumor xenografts can cause a dramatic enrichment of CSCs in post-therapy tumor tissue[10,14]. Likewise, post-treatment tumors in breast cancer patients are also characterized by high CSC numbers, suggesting selective CSC-intrinsic drug resistance[15,16]. Nevertheless, the extent of chemotherapy-induced 'selection' for CSCs varies dramatically between studies, indicating that other mechanisms must play a role. Indeed, resistance of colorectal tumors to Irinotecan is mediated by differentiated cells expressing the drug efflux pump ABCB1[17]. This keeps intra-tumor drug concentrations low and allows CSCs and non-CSCs to survive treatment.

Embryonic SCs contain several genome protection mechanisms, including high expression of DNA repair and anti-oxidant enzymes[18]. Breast CSCs also express high levels of anti-oxidant enzymes that help prevent DNA damage and consequent CSC 'exhaustion'[19]. Furthermore, multiple (C)SC populations, including colorectal CSCs, are characterized by a low proliferation rate, which limits replication-associated DNA damage[20]. Normal SCs of the intestine are an exception as they are actively cycling.

Interestingly, factors secreted by cancer cells can also play a major role in the acquisition of drug resistance. For example, interleukin-4 produced by colorectal cancer cells is a major cytoprotective cytokine that mediates resistance against 5-fluorouracil and oxaliplatin[11]. In addition, the culture supernatant from drug-resistant pancreas carcinoma cells can protect drug-sensitive cells to chemotherapy[21]. In breast cancer, secreted interleukin-6 and -18 contribute to drug resistance[22,23]. Thus, secreted factors in multiple tumor types can modulate drug resistance. In addition, analysis of secreted factors also provides insight into intracellular processes, as many tumor cells shed intracellular and even nuclear proteins into the extracellular space[24].

Given the central role that CSCs are thought to play in mediating drug resistance it is important to identify the plethora of factors that are secreted by them (the 'secretome'). Therefore, we set out to identify secretome differences between paired cultures of highly tumorigenic CSCs and their isogenic non-tumorigenic differentiated progeny. Bioinformatic analysis of the resulting protein lists revealed enrichment of several CSC protection pathways. In addition, we identified several CSC-secreted drug-modifying enzymes that are shown to modulate drug responsiveness of nearby non-CSCs.

EXPERIMENTAL PROCEDURES

Collection, isolation and expansion of colorectal cancer stem cells and differentiated tumor cells

Collection of tumor specimens was performed as described[12,17]. In short, human colorectal tumor specimens were obtained from patients undergoing a liver resection for metastatic adenocarcinoma, in accordance with the ethical committee on human experimentation. Informed consent was obtained from all patients. The obtained tissue fragments were washed extensively with phosphate-buffered saline and were mechanically dissociated using scalpels and vigorous trituration to yield small fragments (< 1 mm3) and single cells. Enzymatic digestion was performed using thermolysin 0.05% (Sigma, Type X) in Dulbecco's modified Eagle's medium/F12 containing 5 mm HEPES (Invitrogen, Carlsbad, CA) for 2 h at 37 °C. The suspension was then filtered through a 40-µm-pore size nylon cell strainer (BD Falcon) to separate the tissue fragments from the single cells. The single cell suspension was cultured in advanced Dulbecco's modified Eagle's medium/F12 (Invitrogen) supplemented with 0.6% glucose (BDH Lab. Supplies), 2 mm l-glutamine (Biowhittaker, Rockland, ME), 9.6 µg/ml putrescin (Sigma), 6.3 ng/ml progesterone (Sigma), 5.2 ng/ml sodium selenite (Sigma), 25 µg/ml insulin (Sigma), 100 µg/ml apotransferrin (Sigma), 5 mm HEPES (Invitrogen), 0.005 µg/ml trace element A (Cellgro), 0.01 µg/ml trace element B (Cellgro), 0.01 µg/ml trace element C (Cellgro), 100 µm β-mercaptoethanol (Merck), 10 ml antibiotic–antimycotic (Invitrogen), 4 µg/ml gentamicine (Invitrogen), 0.002% lipid mixture (Sigma), 5 µg/ml glutathione (Roche), and 4 µg/ml Heparin (Sigma). Growth factors (20 ng/ml EGF (Invitrogen) and 10 ng/ml b-FGF (Abcam, Cambridge, UK)) were added to the cell culture medium freshly each week. All cell cultures were carried out in nontissue culture treated flasks (BD Falcon) at 37 °C in a 5% CO2 humidified incubator. In vitro differentiation was induced by culturing colon CSC cultures for 3 weeks on collagen-coated dishes in Dulbecco's modified Eagle's medium/F12 (GIBCO) supplemented with 20% fetal bovine serum. Passage numbers of the clones used (n = 10) CSC cultures and the accompanying differentiated tumor cell cultures were all below 15.

Protein extraction from conditioned medium

All differentiated cell cultures were washed three times with serum-free medium to remove all serum residues. Paired CSC and differentiated TC cultures were seeded in 10 cm2 dishes and cultured for 48 h in serum-free Stem Cell Medium (described in[17]). After incubation, the conditioned medium of both cultures was collected. Floating cells and cellular debris were removed by centrifugation (2000 rpm, 5 min at 4 °C) and filtration using a 0.22 µm pore size filter. The resulting conditioned medium was concentrated by ultrafiltration using "Amicon Ultra-15" (3 kDa cutoff) centrifugal filter devices according to the manufacturer's instructions (Millipore). Proteinase inhibitors were added to the secreted proteins. Equal amounts of protein (50 µg) were separated on NuPAGE Novex Bis-Tris Mini Gels (Invitrogen). Gels were stained with Coomassie brilliant blue G-250 (Pierce, Rockford, IL) washed and each lane was sliced into ten bands using a band pattern to guide the slicing. The gel slicing and in-gel digestion were performed in a laminar flow under keratin-free conditions.

In-gel digestion

Before MS analysis, separated proteins were in-gel digested as described[12]. Gel lanes corresponding to the different protein samples were sliced into ten bands. Cysteine bonds were reduced with

10 mM dithiotreitol for 1 h at 56 °C and alkylated with 50 mM iodoacetamide for 45 min at RT in the dark. Subsequently proteins were digested with 0.06 µg/µl trypsin o/n at 25 °C. Details can be found in[12].

NanoLC–MS/MS analysis

Peptides were separated by an Ultimate 3000 nanoLC–MS/MS system (Dionex LC-Packings, Amsterdam, The Netherlands) as described previously[12]. Eluting peptides were ionized at 1.7 kV in a Nanomate Triversa Chip-based nanospray source using a Triversa LC coupler (Advion, Ithaca, NJ). Intact peptide mass spectra and fragmentation spectra were acquired on a LTQ-FT hybrid mass spectrometer (Thermo Fisher, Bremen, Germany). Intact masses were measured at resolution 50.000 in the ICR cell, MS/MS spectra were acquired in the linear ion trap in a top 5 experiment. Instrument settings can be found in[12].

Database searching, statistics and Ingenuity Pathway Analysis

MS/MS spectra were searched against the human IPI database 3.31 (67511 entries) using Sequest (version 27, rev 12), which is part of the BioWorks 3.3 data analysis package (Thermo Fisher, San Jose, CA). MS/MS spectra were searched with a maximum allowed deviation of 10 ppm for the precursor mass and 1 amu for the fragment masses. Methionine oxidation and cysteine carboxamidomethylation were allowed as variable modifications, two missed cleavages were allowed and the minimum number of tryptic termini was 1. After database searching the DTA and OUT files were imported into Scaffold 2.01.01 (Proteome software, Portland, OR). Scaffold was used to organize the gel-band data and to validate peptide identifications using the Peptide Prophet algorithm[25]. Only peptide identifications with a probability > 95% were retained. Subsequently, the ProteinProphet algorithm[26] was applied and protein identifications with a probability of > 99% with 2 peptides or more in at least one of the samples were retained. Proteins that contained similar peptides and could not be differentiated based on MS/MS analysis alone were grouped. For each protein identified, the number of spectral counts (identified MS/MS spectra) in each sample (10 gel bands) was exported to Excel. Spectral counts were normalized by dividing the spectral counts per protein by the sum of all counts per sample and multiplying by the average sum across all samples. The list of differentially expressed proteins, including fold changes was imported in the online software package Ingenuity (Ingenuity IPA, version 7.6) and pathway and network analysis was performed with only direct relationships. Furthermore the list of differentially expressed proteins was imported in the online STRING database of known and predicted protein interactions. The interactions include direct (physical) and indirect (functional) associations between proteins. Confidence levels were set to high.

Validation of mass-spectrometry results by Western blotting

Preparation and collection of conditioned medium of CSC and differentiated tumor cell cultures were done as described above in Protein extraction from conditioned medium. Lysates of CSC-cultures and their isogenic differentiated tumor cell offspring were prepared in lysis buffer (20 mM HEPES pH 7.4, 1% NP40, 150 mM NaCl, 5 mM MgCl2, 10% glycerol). Equal amounts of protein derived from lysates and conditioned medium were run out on NuPAGE Novex Tris-Acetate Mini Gel (Invitrogen) and were analyzed by Western blotting using antibodies directed against ALDH1A1 (Abcam, Cambridge, UK), BLMH (Sigma-Aldrich, Zwijndrecht, NL) and β-Actin (AC-15, Novus Biologicals, Littleton, CO, USA).

Maphosphamide and bleomycin cytotoxicity assays

CSC-cultures and their differentiated progeny were cultured in the presence of maphosphamide (Niomech — IIT GmbH, Bielefeld, Germany) or bleomycin (PHARMACHEMIE B, Haarlem) at the indicated concentrations for 72 h. In addition, for both maphosphamide and bleomycin experiments, differentiated TCs were treated with conditioned medium derived from CSC-cultures. Conditioned medium was harvested from CSC-cultures after 48 h of culturing. Mitochondrial activity was evaluated using CellTiter 96® AQueous Non-Radioactive Cell Proliferation Assay (MTS) (Promega). All absorbance values are expressed as percentages of vehicle-treated control wells.

Flow cytometry and cell sorting

Dead cells were excluded using viability marker 7-aminoactinomycin D (7-AAD) (R&D, Detroit, MI) and cell doublets and clumps were excluded using doublet discrimination gating. Aldefluor®-positive cells were analyzed according to the manufacturer's protocol by using Aldefluor® and DEAB (STEMCELL Technologies). The cell sorting experiments were conducted with FACS Aria IIU (BD), using FACS Diva version 6.1 software.

Statistical analysis

The paired beta-binomial test was used to analyze fold changes and statistically significant differences between spectral count data generated from CSC and their differentiated tumor cells. This statistical test takes into account both technical variation and biological variation within a single statistical framework[27]. The Student t test (unpaired, 2-tailed) was performed to analyze statistically significant differences between groups (GraphPad, San Diego, CA). Differences with a p-value of less than .05 were considered statistically significant.

RESULTS

Overlap between the CSC secretome and proteome

We have previously reported on the isolation and characterization of cancer stem cell (CSC)-enriched tumor cell cultures from human colorectal tumors (colonospheres) and the stably differentiated cultures that were derived from them[12,17]. Three of these paired cultures were used to analyze potential differences in the collection of proteins secreted by CSCs and their differentiated offspring respectively. The total of secreted proteins is frequently referred to as the 'secretome'. Conditioned medium from all six cell cultures was collected and run out on a SDS-PAGE gel (Fig. 1A). After tryptic digestion the eluted peptides were analyzed by nanoLC–MS/MS. The total number of unique proteins identified in all secretomes was 1254. Of these, 547 were expressed in all three pairs and 268 proteins in two of the three pairs (Fig. 1B). Unsupervised clustering of all six cell cultures shows that the isogenic pairs cluster together (Fig. 1C). Supervised clustering on the basis of proteins enriched in CSC cultures (Table 1, Supplemental Table 1) shows that all CSC cultures and differentiated cultures now cluster together (Fig. 1D). Of all proteins identified, 48 proteins were enriched more than 1.5 fold in the CSC cultures of all three tumors (Table 1). An additional 100 proteins were enriched more than 1.5-fold in the CSC cultures of two out of three tumors (Supplemental Table 1). All the above mentioned proteins enriched in CSC cultures were analyzed with SecretomeP 2.0 as a computational tool to predict their secretory potential[28]. This revealed that about 60% of all proteins were potentially secreted by means of the classical or non-classical secretion pathways (Table 1, Supplemental Table 1). In

addition, we analyzed our dataset for the presence of exosomal proteins. Testing our dataset against the Human Exocarta Database 4.1 revealed that 55% of all enriched proteins in the CSC cultures were predicted to be exosome-derived (Table 1, Supplemental Table 1). Moreover, of all proteins predicted to be secreted by the non-classical pathway 50% were predicted to be exosome-derived.

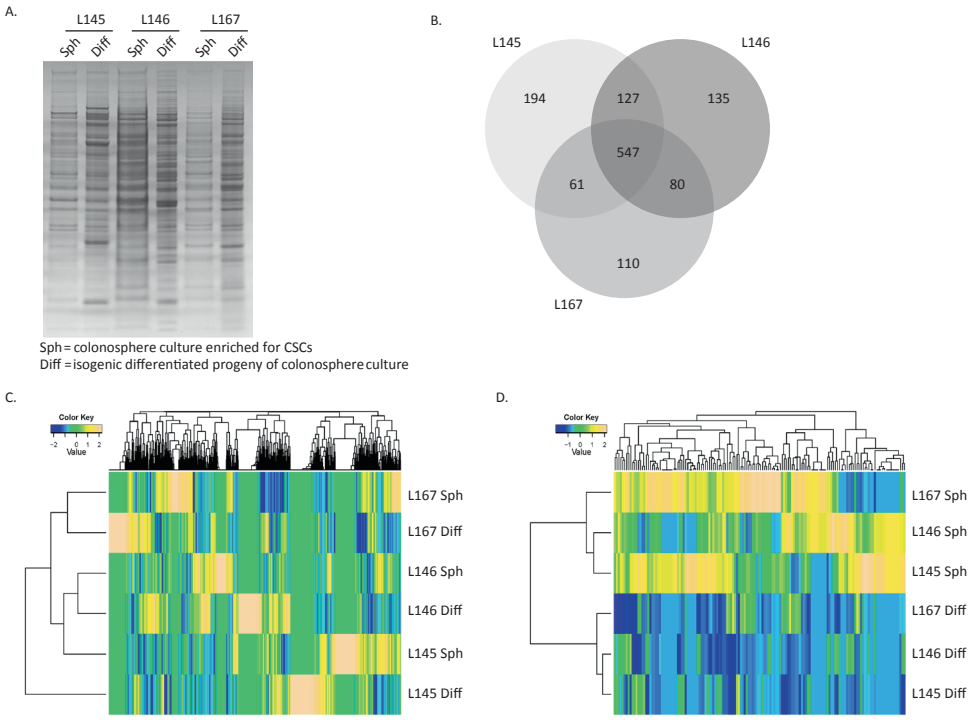

Fig. 1. Secretome analysis of CSC-cultures and isogenic differentiated tumor cells.
(A.) Coomassie-stained protein gradient gel loaded with protein samples from CSC enriched cultures (Sph), and differentiated tumor cells (Diff) from three distinct colorectal liver metastases: L145, L146 and L167. This gel was used for mass-spectrometry analysis.
(B.) Venn diagram of all proteins detected in CSC cultures and differentiated TCs.
(C.) Heatmap of unsupervised cluster analysis of all identified proteins.
(D.) Heatmap of supervised cluster analysis, only including proteins enriched in CSC cultures (Table 1 and Supplemental Table 1) and differentiated cultures.

Table 1. Proteins enriched in the secretomes of cancer stem cell (CSC) cultures were compared to the secretomes of paired differentiated tumor cell cultures. Three tumors were analyzed (L145, L146, L167). Proteins are categorized according to the average fold-enrichment in CSC secretomes with a cut-off at 2-fold. All proteins showed ≥ 1.5-fold enrichment in all 3 single comparisons. The p-values and fold change are based on the paired beta-binomial test. SecretomeP, NN-score above 0,5 indicates possible non-classical secretion, classical secreted proteins (having signaling peptide) are marked with *. Predicted exosome-derived proteins identified by the Exocarta database are marked.

			L145		L146		L167						
Protein	**Gene**	**Accession number**	**Diff**	**CSC**	**Diff**	**CSC**	**Diff**	**CSC**	**fold change**	**p-value**	**location**	**SecretomeP NN-score**	**Human entries Exocarta 4.1**
Chaperonin containing TCP1, subunit 7 (eta)	CCT7	IPI00018465	0	6	0	5	0	4	8	0.000	Cytoplasm	0.382	x
Fc fragment of IgG binding protein	FCGBP	IPI00242956	0	2	0	19	0	7	8	0.000	Extracell space	0.706*	x
Fibroblast growth factor 2 (basic)	FGF2	IPI00154603	0	3	0	2	0	4	8	0.002	Extracell space	0.239	
Fumarate hydratase	FH	IPI00296053	0	2	0	2	0	3	8	0.005	Cytoplasm	0.493	x
Glutathione synthetase	GSS	IPI00010706	0	5	0	2	0	4	8	0.001	Cytoplasm	0.484	x
N-sulfoglucosamine sulfohydrolase	SGSH	IPI00019988	0	4	0	2	0	7	8	0.001	Cytoplasm	0.808*	
Proteasome (prosome, macropain) subunit, alpha type, 6	PSMA6	IPI00029623	0	3	0	3	0	3	8	0.002	Cytoplasm	0.429	x
Ribosomal protein L23a	RPL23A	IPI00021266	0	3	0	4	0	3	8	0.001	Cytoplasm	0.418	
T-complex 1	TCP1	IPI00290566	0	7	0	4	0	5	8	0.000	Cytoplasm	0.518	x
Transferrin	TF	IPI00022463	0	32	0	12	0	46	8	0.000	Extracell space	0.478*	x
WD repeat domain 1	WDR1	IPI00746165	0	6	0	4	0	9	8	0.000	Extracell space	0.518	x
Phosphoglucomutase 1	PGM1	IPI00844159	3	10	0	10	0	28	15.3	0.000	Cytoplasm	0.43	x
Ferritin, light polypeptide	FTL	IPI00852596	0	11	0	9	2	4	14.7	0.001	Cytoplasm	0.383	x
Chaperonin containing TCP1, subunit 5 (epsilon)	CCT5	IPI00010720	2	11	0	6	0	7	12.3	0.001	Cytoplasm	0.425	x
Aldehyde dehydrogenase 1 family, member A1	ALDH1A1	IPI00218914	0	10	2	14	2	22	11.7	0.000	Cytoplasm	0.501	x
NAD synthetase 1	NADSYN1	IPI00306689	0	3	0	3	2	11	8.8	0.005	Cytoplasm	0.444	
Discoidin domain receptor tyrosine kinase 1	DDR1	IPI00001477	2	5	0	4	0	5	6.8	0.010	Plasma membr	0.094*	x
Neurolysin (metallopeptidase M3 family)	NLN	IPI00010346	3	6	0	2	0	12	6.4	0.008	Cytoplasm	0.450*	
Ribosomal protein S13	RPS13	IPI00221089	2	3	0	5	0	5	6.2	0.017	Unknown	0.816	x
Olfactomedin 4	OLFM4	IPI00022255	0	5	12	36	0	31	5.6	0.000	Extracell space	0.649*	x
Serine/arginine-rich splicing factor 1	SRSF1	IPI00215884	0	6	0	4	3	5	5.6	0.016	Extracell space	0.919*	
Malic enzyme 1, NADP(+)-dependent, cytosolic	ME1	IPI00008215	5	17	2	8	0	12	5.3	0.003	Cytoplasm	0.378	x
EPH receptor B4	EPHB4	IPI00289342	0	2	0	3	3	9	5	0.018	Plasma membr	0.366*	x
Serpin peptidase inhibitor, clade B (ovalbumin), member 6	SERPINB6	IPI00413451	5	20	0	11	5	12	4.8	0.006	Cytoplasm	0.44	x
Leucyl/cystinyl aminopeptidase	LNPEP	IPI00221240	5	12	0	11	3	8	4.2	0.015	Cytoplasm	0.63	

CNDP dipeptidase 2 (metallopeptidase M20 family)	CNDP2	IPI00177728	2	4	0	2	0	3	4.1	0.050	Cytoplasm	0.443 x		
LSM4 homolog, U6 small nuclear RNA associated (S, cerevisiae)	LSM4	IPI00294955	0	2	2	4	0	3	4	0.054	Nucleus	0.426		
Ribosomal protein L23	RPL23	IPI00010153	2	3	0	2	0	3	3.6	0.078	Cytoplasm	0.582*		x
Glutathione peroxidase 2 (gastrointestinal)	GPX2	IPI00298176	0	7	3	6	2	3	3.6	0.066	Nucleus	0.233		
Angiogenin, ribonuclease, RNase A family, 5	ANG	IPI00008554	0	6	3	8	4	8	3.5	0.024	Extracell space	0.889*		x
N-acylaminoacyl-peptide hydrolase	APEH	IPI00337741	8	12	5	10	0	28	3.4	0.016	Nucleus	0.577		x
GTP cyclohydrolase I feedback regulator	GCHFR	IPI00217253	0	2	3	6	0	3	3.3	0.054	Cytoplasm	0.93		
Ribosomal protein S11	RPS11	IPI00025091	3	5	3	6	0	5	2.7	0.050	Cytoplasm	0.289		x
Ferritin, heavy polypeptide 1	FTH1	IPI00554521	4	11	0	2	4	7	2.7	0.038	Cytoplasm	0.526 x		
Poliovirus receptor	PVR	IPI00219425	2	4	2	3	0	4	2.6	0.093	Cytoplasm	0.754		
Protein disulfide isomerase family A, member 4	PDIA4	IPI00009904	13	23	12	22	11	51	2.6	0.022	Cytoplasm	0.621 x		
Heat shock 60 kDa protein 1 (chaperonin)	HSPD1	IPI00472102	8	14	7	18	6	27	2.6	0.014	Cytoplasm	0.331 x		
Desmoglein 2	DSG2	IPI00028931	6	10	8	11	4	26	2.5	0.062	Plasma membr	0.838*		x
Vacuolar protein sorting 35 homolog (S, cerevisiae)	VPS35	IPI00018931	3	6	4	6	0	5	2.5	0.061	Cytoplasm	0.682 x		
Ribonuclease, RNase A family, 4	RNASE4	IPI00029699	0	6	5	12	10	16	2.4	0.035	Cytoplasm	0.543*		
Glucuronidase, beta	GUSB	IPI00027745	0	6	2	4	8	12	2.3	0.085	Cytoplasm	0.485		x
Leukotriene A4 hydrolase	LTA4H	IPI00219077	14	26	13	19	7	35	2.3	0.035	Cytoplasm	0.786		x
Phosphoribosylglycinamide formyltransferase	GART	IPI00025273	6	14	7	17	3	5	2.2	0.021	Cytoplasm	0.753*		x
Lectin, galactoside-binding, soluble, 3	LGALS3	IPI00465431	8	21	13	35	18	27	2.2	0.012	Plasma membr	0.678		x
Serine/arginine-rich splicing factor 2	SRSF2	IPI00005978	4	6	0	2	3	5	2.1	0.115	Plasma membr	0.375*		
Suppression of tumorigenicity 14 (colon carcinoma)	ST14	IPI00001922	6	9	2	5	4	12	2	0.050	Cytoplasm	0.547		
Desmocollin 2	DSC2	IPI00025846	8	13	6	12	5	13	2	0.025	Extracell space	0.77		x
Heat shock 70 kDa protein 5 (glucose-regulated protein, 78 kDa)	HSPA5	IPI00003362	17	29	10	19	14	34	2	0.008	Plasma membr	0.313*		x

Seventy-two percent (903/1254) of the CSC-enriched secretome factors were previously identified in the corresponding CSC proteomes (Fig. 2A)[12]. Indeed, the percentages of proteins derived from the nucleus, the cytoplasm, the plasma membrane and the extracellular space for these overlapping proteins were roughly similar in the secretome and the proteome (Fig. 2B). This suggests that the secretome provides an approximate extracellular image of the CSCs themselves. Three-hundred-fifty-one proteins were identified in the secretome alone, but not in the proteome. As may be expected, extracellular space and plasma membrane proteins were strongly enriched in this group of secretome-only proteins (Fig. 2C).

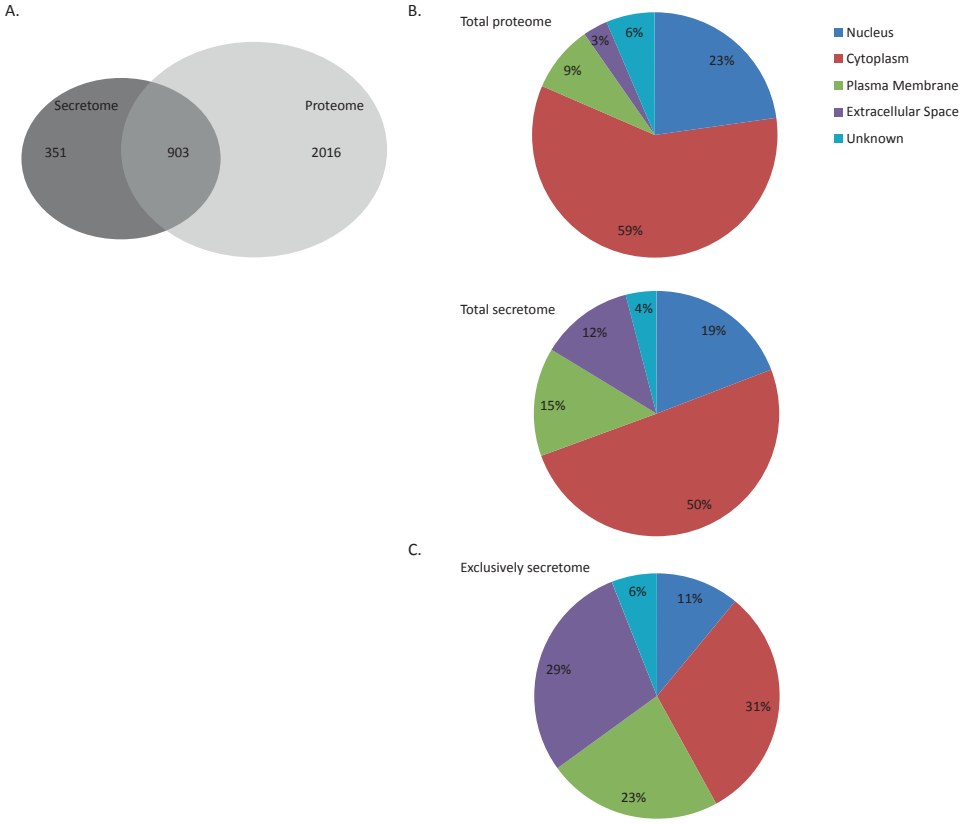

Fig. 2. Overlap between proteomes and secretomes.
(A.) Venn diagram of all proteins detected in the proteomes and secretomes of all three tumors (L145, L146 and L167) including both CSC and differentiated cells.
(B.) Pie-charts showing the percentage of identified proteins in the proteome and secretome, ordered according to their intracellular localization (nucleus, cytoplasm, plasma membrane, extracellular space and unknown).
(C.) Pie-chart showing the percentage of identified proteins exclusively detected in the secretome, ordered according to their intracellular localization (nucleus, cytoplasm, plasma membrane, extracellular space and unknown).

CSCs secrete CSC markers

The list of 148 CSC-enriched secretome proteins (all proteins described in Table 1, Supplemental Table 1) was analyzed for potential functional connectivity by Ingenuity Pathway Analysis (IPA) and extensive PubMed searches (Supplementary Table 2). Strikingly, we found that many putative markers for (cancer-)SCs were identified in the CSC secretomes, including OLFM4, EphB2 and ALDH1A1 (Supplementary Table 2)[29-31].

The CSC secretome is enriched in survival factors

IPA analysis identified 'Cancer' as the most significantly associated disease with the CSC secretome. Proteins governing Cell Death and Survival regulation were most significantly enriched in the category 'Molecular and Cellular Functions' (Supplementary Table 3). Extensive literature analysis revealed that the vast majority of these (37 out of 43 molecules) were anti-apoptotic (Supplementary Table 2). This could reflect a general increase in CSC survival capacity.

Protein synthesis, folding, modification, and processing

Supplementary Table 2 shows that many CSC-secreted proteins are involved in protein synthesis, including 10 ribosomal proteins, 4 tRNA synthetases, a translation initiation factor (EIF2C2), and a ribosome recycling factor (ABCE1). IPA analysis further revealed that EIF2 signaling is one of the top canonical pathways overrepresented in the CSC secretome (Supplementary Table 3). STRING analysis also identified a 14-protein network governing protein synthesis (Fig. 3A).

Furthermore, the list of CSC-enriched proteins also contains multiple protein chaperones located in the cytosol, in the mitochondria, and in the ER. In the cytosol these are components of the TCP and the prefoldin complexes (Supplementary Table 2). The protein folding machinery in the ER is represented by chaperones and disulfide bridge isomerases. Some of these factors not only control protein folding, but also protect against oxidative ER stress. Indeed, GRP78 and ERp72 play an important role in the unfolded protein response (UPR) which is activated upon ER stress. Strikingly, UPR proteins were also found to be upregulated in breast CSCs[32], suggesting that an increased capacity for ER protein folding may be an intrinsic property of various types of CSCs. STRING analysis revealed the presence of two chaperone complexes of 5 and 9 proteins in the CSC secretome (Fig. 3B). Both Ingenuity and STRING analyses showed that factors involved in protein modification are also enriched in the CSC secretome (Supplementary Table 2). These include enzymes involved in glycosaminoglycan degradation and glycosylation (Fig. 3C). Although not identified by STRING or Ingenuity as a separate functional group, we also found 8 proteins that regulate protein tyrosine phosphorylation in the CSC secretome (Supplementary Table 2).

Energy metabolism

IPA analysis also revealed that proteins involved in energy metabolism (Glycolysis/Gluconeogenesis, Pentose phosphate shunt) and glutamate metabolism are enriched in the CSC secretome. Likewise, STRING analysis identified a functional protein network governing glycolysis (Fig. 3D). In general, cancer cells utilize glycolysis rather than oxidative phosphorylation to produce ATP, despite sufficient oxygen supply. This phenomenon, known as the Warburg effect, may therefore be particularly relevant to CSCs.

Oxidative stress

The top Toxicity Pathway identified by IPA is 'Oxidative Stress' (p = 1.0e – 4) (Supplementary Table 3). All 11 proteins involved in the regulation of oxidative stress are listed in Supplementary Table 2. Interestingly, there is a significant overlap between the set of proteins in the secretome and those that are known to be activated by the transcription factor NRF2 (NFE2L2), a key activator of the anti-oxidant response (p = 2.7e – 4; CCT7, FTL, GPX2, GCLC, TXNRD1, FTH1) (Supplementary Table 3). This suggests that CSCs may protect themselves from oxidative stress in part by activating the NRF2 antioxidant pathway. In addition, STRING analysis identified an antioxidant functional interaction network consisting of GPX2, GPX3, GSS, TXNDC12, TXNRD1 and GCLC (Fig. 3E).

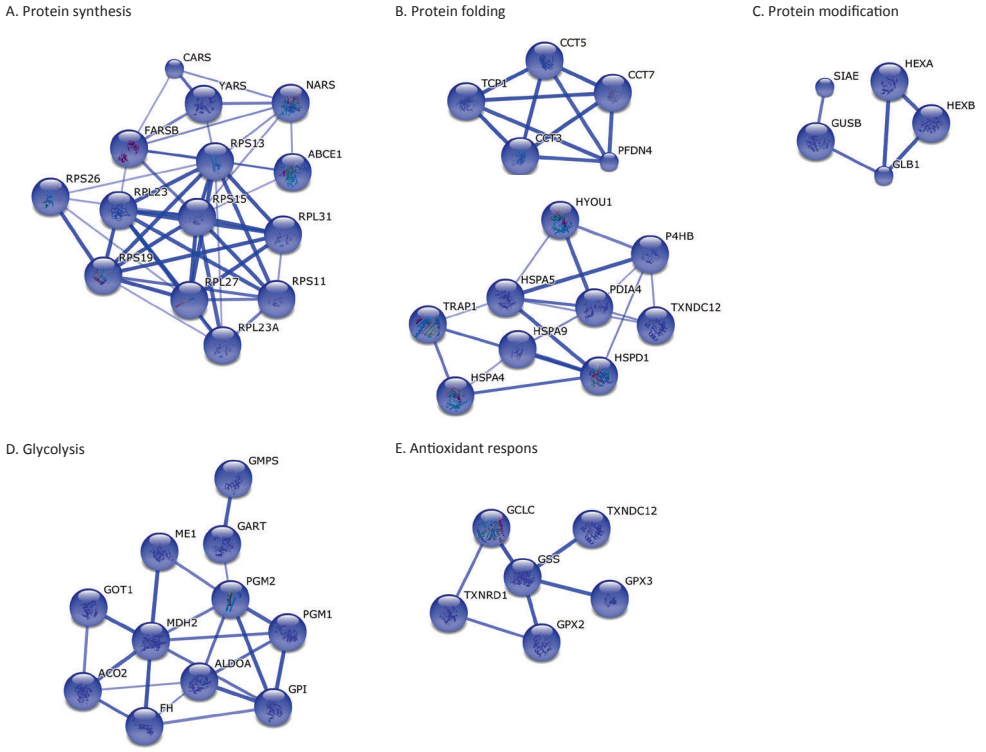

Fig. 3. STRING analysis of CSC-culture secretomes reveals the presence of proteome maintenance, glycolysis, and antioxidant networks.
All CSC-enriched proteins (148) were analyzed by using the STRING web application for functional protein association networks. The strength of the associations is represented by line thickness. The required confidence scores for all associations were set to 0.700 (high). The identified protein networks control (A.) protein synthesis, (B.) protein folding, (C.) protein modification, (D.) glycolysis, and (E.) antioxidant response.

CSCs express ALDH1A1 and BLMH

Extensive PubMed analysis of all secreted factors revealed that CSCs secrete a number of factors that have been implicated in the detoxification and/or conversion of different types of anti-cancer drugs (Supplementary Table 2). These are ALDH1A1, ALDH2, BLMH, CES2, and CD46. Although colonosphere cultures are highly enriched in CSCs, they also contain a subpopulation

of differentiated non-tumorigenic cells. By using Aldefluor®, a fluorescent probe for aldehyde dehydrogenase activity, the tumorigenic CSCs can be separated from the non-tumorigenic cells by FACS sorting[12,17,33]. FACS sorting based on Aldefluor revealed that Aldefluorhigh CSCs, but not the non-tumorigenic Aldefluorlow cells, selectively express ALDH1A1 and BLHM (Fig. 4A).

CSCs secrete ALDH activity and protect differentiated tumor cells from maphosphamide

ALDH1A1 and ALDH2 can detoxify aldehyde-containing anti-cancer drugs such as cyclophosphamide (CPP) and may play a role in drug resistance[34,35]. Maphosphamide is the active analogue of cyclophosphamide which is frequently used for in vitro experiments. In line with the results presented in Fig. 4A we found that ALDH1A1 is expressed in and secreted by the CSC cultures, but to far lower levels by the isogenic differentiated tumor cell cultures (Fig. 4B). Treatment of two distinct CSC lines (L145; L167) and their differentiated progeny showed that CSCs were far more resistant to the drug than differentiated tumor cells (Fig. 4C, D).

To test whether ALDH activity secreted from CSCs was able to cross-protect differentiated tumor cells from maphosphamide, the latter were cultured in the presence of CSC-conditioned medium, and in the presence or absence of the ALDH-inhibitor DEAB. Maphosphamide treatment (40 μM) killed the vast majority (72 ± 2%) of differentiated tumor cells. However, CSC-conditioned medium largely neutralized the cytotoxic effect of maphosphamide (27 ± 5% cell death; $p < 0.05$) (Fig. 4E). Addition of DEAB to the conditioned medium reduced cross-protection by more than 50%. This suggests that approximately half of the protective effect of the CSC-conditioned medium was due to secreted ALDH activity. Survival-signaling growth factors (Supplementary Table 2) and/or additional drug-detoxifying enzymes may account for the remaining protective activity in CSC-conditioned medium.

CSCs secrete bleomycin-hydrolase and protect differentiated tumor cells from bleomycin

BLMH (bleomycin hydrolase, a cysteine peptidase) provides protection against the glycopeptide anti-cancer drug bleomycin by hydrolyzing its first peptide bond[36]. Although bleomycin is not used for the treatment of CRC, in vitro data have shown that it is effective particularly against cell lines displaying microsatellite instability[37]. Furthermore, the finding that high levels of BLMH are secreted by CSCs may have implications for the treatment of other types of cancer in which bleomycin is part of the standard treatment regimen. These include Hodgkin's lymphoma, squamous cell carcinoma and testicular cancer[38].

We first validated that CSCs secrete bleomycin hydrolase (BLMH) to much higher levels than differentiated tumor cells (Figs. 4A and 5A). In line with this, CSCs were markedly resistant to bleomycin while differentiated tumor cells were effectively killed in two distinct cell cultures (L145; L167) (Fig. 5B). Moreover, CSC-conditioned medium protected differentiated tumor cells from bleomycin (Fig. 5C) as it did against maphosphamide (Fig. 4E).

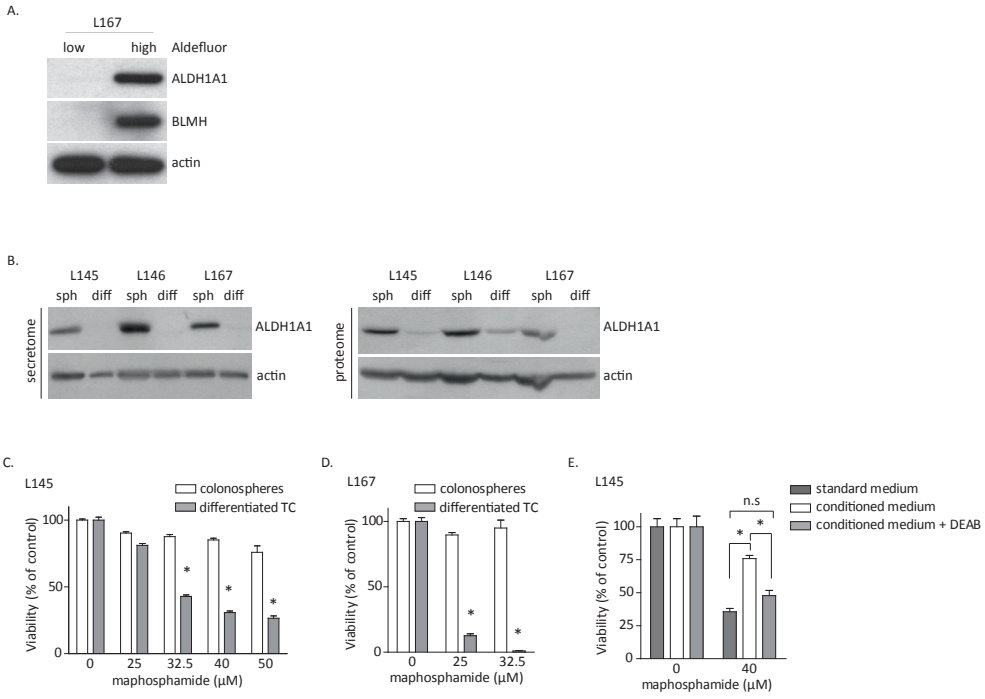

Fig. 4. ALDH1A1 is expressed in the tumorigenic Aldefluorhigh fraction of colonosphere cells and secreted ALDH1A1 protects differentiated cells from maphosphamide.

(A.) Single cell cultures of L167 colonospheres were separated into Aldefluor®high and Aldefluor®low cell populations by FACS sorting. Western blot analysis of Aldefluor®high and Aldefluor®low cell populations was performed to determine ALDH1A1 and BLMH expression in both populations. (B.) Western blot analysis of ALDH1A1 levels in the secretomes (left) and proteomes (right) of CSC-cultures and differentiated TC (L145, L146 and L167).

(C.) and (D.) L145 and L167 CSC-cultures and their differentiated progeny were treated with maphosphamide for 72 h using the indicated concentrations. Cell viability was then assessed by MTS assays for mitochondrial activity. Absorbance values (in triplicate) are expressed as percentage of vehicle-treated control wells.

(E.) Differentiated cells (L145) were cultured in normal culturing medium, conditioned medium derived from CSC-cultures or conditioned medium + DEAB (15 μM) and subsequently treated with 40 μM maphosphamide for 72 h. Cell viability was then assessed by MTS assays. Absorbance values (in triplicate) are expressed as percentage of vehicle-treated control wells.

*Statistical significance (unpaired, 2-tailed t test: $p < 0.05$).

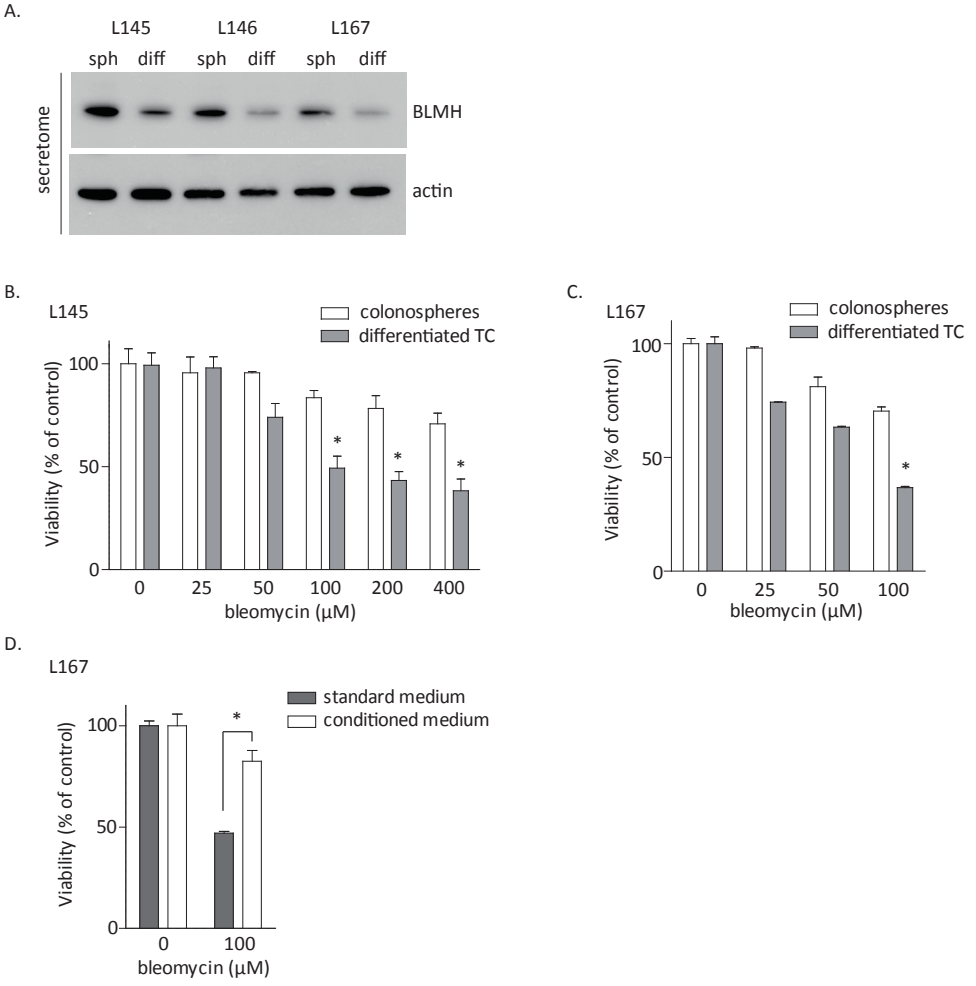

Fig. 5. Bleomycin hydrolase secreted by CSC-cultures protects differentiated cells from bleomycin.
(A.) Western blot analysis of BLMH expression in the secretomes of L145, L146 and L167 CSC-cultures and their differentiated progeny.
(B.) and (C.) L145 and L167 CSC-cultures and their differentiated progeny were treated with bleomycin for 72 h using the indicated concentrations. Cell viability was then assessed by MTS assays. Absorbance values (in triplicate) are expressed as percentage of vehicle-treated control wells.
(D.) Differentiated tumor cells (L167) were cultured in normal culturing medium or conditioned medium derived from the L167 CSC-culture for 72 h. Cell viability was then assessed by MTS assays. Absorbance values (in triplicate) are expressed as percentage of vehicle-treated control wells. *Statistical significance (unpaired, 2-tailed t test: $p < 0.05$).

DISCUSSION

Normal stem cells use multiple mechanisms to maintain their genomic integrity over time, without having been exposed to chemotherapy. Recent evidence indicates that intestinal cancer originates from normal tissue SCs[39,40]. By inference, CSCs may be direct (albeit deranged) descendants from tissue SCs and, as such, have inherited the natural resistance pathways that prevent SC exhaustion. The relationship between CSCs and chemoresistance is highly complex and needs to be investigated for each specific chemotherapeutic drug. The most straightforward relationship is when CSCs express enzymes that directly detoxify anti-tumor drugs, such as the inactivation of CPP/MPP by CSC-produced ALDHs. However, drug resistance can be acquired in many different ways, for instance through increased expression of drug efflux pumps, antioxidant enzymes and DNA repair enzymes[41]. The relationship between CSCs and resistance to a particular drug will therefore depend on whether or not CSCs express the major resistance mechanism to that drug.

Our studies have shown that CSCs express and secrete high levels of many different survival proteins, including those that reduce oxidative stress. Recent evidence shows that breast CSCs are relatively resistant to oxidative stress and that this prevents their exhaustion[19]. The Nrf2 antioxidant program has previously been identified as an important mediator of chemoresistance in cell lines derived from multiple tumor types[42-44]. Our results suggest that Nrf2 may play a similar role in colon cancer, but also that this may occur mainly in the CSC subpopulation. The relatively recent discoveries that the Nrf2 program has pro-tumorigenic properties[45] and that it plays an important role in chemoresistance[42-44] have intensified efforts to search for and develop Nrf2 inhibitors[46]. We propose that such inhibitors may neutralize the intrinsic (Nrf2-mediated) resistance of colorectal CSCs to chemotherapy.

Several DNA repair pathways have been implicated in the protection of stem cells against DNA damage, thereby maintaining genome integrity[47]. Perhaps surprisingly, we have not found any evidence for the enrichment of DNA repair proteins in the proteome or secretome of colorectal CSCs. Rather, we found many factors governing maintenance of proteome integrity being enriched in CSCs. These included factors involved in protein synthesis, folding, modification and destruction. An increased capacity for maintaining proteome integrity therefore appears to be a novel property of the CSC phenotype. However, we also noted that proteins governing protein synthesis and folding are frequently found in secretomes. Therefore, the overrepresentation of this class of proteins in the CSC-secretomes needs to be interpreted with caution and the relevance of this finding for CSC maintenance needs to be tested experimentally.

An important new concept from the current study is that secretion of specific proteins from CSCs modulates drug responses in nearby tumor cells. Thus, CSCs not only possess multiple mechanisms that promote self-preservation, but may also preserve cells in their direct vicinity by secreting drug-detoxifying enzymes. Recently, it was shown that normal intestinal stem cells are flanked by Paneth cells that act as critical SC support cells[48]. Differentiated tumor cells in colorectal tumors may act in the same way by providing support to the CSCs from which they originated. Thus, by secreting drug-detoxifying enzymes CSCs may provide survival signals to their own closely associated support cells and this may be essential for their own survival.

To what extent the mechanisms described above are operating within CRC tumors during chemotherapy needs to be addressed in future experiments. The colonosphere model would be ideal in such studies as they contain CSCs and differentiated tumor cells. They are also highly tumorigenic in mice while preserving the phenotype of the original patient tumor[17].

REFERENCES

1. Ferlay,J. *et al.* Estimates of worldwide burden of cancer in 2008: GLOBOCAN 2008. *Int. J. Cancer* 127, 2893-2917 (2010).
2. Saltz,L.B. *et al.* Bevacizumab in combination with oxaliplatin-based chemotherapy as first-line therapy in metastatic colorectal cancer: a randomized phase III study. *J. Clin. Oncol.* 26, 2013-2019 (2008).
3. Hurwitz,H. *et al.* Bevacizumab plus irinotecan, fluorouracil, and leucovorin for metastatic colorectal cancer. *N. Engl. J. Med.* 350, 2335-2342 (2004).
4. Broadbridge,V.T. *et al.*Cetuximab in metastatic colorectal cancer. *Expert. Rev. Anticancer Ther.* 12, 555-565 (2012).
5. Iqbal,S. & Lenz,H.J. Integration of novel agents in the treatment of colorectal cancer. *Cancer Chemother. Pharmacol.* 54 Suppl 1, S32-S39 (2004).
6. O'Brien,C.A. *et al.* A human colon cancer cell capable of initiating tumour growth in immunodeficient mice. *Nature* 445, 106-110 (2007).
7. Ricci-Vitiani,L. *et al.* Identification and expansion of human colon-cancer-initiating cells. *Nature* 445, 111-115 (2007).
8. Todaro,M. *et al.* Colon cancer stem cells: promise of targeted therapy. *Gastroenterology* 138, 2151-2162 (2010).
9. Vermeulen,L. *et al.* Single-cell cloning of colon cancer stem cells reveals a multi-lineage differentiation capacity. *Proc. Natl. Acad. Sci. U. S. A* 105, 13427-13432 (2008).
10. Pang,R. *et al.* A subpopulation of CD26+ cancer stem cells with metastatic capacity in human colorectal cancer. *Cell Stem Cell* 6, 603-615 (2010).
11. Todaro,M. *et al.* Colon cancer stem cells dictate tumor growth and resist cell death by production of interleukin-4. *Cell Stem Cell* 1, 389-402 (2007).
12. Van Houdt,W.J. *et al.* Comparative proteomics of colon cancer stem cells and differentiated tumor cells identifies BIRC6 as a potential therapeutic target. *Mol. Cell Proteomics.* 10, M111 (2011).
13. Cho,R.W. & Clarke,M.F. Recent advances in cancer stem cells. *Curr. Opin. Genet. Dev.* 18, 48-53 (2008).
14. Dylla,S.J. *et al.* Colorectal cancer stem cells are enriched in xenogeneic tumors following chemotherapy. *PLoS. One.* 3, e2428 (2008).
15. Creighton,C.J. *et al.* Residual breast cancers after conventional therapy display mesenchymal as well as tumor-initiating features. *Proc. Natl. Acad. Sci. U. S. A* 106, 13820-13825 (2009).
16. Li,X. *et al.* Intrinsic resistance of tumorigenic breast cancer cells to chemotherapy. *J. Natl. Cancer Inst.* 100, 672-679 (2008).
17. Emmink,B.L. *et al.* Differentiated human colorectal cancer cells protect tumor-initiating cells from irinotecan. *Gastroenterology* 141, 269-278 (2011).
18. Nagaria,P. *et al.* DNA double-strand break response in stem cells: Mechanisms to maintain genomic integrity. *Biochim. Biophys. Acta*(2012).
19. Diehn,M. *et al.* Association of reactive oxygen species levels and radioresistance in cancer stem cells. *Nature* 458, 780-783 (2009).
20. O'Brien,C.A. *et al.* ID1 and ID3 regulate the self-renewal capacity of human colon cancer-initiating cells through p21. *Cancer Cell* 21, 777-792 (2012).
21. Arlt,A. *et al.* Autocrine production of interleukin 1beta confers constitutive nuclear factor kappaB activity and chemoresistance in pancreatic carcinoma cell lines. *Cancer Res.* 62, 910-916 (2002).
22. Yao,L. *et al.* Discovery of IL-18 as a novel secreted protein contributing to doxorubicin resistance by comparative secretome analysis of MCF-7 and MCF-7/Dox. *PLoS. One.* 6, e24684 (2011).
23. Conze,D. *et al.* Autocrine production of interleukin 6 causes multidrug resistance in breast cancer cells. *Cancer Res.* 61, 8851-8858 (2001).
24. Karagiannis,G.S. *et al.*Cancer secretomics reveal pathophysiological pathways in cancer molecular oncology. *Mol. Oncol.* 4, 496-510 (2010).
25. Shevchenko,A. *et al.* Mass spectrometric sequencing of proteins silver-stained polyacrylamide gels. *Anal. Chem.* 68, 850-858 (1996).
26. Keller,A. *et al.*Empirical statistical model to estimate the accuracy of peptide identifications made by MS/MS and database search. *Anal. Chem.* 74, 5383-5392 (2002).
27. Pham,T.V. & Jimenez,C.R. An accurate paired sample test for count data. *Bioinformatics.* 28, i596-i602 (2012).

28. Bendtsen,J.D. *et al.* Feature-based prediction of non-classical and leaderless protein secretion. *Protein Eng Des Sel* 17, 349-356 (2004).
29. van der Flier,L.G. *et al.* OLFM4 is a robust marker for stem cells in human intestine and marks a subset of colorectal cancer cells. *Gastroenterology* 137, 15-17 (2009).
30. Merlos-Suarez,A. *et al.* The intestinal stem cell signature identifies colorectal cancer stem cells and predicts disease relapse. *Cell Stem Cell* 8, 511-524 (2011).
31. Huang,E.H. *et al.* Aldehyde dehydrogenase 1 is a marker for normal and malignant human colonic stem cells (SC) and tracks SC overpopulation during colon tumorigenesis. *Cancer Res.* 69, 3382-3389 (2009).
32. Bartkowiak,K. *et al.* Discovery of a novel unfolded protein response phenotype of cancer stem/progenitor cells from the bone marrow of breast cancer patients. *J. Proteome. Res.* 9, 3158-3168 (2010).
33. Shenoy,A. *et al.* ALDH as a marker for enriching tumorigenic human colonic stem cells. *Methods Mol. Biol.* 916, 373-385 (2012).
34. Emadi,A. *et al.* Cyclophosphamide and cancer: golden anniversary. *Nat. Rev. Clin. Oncol.* 6, 638-647 (2009).
35. Ma,I. & Allan,A.L. The role of human aldehyde dehydrogenase in normal and cancer stem cells. *Stem Cell Rev.* 7, 292-306 (2011).
36. Zheng,W. *et al.* The unusual active site of Gal6/bleomycin hydrolase can act as a carboxypeptidase, aminopeptidase, and peptide ligase. *Cell* 93, 103-109 (1998).
37. Li,H.R. *et al.* Hypersensitivity of tumor cell lines with microsatellite instability to DNA double strand break producing chemotherapeutic agent bleomycin. *Cancer Res.* 64, 4760-4767 (2004).
38. Chen,J. & Stubbe,J. Bleomycins: towards better therapeutics. *Nat. Rev. Cancer* 5, 102-112 (2005).
39. Barker,N. *et al.* Crypt stem cells as the cells-of-origin of intestinal cancer. *Nature* 457, 608-611 (2009).
40. Zhu,L. *et al.* Prominin 1 marks intestinal stem cells that are susceptible to neoplastic transformation. *Nature* 457, 603-607 (2009).
41. Dean,M. *et al.* Tumour stem cells and drug resistance. *Nat. Rev. Cancer* 5, 275-284 (2005).
42. Wang,X.J. *et al.* Nrf2 enhances resistance of cancer cells to chemotherapeutic drugs, the dark side of Nrf2. *Carcinogenesis* 29, 1235-1243 (2008).
43. Jiang,T. *et al.* High levels of Nrf2 determine chemoresistance in type II endometrial cancer. *Cancer Res.* 70, 5486-5496 (2010).
44. Zhang,P. *et al.* Loss of Kelch-like ECH-associated protein 1 function in prostate cancer cells causes chemoresistance and radioresistance and promotes tumor growth. *Mol. Cancer Ther.* 9, 336-346 (2010).
45. DeNicola,G.M. *et al.* Oncogene-induced Nrf2 transcription promotes ROS detoxification and tumorigenesis. *Nature* 475, 106-109 (2011).
46. Magesh,S. *et al.* Small molecule modulators of Keap1-Nrf2-ARE pathway as potential preventive and therapeutic agents. *Med. Res. Rev.* 32, 687-726 (2012).
47. Tichy,E.D. Mechanisms maintaining genomic integrity in embryonic stem cells and induced pluripotent stem cells. *Exp. Biol. Med. (Maywood.)* 236, 987-996 (2011).
48. Sato,T. *et al.* Paneth cells constitute the niche for Lgr5 stem cells in intestinal crypts. *Nature* 469, 415-418 (2011).

SUPPPLEMENTAL TABLES

Suppplemental table 1. Proteins enriched in the secretomes of CSC cultures when compared to the secretomes of paired differentiated tumor cell cultures. Three tumors were analyzed (L145, L146, L167). Proteins are categorized according to the average fold-enrichment in CSC secretomes with a cut-off at 2-fold. All proteins showed ≥1,5-fold enrichment in 2/3 single comparisons. The p-values and fold change are based on the paired beta-binomial test. SecretomeP, NN-score above 0,5 indicates possible non-classical secretion, classical secreted proteins (having signaling peptide) are marked with *. Predicted exosome-derived proteins identified by the Exocarta database are marked.

			Spectral counts identified										
			L145		L146		L167						
Protein	Gene	Accession number	Diff	CSC	Diff	CSC	Diff	CSC	fold change	p-value	location	SecretomeP NN-score	Human Entries
													Exocarta4.1
apoptosis-inducing factor, mitochondrion-associated, 1	AIFM1	IPI00000690	0	0	0	4	0	5	∞	0,012	Cytoplasm	0,438	
hypoxia up-regulated 1	HYOU1	IPI00000877	0	4	0	3	0	0	∞	0,022	Cytoplasm	0,320*	x
acetyl-CoA acyltransferase 2	ACAA2	IPI00001539	0	2	0	0	0	4	∞	0,036	Cytoplasm	0,403	x
cathepsin Z	CTSZ	IPI00002745	0	5	0	0	0	4	∞	0,012	Cytoplasm	0,861*	
poliovirus receptor-related 1 (herpesvirus entry mediator C)	PVRL1	IPI00003648	0	2	0	0	0	5	∞	0,025	Plasma Membrane	0,246*	
Uncharacterized protein	-	IPI00005589	0	0	0	3	0	3	∞	0,040	-	0,339	
aldehyde dehydrogenase 2 family (mitochondrial)	ALDH2	IPI00006663	0	3	0	0	0	4	∞	0,024	Cytoplasm	0,629	x
tyrosyl-tRNA synthetase	YARS	IPI00007074	0	7	0	0	0	7	∞	0,003	Cytoplasm	0,263	
Ewing sarcoma breakpoint region 1	EWSR1	IPI00009841	0	3	0	3	0	0	∞	0,032	Nucleus	0,267	
regenerating islet-derived family, member 4	REG4	IPI00012501	0	7	0	15	0	0	∞	0,001	Extracellular Space	0,900*	x
RAB5C, member RAS oncogene family	RAB5C	IPI00016339	0	2	0	0	0	3	∞	0,058	Cytoplasm	0,498	x
prolactin-induced protein	PIP	IPI00022974	0	3	0	2	0	0	∞	0,048	Extracellular Space	0,574*	x
methylmalonyl CoA mutase	MUT	IPI00024934	0	3	0	0	0	4	∞	0,024	Cytoplasm	0,437	
latent transforming growth factor beta binding protein 4	LTBP4	IPI00025686	0	8	0	2	0	0	∞	0,010	Extracellular Space	0,238	
UDP-N-acetyl-alpha-D-galactosamine:polypeptide N-acetylgalactosaminyltransferase 1 (GalNAc-T1)	GALNT1	IPI00025818	0	2	0	2	0	0	∞	0,073	Cytoplasm	0,508*	
glutathione peroxidase 3 (plasma)	GPX3	IPI00026199	0	0	0	2	0	3	∞	0,061	Extracellular Space	0,895*	x
ribosomal protein L18a	RPL18A	IPI00026202	0	2	0	2	0	0	∞	0,073	Cytoplasm	0,768	
cleavage and polyadenylation specific factor 1, 160kDa	CPSF1	IPI00026219	0	4	0	2	0	0	∞	0,034	Nucleus	0,416	
ribosomal protein L31	RPL31	IPI00026302	0	3	0	2	0	0	∞	0,048	Cytoplasm	0,402	x
guanine monphosphate synthetase	GMPS	IPI00029079	0	3	0	0	0	7	∞	0,011	Nucleus	0,456	
TNF receptor-associated protein 1	TRAP1	IPI00030275	0	0	0	3	0	3	∞	0,040	Cytoplasm	0,619	x
sema domain, immunoglobulin domain (Ig), short basic domain, secreted, (semaphorin) 3A	SEMA3A	IPI00031510	0	0	0	3	0	9	∞	0,007	Extracellular Space	0,487*	

Protein	Gene	Accession number	Spectral counts identified						fold change	p-value	location	SecretomeP NN-score	Human Entries
			L145		L146		L167						Exocarta4.1
			Diff	CSC	Diff	CSC	Diff	CSC					
transmembrane protein 2	TMEM2	IPI00170706	0	2	0	3	0	0	∞	0,049	unknown	0,55	x
meningioma expressed antigen 5 (hyaluronidase)	MGEA5	IPI00181391	0	2	0	2	0	0	∞	0,073	Cytoplasm	0,44	
ribosomal protein S26	RPS26	IPI00186712	0	3	0	3	0	0	∞	0,032	Cytoplasm	0,325	x
ribosomal protein S15	RPS15	IPI00216153	0	2	0	3	0	0	∞	0,049	Cytoplasm	0,772	
plastin 3	PLS3	IPI00216694	0	6	0	2	0	0	∞	0,015	Cytoplasm	0,429	
polymerase (RNA) II (DNA directed) polypeptide G	POLR2G	IPI00218895	0	2	0	0	0	3	∞	0,058	Nucleus	0,46	
ribosomal protein L27	RPL27	IPI00219155	0	0	0	5	0	3	∞	0,021	Cytoplasm	0,612	x
cystathionine-beta-synthase	CBS	IPI00219352	0	0	0	2	0	3	∞	0,061	Cytoplasm	0,646	
bleomycin hydrolase	BLMH	IPI00219575	0	0	0	2	0	4	∞	0,038	Cytoplasm	0,514	x
CD46 molecule, complement regulatory protein	CD46	IPI00219852	0	4	0	4	0	0	∞	0,016	Plasma Membrane	0,178*	x
eukaryotic translation initiation factor 2C, 2	EIF2C2	IPI00220349	0	6	0	0	0	4	∞	0,007	Cytoplasm	0,33	
tyrosine 3-monooxygenase/tryptophan 5-monooxygenase activation protein, gamma polypeptide	YWHAG	IPI00220642	0	6	0	6	0	0	∞	0,005	Cytoplasm	0,29	x
p21 protein (Cdc42/Rac)-activated kinase 1	PAK1	IPI00289746	0	2	0	0	0	3	∞	0,058	Cytoplasm	0,495	
adaptor-related protein complex 1, gamma 1 subunit	AP1G1	IPI00293396	0	2	0	0	0	5	∞	0,025	Cytoplasm	0,4	
phenylalanyl-tRNA synthetase, beta subunit	FARSB	IPI00300074	0	6	0	0	0	4	∞	0,009	Cytoplasm	0,405	
ATP-binding cassette, sub-family E (OABP), member 1	ABCE1	IPI00303207	0	3	0	0	0	4	∞	0,024	Cytoplasm	0,296	
carboxylesterase 2	CES2	IPI00332828	0	3	0	2	0	0	∞	0,048	Cytoplasm	0,685	
ladinin 1	LAD1	IPI00386700	0	5	0	4	0	0	∞	0,012	Extracellular Space	0,521	
Uncharacterized protein	-	IPI00398135	0	0	0	3	0	3	∞	0,040	-	0,655	
leucine aminopeptidase 3	LAP3	IPI00419237	0	6	0	0	0	3	∞	0,015	Cytoplasm	0,463	x
retinol binding protein 2, cellular	RBP2	IPI00419986	0	0	0	3	0	3	∞	0,040	Cytoplasm	0,635	
inositol-3-phosphate synthase 1	ISYNA1	IPI00478861	0	0	0	2	0	3	∞	0,061	unknown	0,611	
protein phosphatase 2, regulatory subunit A, alpha	PPP2R1A	IPI00554737	0	5	0	0	0	3	∞	0,020	Cytoplasm	0,562	x
thioredoxin reductase 1	TXNRD1	IPI00743646	0	4	0	2	0	0	∞	0,034	Cytoplasm	0,323	
DEAD (Asp-Glu-Ala-Asp) box polypeptide 39B	DDX39B	IPI00790636	0	4	0	0	0	3	∞	0,027	Nucleus	0,427	x
fatty acid binding protein 2, intestinal	FABP2	IPI00218477	0	5	2	6	0	0	5,3	0,051	Cytoplasm	0,638	
exostosin 2	EXT2	IPI00004047	0	3	0	0	2	5	4,4	0,082	Cytoplasm	0,705	x
anterior gradient homolog 3 (Xenopus laevis)	AGR3	IPI00152409	0	3	0	6	3	3	4,3	0,047	Extracellular Space	0,799*	x
Uncharacterized protein	-	IPI00795150	0	4	0	3	3	4	4	0,049	-	0,173	
carboxyl ester lipase (bile salt-stimulated lipase)	CEL	IPI00099670	0	0	0	8	5	9	3,9	0,071	Extracellular Space	0,742*	x
glutamate-cysteine ligase, catalytic subunit	GCLC	IPI00215768	0	7	2	2	2	5	3,9	0,079	Cytoplasm	0,414	

glutamic-oxaloacetic transaminase 1, soluble (aspartate aminotransferase 1)	GOT1	IPI00219029	0	4	2	4	0	0	3,8	0,112	Cytoplasm	0,439	x
thioredoxin domain containing 12 (endoplasmic reticulum)	TXNDC12	IPI00026328	0	0	0	3	2	4	3,7	0,127	Cytoplasm	0,836*	
prolyl endopeptidase	PREP	IPI00747355	3	14	5	6	2	16	3,6	0,026	Cytoplasm	0,543	
Uncharacterized protein	-	IPI00797038	0	6	0	0	6	15	3,6	0,048	-	0,489	
Uncharacterized protein	-	IPI00232533	0	3	0	4	4	5	3,4	0,053	-	0,321	
prefoldin subunit 6	PFDN6	IPI00005657	0	3	2	4	0	0	3,3	0,128	Cytoplasm	0,665	
dipeptidyl-peptidase 3	DPP3	IPI00020672	4	15	6	6	0	12	3,2	0,036	Cytoplasm	0,408	x
glucose-6-phosphate isomerase	GPI	IPI00027497	5	7	0	6	2	8	3,2	0,034	Extracellular Space	0,453	x
heterogeneous nuclear ribonucleoprotein L	HNRNPL	IPI00027834	2	4	0	0	0	3	3,2	0,144	Nucleus	0,477	x
aldolase A, fructose-bisphosphate	ALDOA	IPI00465439	2	3	0	0	0	4	3,2	0,165	Cytoplasm	0,356	x
cleavage stimulation factor, 3′ pre-RNA, subunit 3, 77kDa	CSTF3	IPI00015195	0	0	0	2	2	4	3,1	0,190	Nucleus	0,211	
coxsackie virus and adenovirus receptor	CXADR	IPI00019146	0	0	0	2	2	4	3,1	0,190	Plasma Membrane	0,414*	
xylosyltransferase I	XYLT1	IPI00183487	0	5	0	3	3	0	3,1	0,169	Cytoplasm	0,381*	
phosphoglucomutase 2	PGM2	IPI00550364	3	11	5	5	3	19	3,1	0,065	Cytoplasm	0,414	
cullin 1	CUL1	IPI00014310	0	3	5	5	0	8	2,9	0,038	Nucleus	0,278	
EPH receptor B2	EPHB2	IPI00021275	0	2	0	0	4	9	2,9	0,093	Plasma Membrane	0,336*	x
epidermal growth factor receptor pathway substrate 8	EPS8	IPI00290337	0	2	2	4	0	0	2,9	0,193	Plasma Membrane	0,14	x
malate dehydrogenase 2, NAD (mitochondrial)	MDH2	IPI00291006	0	5	0	3	5	5	2,9	0,056	Cytoplasm	0,595	x
prolyl 4-hydroxylase, beta polypeptide	P4HB	IPI00010796	4	11	3	7	0	0	2,8	0,044	Cytoplasm	0,679*	x
aconitase 2, mitochondrial	ACO2	IPI00017855	0	2	0	8	6	4	2,8	0,068	Cytoplasm	0,413	
sialic acid acetylesterase	SIAE	IPI00010949	5	6	4	9	3	19	2,7	0,060	Cytoplasm	0,786*	x
X-prolyl aminopeptidase (aminopeptidase P) 1, soluble	XPNPEP1	IPI00793375	0	8	7	5	0	7	2,7	0,022	Cytoplasm	0,531	
protein tyrosine phosphatase, receptor type, G	PTPRG	IPI00011651	0	5	2	6	4	4	2,6	0,112	Plasma Membrane	0,148*	
cathepsin C	CTSC	IPI00022810	6	7	3	11	2	13	2,6	0,057	Cytoplasm	0,767*	x
hexosaminidase A (alpha polypeptide)	HEXA	IPI00027851	8	10	0	6	0	8	2,6	0,016	Cytoplasm	0,700*	
heat shock 70kDa protein 9 (mortalin)	HSPA9	IPI00007765	2	12	3	9	7	5	2,5	0,138	Cytoplasm	0,28	x
cysteinyl-tRNA synthetase	CARS	IPI00027443	5	7	0	0	0	5	2,5	0,129	Cytoplasm	0,177	
angiotensin I converting enzyme (peptidyl-dipeptidase A) 1	ACE	IPI00437751	6	24	7	12	4	4	2,5	0,083	Plasma Membrane	0,668*	x
gamma-glutamyl hydrolase (conjugase, folylpolygammaglutamyl hydrolase)	GGH	IPI00023728	0	2	0	0	7	15	2,4	0,086	Cytoplasm	0,628*	x
asparaginyl-tRNA synthetase	NARS	IPI00306960	0	6	4	2	4	11	2,4	0,171	Cytoplasm	0,406	x
galactosidase, beta 1	GLB1	IPI00441344	3	6	0	0	5	12	2,4	0,065	Cytoplasm	0,690*	x
adaptor-related protein complex 2, alpha 2 subunit	AP2A2	IPI00016621	2	0	2	6	0	4	2,3	0,359	Cytoplasm	0,438	x
nephronectin	NPNT	IPI00157556	0	4	0	2	3	0	2,3	0,298	Plasma Membrane	0,321*	x

Protein	Gene	Accession number	Spectral counts identified						fold change	p-value	location	SecretomeP NN-score	Human Entries
			L145		L146		L167						Exocarta4.1
			Diff	CSC	Diff	CSC	Diff	CSC					
dipeptidyl-peptidase 7	DPP7	IPI00296141	5	3	0	4	0	5	2,3	0,080	Cytoplasm	0,805*	
arginyl aminopeptidase (aminopeptidase B)	RNPEP	IPI00642211	9	22	16	21	4	27	2,3	0,046	Cytoplasm	0,535	x
procollagen-lysine, 2-oxoglutarate 5-dioxygenase 3	PLOD3	IPI00030255	13	34	19	22	6	30	2,2	0,050	Cytoplasm	0,561*	x
Uncharacterized protein	-	IPI00479477	2	9	3	8	4	0	2,2	0,500	-	0,618	
thimet oligopeptidase 1	THOP1	IPI00549189	3	5	4	4	2	12	2,2	0,151	Cytoplasm	0,374	
acireductone dioxygenase 1	ADI1	IPI00651738	3	5	4	4	0	8	2,2	0,154	Nucleus	0,459	
prefoldin subunit 4	PFDN4	IPI00015891	2	0	0	2	0	3	2,1	0,371	Cytoplasm	0,724	
plastin 1	PLS1	IPI00032304	3	15	10	7	5	16	2,1	0,148	Cytoplasm	0,412	x
ribosomal protein S19	RPS19	IPI00215780	6	6	5	7	0	9	2,1	0,126	Cytoplasm	0,821	x
lysosomal-associated membrane protein 1	LAMP1	IPI00004503	3	10	3	6	4	3	2	0,165	Plasma Membrane	0,388*	x
hexosaminidase B (beta polypeptide)	HEXB	IPI00012585	11	25	9	12	8	20	2	0,018	Cytoplasm	0,712*	
tyrosine 3-monooxygenase/tryptophan 5-monooxygenase activation protein, zeta polypeptide	YWHAZ	IPI00021263	3	13	2	4	10	11	2	0,136	Cytoplasm	0,252	x
chaperonin containing TCP1, subunit 3 (gamma)	CCT3	IPI00290770	11	14	7	12	0	13	2	0,069	Cytoplasm	0,484	x
carbamoyl-phosphate synthetase 2, aspartate transcarbamylase, and dihydroorotase	CAD	IPI00301263	5	21	11	17	9	8	2	0,160	Cytoplasm	0,402	x

Supplementary Table II. All CSC-enriched secretome proteins were classified into functional categories, based on Ingenuity and STRING analyses and literature searches.

Protein	Function	
(Cancer) Stem Cell signaling		
ALDH1A1	Marks tumor-initiating cells; provides resistance to cyclophosphamide	
EPHB2	Marks tumor-initiating cells; Wnt target; tyrosine kinase receptor	
OLFM4	Wnt and Notch target gene; cell-cell adhesion, anti-apoptosis	
AP2A2	Endocytosis; asymmetric division in HSC	
FGF2	Self-renewal	
Drug resistance/Detoxification		
ALDH1A1	Detoxification of aldehydes, including cyclophosphamide and maphosphamide; Converts vitamin A into RA	
ALDH2	Detoxification of alcohol	
BLMH	Bleomycin hydrolase; resistance to bleomycin	
CES2	Hydrolysis of cocain & heroin; Intestinal drug clearance; activates irinotecan	
CD46	Complement inhibitor; Resistance to antibody-mediated cytotoxicity	
Cell Death and Survival		
ABCE1	unknown	Survival
ACAA2	binds and suppresses pro-apoptotic BNIP	Survival
ADI1	unknown	Death
AGR2	unknown	Survival
AIFM1	caspase-independent DNA cleavage	Death
ALDH1A1	detoxification of aldehydes, including cyclophosphamide	Survival
ANG	inhibits p53 function	Survival
AP2A2	regulates endocytosis to prevent apoptosis by GPCRs	Survival
BLMH	detoxification of Bleomycin	Survival
CCL2	survival signalling through CCR2	Survival
CD46	prevents complement-induced cell death	Survival
CES2	generates SN38 from irinotecan	Survival
CXCL1	survival signalling through CXCR2	Survival
DDR1	survival signalling, partly through Notch1	Survival
DPP3	activation of anti-oxidant response	Survival
DPP7	maintenance of quiescence	Survival
DSG2	truncation product promotes apoptosis	Death
EPHB2	tumor suppressor	Death
EPHB4	survial signalling	Survival
EWSR1	unknown	Survival
FGF2	survival signalling through FGFR	Survival
GCLC	NRF1 target, antioxidant response	Survival
GPX2	ROS neutralization	Survival
HSPA5	protein folding; protects against ER stress	Survival
HSPA9	protein folding in the mitochondria; protection against ox stress	Survival
HSPA1A	cytoplasmic chaperone	Survival
HSPD1	protein folding in the mitochondria; protection against ox stress	Survival
LAMP1	protection against lysosomal death pathway	Survival
LGALS3	prevents mitochondrial membrane depolarization	Survival
MIF	survival signalling through CD44/CD74	Survival
P4HB	main cellular protein disulfide isomerase	Survival
PAK1	phosphorylates and inactivates Bad	Survival

PPP2R1A	dephosphorylation of Bad	Death
PTPRG	tyrosine phosphatase; tumor suppressor	Death
RPS19	regulation of Bcl2 family members	Survival
SERPINB2	inhibition of TNFR-induced apoptosis	Survival
SRSF1	alternative splicing of BIM and BIN	Survival
TF	essential for cell growth and survival	Survival
TRAP1	protein folding in the mitochondria; protection against ox stress	Survival
TXNRD1	ROS neutralization	Survival
YARS	IL-8-like cytokine activity	Survival
YWHAG	14-3-3-gamma; binds and inactivates Bad	Survival
YWHAZ	14-3-3-gamma; binds and inactivates Bax	Survival
Protein synthesis		
EIF2C2	Translation initiation factor	
RPL23A	ribosomal protein	
RPL23	ribosomal protein	
RPS13	ribosomal protein	
RPS11	ribosomal protein	
RPS11	ribosomal protein	
RPS15	ribosomal protein	
RPS19	ribosomal protein	
RPS26	ribosomal protein	
RPL31	ribosomal protein	
RPL27	ribosomal protein	
YARS	tRNA synthetase, links tyrosine to cognate tRNA; cytokine activity	
FARSB	tRNA synthetase, links phenylalanine to cognate tRNA	
CARS	tRNA synthetase, links cysteine to cognate tRNA	
NARS	tRNA synthetase, links asparagine to cognate tRNA	
ABCE1	Ribosome recycling	
Protein folding		
CCT1/TCP1	protein folding in the cytosol	
CCT3	protein folding in the cytosol	
CCT5	protein folding in the cytosol	
CCT7	protein folding in the cytosol	
HSPA1A/HSP70	protein folding in the cytosol	
PFDN6	protein folding in the cytosol; co-chaperone for CCT	
PFDN4	protein folding in the cytosol; co-chaperone for CCT	
HSPD1/HSP60	protein folding in the mitochondria	
TRAP1	protein folding in the mitochondria; protection against ox stress; drug target	
HSPA9	protein folding in the mitochondria	
HYOU/GRP170	protein folding in the ER; hypoxia-induced	
HSPA5/GRP78	protein folding in the ER; part of the UPR	
PDIA4/ERp72	S=S bridge isomerase in the ER; part of the UPR	
TXNDC12/ERp16	S=S bridge isomerase in the ER; protection against ER stress and apoptosis	
P4HB	S=S bridge isomerase in the ER; protection against ER stress and apoptosis	
Protein modification		
GALNT1	mucin-type O-glycosylation	
MGEA5	hyluronidase; PcG-repressed gene	

PPP2R1A	ser/thr phosphatase 2, regulatory subunit
EXT2	Glycosyltransferase; heparan sulfate biosynthesis
GUSB	degrades heparan sulfate in the lysosomes
SGSH	degrades heparan sulfate in the lysosomes
XYLT1	Xylosyltransferase; glycosaminoglycan biosynthesis
CUL1	cullin1; ubiquitin ligase complex
SIAE	acetylesterase; removes acetyl groups from sialic acids
HEXA	hexosaminadase A; removes N-acetyl hexosamines
HEXB	hexosaminadase B; removes N-acetyl hexosamines
GGH	gamma glutamyl hydrolase; removes polyglutamates and glutamate
GLB1	b-galactosidase; removes b-galactose from glycoconjugates
Proteases and peptidases	
PSMA6	proteasome component
serpin B6	cathepsin D inhibitor
APEH	aminoacylhydrolase; destruction of oxidatively damaged proteins
CTSZ	cathepsin Z, lysosomal protease
CTSC	cathepsin C,
LAP3/ICE	caspase-7
NLN	neurolysin, metallopeptidase, ECM remodelling
LNPEP	aminopeptidase, cleaves several peptide hormones
PREP	prolylendopeptidase, cleaves several peptide hormones
CNDP2	nonspecific di-peptidase
XPNPEP1	aminopeptidase; cleaves several peptide hormones
ACE	aminopeptidase; angiotensin-converting enzyme
RNPEP	arginyl aminopeptidase
DPP3	peptidase; Activation of the antioxidant response element via NRF2
DPP7	prolyl peptidase
THOP1	oligopeptidase, medium-sized peptides
Actin cytoskeleton	
WDR1	co-factor for cofilin
PAK1	CDC42/Rac-activated kinase
PLS1	Plastin-1; actin-bundling protein
PLS3	Plastin-3; actin-bundling protein
Redox regulation	
GPX2	glutathione peroxidase; neutralization of peroxides; NRF2 target gene
GPX3	glutathione peroxidase; neutralization of peroxides
GSS	glutathione synthesis
GCLC	glutathione synthesis; NRF2 target gene
DPP3	peptidase; Activation of the antioxidant response element via NRF2
TXNRD1	thioredoxin reductase; selenoprotein; protection against oxidative stress; NRF2 target gene
TXNDC12	thioredoxin, protection against oxidative ER stress
NADSYN1	NAD synthesis
ME1	malic enzyme 1; generates NADPH
CCT7	NRF2 target gene
FTL	NRF2 target gene

Metabolism	
NADSYN	NAD synthesis > SIRT1 > gluconeogenesis
PGM1	phosphoglucomutase; Gluc-1-P > Gluc-6-P; Glycolysis
PGM2	phosphoglucomutase; Gluc-1-P > Gluc-6-P; Glycolysis
GPI	glucose-6-phosphate isomerase; Glycolysis
ALDOA	Alodalse A; Glycolysis
FH	fumarate hydratase, TCA cycle, tumor suppressor
GOT1	amino acid metabolism; TCA cycle
MDH2	malate dehydrogenase; TCA cycle
ACO2	aconitase; TCA cycle
ADI1	methionine salvage
ME1	malic enzyme 1; converts cytosolic malate to pyruvate, generates NADPH
GART	synthesis of purine nucleotides
GMPS	synthesis of purine nucleotides
ACAA2	acetyl-coA acyltransferase 2
ISYNA1	generates myoinositol-3-phosphate from glucose-6-phosphate
AIFM1	oxidative phosphorylation
MUT	generates succinyl-co-A in mitochondria
FABP2	transport and metabolism of fatty acids
CEL	carboxyl ester lipase; absorption and digestion of lipid nutrients
RNA synthesis and processing	
LSM4	Splicing factor, RNA-binding protein, splicing
SRSF1	Splicing factor, oncogene, Wnt target
SRSF2	Splicing factor, tumor suppressor in leukemia?
DDX39B	Splicing factor
ADI1	Splicing factor
CPSF1	polyAdenylation
CSTF3	polyAdenylation
POLR2G	subunit of RNA polymerase II; synthesis of mRNA
HNRNPL	binds hnRNA; formation of mRNA
EWSR1	Ewing sarcoma region 1, Transcription activation, RNA binding,
Angiogenin	RNAse; hydrolysis of tRNA; rRNA transcription; essential for angiogenesis
RNAse4	RNAse
Extracellular matrix/adhesion	
Necl-5/PVR	vitronectin receptor
PVRL1/nectin	binds Necl-5; formation of cell-cell junctions
DDR1	collagen receptor
PLOD3	lysyl hydroxylation of collagen
P4HB	prolyl-4 hydroxylation of collagen
LGALS3	carbohydrate-binding protein in the ECM
REG4	carbohydrate-binding protein in the ECM, also serum tumor marker
LTBP4	Binds TGFbeta in the ECM
Ladinin-1	Component of basement membranes
NPNT	nephronectin; integrin ligand
Chemokines/growth factors	
FGF2/bFGF	stimulates angiogenesis
CCL2	Chemokine
CXCL1	Chemokine

MIF	Chemokine
LTA4H	generates leukotriene B4; neutrophil attraction
YARS	N-terminus has IL-8-like cytokine activity
LTBP4	Binds TGFbeta in the ECM
Sema3A	ligand for neuropilin1; tumor suppressor
GPI/AMF	glucose-6-phosphate isomerase; Cytokine activity: Autocrine Motility Factor,
Tyrosine kinase signaling	
DDR1	collagen receptor
EPHB4	Receptor tyrosine kinase; pro-tumorigenic
EPHB2	Receptor tyrosine kinase; Marks tumor-initiating cells; Wnt target
Agr2	Oncogene (ER); stimulates expression of EGFR ligand Aregulin
ST14	membrane protease; activates HGF, uPA
EPS8	EGFR substrate
PTPRG	protein tyrosine phosphatase receptor G; potential tumor suppressor in CRC
FGF2	Receptor tyrosine kinase ligand
Membrane trafficking	
Vps35	retrograde transport Golgi
Rab5c	Endocytosis
AP2A2	Endocytosis; asymmetric division in HSC
AP1G1	formation of clathrin-coated vesicles
LAMP1	lysosome biogenesis; autophagy
Cell-cell adhesion	
DSC2	desmosome component; reduced in CRC tumors
DSG2	desmosome component
PVRL1/nectin	formation of cell-cell junctions; tight jnctns, adherens jnctns, desmosomes
Iron	
Transferrin	iron transport
Ferritin-light	iron storage
Ferritin-heavy	iron storage
RA signaling	
ALDH1A1	converts vitamin A into RA
RBP2	uptake of vitamin A

Supplementary Table III. Ingenuity analysis of colonosphere-enriched proteins. All 148 up-regulated proteins were analyzed by IPA. The main Molecular and Cellular functions, Canonical Pathways and Toxicity Pathways represented by this protein group are shown.

Main Molecular and cellular functions	Associated molecules	Focus molecules	
Cell Death and Survival	SRSF2,CARS,LGALS3,EPHB2,FGF2,DPP7,TRAP1, HYOU1,GCLC,CD46,HSPA5,AP2A2,ACAA2,SRSF1, ALDH2,PAK1,ALDH1A1,DPP3,LAMP1,TCP1,ACE, AIFM1,PTPRG,PSMA6,EPHB4,P4HB,EWSR1,YWHAG, RPL27,HSPA9,RPS19,YWHAZ,HSPD1,PVR,TXNRD1, ADI1,DDR,SEMA3A,PPP2R1A,GPI,TF,CBS,YARS,GPX2, DSG2,ANG,ABCE1,FTH1	48	
Cellular Growth and Proliferation	SRSF2,FTL,EPS8,LGALS3,FGF2,CUL1,TRAP1,CES2, CD46,HSPA5,GSS,CTSZ,GPX3, SRSF1,PAK1,ALDH1A1, CCT5,TCP1,HEXB,LTBP4,PTPRG,EPHB4,YWHAG,EWSR1, RPS19,EIF2C2,RPL23A,HSPD1,DDR1,SEMA3A,PPP2R1A, FABP2,GPI,TF,CBS,CCT7,CCT3,CTSC,CXADR,ANG,FTH1	41	
Main Canonical Pathways	Associated molecules	Molecules	Number of molecules in pathway
EIF2 Signaling	RPL31,RPL18A,EIF1AX,RPS26,RPL27,RPS15,RPS19, RPS13,EIF2C2,RPL23,RPL23A,RPS11	12	190
tRNA Charging	NARS,CARS,YARS,FARSB	4	81
Gluconeogenesis I	GPI,ALDOA,ME1,MDH2	4	48
Regulation of eIF4 and p70S6K Signaling	PPP2R1A,EIF1AX,RPS26,RPS15,RPS19,RPS13,EIF2C2, RPS11	8	170
Main Toxicity Pathways	Associated molecules	Molecules	Number of molecules in pathway
Oxidative Stress	GPX3,GPX2,GCLC,ME1,GSS	5	56
G2/M DNA Damage Checkpoint Regulation	YWHAG,CUL1,YWHAZ	3	45
NRF2-mediated Oxidative Stress Response	FTL,GPX2,CCT7,GCLC,TXNRD1,FTH1	6	206

6

GPX2 SUPPRESSION OF H2O2 STRESS LINKS THE FORMATION OF DIFFERENTIATED TUMOR MASS TO METASTATIC CAPACITY IN COLORECTAL CANCER

Benjamin L Emmink[1]*, Jamila Laoukili[1]*, Anna P Kipp[2], Jan Koster[3], Klaas M Govaert[1], Szabolcs Fatrai[1], Andre Verheem[1], Ernst JA Steller[1], Regina Brigelius-Flohé[2], Connie R Jimenez[4], Inne HM Borel Rinkes[1] and Onno Kranenburg[1]

[1] Department of Surgery, University Medical Center Utrecht, The Netherlands
[2] Department Biochemistry, German Institute of Human Nutrition, Germany
[3] Department of Oncogenomics, Academic Medical Center Amsterdam, The Netherlands
[4] OncoProteomics Laboratory, VU Medical Center, Amsterdam, The Netherlands

*Equal contribution

Cancer Research. 2014 Sep; in press

ABSTRACT

Colorectal tumorigenesis is accompanied by the generation of oxidative stress, but how this controls tumor development is poorly understood. Here, we studied how the H_2O_2-reducing enzyme glutathione peroxidase 2 (GPx2) regulates H_2O_2 stress and differentiation in patient-derived 'colonosphere' cultures. GPx2 silencing caused accumulation of radical oxygen species, sensitization to H_2O_2-induced apoptosis and strongly reduced clone- and metastasis-forming capacity. Neutralization of radical oxygen species restored clonogenic capacity. Surprisingly, GPx2-suppressed cells also lacked differentiation potential and formed slow-growing undifferentiated tumors. GPx2 overexpression stimulated multi-lineage differentiation, proliferation and tumor growth without reducing tumor-initiating capacity. Finally, GPx2 expression was inversely correlated with H_2O_2-stress signatures in human colon tumor cohorts, but positively with differentiation and proliferation. Moreover, high GPx2 expression was associated with early tumor recurrence, particularly in the recently identified aggressive subtype of human colon cancer. We conclude that H_2O_2 neutralization by GPx2 is essential for maintaining clonogenic and metastatic capacity but also for the generation of differentiated proliferating tumor mass. The results reveal an unexpected redox-controlled link between tumor mass formation and metastatic capacity.

INTRODUCTION

Oxidative stress due to accumulation of reactive oxygen species (ROS) like superoxide or hydrogen peroxide is commonly observed in many types of cancer cells[1-3]. In human colon cancer, several parameters of oxidative stress, such as lipid peroxidation and DNA hydroxylation, are increased with increasing stage[4-6]. Specific ROS, like H_2O_2, can act as second messengers in pro-tumorigenic signalling pathways. For instance, ROS generation is required for the expansion of intestinal stem cells during tumor initiation in the intestine[7]. However, excessive ROS generation can also lead to cell cycle arrest, senescence and programmed cell death[1, 8, 9]. To prevent this, tumor cells have to engage antioxidant programs to ensure redox homeostasis.

Colon tumors consist of tumor cells at different stages of differentiation. Transplantation studies of FACS-separated tumor cell subpopulations have indicated that clonogenic and tumor-initiating potential resides in a subset of undifferentiated cancer cells, frequently referred to as 'cancer stem cells' (CSCs) or 'tumor-initiating cells'[10, 11]. The factors and conditions that control maintenance of the undifferentiated clonogenic tumor cell fraction and their differentiation are incompletely defined, but redox homeostasis is likely to play an important role[12-14]. How redox homeostasis is achieved in colon tumors and whether this influences differentiation is largely unclear. In the current report we have identified the H_2O_2-scavenging enzyme intestinal glutathione peroxidase (GPx2) as a critical determinant of differentiation, tumor growth and metastasis. GPx2 keeps intracellular H_2O_2 levels low and thereby maintains the clonogenic and metastatic tumor cell population. In addition, we demonstrate that GPx2 promotes the formation of differentiated proliferating tumor bulk without exhausting tumor-initiating potential. The results identify redox control by GPx2 as a molecular link between the formation of differentiated tumor mass and metastatic capacity.

MATERIALS & METHODS

Collection, isolation, expansion and tumor formation of colorectal cancer colonospheres
Collection of tumor specimens was performed as described[15]. Human colorectal tumor specimens were obtained from patients undergoing a colon or liver resection for respectively primary or metastatic adenocarcinoma, in accordance with the ethical committee on human experimentation. Informed consent was obtained from all patients. The isolation, expansion and tumor formation of colorectal cancer colonospheres was performed as described[15], for a detailed description of each colonosphere culture used see Supplementary Methods.

Measurement of reactive oxygen species
To assay intracellular ROS, cells were incubated with 10μM CM-H2DCFDA) for 25 min at 37°C. The increase in fluorescence resulting from the oxidation of DCFDA to DCF was measured by microplate reader with emission and excitation of 492–495 and 517–527 nm respectively. To measure increase in intracellular ROS levels after H_2O_2 treatment cells were treated with 800μM H_2O_2, washed with PBS and loaded CM-H2DCFDA. To separate ROS high (top 10%) and low (bottom 10%) cells, colonospheres were made single cell, loaded with CM-H2DCFDA (25 minutes) and sorted with FACS Aria IIU (BD), using FACS Diva version 6.1 software. Dead cells were excluded using viability marker 7-aminoactinomycin D (7-AAD) (R&D, Detroit, MI) and cell doublets and clumps were excluded using doublet discrimination gating.

Transfection of colonosphere cultures

Generation of colonosphere cells stably expressing control scrambled shRNAs, shGPx2#1, or shGPx2#2 was performed as described previously[16]. Briefly, $1x10^5$ cells were transfected with 1ug of the corresponding plasmids by using SuperFect reagent (Qiagen, Hilden, Germany). Stable monoclonal cultures were generated by single-cell cloning and selected with 800ug/ml Geneticin.

Generation of Lentiviral GPx2-expression constructs

For cloning YFP-GPx2 into PLV-lentiviral vector, PCR amplified GPx2 was first cloned into pE-YFP-C1 using the following primers forward 5′-CGCGGATCCGCTTTCATTGCCAAGTCC-3′ and reverse 5′-CCGGAATTCGTCGACCTACCCTTTATTGGTCTCTTCTAGCAGAGTGGC-3′. The PCR product was digested with BamH1 and EcoR1, ligated to the pEYFP-C1 vector cut with BglII and EcoR1, and sequence verified. YFP-GPx2 segment was PCR amplified using primers 5′-CGCGGATCCACGCGT GCCGCCACCATGGTGAGCAAGGGCG-3′ and 5′-CCGATTGCTAGCCTACCCTTTATTGGTCTC TTCTAGCAGAGTGGC-3′. The PCR product was digested with Mlu1 and Nhe1, ligated to the PLV vector, and sequence verified. Flag-GPx2 was generated by PCR amplification from pCDNA3-GPx2 using the following primer pair Forward 5′-CGCATTACGCGTGGATCCGCCGCACCATGGATTAC AAGGATGACGACGATAAGGCTTTCATTGCCAAGTCC-3′, and reverse 5′-CCGATTGCTAGC CTACCC TTTATTGGTCTCTTCTAGCAGAGTGGC-3′. The PCR product was then cloned into PLV-lentiviral vector with Mlu1 and Nhe1. The final product was sequence verified. The sh-RNA insensitive versions of Flag or YFP-GPx2 were constructed using Quickchange mutagenesis kit (Stratagene) according to manufacturer's instructions and using the following pair of primers Forward: 5′-GAGGAGATCCTGAATAGCCTAAAGTATGTCCGTCC-3′ and Reverse: 5′-GGACGGACATACTTTAGG CTATTCAGGATCTCCTC-3′.

Generation of Lentiviral plasmid with GPx2-promoter-driven EGFP

The human GPx2 promoter (2111bp) was PCR amplified from pGL3-reporter plasmid using the following primers: forward CGCTTAATTAACCACTGAATTGGAATCACTGGAGG, and reverse 5′ CCGATTACCGGTTTGGCAATGAAACGCGTGGTGAAG C 3′, containing PAK1 restriction site at the 5′end and Age1 restriction site at the 3′end. The FUGW lentiviral vector with human ubiquitin promoter-driven EGFP [17] was cut with Pak1 and Age1 to release the ubiquitin promoter and was ligated back to the PCR product for human GPx2 promoter digested with Pak1 and Age1.

Liver metastasis model and tumor analysis

Pathogen-free, 10–11-week-old female SCID mice were purchased from Taconic (Ejby, Denmark). Colorectal liver metastases were induced, by injecting single cell suspensions (7.5×10^4 cells/100 µl) into the parenchyma of the spleen of 125-day-old SCID mice using a 27-gauge needle. After six weeks mice were sacrificed and tumor load in the liver was assessed in all liver lobes. Tumor load was scored as hepatic replacement area (HRA), that is, the percentage of liver tissue that had been replaced by tumor tissue. A fully detailed description of liver metastasis model and statistical analysis is provided in the Supplementary Methods.

Cell viability assay

To measure the viability of H_2O_2-treated colonosphere lines, $2x10^4$ cells were seeded in low adherent 24-well plates (Millipore). On the following day, cells were treated with H2O2, and viability was measured over time using CellTiter 96 Aqueous Non-Radioactive Cell-Proliferation assay or multi-tox viability assay (Promega, Madison, WI) according to the manufacturer's instructions.

Immunofluorescence
Colonospheres growing in suspension were harvested and fixed in PBS containing 4% of formaldehyde and permeabilized with ice-cold (-20°C) methanol. Cells were blocked in PBS containing 0.1% tween and 5%BSA, cells were incubated with primary antibodies for 2 hours at room temperature or overnight at 4°C. Colonospheres were subsequently washed and incubated with secondary antibodies (goat anti-rabbit Alexa Fluor 568, and goat anti-mouse Alexa Fluor 647) (Invitrogen) for 1 hour at room temperature. 0.5 µg/mL of DAPI was used to stain nuclei. Images were acquired using a Zeiss LSM510 Meta Confocal microscope and Zeiss LSM5 Software. All images were acquired with identical illumination-settings.

Western Blot analysis
Lysates of colonospheres were prepared either in NP-40 lysis buffer (20 mm HEPES pH7.4, 1% Nonidet P-40, 150 mm NaCl, 5 mm MgCl2, 10% glycerol), or in laemmli buffer. Equal amounts of protein were loaded on NuPAGE Novex Tris-Acetate Mini Gel (Invitrogen) and were analyzed by Western blotting.

Clone forming assay
Colonosphere cell cultures were dissociated as single cells using Accumax (Innovative Cell Technologies). Single-cell suspensions were then filtered through a 40-µm-pore size nylon cell strainer (BD Falcon), and counted. Single cells were then suspended in Matrigel (500 cells in 50 µL) (BD Biosciences, Franklin Lakes, NJ), and allowed to set in 12-well plates at 37°C in a 5% CO2 humidified incubator. After setting, stem cell medium containing fresh growth factors, supplemented or not with 0.2mM NAC, was added. Number of single clones was analyzed after 2 weeks of culture. Colonies were counted using a Leica DM IRBE microscope (Leica, Solms, Germany).

Flow cytometry, cell sorting and immunohistochemistry
Procedure of flow cytometry, cell sorting and immunohistochemistry have been described[15, 16]. A detailed description of methods is provided in the Supplementary Methods.

RNA extraction and Quantitative RT-qPCR
Total RNA was isolated using the RNeasy Mini kit (Qiagen) according to the manufacturer's instructions. cDNA from xenografts and colonospheres was synthesised from 1µg total RNA using iScript cDNA synthesis kit (BioRad). The PCR reactions were set up in a volume of 25µl containing 4µl diluted cDNA, 12.5µl 2xiQ SYBR Green Supermix (BioRad), 8.25 µl H2O and 300nM forward and reverse primer each. The primers (Supplementary Table S5) were mRNA specific to prevent signal information from contaminating genomic DNA. RPL13A and HPRT1 were used as housekeeping genes. All cDNA samples were analysed in triplicate.

Bioinformatic analyses
All analyses were performed using the R2 microarray analysis and visualization platform (http://r2.amc.nl). A fully detailed description of how the GPx2-coexpression and differentiation signature was generated is provided in the Supplementary Methods.

Statistics

All values are presented as mean ± SEM. The Student t test (unpaired, 2-tailed) was performed to analyse if differences between the groups are statistically significant. Differences with a P value of less than 0.05 were considered statistically significant.

Antibodies and reagents

A detailed description of all products used is provided in the Supplementary Methods.

RESULTS

Identification of GPx2 as a key regulator of intracellular H_2O_2 levels and sensitivity to H_2O_2 stress.

Multiple anti-oxidant enzymes control the levels of reactive oxygen species in (tumor) cells. To identify factors regulating redox status in colon cancer, we used three independent H_2O_2-stress-reflecting gene signatures ([18, 19] and http://speed.sys-bio.net) and combined them into a single H_2O_2-stress 'metagene' (Supplementary Table S1). Although there was little overlap between the gene sets, their expression was strongly correlated (Supplementary Table S1). Expression of the metagene was compared to expression of genes encoding major ROS-neutralizing enzymes in three large cohorts of colon cancer patients[20-23]. Of all genes analysed, only one was significantly inversely correlated with expression of the H_2O_2-stress metagene in all three datasets: intestinal glutathione peroxidase (GPx2) (Supplementary Table S2).

Figure 1 GPx2 regulates intracellular H_2O_2 levels and sensitivity to H_2O_2-induced stress in colon cancer cells.
A, Western blot analysis of GPx2 protein levels in L145 colonospheres following short-hairpin RNA mediated GPx2 silencing by two independent shRNAs (#1 and #2).
B, FACS analysis of ROS levels using H2DCFDA probe in L145 colonospheres expressing either scrambled or GPx2-targeting shRNAs.
C, Fluorimetric analysis of ROS levels with H2DCFDA in L145 colonospheres expressing either scrambled or GPx2-targeting shRNAs. Data are shown as means +SEM and represent data from 3 independent experiments. *p≤ 0.05.
D, Western blot analysis of GPx2 levels in ROS^{low} and ROS^{high} cells (L145 and L167) separated by FACS-sorting on the basis of H2DCFDA probe.
E, Fluorimetric analysis of ROS levels with H2DCFDA in L145 colonospheres expressing either scrambled or GPx2-targeting shRNAs after treatment with exogenous H_2O_2. The data are plotted as H_2O_2-induced increase of the absorbance values over (untreated) control values. Data are shown as means +SEM and represent data from 3 independent experiments. *p≤ 0.05.
F, Analysis of cell viability in L145 colonospheres expressing either scrambled or GPx2-targeting shRNAs after treatment with exogenous H2O2 using multitox-fluor viability probe (Promega). Data are shown as means +SD and represent data from 3 independent experiments. *p≤ 0.05.
G, Analysis of cell viability in L145 colonospheres expressing either scrambled or GPx2-targeting shRNAs and rescue vectors encoding the FLAG-tag alone or GPx2-FLAG after treatment with exogenous H2O2 using multitox-fluor viability probe. Data are shown as means +SEM and represent data from 3 independent experiments. *p≤ 0.05, ns = not significant.
H, Clone,-forming assay in Matrigel of L145 and HT29 cells expressing scrambled or GPx2-targeting shRNAs in the presence or absence of N-acetyl-cysteine (NAC). The plots show the number of clones in each group as means ± SEM, *p<0.05, **p<0.01.
See also Supplementary Figure S1

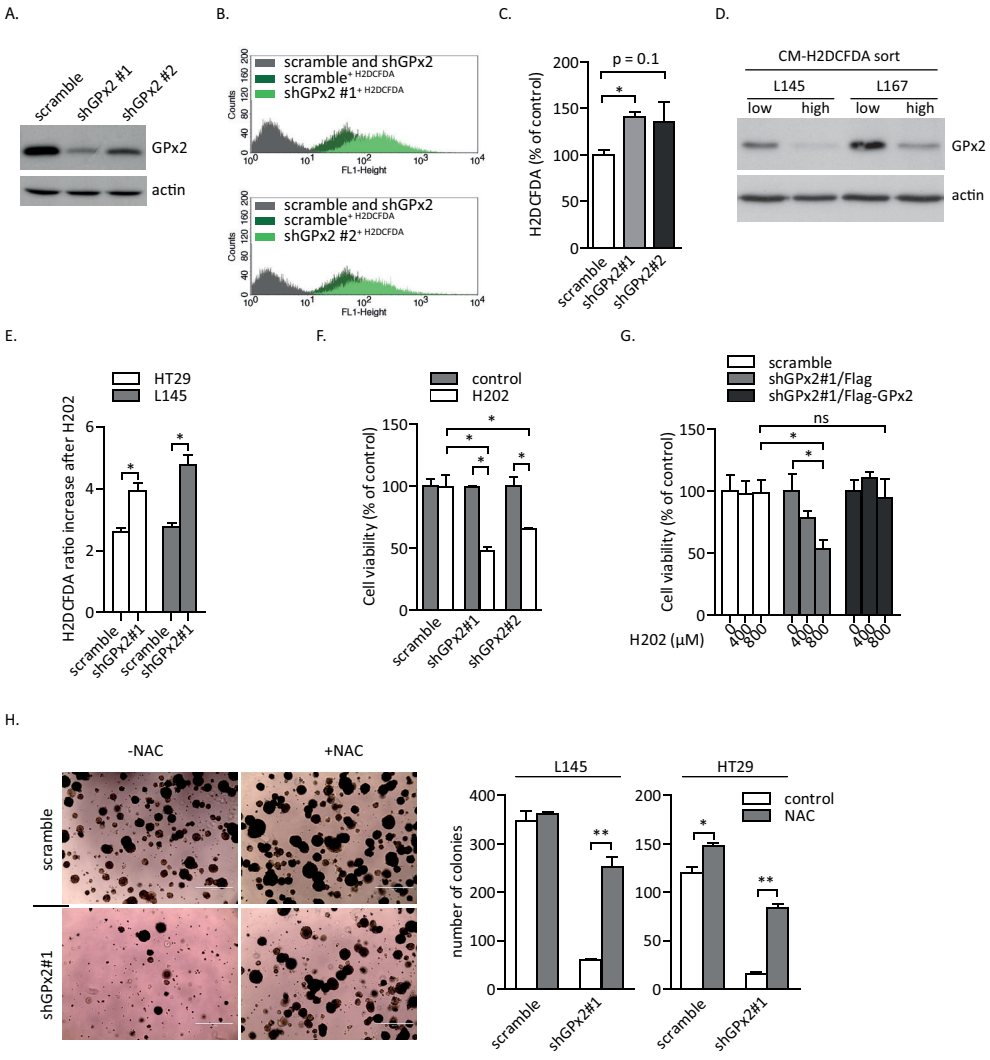

GPx2 reduces H_2O_2 by using glutathione as a thiol substrate[24]. It is mainly expressed in epithelial cells of the gastrointestinal tract, particularly those at the proliferating crypt base[25-27] and is also highly expressed in intestinal adenomas and in colon tumors[27]. This suggests that GPx2 may regulate redox homeostasis in colon cancer. To assess its function in colon cancer cells we suppressed GPx2 expression by using two independent short-hairpin RNAs (shRNAs) in patient-derived colonosphere cultures (Fig. 1A, Supplementary Fig. S1A and S2A). First, we assessed how depletion of GPx2 would affect intracellular redox status by using the 2'- 7'dichlorofluorescein (CM-H2DCFDA) probe. GPx2-depleted cells contained significantly higher basal levels of reactive oxygen species (ROS) than control cells (Fig. 1B and 1C). Furthermore, cell sorting on the basis of intracellular ROS levels with CM-H2DCFDA showed that ROS^{high} cells express far lower levels of GPx2 than ROS^{low} cells (Fig. 1D). Upon treatment with increasing concentrations of H_2O_2, GPx2-depleted cells showed a significantly more pronounced increase in intracellular ROS levels

when compared to control cells (Fig. 1E) and this resulted in a concomitant sensitization to H_2O_2-induced cell death (Fig. 1F). Rescue with an shRNA-insensitive GPx2 mutant completely restored tumor cell resistance to H_2O_2-induced cell death (Fig. 1G). Moreover, loss of GPx2 greatly augmented apoptosis induced by loss of cell-cell adhesion (Supplementary Fig. S1B) which is known to be ROS-mediated[28]. In addition, treatment of colonospheres with Elesclomol or Cisplatin, two drugs known to induce high intracellular ROS levels, resulted in a clear sensitization of the GPX2-depleted cells to both drugs (Supplementary Fig. S1C). Next, we tested how GPx2-depletion affects *in vitro* clone-forming potential. GPx2 silencing strongly reduced the capacity of colonosphere cells to proliferate and to form single-cell-derived clones (Supplementary Fig. S1D). Next, we examined whether elevated ROS levels were the cause of reduced proliferation and clonogenic potential in GPx2-depleted tumor cells, by using the ROS scavenger N-acetylcysteine (NAC). NAC treatment largely restored clone-forming capacity of GPx2-suppressed cells (Fig. 1H) and significantly increased expression of the proliferation marker Ki67 (Supplementary Fig. S1E). Consistent with this observation, H_2O_2 treatment decreased expression of Ki67 in control and GPx2-depleted cells (Supplementary Fig. S1F). These results identify redox control by GPx2 as an important determinant of proliferation and clonogenic capacity in colon cancer cells.

GPx2 silencing generates stem-like cancer cells that lack multi-lineage differentiation capacity.

Increased ROS levels in GPx2-suppressed colonospheres may lead to exhaustion of the fraction of tumor-initiating cells. Therefore, we analysed how GPx2 silencing would affect expression of markers reflecting the presence of stem-like cells and differentiation. Surprisingly, despite reducing clone-forming capacity, GPx2 silencing resulted in a marked increase in aldehyde dehydrogenase (ALDH) activity which marks the clonogenic tumor cell population in these colonosphere lines (Fig. 2A,[15]). In addition, loss of GPx2 resulted in a strongly increased expression of several stem cell genes including OLFM4, Nanog, Sox2 and EphB2 in three independent colonosphere cell lines (Fig. 2B and Supplementary Fig. S2B). Add-back of an shRNA-insensitive form of GPx2, or ROS neutralization with NAC, reduced stem cell marker expression to (near) normal levels while H_2O_2 treatment further augmented it (Fig. 2C and Supplementary Fig. S2C). H_2O_2 and NAC treatment had no effect on GPx2 gene expression (Fig. 2D).

Figure 2 GPx2 silencing generates stem-like cancer cells that lack multi-lineage differentiation capacity.
A, FACS-analysis using the Aldefluor® assay in L145 colonospheres and in HT29 cell variants expressing either scrambled, shGPx2#1, or shGPx2#2 shRNAs. Cells incubated with the Aldefluor substrate BAAA and the ALDH specific DEAB inhibitor were used to set the gate.
B, qPCR analysis of mRNA levels of GPx2 and the indicated stem cell markers in L145 and HT29 colonospheres cells stably expressing scrambled shRNAs or shGPx2#1. Graphs show mean ± SEM,* $p<0.05$.
C, qPCR analysis of mRNA levels of OLFM4 and SOX2 in L145 and HT29 colonospheres expressing scrambled shRNAs, or shGPx2#1 in combination with either YFP (control) or shGPx2-insensitive YFP-GPx2. Graphs show mean ± SEM.
D, qPCR analysis of mRNA levels of the indicated differentiation markers in L145 and HT29 colonospheres cells stably expressing scrambled shRNAs or shGPx2#1. Graphs show mean ± SEM,* $p<0.05$. Expression of all stem cell and differentiation markers was tested in all cell lines. qPCR data are only shown for the genes that were expressed above background levels.
See also supplementary Figure. S2
E, Immunoblot analysis of GPx2 and differentiation markers (MUC2 and CK20) in control and shGPx2#1-expressing HT29 colonospheres at the indicated time points following single-cell making.
F, Alkaline Phosphatase (ALP) activity analysis in L145 colonospheres (left panel) expressing scrambled shRNAs or shGPx2#. Measurement of ALP activity in HT29 colonospheres (right panel) expressing scrambled shRNAs or shGPx2#1 in the absence or presence of butyrate. Graphs show mean ± SEM,* $p<0.05$
G, ALP activity analysis (left panel) in L145 colonosphere cells expressing scrambled shRNAs and shGPx2#1 reconstituted with either YFP or shRNA-insensitive YFP-GPx2. Graphs show mean ± SEM,* $p<0.05$.

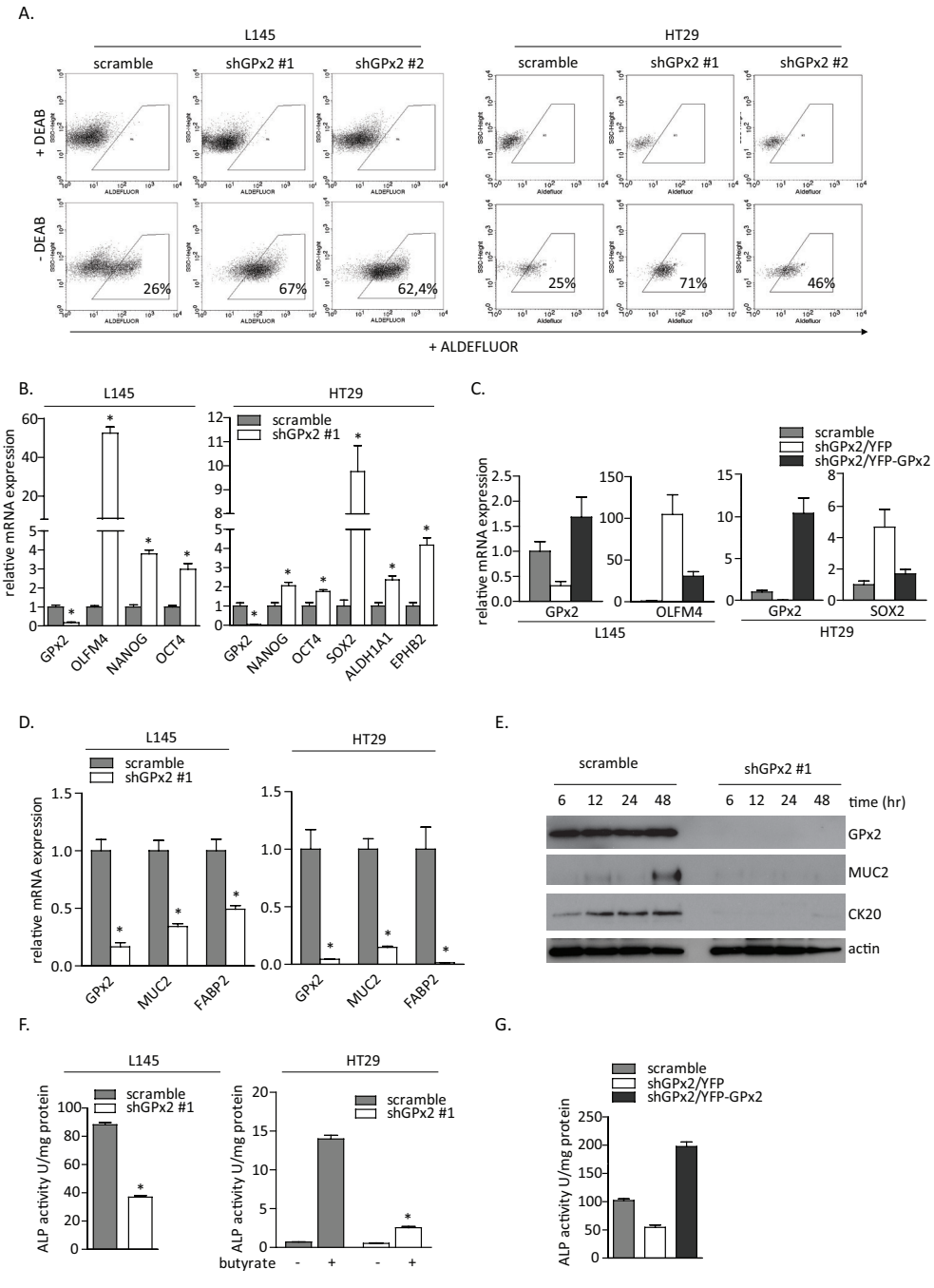
A.
L145
HT29
scramble
shGPx2 #1
shGPx2 #2
+ DEAB
- DEAB
26%
67%
62,4%
25%
71%
46%
+ ALDEFLUOR
B.
L145
HT29
scramble
shGPx2 #1
relative mRNA expression
GPx2
OLFM4
NANOG
OCT4
SOX2
ALDH1A1
EPHB2
C.
scramble
shGPx2/YFP
shGPx2/YFP-GPx2
relative mRNA expression
GPx2
OLFM4
SOX2
L145
HT29
D.
L145
HT29
scramble
shGPx2 #1
relative mRNA expression
GPx2
MUC2
FABP2
E.
scramble
shGPx2 #1
6
12
24
48
time (hr)
GPx2
MUC2
CK20
actin
F.
L145
HT29
scramble
shGPx2 #1
ALP activity U/mg protein
butyrate
G.
scramble
shGPx2/YFP
shGPx2/YFP-GPx2
ALP activity U/mg protein

The increase in stem cell marker expression was accompanied by a concomitant loss of differentiation markers, including cytokeratin 20 (CK20), Mucin2 (MUC2; goblet cells) and FABP1/2 (enterocytes) (Fig. 2D, Supplementary Fig. S2E and S2F). Normally, differentiation marker expression increases over time as colonospheres grow from single cells, but this was completely prevented in the absence of GPx2 (Fig. 2E). Furthermore, GPx2 suppression greatly decreased basal and butyrate-induced Alkaline Phosphatase (ALP) activity, a marker for differentiation (Fig. 2F). Add-back of the shRNA-insensitive form of GPx2 restored ALP activity and differentiation marker expression (Fig. 2G and Supplementary Fig. S2G).

To assess whether the reduced differentiation capacity of GPx2-suppressed cells was the result of a selection process due to their apoptosis sensitivity (Fig. 1F, Supplementary Fig. S1B and S2H) we tested whether blocking apoptosis would rescue their differentiation capacity. Supplementary Fig. S2H shows that blocking apoptosis with the z-VAD peptide did not rescue differentiation in GPx2-suppressed cells. There was no effect of GPx2 suppression on markers of senescence, including the expression of p16 and nuclear heterochromatin foci (Supplementary Fig. S2H and S2I and data not shown).

Together, the above findings show that GPx2 loss generates a population of stem-like cancer cells that are prone to H_2O_2-induced stress and that have lost multi-lineage differentiation capacity.

GPx2-suppressed cells from slow growing tumors with a stem-like phenotype but lack metastatic capacity

The above results show that GPx2 regulates both stress sensitivity and differentiation potential and may therefore affect tumor and metastasis formation. To test this, we injected control and GPx2-depleted colonospheres into immunodeficient mice. Colonospheres lacking GPx2 formed significantly smaller tumors than control cultures (2 independent shRNAs; 3 independent clones; Fig. 3A and Supplementary Fig. S3A). In all cases, the incidence of tumor formation was similar to that of control cultures (>80%). Phenotypic analysis of the resulting tumors by RT-qPCR and FACS revealed high expression of stem cell markers and high ALDH activity (Fig. 3B, 3C and Supplementary Fig. S3B), and an accompanying loss of differentiation marker expression (Fig. 3D). Analysis of tumor sections by immunohistochemistry showed that reduced tumor growth was associated with a significant decrease in the number of proliferating (Ki67-positive) cells (Fig. 3E), which is in line with the results obtained in vitro. By contrast, we did not observe an effect of GPx2 suppression on tumor cell apoptosis (Fig. 3E).

Next, we investigated the requirement for GPx2 during metastasis formation. The most common site for colon cancer metastasis is the liver. To induce liver metastases we injected control and GPx2-depleted tumor cells into the spleen, from where they reach the liver through the portal vein. Despite their stem-like phenotype, GPx2-depleted cells displayed a dramatic reduction in metastatic capacity (Fig. 4A-4C). The few metastatic nodules that did develop from GPx2-depleted cell populations had retained expression of GPx2 (Fig. 4D and 4E). These GPx2-positive cell populations were pre-existent as demonstrated by the presence of GPx2-positive patches in the developing spleen tumors (Fig. 4D and 4E).

Taken together, GPx2-suppressed colonospheres form slowly proliferating tumors with an undifferentiated CSC-like phenotype, but they are unable to establish liver metastases.

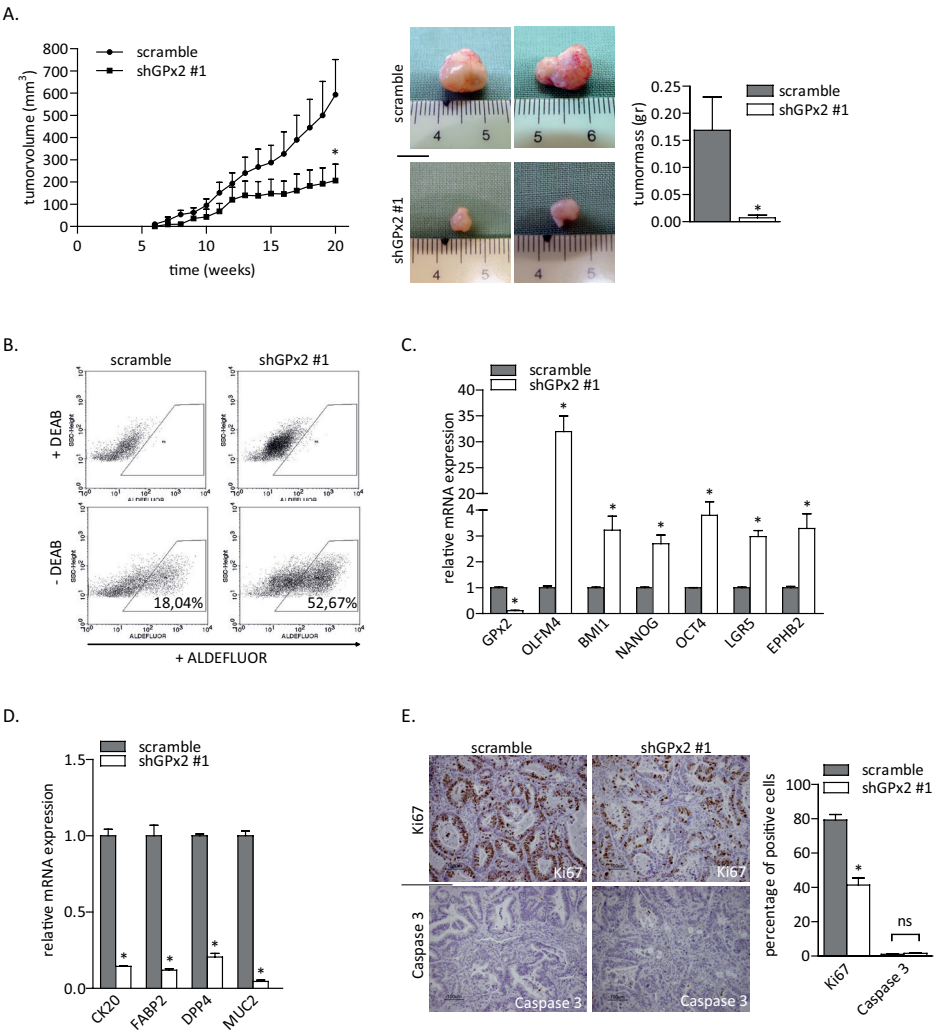

Figure 3 GPx2-suppressed cells from slow growing undifferentiated tumors.
A, In vivo tumorigenicity assay comparing colonospheres derived from L145 cells expressing scrambled shRNAs or shGPx2#1. The equivalent of 3000 cells was inoculated subcutaneously into both flanks of immunodeficient mice (n=4). Volume (left panel) and tumor mass (right panel) measurement of subcutaneous tumors from both groups are shown. The incidence of tumor formation was 7 out of 8 in both groups. The photograph shows tumors formed in both groups (middle panel). Graphs show mean ± SEM,* p<0.05.
B, FACS-analysis (left panel) using Aldefluor® assay in cells isolated from subcutaneous L145 tumors expressing either scrambled shRNAs or shGPx2#1. Cells incubated with the Aldefluor® substrate BAAA and the ALDH specific inhibitor DEAB were used to set the gate.
C, qPCR analysis of mRNA levels of the indicated stem cell genes in xenografts expressing scrambled shRNAs or shGPx2#1. Graphs show mean ± SEM,* p<0.05.
D, qPCR analysis of mRNA levels of the indicated differenation genes in xenografts expressing scrambled shRNAs or shGPx2#1. Graphs show mean ± SEM,* p<0.05.
E, Immunohistological staining of paraffin-embedded sections of subcutaneous tumors derived from scrambled and shGPx2#1-expressing L145 cells using anti-Ki67 or anti-active-caspase 3 antibodies. Quantification of the number of marker-positive cells is shown in the graph (mean ± SEM) ,* p<0.05.
See also supplementary figure S3

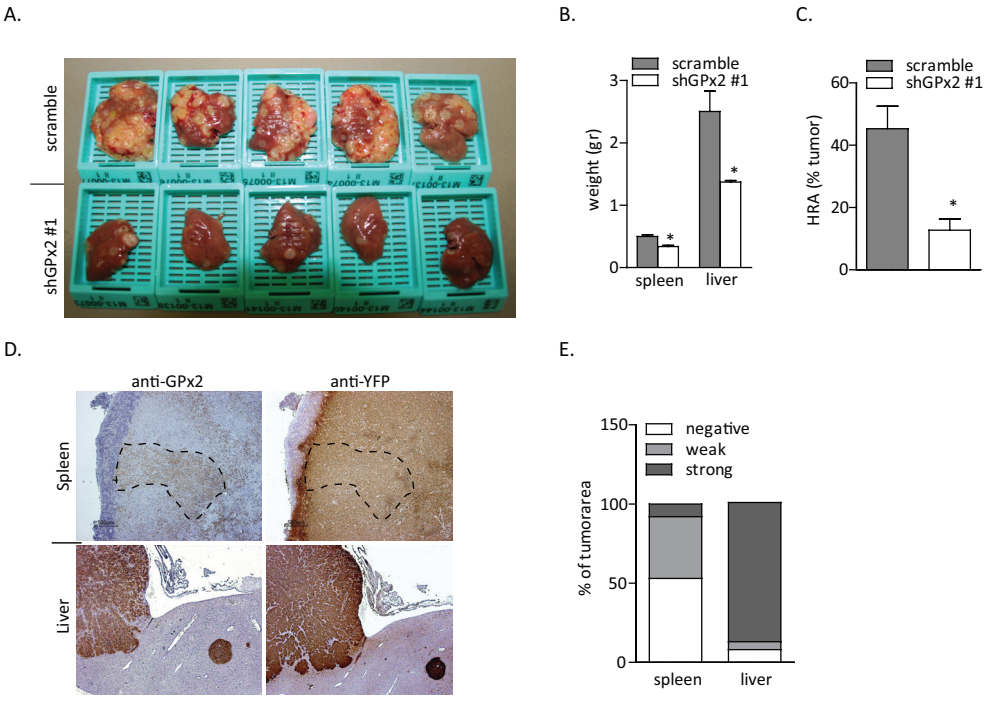

Figure 4 GPx2-suppressed cells lack metastatic capacity.
A, Photograph showing liver metastasis derived from scrambled-YFP-HT29 or shGPx2#1-YFP-HT29 cells after injection of $7{,}5.10^4$ cells into the spleen of SCID mice.
B, Measurement of organ weight of livers and spleens derived from mice injected with scrambled-YFP-HT29 or shGPx2#1-YFP-HT29 cells. Graph show mean ± SEM,* $p<0.05$.
C, The graph shows measurement of the Hepatic Replacement Area (HRA) for each group. Graph in show mean ± SEM, *$p<0.05$.
D, Immunostaining of paraffin-embedded tissue sections of spleen tumors and liver metastases derived from YFP-HT29 shGPx2#1-expressing cells using anti-GPx2 and anti-YFP antibodies. The dashed line delineates a GPx2-positive patch in a shGPx2#1 spleen tumor.
E, Quantification of GPx2 expression (% positive tumor area and intensity of staining) in spleen and liver tumors formed by YFP-HT-29 shGPx2#1 cells.

Overexpression of GPx2 stimulates the formation of proliferating differentiated tumor mass.

The above results suggest that GPx2 is required for the formation of differentiated proliferating tumor mass. To determine whether GPx2 levels regulate differentiation and drive tumor mass formation in vivo, we expressed flag- or YFP-tagged GPx2 in colonosphere cell lines with relatively low levels of endogenous GPx2 (Fig. 5A and Supplementary Fig. S4A). Overexpression of YFP-GPx2 caused a marked increase in the expression of markers associated with various differentiation lineages present in the colon, including MUC2 (goblet cells), FABP1 (enterocytes) and Chromogranin A (enteroendocrine cells) (Fig. 5B and Supplementary Fig. S4B and S4C). By contrast, stem cell markers were suppressed following GPx2 expression (Fig. 5D and Supplementary Fig. S4D). Similar results were obtained with Flag-GPx2-expressing colonosphere lines (data not shown). Importantly, when injected subcutaneously into immunodeficient mice, YFP-GPx2 or flag-GPx2 overexpressing colonospheres (3 independent lines) grew more rapidly when compared to control (YFP-expressing) cells and with a reduced latency (Fig. 5E and Supplementary Fig. S4E). This was even more pronounced in a secondary transplantation experiment (Fig. 5F), indicating that GPx2 overexpression does not lead to exhaustion of the tumor-initiating cell fraction but rather that these cells are more prone to form rapidly proliferating and differentiating offspring expanding the tumor mass. Tumors derived from GPx2-overexpressing colonospheres also displayed increased basal Alkaline Phosphatase activity and elevated expression of multi-lineage differentiation markers and the proliferation marker Ki67 (Fig. 5H and 5G), while stem cell genes were strongly suppressed (Fig. 5I).

To assess whether *endogenous* expression levels of GPx2 correlate with proliferation and differentiation potential, we generated a lentiviral construct in which the GPx2 promoter drives expression of GFP. Colonospheres were transduced with this construct and monoclonal cultures were generated by single-cell cloning to exclude variations in promoter activity due to differential transduction efficiency. FACS analysis showed heterogeneous expression of GFP in these cultures (Fig. 6A). Next, we used FACS sorting to separate GFP-high from GFP-low cells. This generated subpopulations of GPx2-high and GPx2-low tumor cells (Fig. 6A). GPx2-high cells expressed high levels of differentiation and proliferation markers whereas GPx2-low cells expressed high levels of stem cell genes (Fig. 6B and 6C). In addition, GPx2-high cells had a significantly higher tumor-initiating potential than GPx2-low cells (Fig. 6D). Collectively, our results identify GPx2 as a critical regulator of the formation of proliferating differentiated tumor mass.

Figure 5 Overexpression of GPx2 stimulates the formation of proliferating differentiated tumor mass.
A, Immunoblot analysis of GPx2 protein and the indicated differentiation markers in L169 colonosphere lines stably expressing Flag- or YFP-tagged GPx2. *Indicates endogenous GPx2 protein.
B, qPCR analysis of mRNA levels of the indicated differentiation markers was performed on L169 colonosphere line stably expressing YFP-GPx2 protein. Data are shown as means +SEM and represent data from 3 independent experiments. *p≤ 0.05.
C, Immunofluorescence staining of the differentiation markers MUC2, FABP1, CK20 and ChrA on control L169 colonospheres and those stably expressing YFP-GPx2.
D, q-PCR analysis of mRNA levels of the indicated stem cell genes in L169 colonosphere line stably expressing YFP-GPx2 protein. Data are shown as means +SEM and represent data from 3 independent experiments. *p≤ 0.05.
E, Tumor formation by L169 colonospheres expressing YFP or YFP-GPx2 injected subcutaneously into immunodeficient mice. n=10. Graph shows mean ± SEM, *p<0.05.
F, Subcutaneous Xenografts derived from L169 colonospheres expressing YFP or YFP-GPx2 as described in F were digested into single cells, re-transplanted into immunodeficient mice, and measured for tumor growth. Graph shows mean ± SEM, *p<0.05.
G, Measurement of ALP activity in Xenografts derived from L169 colonospheres expressing YFP or YFP-GPx2 as described in (E). Graph shows mean ± SEM,* p<0.05.
H, q-PCR analysis of mRNA levels of GPx2, the indicated differentiation genes and the proliferation gene Ki67 in L169 xenografts stably expressing YFP-GPx2 protein. Graphs show mean ± SEM, *p<0.05
I, q-PCR analysis of mRNA levels of the indicated stem cell genes in L169 xenografts stably expressing YFP-GPx2 protein. Graphs show mean ± SEM, *p<0.05
See also supplementary figure S4

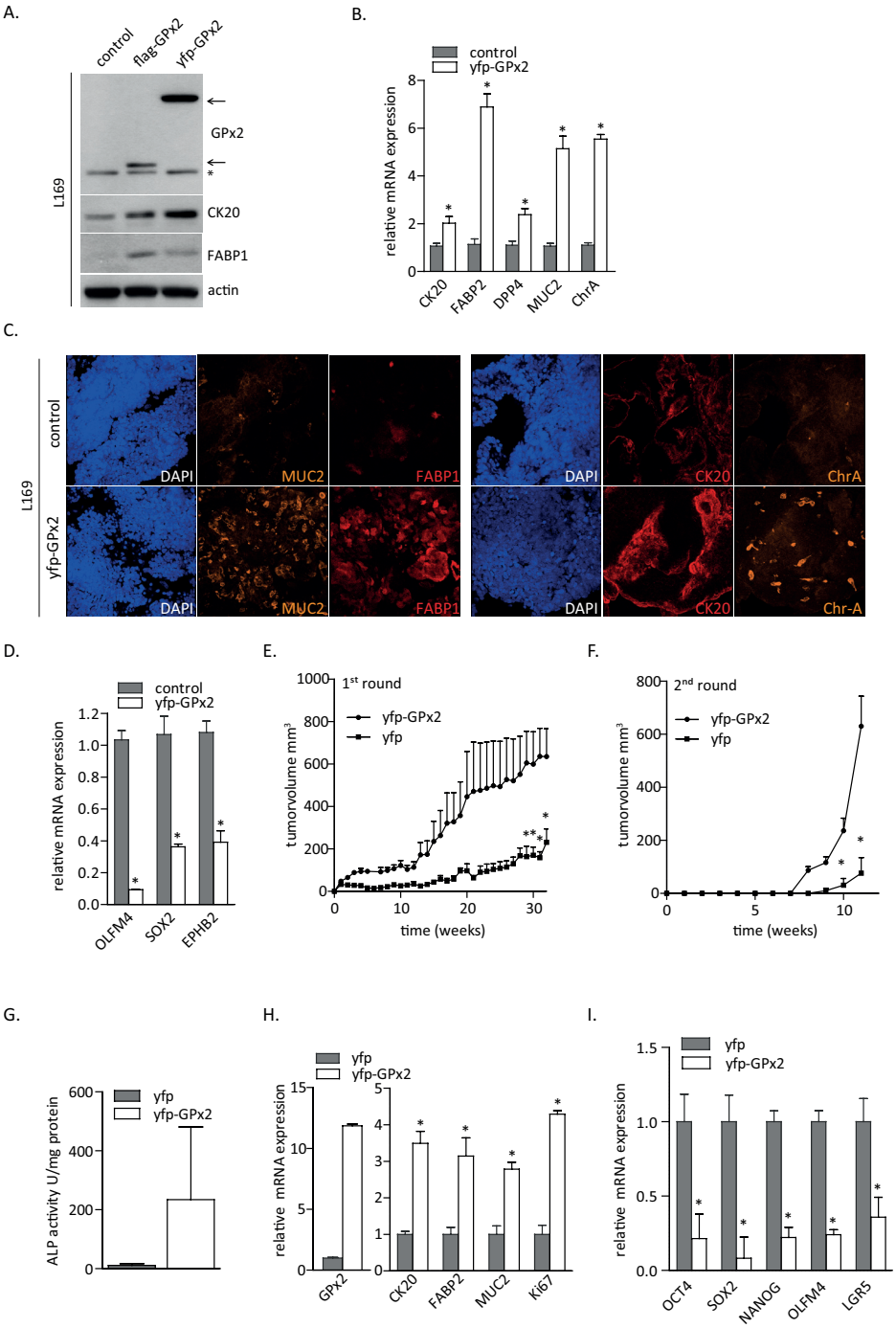
A.
control
flag-GPx2
yfp-GPx2
L169
GPx2
CK20
FABP1
actin
B.
control
yfp-GPx2
relative mRNA expression
CK20
FABP2
DPP4
MUC2
ChrA
C.
L169
control
yfp-GPx2
DAPI
MUC2
FABP1
DAPI
CK20
ChrA
DAPI
MUC2
FABP1
DAPI
CK20
Chr-A
D.
control
yfp-GPx2
relative mRNA expression
OLFM4
SOX2
EPHB2
E.
1st round
yfp-GPx2
yfp
tumorvolume mm3
time (weeks)
F.
2nd round
yfp-GPx2
yfp
tumorvolume mm3
time (weeks)
G.
yfp
yfp-GPx2
ALP activity U/mg protein
H.
yfp
yfp-GPx2
relative mRNA expression
GPx2
CK20
FABP2
MUC2
Ki67
I.
yfp
yfp-GPx2
relative mRNA expression
OCT4
SOX2
NANOG
OLFM4
LGR5

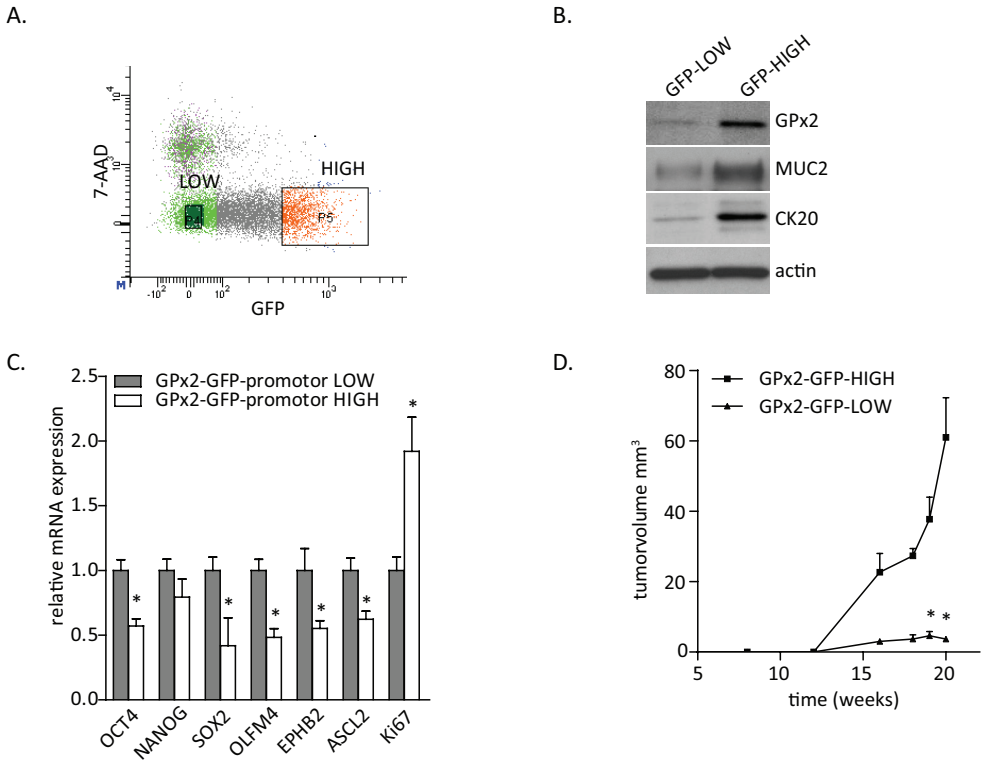

Figure 6 High GPx2-promotor activity defines a cancer cell population with increased proliferation, differentiation and tumor forming potential**.**

A, FACS sort of GFP-low and GFP-high expressing cells in single-cell suspensions derived from L145 sub-cloned line where GFP expression is driven by endogenous GPx2-promoter. 7-AAD staining was used to exclude dead cells.

B, FACS-sorted GFP^{low} and GFP^{high} samples were collected and processed for Western blot for the expression of GPx2 protein and the indicated differentiation markers.

C, q-PCR analysis of the FACS-sorted GFP^{low} and GFP^{high} samples for the expression of the indicated stem cell genes and proliferation marker Ki67. Graphs show mean ± SEM, *p<0.05.

D, Tumor formation assay comparing FACS-sorted GFP^{low} and GFP^{high} L145 cells. The equivalent of 1000 cells was inoculated subcutaneously into immunodeficient mice (n=6). Graph shows mean ± SEM, *p<0.05

GPx2 expression defines a subgroup of colon tumors displaying differentiation, proliferation and low H_2O_2 stress.

The data so far link GPx2 to differentiation and proliferation of patient-derived colonosphere cultures and the experimental tumors that are derived from them. We next assessed the relevance of these findings for human colon cancer. To this end we used transcriptomic profiles of two distinct cohorts[20, 23] of colorectal tumors and identified the genes whose expression was significantly correlated with GPx2. The 100 genes that were most significantly co-expressed with GPx2 in both cohorts were identified. The overlapping gene set (53 genes, Supplementary Table S3) was then used to cluster the tumors of three large cohorts[20-23] into GPx2-expression subgroups with low, median and high expression of GPx2 (Fig. 7A and 7B). GPx2^{high} tumors were characterized by high expression of Wnt target genes and markers of epithelial differentiation, while being inversely correlated with mesenchymal gene expression (Fig. 7B). The GPx2^{high} group almost completely overlapped with the well-differentiated Wnt^{high} Colon Cancer Subtype 1 (CCS1 (22); Supplementary Fig. S5A). Gene Set Enrichment Analysis (GSEA) shows that signatures reflecting epithelial differentiation (Methods, Supplementary Table S4), WNT pathway activity[29] and proliferation[30] are strongly enriched in GPx2^{high} tumors (Fig. 7C). Indeed, histologically well-differentiated human colon tumors express significantly higher levels of GPx2[31] as well as the GPx2 co-expression signature (Supplementary Fig. S6A). Conversely, GPx2 was inversely correlated with a signature for primitive undifferentiated tumors (Nanog/Oct4/Sox2-target genes)[32] (Fig. 7D). In line with its function as an H_2O_2 scavenger, GPx2 expression was also inversely correlated with expression of the H_2O_2-metagene (Supplementary Table S1, Fig. 7D, Supplementary Fig. S5C). Indeed, NOS^{high}/GPx2^{low} (stem cell-like) tumors displayed far higher expression of the H_2O_2 metagene than differentiated NOS^{low}/GPx2^{high} tumors (Fig. 7D).

While GPx2 is clearly more highly expressed in the less aggressive CCS1 subtype, its expression is also considerable in the aggressive CCS3 subtype (median 2log expression ~9). In fact, the HT29 cell line that was used for the metastasis experiments belongs to this CCS3 subgroup[22]. Strikingly, when only considering the CCS3 subtype, high GPx2 expression levels were associated with a significantly increased risk of metastasis formation in two independent large human colon tumor cohorts (AMC-90[22] and MVRM-345[20, 23]; Supplementary Fig. S6B and S6C).

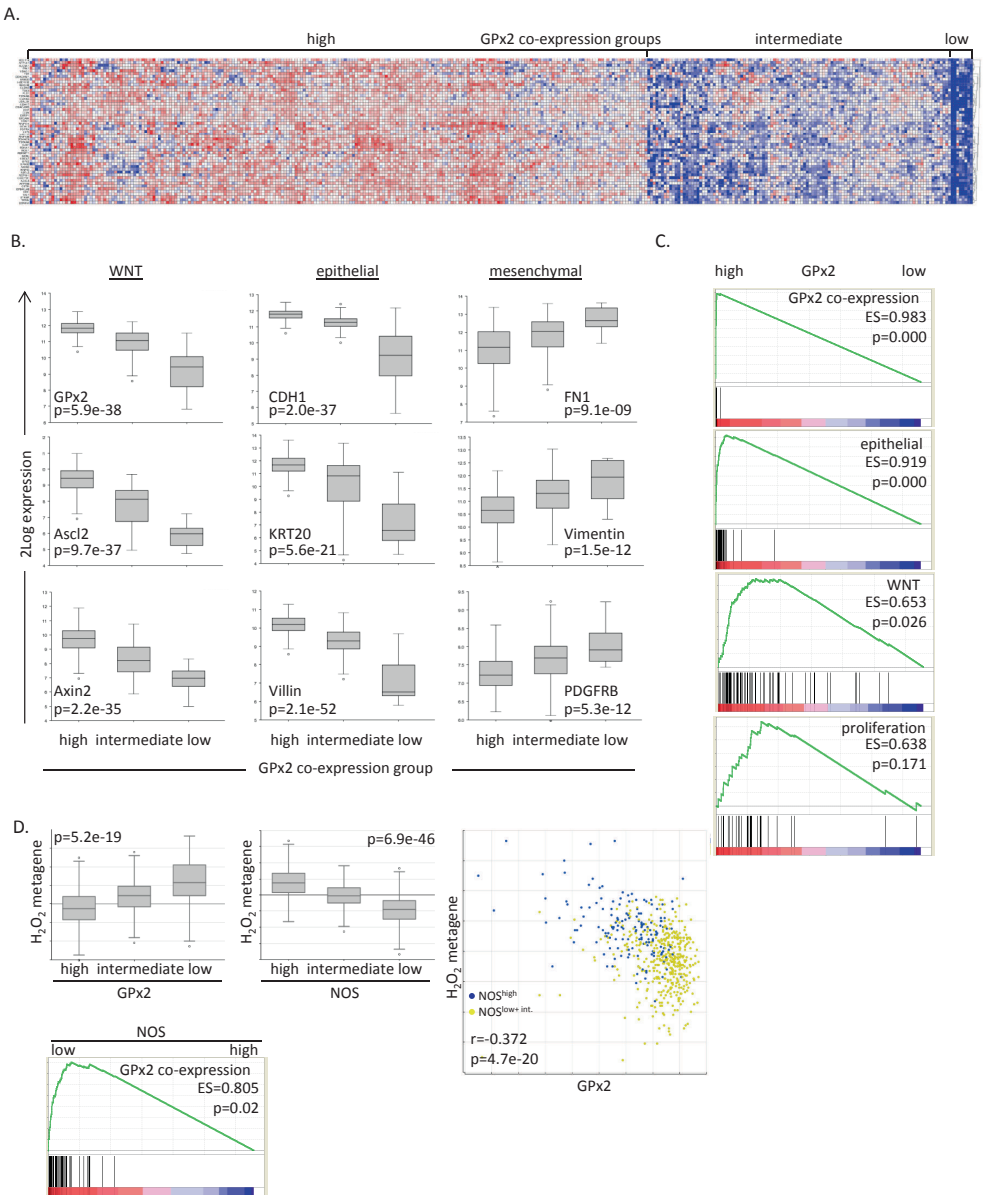

Figure 7 GPx2 expression defines a subgroup of colon tumors characterized by epithelial differentiation, expression of Wnt targets, and proliferation.

A, K-means clustering of tumors in the MVRM meta-cohort (n=345) into three subgroups with high, intermediate and low expression of GPx2 co-expressed genes.

B, Analysis of the expression of single genes (Wnt targets, epithelial, mesenchymal) in the GPx2-low, -intermediate and -high groups.

C, Gene set enrichment analyses (GSEA) of the enrichment of the indicated signatures in GPx2 high versus low tumors.

D, Correlation of expression of the H_2O_2 metagene with the GPx2 co-expression signature and with the Nanog/Oct4/Sox2 (NOS) signature for primitive undifferentiated tumors. The XY plot shows the inverse correlation of H_2O_2 metagene with the GPx2 co-expression signature. NOS^{high} tumors are depicted in blue. Gene set enrichment analysis (GSEA) shows enrichment of the GPx2 signature in NOS^{low} tumors.

See also supplementary figure S5

DISCUSSION

In the present report we show that GPx2 regulates two aspects of colon tumor growth. First, it is required for the survival of clonogenic tumor cells in response to H_2O_2-stress. Second, it is essential for the generation of proliferating differentiated tumor mass. Thus, by maintaining redox homeostasis, GPx2 controls the balance between survival, proliferation and differentiation. These results are in line with the general idea that ROS generation supports tumor growth, but also creates a vulnerability that may be exploited therapeutically[8, 33, 34]. While high ROS level may be associated with and contribute to tumor development, tumor cells have to prevent excessive ROS accumulation as this may lead to cell death, cell cycle arrest and senescence[35]. In the intestine, loss of the APC tumor suppressor causes ROS accumulation and this is required for the formation of proliferative progenitors during tumor initiation[7]. However, intestinal adenoma formation also requires neutralization of excessive ROS via the metabolic enzyme TIGAR[36]. In addition, the Nrf2 antioxidant program is essential for the development of lung and pancreas carcinomas in mice[37]. Nrf2 induces expression of GPx2[38] and other antioxidant enzymes, including thioredoxin reductase 1 (TR1) and peroxiredoxins. Interestingly, like GPx2-deficient tumor cells (this report), TR1-deficient tumor cells show strongly reduced tumor- and metastasis-forming capacity[39]. Together, these studies highlight the importance of maintaining redox balance during tumor initiation and progression. We propose that GPx2, possibly in concert with other anti-oxidant enzymes such as GPx1[40], TIGAR[36] and TR1[39] promotes survival and tumor growth in colon cancer by neutralizing the overproduction of ROS that is associated with tumor development. This ensures maintenance of clonogenic tumor cells and differentiation potential resulting in tumor mass formation.

Another important aspect of the regulation of tumor development by GPx2 is inflammation. Mice deficient for both GPx1 and GPx2 show increased intestinal inflammation and spontaneous development of ileocolitis and intestinal cancer. The restoration of one GPx2 (but not GPx1) allele almost fully rescued these phenotypes[41]. Furthermore, GPx2-knockout mice show severe inflammation and an increased number of tumors in a mouse model for inflammation-triggered colon cancer[42]. GPx2 may suppress inflammation by inhibiting cyclooxygenase-2 (COX-2) expression or activity[16, 31]. Interestingly, while tumor multiplicity was higher in GPx2 knockout mice, presumably due to more severe inflammation, tumor size was significantly smaller[42]. This is consistent with a model in which GPx2 prevents colon tumor initiation by limiting inflammation, but promotes the growth of established tumors by stimulating the formation of differentiated tumor mass (this report). In our experiments GPx2 knockdown had no measurable effect on tumor inflammation score or tumor stroma content, as judged by histology. However, these experiments were performed in immune-deficient mice which lack a large part of their immune cell repertoire. Therefore the absence of differences relating to immune infiltrate and other stromal parameters in our experiments has to be interpreted carefully.

The observed requirement for GPx2 in generating differentiated tumor mass is supported by analysis of transcriptomics data, demonstrating a strong positive correlation between GPx2 expression and epithelial differentiation, proliferation and Wnt activity. *Vice versa*, we found a strong negative correlation between GPx2 expression and expression of a signature for undifferentiated tumor cells and the H_2O_2–response metagene. Interestingly, the epithelial-type Wnt^{high} subgroup of colon tumors has a reduced propensity to develop metastases[22, 43]. This seems to be at odds with our finding that GPx2 is required for metastasis formation. Strikingly, high expression of Wnt target genes is also associated with low metastatic potential[43], while being

essential for the maintenance of colon cancer stem cells[44]. These results highlight the importance of considering colon cancer subgroups when analysing gene associations with clinical outcome. Indeed, we found that GPx2 is required for metastasis formation by CCS3-type tumor cells (HT-29) and that high GPx2 levels were significantly correlated with increased risk of metastasis within that aggressive CCS3 subtype of colon tumors.

Together the data identify GPx2 as an enzyme that is required to protect colon cancer cells against a variety of stress sources (H_2O_2, loss of cell-cell adhesion, chemotherapeutic drugs). GPx2 levels are associated with metastasis formation particularly in the aggressive CCS3 subtype, which has a primitive stem-like phenotype[22, 45] and is relatively resistant to current systemic therapy[22]. We therefore propose that therapeutically increasing ROS levels, either through targeting GPx2 or by other means, may be particularly effective in sensitizing the aggressive colon tumor subtype to chemotherapy and/or in reducing their propensity to form metastases.

REFERENCES

1. Nogueira V, *et al.* Molecular Pathways: Reactive Oxygen Species Homeostasis in Cancer Cells and Implications for Cancer Therapy. ClinCancer Res. 2013.
2. Szatrowski TP, *et al.* Production of large amounts of hydrogen peroxide by human tumor cells. Cancer Res. 1991;51:794-8.
3. Toyokuni S, *et al.* Persistent oxidative stress in cancer. FEBS Lett. 1995;358:1-3.
4. Hendrickse CW, *et al.* Neoptolemos JP. Lipid peroxidation and prostaglandins in colorectal cancer. BrJSurg. 1994;81:1219-23.
5. Skrzydlewska E, *et al.* Antioxidant status and lipid peroxidation in colorectal cancer. JToxicolEnvironHealth A. 2001;64:213-22.
6. Wiseman H, *et al.* Damage to DNA by reactive oxygen and nitrogen species: role in inflammatory disease and progression to cancer. BiochemJ. 1996;313 (Pt 1):17-29.
7. Myant KB, *et al.* ROS Production and NF-kappaB Activation Triggered by RAC1 Facilitate WNT-Driven Intestinal Stem Cell Proliferation and Colorectal Cancer Initiation. Cell Stem Cell. 2013.
8. Trachootham D, *et al.* Redox regulation of cell survival. AntioxidRedoxSignal. 2008;10:1343-74.
9. Trachootham D, *et al.* Targeting cancer cells by ROS-mediated mechanisms: a radical therapeutic approach? NatRevDrug Discov. 2009;8:579-91.
10. O'Brien CA, *et al.* A human colon cancer cell capable of initiating tumour growth in immunodeficient mice. Nature. 2007;445:106-10.
11. Ricci-Vitiani L, *et al.* Identification and expansion of human colon-cancer-initiating cells. Nature. 2007;445:111-5.
12. Baumann M, *et al.* Exploring the role of cancer stem cells in radioresistance. NatRevCancer. 2008;8:545-54.
13. Diehn M, *et al.* Association of reactive oxygen species levels and radioresistance in cancer stem cells. Nature. 2009;458:780-3.
14. Phillips TM, *et al.* The response of CD24(-/low)/CD44+ breast cancer-initiating cells to radiation. JNatlCancer Inst. 2006;98:1777-85.
15. Emmink BL, *et al.* Differentiated human colorectal cancer cells protect tumor-initiating cells from irinotecan. Gastroenterology. 2011;141:269-78.
16. Banning A, *et al.* Glutathione Peroxidase 2 Inhibits Cyclooxygenase-2-Mediated Migration and Invasion of HT-29 Adenocarcinoma Cells but Supports Their Growth as Tumors in Nude Mice. Cancer Res. 2008;68:9746-53.
17. Lois C, *et al.* Germline transmission and tissue-specific expression of transgenes delivered by lentiviral vectors. Science. 2002;295:868-72.
18. Koh LW, *et al.* A Distinct Reactive Oxygen Species Profile Confers Chemoresistance in Glioma-Propagating Cells and Associates with Patient Survival Outcome. AntioxidRedoxSignal. 2013.
19. Kyng KJ, *et al.* The transcriptional response after oxidative stress is defective in Cockayne syndrome group B cells. Oncogene. 2003;22:1135-49.
20. Jorissen RN, *et al.* Metastasis-Associated Gene Expression Changes Predict Poor Outcomes in Patients with Dukes Stage B and C Colorectal Cancer. ClinCancer Res. 2009;15:7642-51.
21. Marisa L, *et al.* Gene expression classification of colon cancer into molecular subtypes: characterization, validation, and prognostic value. PLoSMed. 2013;10:e1001453.
22. Melo DSE, *et al.* Poor-prognosis colon cancer is defined by a molecularly distinct subtype and develops from serrated precursor lesions. NatMed. 2013;19:614-8.
23. Smith JJ, *et al.* Experimentally derived metastasis gene expression profile predicts recurrence and death in patients with colon cancer. Gastroenterology. 2010;138:958-68.
24. Brigelius-Flohe R. Tissue-specific functions of individual glutathione peroxidases. Free RadicBiolMed. 1999;27:951-65.
25. Brigelius-Flohe R, Maiorino M. Glutathione peroxidases. BiochimBiophysActa. 2013;1830:3289-303.
26. Chu FF, *et al.* Expression, characterization, and tissue distribution of a new cellular selenium-dependent glutathione peroxidase, GSHPx-GI. JBiolChem. 1993;268:2571-6.
27. Florian S, *et al.* Cellular and subcellular localization of gastrointestinal glutathione peroxidase in normal and malignant human intestinal tissue. Free RadicRes. 2001;35:655-63.
28. Schafer ZT, *et al.* Antioxidant and oncogene rescue of metabolic defects caused by loss of matrix attachment. Nature. 2009;461:109-13.

29. van der Flier LG, *et al.* The Intestinal Wnt/TCF Signature. Gastroenterology. 2007;132:628-32.
30. Anjomshoaa A, *et al.* Reduced expression of a gene proliferation signature is associated with enhanced malignancy in colon cancer. BrJCancer. 2008;99:966-73.
31. Banning A, *et al.* GPx2 counteracts PGE2 production by dampening COX-2 and mPGES-1 expression in human colon cancer cells. AntioxidRedoxSignal. 2008;10:1491-500.
32. Ben-Porath I, *et al.* An embryonic stem cell-like gene expression signature in poorly differentiated aggressive human tumors. NatGenet. 2008;40:499-507.
33. Schumacker PT. Reactive oxygen species in cancer cells: live by the sword, die by the sword. Cancer Cell. 2006;10:175-6.
34. Trachootham D, *et al.* Effective elimination of fludarabine-resistant CLL cells by PEITC through a redox-mediated mechanism. Blood. 2008;112:1912-22.
35. Hamanaka RB, *et al.* Mitochondrial reactive oxygen species regulate cellular signaling and dictate biological outcomes. Trends in biochemical sciences. 2010;35:505-13.
36. Cheung EC, *et al.* TIGAR Is Required for Efficient Intestinal Regeneration and Tumorigenesis. DevCell. 2013;25:463-77.
37. DeNicola GM, *et al.* Oncogene-induced Nrf2 transcription promotes ROS detoxification and tumorigenesis. Nature. 2011;475:106-9.
38. Banning A, *et al.* The GI-GPx gene is a target for Nrf2. MolCell Biol. 2005;25:4914-23.
39. Yoo MH, *et al.* Thioredoxin reductase 1 deficiency reverses tumor phenotype and tumorigenicity of lung carcinoma cells. JBiolChem. 2006;281:13005-8.
40. Chu FF, *et al.* Role of Se-dependent glutathione peroxidases in gastrointestinal inflammation and cancer. Free RadicBiolMed. 2004;36:1481-95.
41. Esworthy RS, *et al.* Epithelium-specific glutathione peroxidase, Gpx2, is involved in the prevention of intestinal inflammation in selenium-deficient mice. The Journal of nutrition. 2005;135:740-5.
42. Krehl S, *et al.* Glutathione peroxidase-2 and selenium decreased inflammation and tumors in a mouse model of inflammation-associated carcinogenesis whereas sulforaphane effects differed with selenium supply. Carcinogenesis. 2012;33:620-8.
43. Melo DSE, *et al.* Methylation of cancer-stem-cell-associated Wnt target genes predicts poor prognosis in colorectal cancer patients. Cell Stem Cell. 2011;9:476-85.
44. Vermeulen L, *et al.* Wnt activity defines colon cancer stem cells and is regulated by the microenvironment. NatCell Biol. 2010;12:468-76.
45. Sadanandam A, *et al.* Reconciliation of classification systems defining molecular subtypes of colorectal cancer: interrelationships and clinical implications. Cell Cycle. 2014;13:353-7.

SUPPLEMENTARY MATERIAL & METHODS

Isolation and expansion of colonospheres

The isolation and expansion of colorectal cancer colonospheres was performed as described (1). In short, the obtained tissue fragments were washed extensively with PBS and were mechanically dissociated using scalpels and vigorous trituration to yield small fragments (<1mm3) and single cells. Enzymatic digestion was performed using thermolysin 0.05% (Sigma, Type X) in DMEM/F12 containing 5 mM Hepes (Gibco) for 2hr at 37ºC. The suspension was then filtered through a 40-µm-pore size nylon cell strainer (BD Falcon) to separate the tissue fragments from the single cells. The single cell suspension was cultured in advanced DMEM/F12 (Gibco) supplemented with 0,6% glucose (BDH Lab. Supplies), 2mM L-glutamine (Biowhittaker), 9.6 µg/ml putrescin (Sigma), 6.3 ng/ml progesterone (Sigma), 5.2 ng/ml sodium selenite (Sigma), 25 µg/ml insulin (Sigma), 100 µg/ml apotransferrin (Sigma), 5 mM hepes (Gibco), 0,005 µg/ml trace element A (Cellgro), 0,01µg/ml trace element B (Cellgro), 0,01 µg/ml trace element C (Cellgro), 100 µM β-mercapto ethanol (Merck), 10 ml antibiotic-antimycotic (Gibco), 4 µg/ml gentamicine (Invitrogen), 0.002% lipid mixture (Sigma) and 5 µg/ml glutathione (Roche). This Advanced DMEM/F12 medium plus supplements is defined as Stem Cell Medium. Growth factor FGF (10 ng/ml, Abcam) were added to the cell culture medium freshly each week. All cell culture was carried out in non-tissue culture treated flasks (BD Falcon) at 37° C in a 5% CO2 humidified incubator.

HT-29 cells (human colon adenocarcinoma cells; German Collection of Microorganisms and Cell Cultures) were grown as colonospheres, under non-adherent conditions in Stem Cell Medium at 37°C in a 5% CO2 humidified incubator.

Cultures used for GPx2 knockdown				
Case	**Tumor site**	**Tumor type**	**Tumor stage**	**Differentiation**
CRC29	Right colon	Adenocarcinoma	T3N0Mx	Poor
L145	Liver segment VII	Adenocarcinoma	metastasis	Moderate
HT29	Colon	Adenocarcinoma	Not known	Mesenchymal subtype (2)
Cultures used for GPx2 overexpression				
Case	**Tumor site**	**Tumor type**	**Tumor stage**	**Differentiation**
CRC29	Right colon	Adenocarcinoma	T3N0Mx	Poor
L145	Liver segment VII	Adenocarcinoma	metastasis	Moderate
L167	Liver segment II-IV	Adenocarcinoma	metastasis	Moderate
L169	Liver segment IV	Adenocarcinoma	metastasis	Well

Isolation of single cells from xenografts and colonospheres

Tumor xenografts were mechanically dissociated to yield small fragments that were further dissociated using dispase II (Roche)/ collagenase XI (Sigma; 30 min 37C). The cells were washed once with PBS and were subsequently incubated with TrypLE express (Invitrogen) including 2,000 U/ml DNase (Sigma; 30 min 37C). To obtain single cell suspensions from colonospheres, they were incubated with Accumax (Innovative Cell Technologies) plus 2 U/ml DNAse1 (Sigma) for 10 minutes in a rotary incubator at 37°C. Both types of cell suspensions were then filtered through a 40-µm-pore size nylon cell strainer (BD Falcon) to obtain single cells.

Tumor formation

Single cell populations (GPx2 knockdown, GPx2 over-expressing cells and controls) were diluted to 10.000 live spheroid-derived cells, mixed with BD Matrigel (BD Biosciences) at a 1:1 ratio (total volume 100 µl) and injected subcutaneous into the flanks of 6 weeks old BALB/cnu/nu mice. The same procedure was followed after FACS sorting experiments in which GPx2-GFP high and low cell populations were mixed with Matrigel (BD Biosciences) at 1000 cells/50µl and injected into the flanks of BALB/cnu/nu mice.

Liver metastasis model

Pathogen-free, 10–11-week-old female SCID (severe combined immunodeficiency) mice were purchased from Taconic (Ejby, Denmark). Animals were quarantined for 2 weeks. HT29 cells expressing YFP were harvested by brief trypsinization. Colorectal liver metastases were induced as previously described (3). In brief, single cell suspensions were prepared in phosphate-buffered saline to a final concentration of 7.5 x 10^4 cells/100 µl. Cells were injected into the parenchyma of the spleen of 125-day-old SCID mice using a 27-gauge needle. The injection site on the spleen was pressed with a cotton stick to ensure hemostasis. The peritoneum and skin were closed in a single layer with surgical thread.

Tumor analysis

After six weeks mice were sacrificed and tumor load in the liver was assessed in all liver lobes. Tumor load was scored as hepatic replacement area (HRA), that is, the percentage of liver tissue that had been replaced by tumor tissue, exactly as described before (3). In brief, on hematoxylin and eosin-stained sections, at least 100 fields were selected using an interactive video overlay system, including an automated microscope (Q-Prodit; Leica Microsystems) at a x40 magnification. Using a four-point grid overlay, the ratio of tumor cells versus normal hepatocytes was determined for each field. Tumor load (HRA) was expressed as the average area ratio of all fields.

Antibodies and reagents

The antibodies used in this study are rabbit anti-human GPx2(2), rabbit anti-FABP1 (Sigma), mouse anti-cleaved-caspase-3 (Cell Signalling), mouse anti-mucin2 (Epitomics), mouse anti-cytokeratin 20 (Ks20.8; Dako), rabbit anti-OLFM4 (Abcam),rabbit anti-oct4 (Cell Signalling), rabbit anti-Ki67 (Novocastra), mouse anti-epithelial antigen (EpCAM, cloneBER-EP4; Dako), mouse anti-GFP (Roche), mouse anit-p16 (clone C20, Santa Cruz), mouse anti-p21WAF (clone OP68, Calbiochem) and mouse anti-β-actin (AC-15; Novis Biologicals). The AldefluorTM reagent was purchased from STEMCELL Technologies and used according to the manufacturer's instructions. The general Caspase Inhibitor Z-VAD-FMK (R&D systems) was used at a concentration of 25µM and added directly after making colonospheres single cell.

Flow cytometry and cell sorting

Aldefluor®-positive cells were analyzed according to the manufacturer's protocol by using the ALDH substrate BAAA (1 µmol/l per 1×10^6 cells)(STEMCELL Technologies). Negative control samples were co-incubated with diethylaminobenzaldehyde (DEAB; 50 mM). The cell sorting experiments were conducted with FACS Aria IIU (BD), using FACS Diva version 6.1 software, and the expression was analyzed using a FACScalibur (BD Biosciences, San Diego, USA). Dead cells were excluded using viability marker 7-aminoactinomycin D (7-AAD) (R&D, Detroit, MI) and cell doublets and clumps were excluded using doublet discrimination gating. For analysis of xenograft

material, anti-human epithelial antigen (Ep-CAM, clone BER-EP4; Dako) was used as a marker to select for epithelial cells.

Immunohistochemistry

For anti-human GPx2 (4) and anti-human cytokeratin 20 (Ks20.8; M7019 Dako), antigen retrieval was performed by boiling samples for 20 min in HIER Citrate Buffer pH 6.0 (Monosan®). The anti-human GPx2 was diluted 1/5000 in PBS 0.05% BSA and incubated overnight at 4ºC, and anti-human cytokeratin 20 was diluted 1/50 in PBS 0.05% BSA and incubated overnight at 4 ºC. Secondary antibodies (polymer HRP conjugated anti-rabbit (for GPx2) and anti-mouse (for CK20), Powervision) were added for 30 min at room temperature. Samples were developed using DAB, counterstained with haematoxylin and mounted.

Bioinformatic analyses

All analyses were performed using the R2 microarray analysis and visualization platform (http://r2.amc.nl). For generation of the GPx2-coexpression signature we identified all genes that were significantly co-expressed with GPx2 in two datasets (5, 6). The cut-off for maximum p values for single gene associations was set to e-6 and False Discovery Rate was used to correct for multiple testing. The 100 genes most significantly co-expressed with GPx2 in both datasets showed a 53-gene overlap (Supplementary Table S3). For k-means clustering the 53-gene GPx2 co-expression signature was uploaded into R2 and was used as a gene category to cluster the tumors into 3 groups in 10x100 draws. The clustering was stored as a track. For generation of the differentiation signature we identified all genes that were significantly co-expressed with CDX2 *and* KRT20 *and* VIL1. The cut-off for maximum p values for single gene associations was set to e-6 and False Discovery Rate was used to correct for multiple testing. The 200 genes most significantly co-expressed with CDX2, KRT20 and VIL1 yielded an overlap of 63 genes (Supplementary Table S4). This list was uploaded into R2 as a category. To compare expression levels of genes in tumor subgroups we used the option 'view gene in groups' and selecting either the GPx2 subgroups or the CCS subgroups as a track.

REFERENCES

1. Emmink BL, Van Houdt WJ, Vries RG, Hoogwater FJ, Govaert KM, Verheem A, et al. Differentiated human colorectal cancer cells protect tumor-initiating cells from irinotecan. Gastroenterology. 2011;141:269-78.
2. Melo DSE, Wang X, Jansen M, Fessler E, Trinh A, de Rooij LP, et al. Poor-prognosis colon cancer is defined by a molecularly distinct subtype and develops from serrated precursor lesions. NatMed. 2013;19:614-8.
3. van der Bilt JD, Kranenburg O, Nijkamp MW, Smakman N, Veenendaal LM, Te Velde EA, et al. Ischemia/reperfusion accelerates the outgrowth of hepatic micrometastases in a highly standardized murine model. Hepatology. 2005;42:165-75.
4. Banning A, Kipp A, Schmitmeier S, Lowinger M, Florian S, Krehl S, et al. Glutathione Peroxidase 2 Inhibits Cyclooxygenase-2-Mediated Migration and Invasion of HT-29 Adenocarcinoma Cells but Supports Their Growth as Tumors in Nude Mice. Cancer Res. 2008;68:9746-53.
5. Jorissen RN, Gibbs P, Christie M, Prakash S, Lipton L, Desai J, et al. Metastasis-Associated Gene Expression Changes Predict Poor Outcomes in Patients with Dukes Stage B and C Colorectal Cancer. ClinCancer Res. 2009;15:7642-51.
6. Smith JJ, Deane NG, Wu F, Merchant NB, Zhang B, Jiang A, et al. Experimentally derived metastasis gene expression profile predicts recurrence and death in patients with colon cancer. Gastroenterology. 2010;138:958-68.

Supplementary figure S1. Suppression of GPx2 reduces proliferation and clone forming potential of colon CSCs. ➔

A, Immunoblot analysis of GPx2 expression in HT29 colonosphere lines stably expressing scrambled shRNAs, shGPx2#1 or shGPx2#2.

B, Western blot analysis of GPx2 and cleaved caspase-3 expression after single cell making of L145 colonospheres expressing scrambled shRNAs, and different clones of shGPx2#1 or shGPx2#2.

C, Analysis of cell viability in L145 colonospheres expressing either scrambled or GPx2-targeting shRNAs after treatment with Elesclomol and Cisplatin using the Multitox-Fluo probe (Promega). Data are shown as means +SD and represent data from 3 independent experiments. *p≤ 0.05.

D, Clone forming assay of L145 and HT29 colonosphere lines expressing scrambled shRNAs, or shGPx2#1 using matrigel 3D-culture system. Graphs show mean ± SEM, *p<0.05.

E, qPCR analysis of mRNA levels of the proliferation cell marker Ki67 in L145 colonosphere line expressing scrambled shRNAs, shGPx2#1 or shGPx2#2, 72 hours after treatment with 0.2mM of N-acetylcyteine (NAC). Graphs show mean ± SEM, *p<0.05, **p<0.01.

F, qPCR analysis of mRNA levels of Ki67 in L145 colonosphere line expressing the indicated shRNAs 72 hours after treatment with 50μM H_2O_2. Graphs show mean ± SEM, *p<0.05.

SUPPLEMENTARY FIGURES

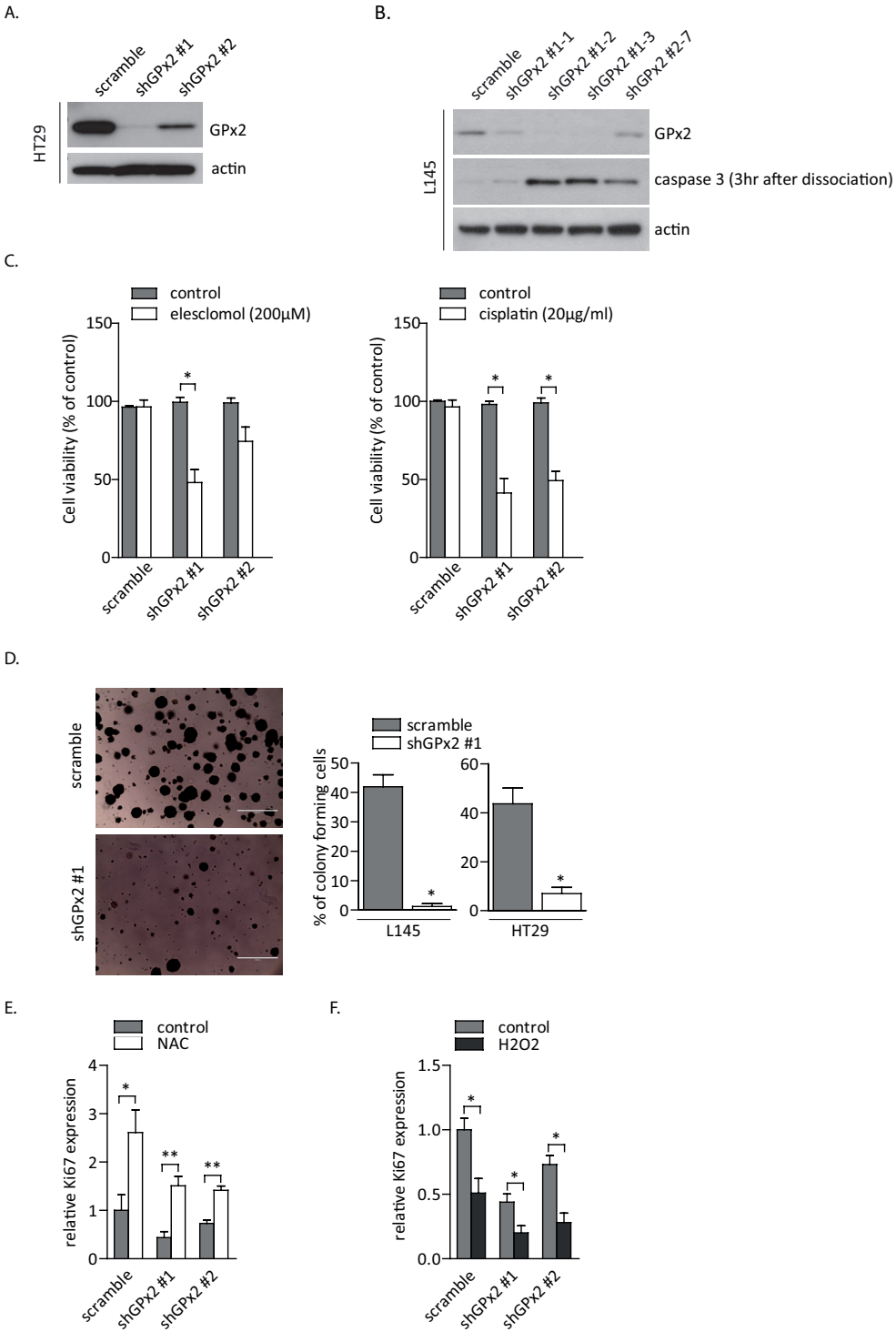

Supplementary figure S2. Loss of GPx2 impairs differentiation of CSCs**.**
A, Immunoblot analysis of GPx2 protein levels in CRC29 cells following short-hairpin RNA-mediated GPx2 silencing.
B, qPCR analysis of mRNA levels of GPx2, and the indicated stem cell markers in CRC29 colonosphere line stably expressing scrambled shRNAs or shGPx2#1. Graphs show mean ± SEM, *p<0.05.
C, qPCR analysis of mRNA levels of the stem cell marker OLFM4 in L145 colonospheres expressing scrambled shRNAs, shGPx2#1 or shGPx2#2, 72 hours after treatment with 0.2mM of N-acetylcyteine (NAC) (left graph) or 50μM H_2O_2 (right graph). Graphs show mean ± SEM, *p<0.05, ***p<0.001.
D, qPCR analysis of mRNA levels for GPx2 inL145 colonosphere line stably expressing scrambled shRNAs or shGPx2#1. Graphs show mean ± SEM.
E, qPCR analysis of mRNA levels for the indicated differentiation markers in CRC29 colonosphere line stably expressing scrambled shRNAs or shGPx2#1. Graphs show mean ± SEM, *p<0.05, ND=Not detectable.
F, Immunoblot analysis of GPx2 protein and the indicated differentiation markers in HT29 colonosphere lines expressing scrambled shRNAs, shGPx2#1 or shGPx2#2.
G, Immunoblot of GPx2 and MUC2 expression in HT29 cells expressing scrambled shRNAs, or shGPx2#1 reconstituted with either FLAG (control) or shRNA-insensitive FLAG-GPx2.
H, Western Blot analysis of GPx2, MUC2, cleaved caspase-3, p16 and p21 expression in HT29 cells colonospheres lines expressing scrambled shRNAsor shGPx2#1, 24 and 48 hours after single cell making, treated with or without the general apoptosis inhibitor z-VAD.
I, qPCR analysis of mRNA levels for the senescence marker p16 in L145 colonosphere line stably expressing scrambled shRNAs or shGPx2#1. Graphs show mean ± SEM.

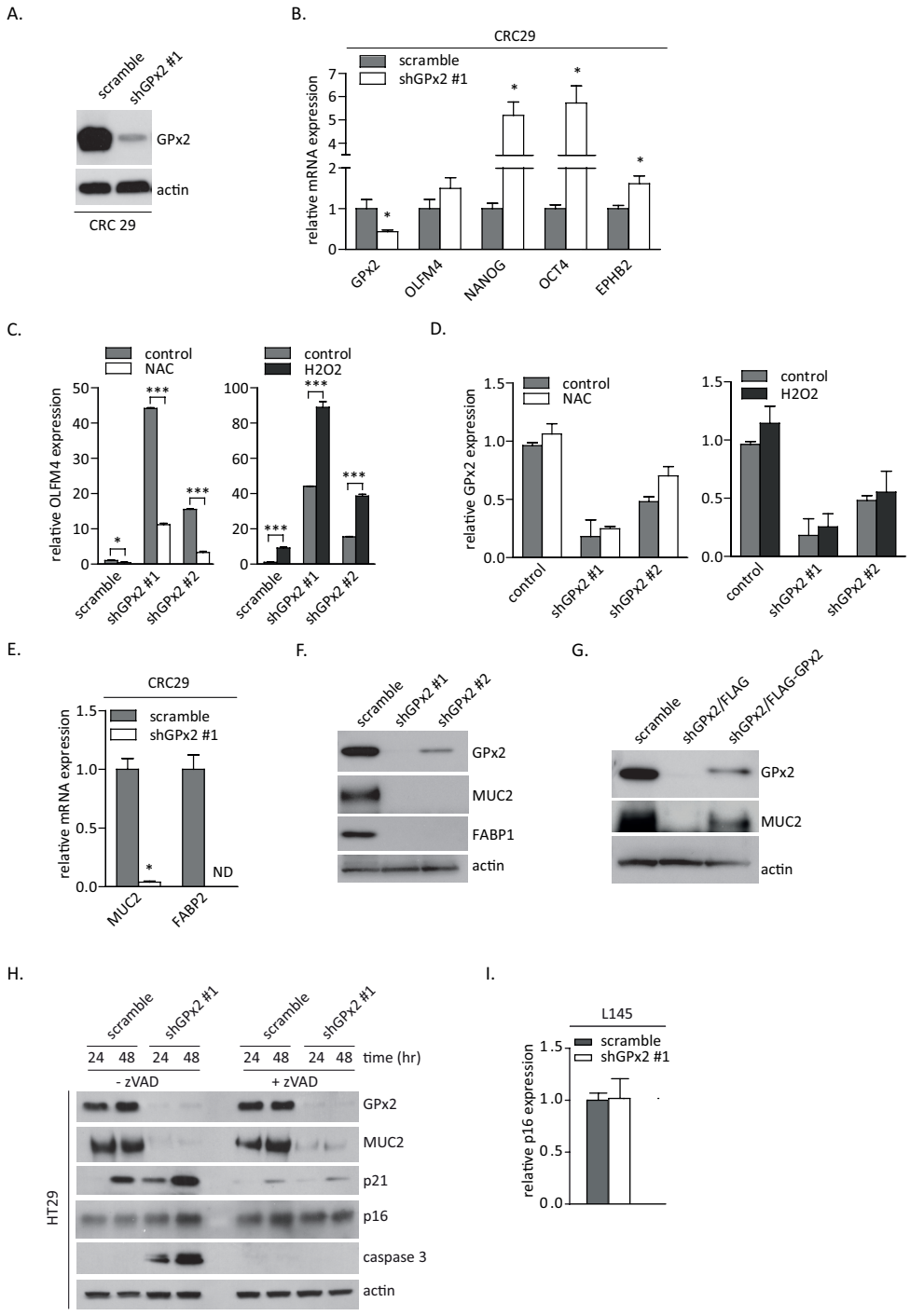
A.
scramble
shGPx2 #1
GPx2
actin
CRC 29
B.
CRC29
scramble
shGPx2 #1
relative mRNA expression
GPx2
OLFM4
NANOG
OCT4
EPHB2
C.
control
NAC
control
H2O2
relative OLFM4 expression
scramble
shGPx2 #1
shGPx2 #2
D.
control
NAC
control
H2O2
relative GPx2 expression
control
shGPx2 #1
shGPx2 #2
E.
CRC29
scramble
shGPx2 #1
relative mRNA expression
ND
MUC2
FABP2
F.
scramble
shGPx2 #1
shGPx2 #2
GPx2
MUC2
FABP1
actin
G.
scramble
shGPx2/FLAG
shGPx2/FLAG-GPx2
GPx2
MUC2
actin
H.
scramble
shGPx2 #1
time (hr)
- zVAD
+ zVAD
HT29
GPx2
MUC2
p21
p16
caspase 3
actin
I.
L145
scramble
shGPx2 #1
relative p16 expression

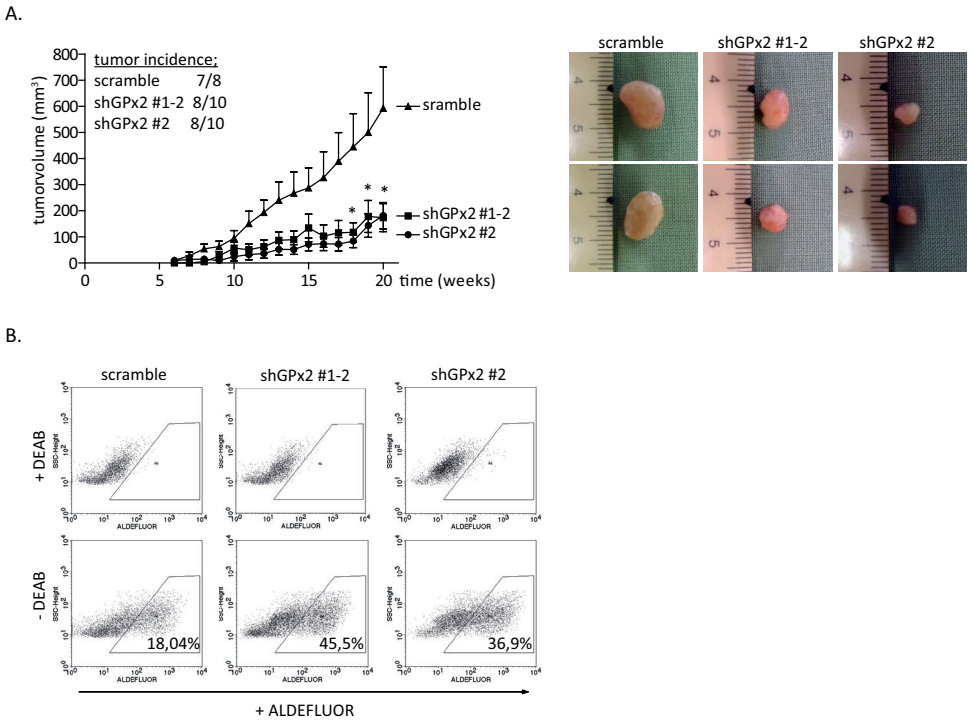

Supplementary figure S3. Loss of GPx2 reduces tumor growth.
A, Subcutaneous tumor formation by L145 colonospheres expressing scrambled shRNAs, shGPx2#1-2, or shGPx2#2. The equivalent of 3000 cells was inoculated subcutaneously into immunodeficient mice and tumor volume was determined over time. The photograph shows tumors formed in all three groups. Graphs show mean ± SEM, *p<0.05.
B, FACS-analysis using the Aldefluor® assay in L145 cells isolated from scrambled, shGPx2#1-2, or shGPx2#2 subcutaneous tumors. Cells incubated with the Aldefluor® substrate BAAA and the ALDH specific inhibitor DEAB were used to set the gate.

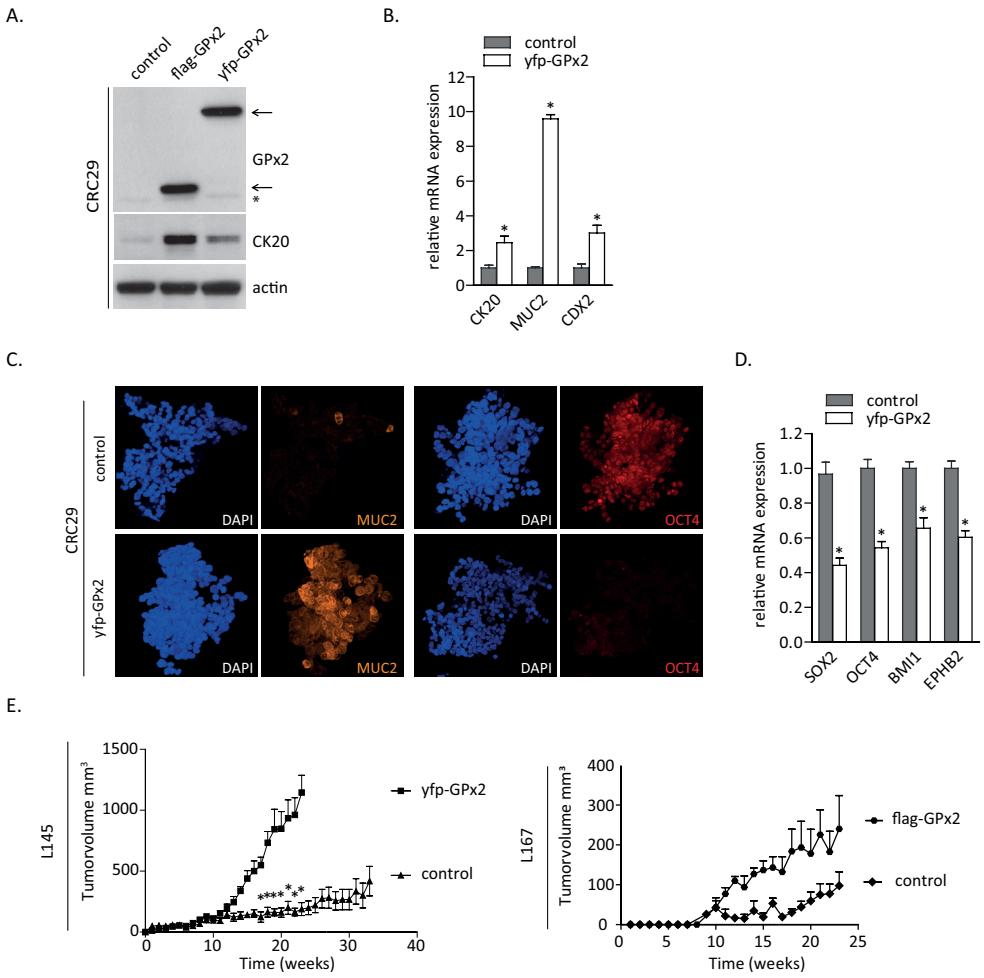

Supplementary figure S4. Overexpression of GPx2 promotes differentiation of CSCs and accelerates tumor growth.

A, Immunoblot analysis of GPx2 protein and the indicated differentiation markers in CRC29 colonosphere lines stably expressing Flag- or YFP-tagged GPx2. *Indicates endogenous GPx2 protein.

B, qPCR analysis of mRNA levels of the indicated differentiation markers was performed on CRC29 colonosphere line stably expressing control YFP or YFP-GPx2 protein. Data are shown as means +SEM and represent data from 3 independent experiments. *p≤ 0.05.

C, Immunofluorescence analysis of the differentiation marker MUC2 and the stem cell marker OCT4 in control or YFP-GPx2-expressing CRC29 cells.

D, q-PCR analysis of mRNA levels of the indicated stem cell genes in CRC29 colonosphere line stably expressing control or YFP-GPx2 protein. Data are shown as means +SEM and represent data from 3 independent experiments. *p≤ 0.05.

E, Tumor forming capacity was performed by injecting L145 and L167 colonospheres expressing control or YFP-GPx2 subcutaneously injected into immunodeficient mice. Tumor volume was measured over time. Graphs show mean ± SEM, *p<0.05.

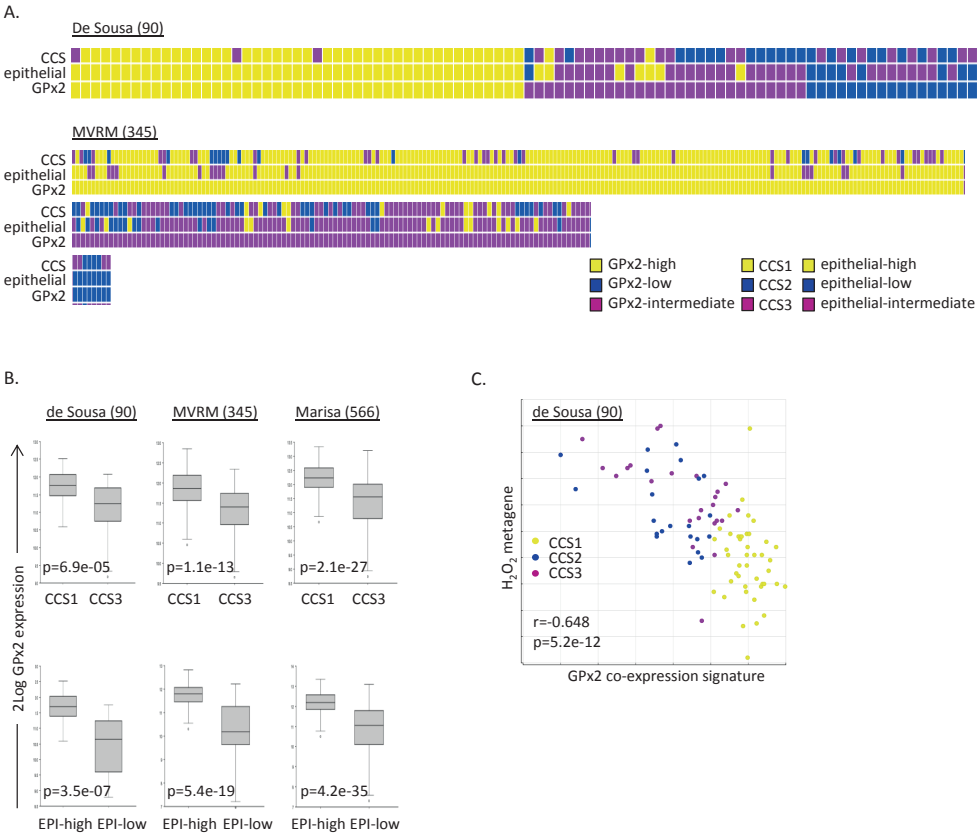

Supplementary figure S5. GPx2 expression in human colon tumor cohorts correlates with epithelial differentiation and low H_2O_2 stress.

A, Comparative clustering by using the GPx2, epithelial and CCS classifiers in the de Sousa and MVRM cohorts shows a near-complete overlap between the CCS1, epithelial-high and GPx2-high subgroups.

B, Expression levels of GPx2 in CCS1 *versus* CCS3 and in epithelial-high *versus* epithelial-low tumors in the de Sousa and MVRM cohorts. The box plots show a significantly higher expression of GPx2 in the CCS1 and epithelial-high tumor subgroups.

C, XY plot showing the inverse correlation of the GPx2 co-expression signature with the H_2O_2 metagene in the De Sousa cohort. CCS subgroups are color-coded, revealing high GPx2 and low H_2O_2 stress in CCS1 tumors.

A.

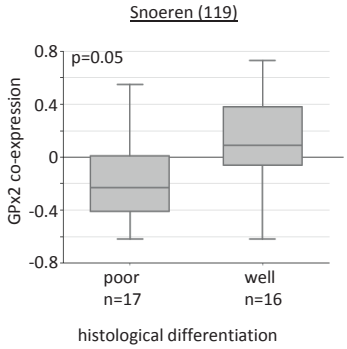

B.

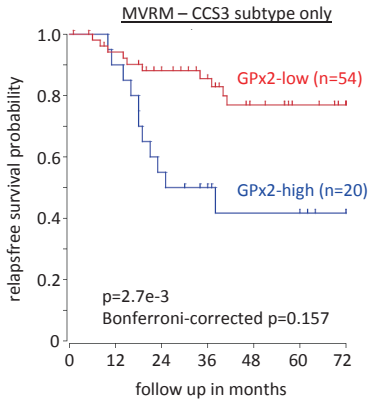

C.

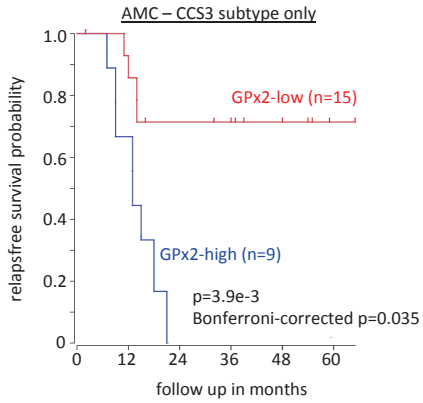

Supplementary figure S6. High GPx2 expression in CCS3 subtype colon tumors is associated with increased metastatic risk.
A, Expression levels of the GPx2 co-expression gene set in histologically well–differentiated metastases (n=16) and poorly differentiated metastases (n=17) in the Snoeren dataset ($p<0.05$).
B, Kaplan-Meier curves of 74 patients with metastasis-prone CCS3-type tumors in the MVRM dataset. Time to recurrence in patients with high GPx2 expression and low GPx2 expression is shown (log rank p=2.7e-3).
C, Kaplan-Meier curves of 24 patients with metastasis-prone CCS3-type tumors in the AMC-90 dataset. Time to recurrence in patients whit high GPx2 expression and low GPx2 expression is shown (log rank p=3.9e-3)

SUPPLEMENTARY TABLES

Supplementary Table S1. The H2O2 stress response metagene**.** Gene lists of three independent H2O2 stress response signatures were from www.speed.sys-bio.net and references (1) and (2). The overlap between the signatures was determined by using Genevenn (http://genevenn.sourceforge.net/). The metagene combines all genes in the three lists. Correlation coefficients between the three signatures was determined by analyzing a large cohort of CRC patients (MVRM; a batch-corrected compiled dataset published in (3, 4)) using the R2 platform (http://r2.amc.nl).

H2O2-1 (SPEED)		**H2O2-2 (KOH)**			**H2O2-3 (KYNG)**		
PCF11	UGCG	ANGPTL2	ADM	SPRY1	AEBP1	PPP1CA	OAZ2
RHOB	NR4A2	CD9	ANKRD37	SPRY1	ANKRD1	PRKCSH	ORAOV1
IL8	TMEM194A	H2AFX	ASCL1	NA	ATP5E	PSMC4	PFDN5
TMEFF1	THAP10	VAMP3	ATF3	ZBED5	ATP6AP1	PTGER4	PKIA
PPP1R10	SPRY2	CENPA	ATF4	ZC3H7A	ATP6V1C2	PTP4A3	PLXNA1
NRIP1	YTHDC2	MELK	CSRNP1	ZFP36	BAG4	RAB36	
JUN	IER2	ZWINT	BAMBI	SLC1A2	C4BPA	RCC1	
JUNB	ATF3	PPP1R3C	CEBPD	PCSK1	CCNA2	RELA	
TRIB1	MAFF	SPC25	CREB5	KDM5B	CCNH	RPL31	
WASL	FLRT3	CKAP2L	DDIT3	RAB6B	CD59	SEPP1	
SERPINB9	HMOX1	PBK	DDIT4	WDR19	CD68	SERPINH1	
NAMPT	BCL6	OIP5	INTS6	DNAJC12	CD81	SLC20A1	
KCNE4	HSP90B1	PLOD1	EGR1	JAZF1	CDC34	SLC39A7	
EFNB2	SLC30A1	NT5E	EIF5	DNAJC12	CFD	SRGN	
OXTR	PHLDA1	AURKB	FOSB	ANK3	CKMT2	TAL1	
KLF10	RAB2A	TK1	GADD45A	GABBR1	COMMD6	TAP1	
ATP6V0E1	LDLR	CEP55	GPR19	MAP1B	COX6C	TCF3	
ATRX	CREM	CDKN3	HERPUD1	GRB10	CRYAB	TGFBR3	
LUC7L3	C1orf103	DLL3	C7orf68	KLC1	CST3	TPT1-AS1	
EGR1	HOMER1	ASCL1	HIST1H4C		CTNNB1	TSPAN4	
SUV420H1	IL6	CREB5	HPS6		CTSB	TUBA4A	
PTPRO	SLC2A3	DUSP1	PELO		CTSS	UNG	
NR4A1	IL6ST	KIFAP3	POU3F2		CUX1	ZBTB7A	
GDF15	C17orf91	UBAP2L	PPP1R15A		DDX52	GDF15	
VEGFA	PMAIP1	SGSM2	RASSF1		DNAJA1	HCFC1R1	
SCAMP1	LRRFIP1	KIDINS220	RASSF1		DNAJB1	HMOX1	
DUSP1	MYBL1	FAM117B	RCVRN		DUT	HNRNPA1	
SP100	KLF2	EFNB3	RGS16		EID1	IFI6	
SOCS5	BAALC	DPYSL3	RGS2		ENG	IL10RB	
DUSP6		DCAF5	SERTAD1		FLOT2	MCAM	
MBNL1		MXD4	SOX21		GADD45A	MPV17	
H2O2 metagene							
ANGPTL2	ADM	JUNB	IL6	IFI6	KDM5B	GADD45A	
CD9	ANKRD37	TRIB1	SLC2A3	IL10RB	RAB6B	GDF15	
H2AFX	ASCL1	WASL	IL6ST	MCAM	WDR19	HCFC1R1	
VAMP3	ATF3	SERPINB9	C17orf91	MPV17	DNAJC12	KLC1	
CENPA	ATF4	NAMPT	PMAIP1	OAZ2	JAZF1	NRIP1	
MELK	CSRNP1	KCNE4	LRRFIP1	ORAOV1	DNAJC12	JUN	
ZWINT	BAMBI	EFNB2	MYBL1	PFDN5	ANK3	C1orf103	
PPP1R3C	CEBPD	OXTR	KLF2	PKIA	GABBR1	HOMER1	
SPC25	CREB5	KLF10	BAALC	PLXNA1	MAP1B	HMOX1	
CKAP2L	DDIT3	ATP6V0E1	AEBP1	PPP1CA	NA	HNRNPA1	
PBK	DDIT4	ATRX	ANKRD1	PRKCSH	ZBED5	PCSK1	
OIP5	INTS6	LUC7L3	ATP5E	PSMC4	ZC3H7A	SPRY1	
PLOD1	EGR1	EGR1	ATP6AP1	PTGER4	ZFP36	MAFF	
NT5E	EIF5	SUV420H1	ATP6V1C2	PTP4A3	PCF11	DDX52	
AURKB	FOSB	PTPRO	BAG4	RAB36	RHOB	GRB10	
TK1	GADD45A	NR4A1	C4BPA	RCC1	IL8	FLOT2	

CEP55	GPR19	GDF15	CCNA2	RELA	TMEFF1
CDKN3	HERPUD1	VEGFA	CCNH	RPL31	PPP1R10
DLL3	C7orf68	SCAMP1	CD59	SEPP1	FLRT3
ASCL1	HIST1H4C	DUSP1	CD68	SERPINH1	HMOX1
CREB5	HPS6	SP100	CD81	SLC20A1	BCL6
DUSP1	PELO	SOCS5	CDC34	SLC39A7	HSP90B1
KIFAP3	POU3F2	DUSP6	CFD	SRGN	SLC30A1
UBAP2L	PPP1R15A	MBNL1	CKMT2	TAL1	PHLDA1
SGSM2	RASSF1	UGCG	COMMD6	TAP1	RAB2A
KIDINS220	RASSF1	NR4A2	COX6C	TCF3	LDLR
FAM117B	RCVRN	TMEM194A	CRYAB	TGFBR3	CREM
EFNB3	RGS16	THAP10	CST3	TPT1-AS1	DNAJA1
DPYSL3	RGS2	SPRY2	CTNNB1	TSPAN4	DNAJB1
DCAF5	SERTAD1	YTHDC2	CTSB	TUBA4A	DUT
MXD4	SOX21	IER2	CTSS	UNG	EID1
SLC1A2	SPRY1	ATF3	CUX1	ZBTB7A	ENG

Limited overlap between H2O2 gene signatures

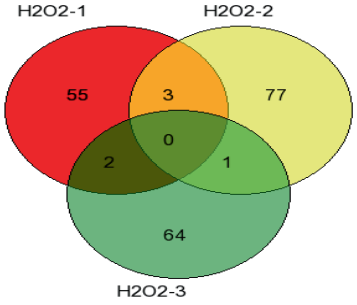

Correlation between expression of H2O2 signatures

signature	r value	p value
H2O2-1 vs H2O2-2	0.759	p=6.0e-66
H2O2-1 vs H2O2-3	0.618	p=8.8e-38
H2O2-2 vs H2O2-3	o.665	p=2.6e-45

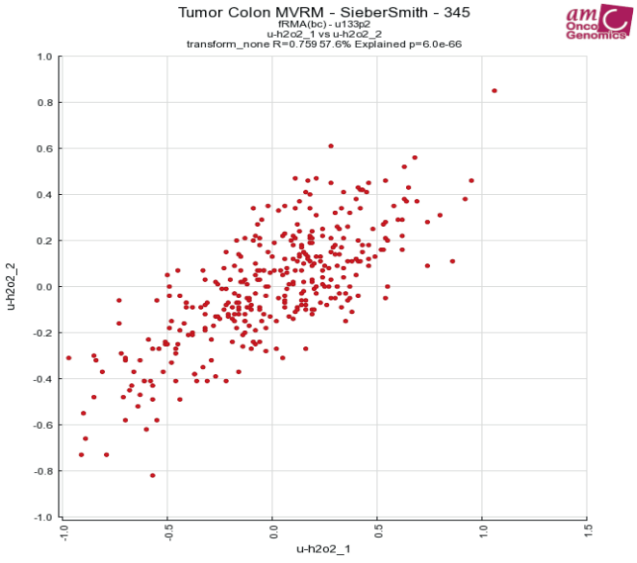

Supplementary Table S2. Correlation of the expression of the H2O2-response metagene and genes en-

coding H2O2-scavenging enzymes. The expression values of the H2O2-response metagene in all individual tumors of three large cohorts (3-6) was determined and correlated with the expression of individual genes encoding H2O2-neutralizing enzymes. Correlation and p-values are shown for each of these associations.

	Datasets		
Gene	**De Sousa e Melo (90)**	**MVRM (345)**	**Marisa (566)**
GPx1	r=0.152 p=0.15	r=0.359 p=6.0e-12	r=0.222 p=9.7e-08
GPx2	**r=-0.393 p=1.3e-04**	**r=-0.205 p=1.3e-04**	**r=-0.319 p=6.9e-15**
GPx3	r=0.494 p=7.3e-07	r=0.244 p=4.4e-06	r=0.325 p=2.1e-15
GPx4	r=-0.023 p=0.83	r=0.350 p=2.3e-11	r=0.211 p=4.2e-07
GPx5	r=0.151 p=0.16	r=0.364 p=3.2e-12	**r=-0.379 p=9.8e-21**
GPx6/7	r=0.349 p=7.4e-04	r=0.364 p=3.2e-12	r=0.348 p=1.3e-17
GPx8	r=0.513 p=2.3e-07	r=0.466 p=5.9e-20	r=0.494 p=3.1e-36
PRDX1	r=0.058 p=0.59	r=0.409 p=2.6e-15	r=0.177 p=2.2e-05
PRDX2	r=-0.006 p=0.95	r=0.247 p=3.3e-06	r=0.105 p=0.01
PRDX3	r=-0.042 p=0.70	r=0.291 p=3.5e-08	r=0.070 p=0.10
PRDX4	r=-0.008 p=0.94	r=0.234 p=1.1e-05	r=0.085 p=0.04
PRDX5	**r=-0.444 p=1.1e-05**	r=-0.078 p=0.15	**r=-0.140 p=8.4e-04**
PRDX6	r=0.294 p=4.9e-03	r=0.382 p=2.0e-13	r=0.206 p=8.1e-07
Catalase	**r=-0.334 p=1.3e-03**	r=0.128 p=0.02	**r=-0.140 p=8.5e-04**

Supplementary Table S3. The GPx2 co-expression signature. The 100 genes that are most significantly co-expressed with GPx2 were identified in two independent datasets. The table shows the 53-gene overlap between these lists, which we designated 'the GPx2 co-expression signature'.

GPx2 co-expression signature	
ACSL5	LY75
ASCL2	MUC3B
ATP10B	NEBL
ATP1A1	NOX1
AXIN2	PDHA1
BCL11B	PLS1
CD24	PPA1
CDCA7	REPIN1
CDH1	RNF114
CDH17	RNF128
CEACAM1	RNF43
CEACAM5	SLC5A1
CFTR	STRBP
CLDN3	TOX3
CLRN3	TPRN
DDC	TSPAN6
EHF	TSPAN8
EPB41L4B	TST
EPCAM	UCHL3
EPHB2	USH1C
ESRP1	VDAC1
ESRRA	VIL1
FAM3D	ZDHHC9
FERMT1	
FGFR4	
GJB1	
GPX2	
GUCY2C	
HSD11B2	
LGALS4	

Supplementary Table S4. The epithelial signature. The 200 genes that are most significantly co-expressed with the epithelial differentiation genes CDX2, KRT20 and VIL1 were identified in a large combination cohort (MVRM). The table shows the 63-gene overlap between these lists, which we designated 'the epithelial signature'.

Epithelial signature		
FABP1	C10orf99	TMPRSS2
CDH17	MOGAT3	KIAA0226L
GUCY2C	NR1I2	DDC
LRRC19	LRRC31	EPS8L3
GPA33	MYO7B	IFNLR1
FLJ22763	PRR15	TRABD2A
CDX2	CLRN3	VIL1
MEP1A	SLC39A5	FAM211A
ABP1	EPB41L4B	IYD
HEPH	A1CF	ATP10B
HSD11B2	GPR160	CTTNBP2
CDX1	NAT2	SOWAHA
CLDN3	CFTR	ATP2C2
NOX1	PRLR	REPS2
PPP1R14D	SLC3A1	MAB21L3
MUC20	ISX	PRAP1
WNK4	TSPAN6	CEBPA
FAM84A	VAV3	LOC100505806
CEACAM5	OVOL1	SATB2
LGALS4	PRSS8	QPRT
		SHROOM1
		SLC25A13
		ZNF823

Supplementary Table S5. Primer pairs used for RT-qPCR analysis. The table lists all primer pairs used for RT-qPCR analysis of the indicated genes.

Primers of genes		Sequences	
	Gene name	Forward	Reverse
	GPx2	GCTCCCCTACCCTTATGATGA	AAATGATGAGCTTGGGATCGG
Stem cell	OLFM4	ACTGTCCGAATTGACATCATGG	TTCTGAGCTTCCACCAAAACTC
	SOX2	TACAGCATGTCCTACTCGCAG	GAGGAAGAGGTAACCACAGGG
	NANOG	TTTGTGGGCCTGAAGAAAACT	AGGGCTGTCCTGAATAAGCAG
	OCT4	CGACCATCTGCCGCTTTGAG	CCCCCTGTCCCCCATTCCTA
	ASCL2	TCTAAGGGCACAGAGAATCC	ACTGCTCGTGTCCAGATC
	LGR5	ACACTGTCATTGCGAGCCC	GAGGTCTAGGTAGGAGGTGAAG
	ALDH1A1	CCGTGGCGTACTATGGATGC	GCAGCAGACGATCTCTTTCGAT
	EPHB2	GCTTTCTGCTTACTGACTTAGG	GGTGGGAGGAGGGAAGAG
	BMI1	AGATTGGATCGGAAAGTAAAC	TCACAGTCATTGCTGCTGGGCA
Differentiation	FABP2	ATGGCGTTTGACAGCACTTG	TCAGTTCCGTCTGCTAGATTGTA
	CK20	GGACGACACCCAGCGTTTAT	CGCTCCCATAGTTCACCGTG
	MUC2	GGAGATCACCAATGACTGCGA	GAATCGTTGTGGTCACCCTTG
	ChrA	TAAAGGGGATACCGAGGTGATG	CCTCAGCCTTGGACTCCTG
	CDX2	GACGTGAGCATGTACCCTAGC	GCGTAGCCATTCCAGTCCT
	DPP4	TACAAAAGTGACATGCCTCAGTT	TGTGTAGAGTATAGAGGGGCAGA
Meschencymal	N-CADHERIN	TGGGAATCCGACGAATGG	TGCAGATCGGACCGGATACT
	VIMENTIN	GGAAGCCGAAAACACCCTG	GAGACGCATTGTCAACATCCT
	SNAIL1	GAGGCGGTGGCAGACTAG	AGATGAGCATTGGCAGCGAG
	TWIST1	CGGGAGTCCGCAGTCTTA	TGAATCTTGCTCAGCTTGTC
	ACTA2	CAGGGCTGTTTTCCCATCCAT	ACGTAGCTGTCTTTTTGTCCC
	FN1	GGCTCACTGCAAAGACTTTGAA	GGCTCACTGCAAAGACTTTGAA
	ZEB1	CAAGAGGCGCAAACAAGCC	GGTTGGCAATACCGTCATCC
Proliferation	Ki67	CGGACTTTGGGTGCGACTT	GTCGACCCCGCTCCTTTT
Housekeeping	HPRT	GAAAAGGACCCCACGAAGTGT	AGTCAAGGGCATATCCTACAA
	RLP13A	GCCATCGTGGCTAAACAGGTA	GTTGGTGTTCATCCGCTTGC

REFERENCES

1. Koh LW, Koh GR, Ng FS, Toh TB, Sandanaraj E, Chong YK, et al. A Distinct Reactive Oxygen Species Profile Confers Chemoresistance in Glioma-Propagating Cells and Associates with Patient Survival Outcome. AntioxidRedoxSignal. 2013.
2. Kyng KJ, May A, Brosh RM, Jr., Cheng WH, Chen C, Becker KG, et al. The transcriptional response after oxidative stress is defective in Cockayne syndrome group B cells. Oncogene. 2003;22:1135-49.
3. Jorissen RN, Gibbs P, Christie M, Prakash S, Lipton L, Desai J, et al. Metastasis-Associated Gene Expression Changes Predict Poor Outcomes in Patients with Dukes Stage B and C Colorectal Cancer. ClinCancer Res. 2009;15:7642-51.
4. Smith JJ, Deane NG, Wu F, Merchant NB, Zhang B, Jiang A, et al. Experimentally derived metastasis gene expression profile predicts recurrence and death in patients with colon cancer. Gastroenterology. 2010;138:958-68.
5. Marisa L, de RA, Duval A, Selves J, Gaub MP, Vescovo L, et al. Gene expression classification of colon cancer into molecular subtypes: characterization, validation, and prognostic value. PLoSMed. 2013;10:e1001453.
6. Melo DSE, Wang X, Jansen M, Fessler E, Trinh A, de Rooij LP, et al. Poor-prognosis colon cancer is defined by a molecularly distinct subtype and develops from serrated precursor lesions. NatMed. 2013;19:614-8.

7

HYPOXIA FOLLOWING LIVER SURGERY IMPOSES AN AGGRESSIVE CANCER STEM CELL PHENOTYPE ON RESIDUAL TUMOR CELLS

Klaas M Govaert, Benjamin L Emmink*, Maarten W Nijkamp*, Zing J Cheung, Ernst JA Steller, Szabolcs Fatrai, Menno T de Bruijn, Onno Kranenburg, Inne HM Borel Rinkes

Department of Surgery, University Medical Center Utrecht, The Netherlands

*Equal contribution

Annals of Surgery. 2014 Apr;259(4):750-9

MINI ABSTRACT

Experimental liver surgery causes localized chronic tissue hypoxia and influx of bone marrow-derived cells. Tumor cells residing in these areas adopt an aggressive immature cancer stem cell (CSC) phenotype. Hypoxia was sufficient to induce the CSC phenotype and stimulate tumor outgrowth. CSCs were readily eliminated by the hypoxia-activated pro-drug tirapazamine.

ABSTRACT

OBJECTIVE: To assess the contribution of hypoxia and bone marrow-derived cells to aggressive outgrowth of micrometastases following liver surgery. **BACKGROUND DATA:** Liver surgery generates a microenvironment that fosters aggressive tumor recurrence. These areas are characterized by chronic hypoxia and influx of bone marrow-derived cells. **METHODS:** The contribution of hematopoietic cell types was studied in mice lacking specific components of the immune system and in irradiated mice lacking all bone marrow-derived cells. Tumor cells were derived from colorectal cancer patients and from a metastatic tumor cell line. Hypoxia-induced changes in stem cell- and differentiation marker expression, clone-forming potential and metastatic capacity were assessed. The effect of vascular clamping on cancer stem cell (CSC) characteristics was performed in mice bearing patient-derived liver metastases. **RESULTS:** Immune cells and bone marrow-derived cells were not required for aggressive outgrowth of micro-metastases in surgery-treated livers. Rather, hypoxia was sufficient to promote invasion and accelerate metastatic outgrowth. This was associated with a rapid loss of differentiation markers and increased expression of CSC markers and clone-forming capacity. Likewise, metastases residing in ischemia-reperfusion-injured liver lobes acquired CSC characteristics. Despite their renowned general resistance to chemotherapy, clone-forming CSCs were readily killed by the hypoxia-activated pro-drug tirapazamine. **CONCLUSIONS:** Surgery-generated hypoxia in the liver causes rapid de-differentiation of tumor cells into immature CSCs with high clone- and metastasis-forming capacity. The results help explain the phenomenon of aggressive local tumor recurrence following liver surgery and offer a potential strategy to kill aggressive CSCs by hypoxia-activated pro-drugs.

INTRODUCTION

The fact that metastases frequently arise at sites of injury has been known for over a century[1]. However, the mechanisms that link surgery-induced tissue injury to the stimulation of metastatic growth are still largely obscure[2]. Metastases from colorectal tumors primarily develop in the liver and the lungs as a result of haematogenous spread and subsequent lodging of circulating tumor cells in the microvasculature of these organs. Results from experimental model systems have demonstrated that injury to liver tissue either caused by surgical trauma,[3,4] ischemia-reperfusion,[5] chemotherapy,[6] or irradiation[7] stimulates the outgrowth of liver metastases. Furthermore, surgical resection of liver metastases in colorectal cancer patients results in a significantly better disease control if ischemia-reperfusion injury is limited[8]. Along the same line, it has been argued that peri-operative therapy aimed at minimizing the consequences of surgery-induced tissue injury could be beneficial[9]. Partial liver resection and/or local ablation strategies are the only potentially curative treatment modalities in patients with metastatic colorectal cancer. Therefore, it is essential to understand the principles of liver injury-stimulated tumor growth in detail.

Our previous work has demonstrated that micro-metastases in the liver adopt a highly aggressive phenotype following liver injury induced by ischemia-reperfusion[5,10,11] or local ablation[3,12]. We found that accelerated tumor growth was primarily observed in tissue areas characterized by hypoxia and inflammation[3,11] and that this was independent of hypoxia-induced angiogenesis[3]. There is no doubt that both hypoxia and inflammation are pro-tumorigenic conditions (reviewed in[13-15]). Inflammatory cells and bone marrow-derived progenitor cells (BMDPCs) homing to injured tissue may promote local tumor growth and metastasis by secreting growth factors, cytokines and matrix-remodeling enzymes[16-18]. Such cells may also play a role in mediating chemotherapy resistance and in suppressing anti-tumor immunity[16]. One of the hallmarks of injured tissue is oxygen deprivation (hypoxia), caused by decreased tissue perfusion. Hypoxia-inducible factors (HIFs) promote tissue inflammation by stimulating expression of pro-inflammatory genes including cyclooxygenase-2, nitric oxide synthase and various cytokines[19]. *Vice versa*, expression of HIF1 itself is stimulated by NFκB, a key regulator of inflammatory gene expression[20,21]. Hypoxia also directly affects tumor cell behavior independently of inflammation by promoting tumor cell de-differentiation, invasion and metastasis (reviewed in[15]). The effects of hypoxia on both tumor cells and stromal cells are likely to contribute to hypoxia-associated therapy resistance and aggressive tumor behavior.

Given the intricate relationship between hypoxia and inflammation it has so far been impossible to identify the major driving force behind aggressive tumor recurrence following liver surgery. In the present report we have explored the contribution of hypoxia and inflammation to surgery-induced stimulation of tumor growth by using primary patient-derived colonosphere cultures and a mouse model for experimental liver metastasis formation. Based on the obtained results we present a potential therapeutic strategy to limit surgery-induced stimulation of tumor growth.

METHODS

Cell Culture

C26 cells were cultured in Dulbecco's modified Eagle's medium (DMEM; ICN Pharmaceuticals, Zoetermeer, The Netherlands) supplemented with 5 per cent (v/v) fetal calf serum, 2mmol/l glutamine, 0.1 mg/ml streptomycin, 100 units/ml penicillin. Human colonospheres cell lines (L145, L146, L167 and L169) were derived from patients harboring colorectal liver metastases and cultured in Stem Cell Medium as described[22]. All cell culture was carried out at 37 °C in a 5% CO2 humidified incubator under normoxic (21% oxygen) or hypoxic (1% oxygen) conditions, the latter using an Invivo2 Hypoxia Workstation (Biotrace International, Spennymoor, UK).

Clone-forming assays

Cells were pre-cultured under normoxic or hypoxic conditions for 24 hour. Following this 24 hour exposure to normoxia/hypoxia, C26 were seeded as single cells at 1000 cells per 10-cm dish in triplicate under normoxic conditions. Colonies were stained after ten days with 0.2 per cent crystal violet and counted. Colonospheres were processed as described by Emmink et al[22]. In short, 1000 single cells were plated in matrigel and colonospheres were counted 3 to 4 weeks after seeding.

The clone-forming potential of cells derived from tumor xenografts was assessed 24 hours following vascular clamping or sham treatment. Tumor-bearing livers were harvested and tumor tissue was cut into small fragments. Tissue fragments were washed with PBS until the supernatant was clear and were incubated in digestion buffer (50 ml DMEM, 1.25ml FCS, 3.5mg collegenase IX (Sigma, St. Louis, MO, USA), 6.2mg dispase type II (Invitrogen, Carlsbad, CA, USA), 500ul Primosin) for 60 minutes at 37°C while shaking. Dissociated cells were washed with PBS and were filtered through a 70-um cell strainer to separate residual tissue fragments from single cells. Cells were plated in matrigel in a concentration of 5000 cells/well and growth factors b-FGF (10 ng/ml, Abcam, Cambridge, United Kingdom) and EGF (20 ng/ml, Invitrogen) were freshly added every week. Tumor cells which were not used for the colonosphere forming assays were processed for flow cytometry to determine the percentage human cells using the epithelial marker anti-EpCAM (1/1000, Dako, Glostrup, Denmark). Five weeks following plating, colonospheres were counted and percentage of colonospheres forming efficacy was corrected for the percentage human cells (EpCAM+) in the clamped and sham treated single cell suspension.

To assess the effect of tirapazamine (TPZ) on the number of clone-forming cells colonospheres were exposed to hypoxia or normoxia with or without TPZ (40 μM; kindly provided by Dr Minchinton, BC Cancer Agency, Vancouver, Canada) for 24 hours. Following drug-exposure, single cells were washed and plated out in matrigel (1000 live cells/well) and colonospheres were counted after 3-4 weeks.

Invasion assay

Invasion assays were performed as described[23]. Following 24 hour incubation under hypoxia or normoxia, 50.000 C26 cells were placed in serum free conditions as single cells in the upper compartment of BioCoat matrigel invasion chambers (#354480; Becton Dickinson (BD) Biosciences, Franklin Lakes, NJ, USA). Following another 8 hours of incubation under respectively hypoxia or normoxia transmigrated (towards a 5% serum gradient) cells were counted. Assays were performed in duplicate.

Western blotting

Colonospheres were cultured under normoxic or hypoxic conditions for up to 48 hours. For the TPZ toxicity experiment colonospheres were cultured for 24 hours under normoxic or hypoxic conditions with or without 40 μM TPZ. Colonospheres were lysed in buffer (containing 20 mmol/l HEPES, pH 7.4, 1 per cent NP40, 150 mmol/l sodium chloride, 5 mmol/l magnesium chloride, 10 per cent glycerol), run out on sodium dodecyl sulphate-containing gels and blotted onto nitrocellulose membranes. After blocking in milk, the blots were probed with antibodies against cytokeratin 20 (CK20, Ks20.8; 1:500, M7019; Dako), cleaved caspase-3 (1:5000, ab9665; Cell Signaling, Littleton, MA, USA) or actin (1:20000, NB600-501; Novus Biologicals, Littleton, CO, USA). Horseradish peroxidase-conjugated secondary antibodies were from Dako. Signals were detected by chemoluminescence.

Immunohistochemistry

Nine days following vascular clamping of livers containing L145 tumors, immunohistochemistry was performed on formalin embedded tissue using antibodies against CK20 (Ks20.8, 1:200, M7019, Dako), fatty acid-binding protein 1 (FABP1; 1:500, HPA 028275, Sigma) and mucin2 (MUC2; 1:200, 15334; Santa Cruz, Santa Cruz, CA, USA). Slides were incubated overnight with primary antibody at 4°C. For detection goat anti Ms/Rb/Rt-poly-HRP (Powervision Immunologic, Immunovision Technologies, Brisbane, CA, USA) was used. All slides were developed with diaminobenzidine followed by heamatoxylin counterstaining. Pictures were made of the whole tumor lesion and the percentage positive stained tissue per high power field(HPF) was calculated using ImageJ software (National Institutes of Health, Bethesda, MD, USA).

Granulocytes in the transition zone(TZ) following radiofrequency ablation (RFA) procedure, were detected by coupling of diazonium salt (pink) to the naphthol-AS-D-chloroacetate esterasecreated free naphthol compound (characteristic for granulocytes) following standard procedures. Pictures of the TZ were made and LEDER positive cells were counted per HPF. All quantifications were performed in a blinded fashion.

Immunofluorescence

L146 cells were exposed for 24 hours to hypoxia or normoxia prior to fixation in 3.7% formaldehyde (30 minutes). After fixation, cells were washed with PBS before being permeabilized with ice-cold (-20°C) methanol (10 minutes). Cells were blocked in PBS containing 2% BSA and 0.1% Tween (1 hour). Cells were incubated overnight with primary antibody against CK20 (Ks20.8, 1:50, M7019; Dako) and stained overnight at 4 degrees with a fluorescence conjugated IgG (chicken anti-mouse Alexa fluor 488) mixed with 0.5 μg/mL DAPI. The slides were cover slipped with Vectashield mounting medium. The samples were analysed using a Zeiss LSM510 META microscope.

Flow Cytometry

Aldefluor activity and the expression of the surface marker SCA1 were analysed by FACS using CellQuest software (BD). C26 cells and the L145 colonosphere cell line were cultured under normoxia or hypoxia for the indicated time points. For the toxicity experiments, colonosphere line L145 was cultured for 24 hours under normoxic or hypoxic conditions with or without TPZ (20- or 40 μM). Next, cells were trypsinized to obtain single cell suspensions. Cell doublets and clumps were excluded by prior filtration and by using doublet discrimination gating during FACS analysis. Aldefluor-positive cells were analyzed according to the manufacturer's protocol by

using the ALDH substrate BAAA (1 µmol/l per 1×106 cells; StemCell Technologies, Vancouver, Canada). Negative control samples were co-incubated with diethylaminobenzaldehyde (DEAB; 50 mM, StemCell Technologies). Percentage of SCA1 expression in C26 cells following 24 hour incubation under normoxia or hypoxia was determined using the antibody against SCA1 (Ly-6A/E(D7), 557403, BD). The cell sorting experiments were conducted with DAKO-Cytomation MoFlo High Speed Sorter.

Quantitative real time polymerase chain reaction

RNA was isolated according to the manufacturer's protocol (RNeasy Mini Kit, Qiagen, Venlo, the Netherlands) from colonospheres cell lines (L145, L146 and L169) exposed up to 48 hours *in vitro* to normoxia and hypoxia and from the L145 xenografted colonosphere tumor tissue 24 hour following clamping. c-DNA was synthesized from 250 ng of total RNA using iScript cDNA Synthesis Kit (Bio-Rad, Hercules, CA, USA). Next cDNA was amplified in an iCycler thermocycler (Bio-Rad) using iQ SYBR Green Supermix (Bio-Rad). mRNA expression levels were quantified using iCycler software (Bio-Rad) and were normalized to B2M. All samples were analyzed in triplicate. qPCR analysis was performed for the markers hexokinase2 (HEX2), fatty acid-binding protein2 (FABP2), MUC2, SOX2, OCT4, NANOG, olfactomedin 4 (OLFM4) and chromogranin A (CHRA) (all primers were ordered from Sigma).

Experimental animal treatments

All experiments were carried out in accordance with the guidelines of the Animal Welfare Committee of the University Medical Centre Utrecht, The Netherlands. For the experiments using C26 cells, male Balb/c mice, nude mice, severe combined immunodeficiency (SCID) mice or non-obese diabetic (NOD) SCID mice were purchased from Charles River (10–12 weeks, 20–25 g; Sulzfeld, Germany). For the human L145 colonosphere in vivo experiments CB17/Icr-Prkdc <scid>Crl (F) were purchased (Charles River). Animals were housed under standard laboratory conditions. All surgical procedures were performed under isoflurane inhalation anaesthesia. Buprenorphine was administered intramuscularly before surgery to provide sufficient preoperative analgesia.

Tumor induction of C26 cells and RFA were performed as described by Nijkamp et al [3]. For the experiments using the colonosphere cell line L145, cells were injected and grown subcutaneously to a maximum of 1 cm^3. Serial transplantation of a little piece of tumor (± 10mm^3) was performed into the left liver lob of a new recipient mice. This tumor was allowed to grow for 8 weeks before hepatic clamping procedure (45 minutes) was performed as described by van der Bilt et al[5]. Control mice underwent surgery and liver handling without the clamping procedure itself.

Radiotherapy was used just to gain complete loss of bone marrow function in Balb/C mice. This was given for one minute at a dose of 6 gray two hours prior to tumor cell induction. Loss of inflammatory cells was validated by LEDER staining for granulocytes on liver sections and by blood analysis for white blood cells using a Cell-Dyn 1800 (Abbott Diagnostics).

Assessment of tumor cell phenotype following radiofrequency ablation

Mice bearing enhanced green fluorescent protein (EGFP)- expressing tumor cells were killed 24 hours after RFA. Confocal microscope images were prepared as described by Nijkamp et al[3]. In short, livers were excised and placed on a coverslip using immersion oil to improve visualization. EGFP was excited at 488 nm and length of largest diameter of metastases was measured in both reference zone (RZ) and transition zone (TZ). The TZ was defined as the area stretching 2 mm

outside the necrotic ablated zone. The RZ was defined as the part of the liver unaffected by the RFA treatment (more than 2 mm from the lesion border).

Tumor load analysis following radiofrequency ablation

For the tumor load studies following RFA in irradiated mice, animals were terminated 10 days following tumor cell injection (seven days following RFA). For the metastases formation experiments using hypoxia or normoxia exposed C26 cells, mice were terminated 7 days following tumor cell injection. Livers were harvested, fixed in 4 per cent buffered formaldehyde and embedded in paraffin for morphometric assessment of tumor growth. Tumor load was scored in the RZ and TZ in the irradiated mice, as described previously[3]. For the experiment using hypoxia or normoxia exposed tumor cells, the number of metastases and HRA were measured in the whole left liver lobe.

Statistics

Data are presented as mean (s.e.m.). All statistical differences between groups were measured by paired (or unpaired when appropriate) Student's *t* tests using GraphPad Prism version 5.0 (Graphpad Software, La Jolla, CA, USA).

RESULTS

Immune cells are dispensable for injury-induced aggressive tumor growth in the liver

We have previously shown that damage to liver tissue induced either by RFA or ischemia-reperfusion injury generates highly localized regions of chronic hypoxia in which aggressive tumor growth is observed[3,5]. To study whether immune cells contribute to the aggressive phenotype of tumor cells in post-surgery livers we made use of irradiation to kill all hematopoietic cells (Fig 1A). Following RFA, neutrophils are the first cells to arrive at the transition zone,[24] which separates the site of injury from the non-affected liver. As expected, the recruitment of neutrophils was not observed in irradiated mice (FIG 1B). Tumor cell invasion into the peri-necrotic region can be quantified by making use of GFP-expressing tumor cells and post-mortem fluorescence microscopy analysis of the liver. Surprisingly, the absence of neutrophils and other inflammatory cells in the hypoxic transition zone had no effect on the highly invasive phenotype that characterizes metastases in this region (FIG 1C,D). Moreover, irradiation did not affect surgery-stimulated outgrowth of metastases in the transition zone (FIG 1E and ref[3]). Similarly, transition zone metastases in mice lacking either T lymphocytes (nude), T and B lymphocytes (SCID) or T lymphocytes, B lymphocytes and natural killer (NK) cells (NOD/SCID) were all characterized by a highly invasive phenotype (FIG 1F). From these experiments we conclude that inflammatory cells are dispensable for establishing an invasive phenotype and accelerated outgrowth of peri-necrotic metastases in RFA-injured livers.

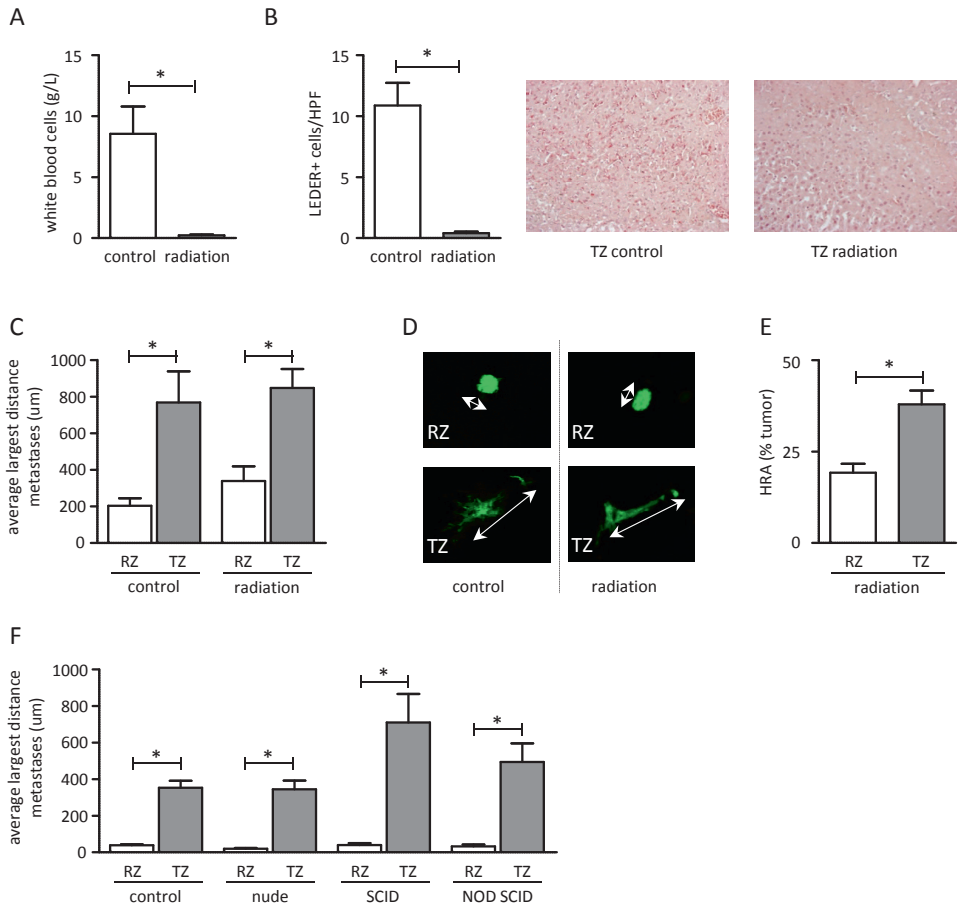

Fig 1. Immune cells and bone marrow-derived cells do not contribute to the invasive metastasis phenotype and accelerated tumor outgrowth induced by liver surgery

Balb/c mice were subjected to radiation or control treatment directly followed by intrasplenic injection of enhanced green fluorescent protein (EGFP)-expressing tumor cells. Three days later liver micrometastases were formed and RFA treatment was performed in the left liver lobe. To assure adequate radiation, white blood cells were measured 24 hrs following RFA in the corresponding blood samples (**A**) and neutrophil influx into the TZ was assessed by LEDER staining on corresponding tissue sections (neutrophils were counted per high power field (HPF))(**B**). 24 hours following RFA treatment invasion of tumor cells was determined by measuring the longest diameter of metastases in the hypoxic transition zone (TZ) and the normoxic reference zone (RZ) (n=4-6)(**C**). Representative pictures are shown (**D**). Ten days following RFA, tumor load (calculated as hepatic replacement area: HRA) was determined in the TZ and RZ in irradiated mice (n=11) (**E**). Invasion of GFP-labeled C26 cells 24 hours following RFA treatment was measured in mice with different immunological backgrounds. Normal Balb/c mice (control), nude mice lacking T lymphocytes, severe combined immunodeficiency (SCID) mice lacking T and B lymphocytes and non-obese diabetic (NOD) SCID mice lacking T lymphocytes, B lymphocytes and natural killer (NK) cells (n=3) (**F**). * $p<0.05$ student's t-test.

Exposure of colorectal tumor cells to hypoxia promotes clone-formation, invasion and metastatic capacity

The finding that inflammatory cells do not play a major role in injury-induced aggressive tumor growth prompted us to test the isolated effect of hypoxia on colorectal cancer cell behavior. To this end, murine colorectal cancer cells and patient-derived 'colonosphere' cultures were exposed to hypoxia or normoxia for 24 hours, after which their colony-forming potential was assessed. In all cultures tested, exposure to hypoxia significantly increased the number of cells with colony-forming potential (FIG 2A). Furthermore, hypoxia also increased the invasive capacity of C26 cells (FIG 2B). Increased colony-forming potential coupled to increased invasive capacity suggested that a short transient exposure to hypoxia may be sufficient to increase the metastatic capacity of the resulting cultures. To test this, we injected normoxic and hypoxic C26 cells into the spleens of Balb/c mice and analyzed metastatic burden in the liver two weeks later. We observed that 5 days of *in vitro* exposure to hypoxia doubled the metastatic potential of C26 tumor cells (FIG 2C,E). Moreover, liver metastases formed by hypoxia-exposed C26 tumor cells occupied approximately threefold more liver tissue than those cultured under normoxia (FIG 2D,E).

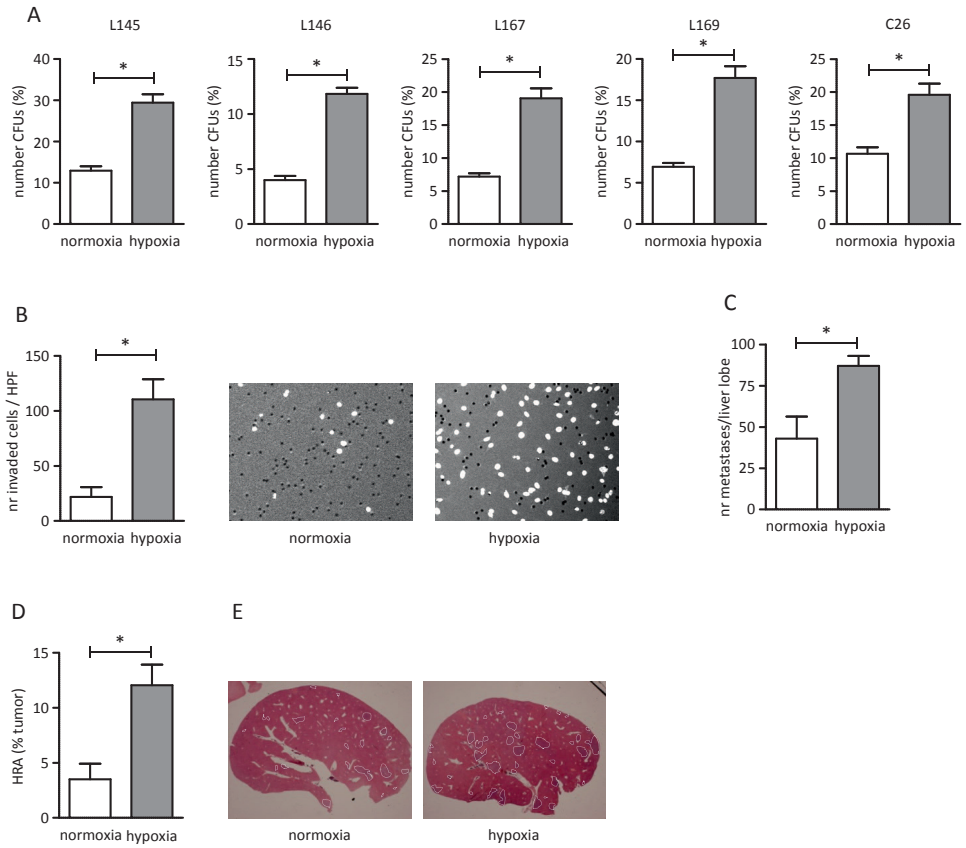

Fig 2. *In vitro* exposure of colorectal tumor cells to hypoxia promotes clone-formation, invasion and metastatic capacity

Five different colorectal cancer cell lines were grown under hypoxia or normoxia for 24 hours and their colony-forming potential was assessed in normoxia. All experimenters were performed in triplicate. The mean % of

colony-forming cells +/- SEM is shown. (**A**). C26 cells were cultured in Transwell migration chambers coated with Matrigel and were exposed to normoxia or hypoxia for 24 hours. Absolute numbers of Matrigel-invaded C26 cells were then quantified in six high power fields (HPFs). Representative HPFs with DAPI stained migrated cells(white) trough semi-permeable membrane(black dots) are shown. The experiment was performed in duplicate (**B**)**.** C26 cells were exposed to normoxia or hypoxia *in vitro* for 5 days. Following intrasplenic tumor cell injection (n=4), the livers were harvested 7 days later to assess the number of metastases (**C**) and the tumor load as hepatic replacement area (% liver tissue occupied by tumor) (**D**). Representative liver sections are shown (**E**).* $p<0.05$ Student's t-test.

Exposure of colorectal tumor cells to hypoxia causes rapid loss of differentiation markers and a concomitant increase in stem cell markers

The above results suggest that hypoxia alone is sufficient to induce a more invasive and aggressive phenotype in colorectal cancer cells. Given that hypoxia can foster the growth of normal and cancer stem cells[15] and that stem cell signatures are associated with poor survival in colorectal cancer[25,26], we analyzed differentiation and stem cell marker expression in colorectal tumor cells exposed to hypoxia or normoxia. Culturing human colonospheres of 4 different patients in hypoxia caused a rapid (24 hours) loss of cytokeratin 20 (CK20), which is a general marker for colorectal tumor cell differentiation (FIG 3A,B). In addition, hypoxia caused loss of the enterocyte marker FABP2 and of the goblet cell marker Mucin-2, whereas hexokinase-2, a marker for hypoxia, was strongly induced (3C). Aldefluor® is a fluorescent probe for aldehyde dehydrogenase activity and frequently used to identify normal and cancer stem cells[27-30]. Indeed, Aldefluor+ cells express high levels of primitive stem cells markers(FIG 3F) and recently we have shown that these cells are clonogenic and tumorigenic [22]. Transplantation studies have identified the cell surface protein Sca1 as a marker for tumor-initiating cells in mice and it is commonly used to identify murine cancer stem cells[31-38]. Exposure of C26 cells and human colonospheres to hypoxia caused a dramatic increase in Sca1- and Aldefluor-positive cells respectively (FIG 3D,E). Together, the results demonstrate that exposure of human and murine colorectal tumor cells to hypoxia causes a rapid and general loss of differentiation markers and a concomitant increase in stem cell markers and clone-forming capacity.

Colorectal cancer is characterized by an enormous genetic heterogeneity between individual tumors. Therefore, it is quite possible that Aldefluor (and/or Sca1), while being good CSC markers for the cell lines that were used in the present study, may not be general markers for CSCs in all colorectal tumors.

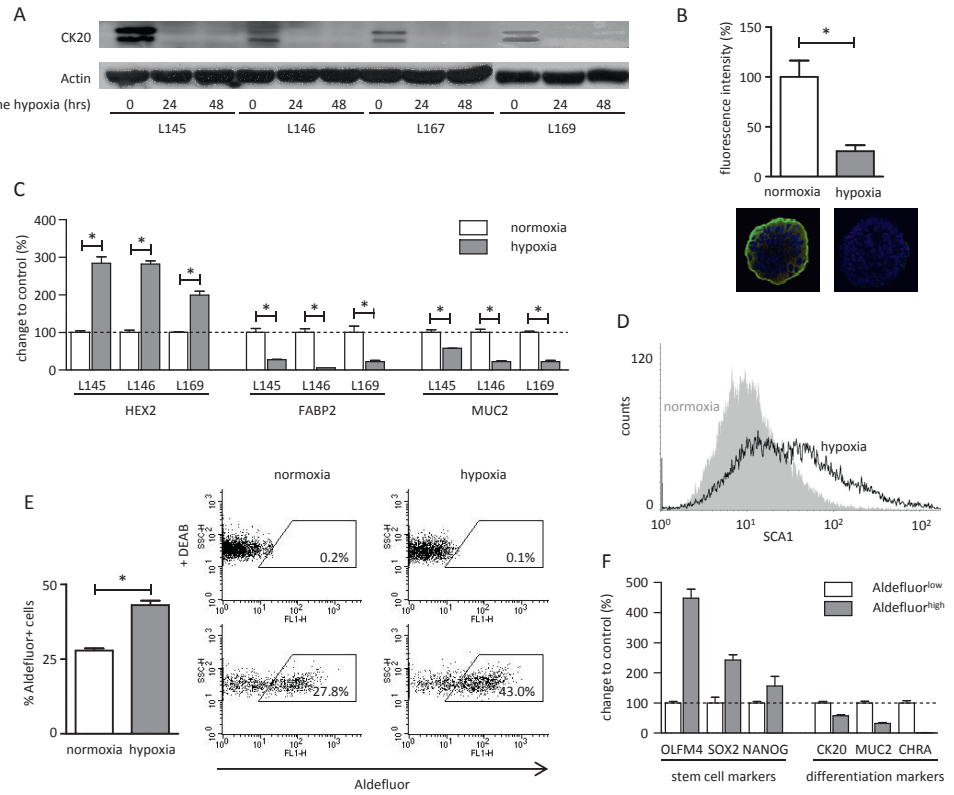

Fig 3. *In vitro* hypoxia suppresses differentiation and causes increased expression of stem cell markers

The indicated human colonosphere cell lines were exposed to hypoxia for 0, 24 or 48 hours. Lysates were analyzed for the differentiation marker cytokeratin 20 (CK20). Actin served as a control for equal protein loading (**A**). L146 cells were cultured as above on glass cover slips and immunofluorescence for CK20 was performed. The intensity of CK20 was measured using LSM software. Mean CK20 signal intensity levels were then plotted as means +/- SEM. The experiment was performed in triplicate. Representative images are shown (**B**). Up to 48 hours following exposure to hypoxia samples of the indicated colonosphere lines were analyzed for RNA levels of the hypoxia marker hexokinase2 (HEX2) and the differentiation markers FABP2 and MUC2 by qPCR. All experiments were performed in triplicate (**C**). C26 cells were exposed to normoxia or hypoxia for 24 hours. Cells were then analysed for stem cell antigen 1 (SCA1) levels by FACS (**D**). L145 cells were exposed to either normoxia or hypoxia for 24 hours and Aldefluor activity was measured using FACS analysis. DEAB was used to identify the negative cell population (**E**). L145 cells were FACS sorted for Aldefluor^{low} and Aldefluor^{high} activity and tested for stem cell marker and differentiation marker expression using qPCR (**F**). All experimenters were performed in triplicate at least two times. Results are shown as means +/- SEM. * $p<0.05$ Student's t-test.

Vascular clamping induces a cancer stem cell (CSC)-like phenotype in resident liver metastases

Next, we analyzed whether the *in vitro* processes described above would also occur in liver metastases following tissue injury. To this end we used patient-derived L145 colonospheres. Implantation of a small piece of tumor tissue into the parenchyma of the left liver lobe resulted in the growth of a single liver tumor in all cases. After 8 weeks, ischemia-reperfusion injury (or

sham treatment) was induced. 24 hours following vascular clamping, the livers were isolated and the tumors were processed for analysis of the expression of stem cell and differentiation markers and for colony-forming potential. The stem cell markers SOX2 and OCT4 were elevated in tumors isolated from clamped versus non-clamped liver lobes while the differentiation markers FABP2 and MUC2 were reduced (FIG 4A). In line with this result, tumor tissue harvested from clamped liver lobes contained significantly more clonogenic tumor cells than tumors isolated from non-clamped lobes (FIG 4B). Immunohistochemistry of tumor tissue 5 days following vascular clamping also showed a strong decrease in the expression of FABP1 and CK20 in tumors isolated from clamped liver lobes. The differences in Muc2 expression were highly variable (FIG 4C). These results demonstrate that ischemia-reperfusion injury rapidly imposes an immature, aggressive phenotype on resident tumor tissue.

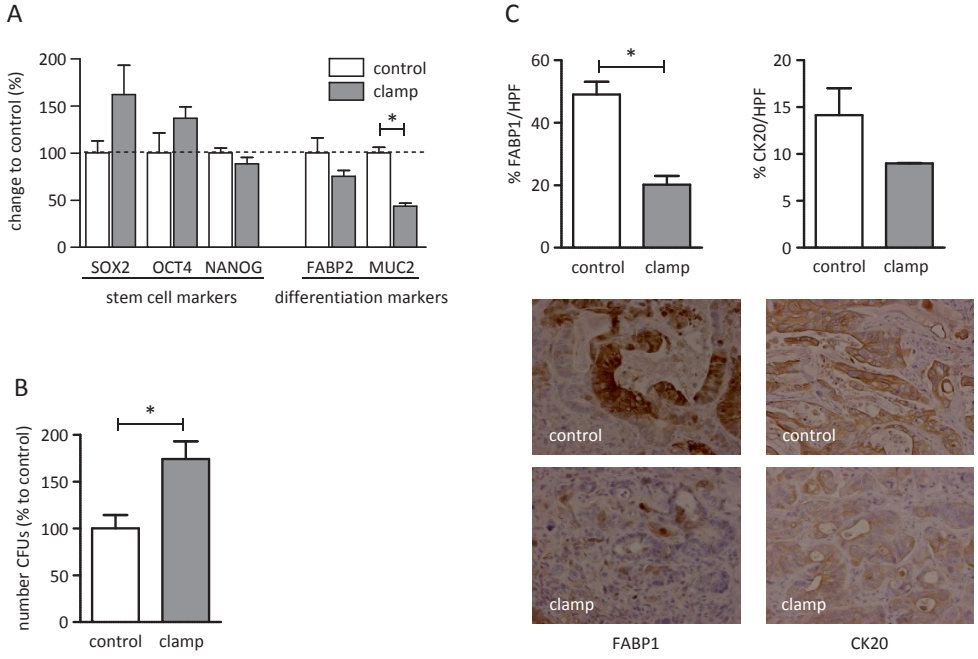

Fig 4. Ischemia-reperfusion in mouse livers bearing human tumor xenografts causes loss of tumor cell differentiation and increased colony-forming potential

Small pieces of subcutaneous L145 human tumor xenografts were implanted into the left liver lobes of immunodeficient mice. Eight weeks following implantation the left liver lobes were subjected to an ischemia (45 minutes) reperfusion (24 hours) procedure. The livers were harvested and tumor tissue was analyzed for stem cell marker and differentiation marker expression using qPCR (**A**) Alternatively, the tumor tissue was processed to single cells. The number of Colony-Forming Units (CFU) was assessed by plating single cells in Matrigel and analyzing the number of colonies five weeks later (**B**). Nine days following the clamping procedure tumor-containing livers were analyzed by immunohistochemistry for the differentiation makers FABP1 and CK20 (**C**). All experimenters were performed in triplicate. * $p<0.05$ Student's t-test.

Tirapazamine as a potentially effective anti-CSC drug

CSCs are thought to be intrinsically resistant to chemotherapy due to their ability to keep intracellular radical oxygen species low and to high activity of the DNA damage checkpoint and DNA repair enzymes[39]. However, CSCs do not display intrinsic resistance to all (chemotherapeutic) drugs, as they are highly sensitive to killing by Akt inhibitors[40] and by the topoisomerase I inhibitor irinotecan[22]. Interestingly, the hypoxia-activated pro-drug tirapazamine (TPZ) is a topoisomerase II inhibitor,[41] which we have previously shown to be effective in preventing injury-associated aggressive tumor recurrence in the liver[42]. Therefore we tested whether TPZ was able to kill hypoxia-exposed CSCs. We found that TPZ readily killed colonopshere cultures from three different patients in a hypoxia-dependent manner (FIG 5A) and completely abolished clone-forming capacity of hypoxia-exposed colonospheres (FIG 5B). Strikingly, TPZ treatment completely prevented the hypoxia-induced increase in Aldefluor+ CSCs in the tumor cell population surviving treatment (FIG 5C).

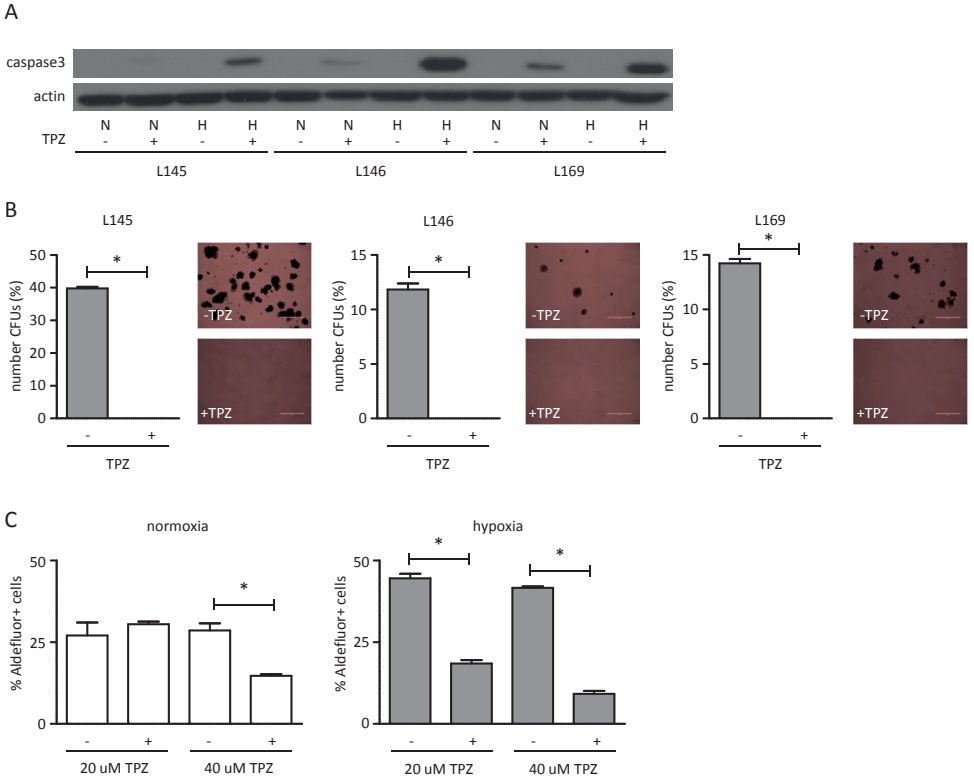

Fig 5. The hypoxia-activated pro-drug tirapazamine kills colorectal cancer stem cells

The indicated colonosphere cell lines were cultured with or without tirapazamine (TPZ; 40 uM) for 24 hours in hypoxia (H) or normoxia (N). Cells were lysed and analyzed for the processing of caspase-3 as an indicator of tumor cell apoptosis. Actin was used as a loading control (**A**). Cells were grown in hypoxia for 24 hours in the presence or absence of TPZ (40 uM). Single cell suspensions were prepared and the colony-forming potential was assessed by plating 1000 live cells in Matrigel. The number of Colony Forming Units (CFUs) was assessed three-four weeks later. Representative pictures are shown (**B**). The effect of TPZ treatment on the number of Aldefluor+ cells population was assessed by FACS. L145 cells were cultured in normoxia or hypoxia for 24 hours with or without TPZ (20uM or 40uM). Cells were then processed for FACS analysis of the % Aldefluor-positive cells as in Figure 4 (**C**). All experimenters were performed in triplicate. * $p<0.05$ Student's t-test.

DISCUSSION

Previously, we have shown that the HSP90-blocker 17-DMAG, a potent destabilizer of HIF1, could prevent hypoxia-associated aggressive tumor growth surrounding RFA-generated lesions.3 In the present report, we provide evidence that tumor cell exposure to hypoxia is sufficient to drive aggressive local outgrowth of liver tumors without the need for infiltrating inflammatory cells or BMDPCs. Exposure of patient-derived "colonosphere" cultures to hypoxia caused a rapid loss of differentiation markers and imposed an invasive CSC phenotype. These effects were also observed in mice harboring human xenotransplant in the liver after ischemia-reperfusion injury. We propose that the hypoxia-induced phenotypic change to a more primitive CSC-like state contributes to the observed aggressive postsurgery phenotype of residual micrometastases. Given the enormous genetic heterogeneity that characterizes colorectal cancer, further work is needed to establish the generality of these findings in a large panel of human colorectal tumors and in patients undergoing partial liver resection. Nonetheless, given that hypoxia-induced increase in cancer stemness was observed in all cell lines analyzed, it may be regarded as a relatively common phenomenon. In line with this, colorectal cancer patients whose tumors are characterized by a primitive stem cell–like expression pattern are at high risk of developing metastases and tumor recurrence[26].

Local recurrence is a major concern after liver surgery. Local recurrence rates of up to 60% have been reported after RFA procedures[43,44]. A key issue is that more than 50% of resected liver tumors harbor microsatellite lesions, which are undetectable by conventional imaging[45]. Moreover, clinically inconspicuous rest liver frequently (up to 70%) contains micrometastases[46,47]. When left behind after surgery, such micrometastases could benefit from the hypoxic protumorigenic microenvironment and undergo the transition into a CSC-like state. It is important to note that the "CSC state" is not a stable feature of a select group of cells but one that may be obtained or lost over time, depending on cues from the microenvironment[48,49]. Our results suggest that postsurgical hypoxia is one such dominant cue.

Although there is no doubt that inflammatory cells and BMDPCs can promote tumor formation,[14,17] these cells were not required for the changes in tumor behavior after liver surgery (this report). Apparently, the mechanisms that link chronic inflammation to tumor development are distinct from those linking postsurgical hypoxia to an aggressive tumor phenotype. Nevertheless, hepatitis is an independent predictor for local recurrence after RFA treatment of hepatocellular carcinoma (HCC)[50]. Whether this is due to inflammation associated hypoxia or to the inflammatory cells themselves is not known.

Our results using human colorectal tumor cell lines freshly isolated from liver metastases in a mouse model demonstrate that liver surgery promotes the CSC phenotype and causes accelerated tumor outgrowth. These results warrant clinical studies in which the phenotype and growth behavior of liver metastases is analyzed before and after the first surgical procedure. Interestingly, a recent study investigated the growth speed of 60 HCC tumors before and after transarterial chemoembolization[51,52]. This procedure induces high levels of hypoxia due to the embolization spheres[53,54]. After transarterial chemoembolization, the mean tumor doubling time was significantly shorter, suggesting hypoxia-associated acceleration of tumor growth. This is in line with the results that we have obtained in the model of surgery-stimulated hypoxia-associated outgrowth of colorectal liver tumors. A clinical imaging study should address the relationship between liver surgery and the rate of local and distant recurrent tumor growth in patients with metastatic colorectal cancer. On the basis of the results so far, we suggest that minimizing surgery-induced hypoxia may help prevent aggressive local tumor recurrence.

Hypoxia not only causes changes in tumor phenotype, it is also strongly associated with poor response to radiotherapy and chemotherapy. This may be due to the lack of oxygen itself (reactive oxygen species cannot be formed in the absence of oxygen), but it may also be directly related to the hypoxia-induced CSC phenotype, as CSC are generally considered to be relatively chemoresistant[55–57]. Overcoming hypoxia-associated resistance of tumor cells to chemotherapy is one of the holy grails in oncology. Approaches include the pharmacological targeting of HIFs and the use of hypoxia-activated prodrugs such as TPZ[58–60]. Previously, we have shown that this drug is effective in overcoming hypoxia-driven aggressive outgrowth of C26 liver metastases after RFA[42]. In the present report, we show that TPZ has the remarkable capacity to lower the CSC fraction in drug-treated cell populations and kill all clone forming capacity, while treatment with most standard chemotherapeutics (such as, oxaliplatin and 5FU) increases the CSC fraction[61,62]. TPZ inhibits topoisomerase II. Recently, we found that irinotecan, a topoisomerase I inhibitor, is also effective in eliminating the CSC population[22]. It follows that CSCs may not be selectively resistant to the type of DNA damage induced by topoisomerase inhibition. An alternative explanation could be that TPZ inhibits expression of HIF1[63]. This could affect cellular differentiation, invasion, and metastasis formation[15]. However, in the colorectal tumor cells studied here, apoptosis was the primary outcome after hypoxic exposure to TPZ, and this completely prevented the hypoxia-induced increase in CSC numbers. This suggests that the cytotoxic effects rather than the effects on HIF1 may be dominant. In any case, this study together with our prior work[22] strongly suggests that topoisomerase inhibition may be a good strategy to kill colorectal CSCs.

How may these results be implicated in the treatment of liver tumors? Surgical procedures, which generate hypoxia in the liver, include RFA and embolization techniques. The clinical value of embolization spheres loaded with doxorubicin has recently been established and may become standard treatment in HCC (reviewed in[64]). We propose that the unique capacity of TPZ to kill colorectal CSCs may be exploited in the treatment of nonresectable metastases. These drugs could be included in embolization beads, ensuring local delivery in areas of hypoxia, or could be administered as adjuvant therapy after RFA. In addition, by locally killing the CSC fraction, these drugs could prevent the initiation of new metastatic clones. The combination of surgical and/or radiological approaches with CSC-targeting chemotherapeutics such as TPZ should reduce intrahepatic recurrence rates in metastatic colorectal cancer.

CONCLUSIONS

Surgery-generated hypoxia in the liver causes rapid dedifferentiation of tumor cells into immature CSCs with high clone and metastasis-forming capacity. The results presented in this report help explain the phenomenon of aggressive local tumor recurrence following liver surgery and offer a potential strategy to kill aggressive CSCs by hypoxia-activated pro-drugs such as TPZ.

Acknowledgments
The authors thank K. Trumpi, T. Vellinga and S. van Schelven for support regarding the animal studies, A. Verheem and D. Raats for providing excellent technical assistance, and J. Vermeulen for his help in conducting the hypoxia experiments. Dr. Minchinton is acknowledged for providing Tirapazamine.

REFERENCES

1. Jones FS, *et al.* On the cause of the localization of secondary tumors at points of injury. J Exp Med 1914; 20:404-412.
2. Demicheli R, *et al.* The effects of surgery on tumor growth: a century of investigations. Ann Oncol 2008; 19:1821-1828.
3. Nijkamp MW, *et al.* Accelerated perinecrotic outgrowth of colorectal liver metastases following radiofrequency ablation is a hypoxia-driven phenomenon. Ann Surg 2009; 249:814-823.
4. Fisher B, Fisher ER. Experimental studies of factors influencing hepatic metastases. III. Effect of surgical trauma with special reference to liver injury. Ann Surg 1959; 150:731-744.
5. van der Bilt JD, *et al.* Ischemia/reperfusion accelerates the outgrowth of hepatic micrometastases in a highly standardized murine model. Hepatology 2005; 42:165-175.
6. Daenen LG, *et al.* Chemotherapy enhances metastasis formation via VEGFR-1-expressing endothelial cells. Cancer Res 2011; 71:6976-6985.
7. van den Brenk HA, *et al.* Stimulation of growth of metastases by local x-irradiation in kidney and liver. Br J Cancer 1973; 28:349-353.
8. Nijkamp MW, *et al.* Prolonged portal triad clamping during liver surgery for colorectal liver metastases is associated with decreased time to hepatic tumour recurrence. Eur J Surg Oncol 2010; 36:182-188.
9. van der Bij GJ, *et al.* The perioperative period is an underutilized window of therapeutic opportunity in patients with colorectal cancer. Ann Surg 2009; 249:727-734.
10. van der Bilt JD, *et al.* Selective portal clamping to minimize hepatic ischaemia-reperfusion damage and avoid accelerated outgrowth of experimental colorectal liver metastases. Br J Surg 2006; 93:1015-1022.
11. van der Bilt JD, *et al.* Perinecrotic hypoxia contributes to ischemia/reperfusion-accelerated outgrowth of colorectal micrometastases. Am J Pathol 2007; 170:1379-1388.
12. Nijkamp MW, *et al.* CD95 is a key mediator of invasion and accelerated outgrowth of mouse colorectal liver metastases following radiofrequency ablation. J Hepatol 2010; 53:1069-1077.
13. Bertout JA, *et al.* The impact of O2 availability on human cancer. Nat Rev Cancer 2008; 8:967-975.
14. Klampfer L. Cytokines, inflammation and colon cancer. Curr Cancer Drug Targets 2011; 11:451-464.
15. Semenza GL. Hypoxia-inducible factors: mediators of cancer progression and targets for cancer therapy. Trends Pharmacol Sci 2012; 33:207-214.
16. Shiao SL, *et al.* Immune microenvironments in solid tumors: new targets for therapy. Genes Dev 2011; 25:2559-2572.
17. Lyden D, *et al.* Impaired recruitment of bone-marrow-derived endothelial and hematopoietic precursor cells blocks tumor angiogenesis and growth. Nat Med 2001; 7:1194-1201.
18. Langenberg MH, *et al.* Liver surgery induces an immediate mobilization of progenitor cells in liver cancer patients: A potential role for G-CSF. Cancer Biol Ther 2010; 9:743-748.
19. Imtiyaz HZ, *et al.* Hypoxia-inducible factors as essential regulators of inflammation. Curr Top Microbiol Immunol 2010; 345:105-120.
20. Taylor CT. Interdependent roles for hypoxia inducible factor and nuclear factor-kappaB in hypoxic inflammation. J Physiol 2008; 586:4055-4059.
21. Taylor CT, Cummins EP. The role of NF-kappaB in hypoxia-induced gene expression. Ann N Y Acad Sci 2009; 1177:178-184.
22. Emmink BL, *et al.* Differentiated human colorectal cancer cells protect tumor-initiating cells from irinotecan. Gastroenterology 2011; 141:269-278.
23. Steller EJ, *et al.* The death receptor CD95 activates the cofilin pathway to stimulate tumour cell invasion. EMBO Rep 2011; 12:931-937.
24. Nijkamp MW, *et al.* Radiofrequency ablation of colorectal liver metastases induces an inflammatory response in distant hepatic metastases but not in local accelerated outgrowth. J Surg Oncol 2010; 101:551-556.
25. de Sousa E Melo, *et al.* Methylation of cancer-stem-cell-associated Wnt target genes predicts poor prognosis in colorectal cancer patients. Cell Stem Cell 2011; 9:476-485.
26. Merlos-Suarez A, *et al.* The intestinal stem cell signature identifies colorectal cancer stem cells and predicts disease relapse. Cell Stem Cell 2011; 8:511-524.
27. Charafe-Jauffret E, *et al.* Aldehyde dehydrogenase 1-positive cancer stem cells mediate metastasis and poor clinical outcome in inflammatory breast cancer. Clin Cancer Res 2010; 16:45-55.

28. Deng S, *et al.* Distinct expression levels and patterns of stem cell marker, aldehyde dehydrogenase isoform 1 (ALDH1), in human epithelial cancers. PLoS One 2010; 5:e10277.
29. Shenoy A, *et al.* ALDH as a marker for enriching tumorigenic human colonic stem cells. Methods Mol Biol 2012; 916:373-385.
30. Shenoy AK, *et al.* Transition from colitis to cancer: high Wnt activity sustains the tumor-initiating potential of colon cancer stem cell precursors. Cancer Res 2012; 72:5091-5100.
31. Weng D, *et al.* Metastasis is an early event in mouse mammary carcinomas and is associated with cells bearing stem cell markers. Breast Cancer Res 2012; 14:R18.
32. Chen MS, *et al.* Wnt/beta-catenin mediates radiation resistance of Sca1+ progenitors in an immortalized mammary gland cell line. J Cell Sci 2007; 120:468-477.
33. Xin L, *et al.* The Sca-1 cell surface marker enriches for a prostate-regenerating cell subpopulation that can initiate prostate tumorigenesis. Proc Natl Acad Sci U S A 2005; 102:6942-6947.
34. Batts TD, *et al.* Stem cell antigen-1 (sca-1) regulates mammary tumor development and cell migration. PLoS One 2011; 6:e27841.
35. Upadhyay G, *et al.* Stem cell antigen-1 enhances tumorigenicity by disruption of growth differentiation factor-10 (GDF10)-dependent TGF-beta signaling. Proc Natl Acad Sci U S A 2011; 108:7820-7825.
36. Mulholland DJ, *et al.* Lin-Sca-1+CD49fhigh stem/progenitors are tumor-initiating cells in the Pten-null prostate cancer model. Cancer Res 2009; 69:8555-8562.
37. Grange C, *et al.* Sca-1 identifies the tumor-initiating cells in mammary tumors of BALB-neuT transgenic mice. Neoplasia 2008; 10:1433-1443.
38. Kruger JA, *et al.* Characterization of stem cell-like cancer cells in immune-competent mice. Blood 2006; 108:3906-3912.
39. Eyler CE, Rich JN. Survival of the fittest: cancer stem cells in therapeutic resistance and angiogenesis. J Clin Oncol 2008; 26:2839-2845.
40. Eyler CE, *et al.* Brain cancer stem cells display preferential sensitivity to Akt inhibition. Stem Cells 2008; 26:3027-3036.
41. Wilson WR, Hay MP. Targeting hypoxia in cancer therapy. Nat Rev Cancer 2011; 11:393-410.
42. Govaert KM, *et al.* Effects of tirapazamine on experimental colorectal liver metastases after radiofrequency ablation. Br J Surg 2012; 99:567-575.
43. Mulier S, *et al.* Local recurrence after hepatic radiofrequency coagulation: multivariate meta-analysis and review of contributing factors. Ann Surg 2005; 242:158-171.
44. Wong SL, *et al.* American Society of Clinical Oncology 2009 clinical evidence review on radiofrequency ablation of hepatic metastases from colorectal cancer. J Clin Oncol 2010; 28:493-508.
45. Nanko M, *et al.* Micrometastatic colorectal cancer lesions in the liver. Surg Today 1998; 28:707-713.
46. Yokoyama N, *et al.* Immunohistochemically detected hepatic micrometastases predict a high risk of intrahepatic recurrence after resection of colorectal carcinoma liver metastases. Cancer 2002; 94:1642-1647.
47. Conzelmann M, *et al.* Detection of disseminated tumour cells in the liver of cancer patients. Eur J Surg Oncol 2005; 31:977-985.
48. Heddleston JM, *et al.* Hypoxia inducible factors in cancer stem cells. Br J Cancer 2010; 102:789-795.
49. Visvader JE, *et al.* Cancer stem cells in solid tumours: accumulating evidence and unresolved questions. Nat Rev Cancer 2008; 8:755-768.
50. Harrison LE, *et al.* Locoregional recurrences are frequent after radiofrequency ablation for hepatocellular carcinoma. J Am Coll Surg 2003; 197:759-764.
51. Tezuka M, *et al.* Growth rate of locally recurrent hepatocellular carcinoma after transcatheter arterial chemoembolization: comparing the growth rate of locally recurrent tumor with that of primary hepatocellular carcinoma. Dig Dis Sci 2007; 52:783-788.
52. Kubota K, *et al.* Growth rate of primary single hepatocellular carcinoma: determining optimal screening interval with contrast enhanced computed tomography. Dig Dis Sci 2003; 48:581-586.
53. Rhee TK, *et al.* Effect of transcatheter arterial embolization on levels of hypoxia-inducible factor-1alpha in rabbit VX2 liver tumors. J Vasc Interv Radiol 2007; 18:639-645.
54. Virmani S, *et al.* Comparison of hypoxia-inducible factor-1alpha expression before and after transcatheter arterial embolization in rabbit VX2 liver tumors. J Vasc Interv Radiol 2008; 19:1483-1489.
55. Keith B, Simon MC. Hypoxia-inducible factors, stem cells, and cancer. Cell. 2007;129:465–72.
56. Todaro M, *et al.* Colon cancer stem cells dictate tumor growth and resist cell death by production of interleukin-4. Cell Stem Cell. 2007;1:389–402.

57. Dean M, *et al.* Tumour stem cells and drug resistance. Nat Rev Cancer. 2005;5:275–284.
58. Brown JM. The hypoxic cell: a target for selective cancer therapy—eighteenth Bruce F. Cain Memorial Award lecture. Cancer Res. 1999;59:5863–5870.
59. Wang J, *et al.* Repair of DNA and chromosome breaks in cells exposed to SR 4233 under hypoxia or to ionizing radiation. Cancer Res. 1992;52:4473–4477.
60. Zeman EM, *et al.* SR-4233: a new bioreductive agent with high selective toxicity for hypoxic mammalian cells. Int J Radiat Oncol Biol Phys. 1986;12:1239–1242.
61. Todaro M, *et al.* Colon cancer stem cells dictate tumor growth and resist cell death by production of interleukin-4. Cell Stem Cell. 2007;1:389–402.
62. Dylla SJ, *et al.* Colorectal cancer stem cells are enriched in xenogeneic tumors following chemotherapy. PLoS One. 2008;3:e2428.
63. Zhang J, *et al.* Suppression of hypoxia-inducible factor 1alpha (HIF-1alpha) by tirapazamine is dependent on eIF2alpha phosphorylation rather than the mTORC1/4E-BP1 pathway. PLoS One. 2010;5:e13910.
64. Lencioni R, *et al.* Transcatheter treatment of hepatocellular carcinoma with Doxorubicin-loaded DC Bead (DEBDOX): technical recommendations. Cardiovasc Intervent Radiol. 2012;35:980–985.

8

MASPIN IS A MARKER FOR EARLY RECURRENCE IN PRIMARY STAGE III AND IV COLORECTAL CANCER

Benjamin L Emmink[1*], Nikol Snoeren[1*], Marian J Groot Koerkamp[3], Sander R van Hooff[3], Jeroen ACM Goos[2], Winan J van Houdt[1], Meike de Wit[2], Anne M Prins[1], Sander R Piersma[4], Thang V Pham[4], Eric J Belt[5], Herman Bril[6], Hein B Stockmann[7], Gerrit A Meijer[2], Richard van Hillegersberg[1], Frank C Holstege[3], Connie R Jimenez[4], Remond JA Fijneman[2], Onno Kranenburg[1], Inne HM Borel Rinkes[1]

[1] Department of Surgery, University Medical Centre Utrecht, The Netherlands
[2] Department of Pathology, VU University Medical Centre, The Netherlands
[3] Department of Molecular Cancer Research, University Medical Centre, The Netherlands
[4] OncoProteomics Laboratory, VU University Medical Centre, The Netherlands
[5] Department of Surgery, VU University Medical Centre, The Netherlands
[6] Department of Pathology, Kennemer Gasthuis, The Netherlands
[7] Department of Surgery, Kennemer Gasthuis, The Netherlands

*Equal contribution

ABSTRACT

BACKGROUND: Little is known about the factors that drive metastasis formation in colorectal cancer (CRC). Here we set out to identify genes and proteins in patients with colorectal liver metastases that correlate with early disease recurrence. Such factors may predict a propensity for metastasis in earlier stages of CRC. **METHODS:** Gene expression profiling and proteomics were used to identify differentially expressed genes/proteins in resected liver metastases that recurred within 6 months following liver surgery versus those that did not recur for more than 24 months. Expression of the identified genes/proteins in stage II (n=243) and III (n=176) tumours was analyzed by immunohistochemistry on tissue microarrays. Correlation of protein levels with stage-specific outcome was assessed by uni- and multivariable analyses. **RESULTS:** Both gene expression profiling and proteomics identified Maspin to be differentially expressed in colorectal liver metastases with early (< 6 months) and prolonged (>24 months) time to recurrence. Immunohistochemical analysis of Maspin expression on tumor sections revealed that it was an independent predictor of time to recurrence (log rank p=0.004) and CRC specific survival (p=0.000) in stage III CRC. High Maspin expression was also correlated with mucinous differentiation. In stage II CRC patients high Maspin expression did not correlate with survival but was correlated with a right sided tumour location. **CONCLUSIONS:** High Maspin expression correlates with poor outcome in CRC after spread to the local lymph nodes. Therefore, Maspin may have a stage-specific function possibly related to tumour cell dissemination and/or metastatic outgrowth.

INTRODUCTION

Five-year survival rates in colorectal cancer (CRC) vary dramatically from ~93% in patients with localized stage I tumours to ~6% in patients with metastasized inoperable disease[1]. The decision to administer adjuvant chemotherapy in CRC is predominantly stage dependent. All stage III and high-risk stage II patients are recommended to receive adjuvant treatment. In contrast, patients with stage I and low-risk II disease generally do not receive adjuvant chemotherapy after resection of the primary tumour, since 5-year survival rates are high and there is only minimal benefit in unselected patients[2, 3]. Recently, gene expression profiling has been used to identify high risk stage II patients who can possibly benefit from adjuvant chemotherapy. Two published gene signatures have proven to be able to select stage II cancer patients for adjuvant treatment: The Oncotype DX Colon Cancer Assay (12-genes) and the ColoPrint (18-genes). Both signatures seem to perform better than most conventional risk factors[4-6] and are currently being further validated. The discovery of novel biomarkers for predicting tumour behavior is not only valuable from a prognostic viewpoint, but can also help to gain insight into the mechanisms that cause disease progression and metastasis formation. Differences in tumour cell survival, migration, invasion and extracellular matrix remodeling are all likely to play a role[7].

To turn a locally invasive colorectal tumour into a metastasizing one very few, if any, additional genetic changes are required[8]. It is possible that the factors driving initial metastasis formation from the primary tumour also promote tumour recurrence at later stages of the disease, following surgical removal of liver metastases[9]. After resection of colorectal liver metastases, the vast majority of patients experience tumour recurrence within two years. However, the patients that remain disease-free beyond two years have a good chance of five-year survival without additional therapy[10-13]. This is most likely due to favorable tumour characteristics.

The rationale of this study was to obtain further insight into the mechanisms causing tumour progression and metastases formation. Gene expression profiling and proteomics were used to detect differences between stage IV CRC patients that recur within 6 months after resection, versus those that fail to recur for more than two years. Subsequently, we analyzed whether expression of the identified factors also predicts metastasis formation in early stages of CRC.

METHODS

Patients and samples

Microarray and mass-spectrometry analysis

Biopsies of thirty liver metastases were used to identify genes and proteins correlating with early recurrence in stage IV CRC patients. Patient, tumour and surgical characteristics, were derived from our prospectively collected database. Thirty frozen tumour biopsies were collected between July 2003 and august 2008 at the University Medical Centre in Utrecht, the Netherlands (Dataset 1) (figure 1). Samples were included if patients were aged 18 years or older and received curative resection for histologically confirmed liver metastases from CRC. Patients with a history of non-colorectal malignancies, extra hepatic disease or microscopic residual disease (R1) after surgery and patients who received local ablation therapy or chemoembolization alone or in combination with resection were excluded. Only specimens were included that were snap frozen in liquid nitrogen within 30 minutes after resection and were stored at -80°C. The study protocol was approved by The Medical Ethical Committee (MEC) of the University Medical Center Utrecht as

recognized by article 16 of the WMO (Dutch Law on Medical Research with human subjects). Written informed consent was obtained from all patients in datataset 1.

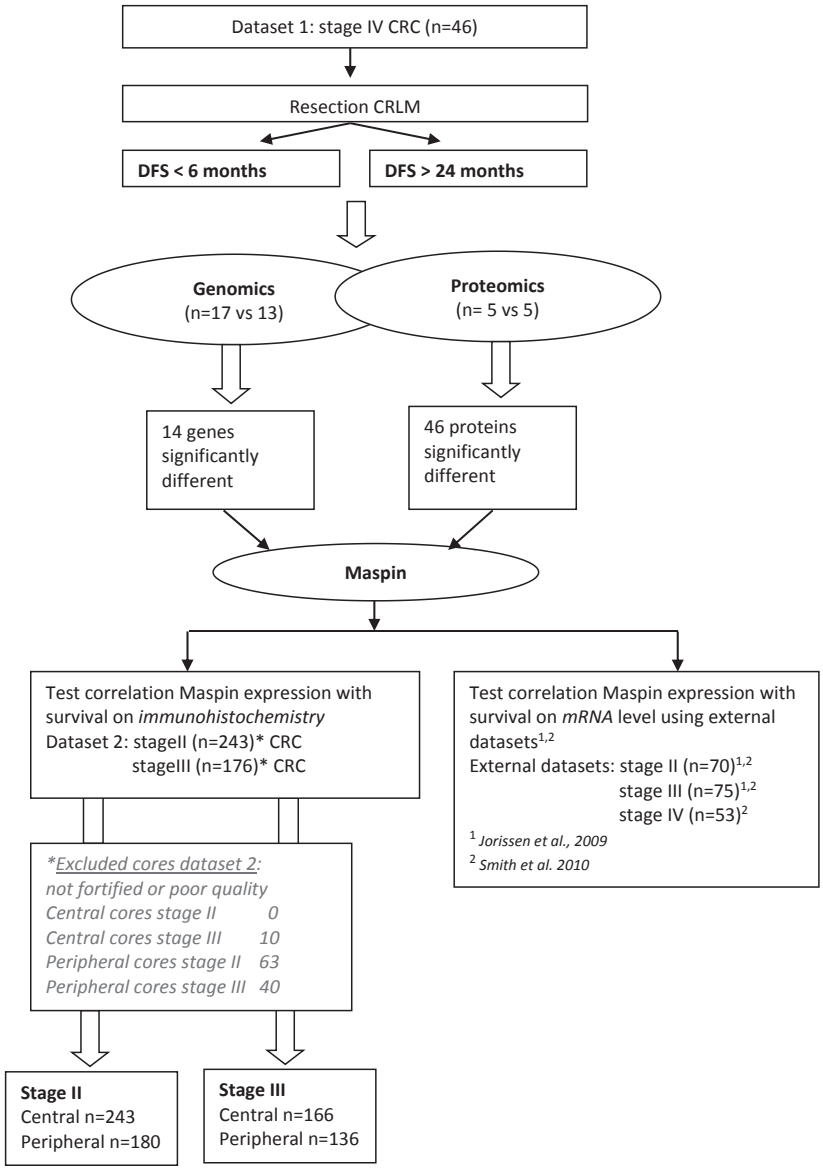

Figure 1. Study workflow

Tissue microarray study

Between 1996 and 2005, 419 patients underwent surgical colon cancer resection at the Kennemer Gasthuis Hospital in Haarlem, The Netherlands, that were classified as stage II (T_{3-4}, N_0, M_0) or stage III (T_{1-4}, N_{1-2}, M_0) according to the 4th edition of the TNM-classification system (Dataset 2) (figure 1). These tumour samples were used to examine any stage-specific role of the biomarkers

retrieved from dataset 1. Patient, tumour and surgical characteristics, were retrospectively drafted from clinical and pathology reports. Collection, storage and use of tissue and patient data were performed in agreement with the 'Code for Proper Secondary Use of Human Tissue in The Netherlands' (Code for Proper Secondary Use of Human Tissue in The Netherlands. Available from: http://www.federa.org/codes-conduct)[14].

Gene expression profiling

RNA isolation, labeling, and hybridization to whole-genome oligonucleotide high-density microarrays were performed as previously described[15]. In short, two expression profiles in dye-swap experiments were generated for each sample. The samples were compared against a commercial reference (Universal Human Reference RNA catalog #740000, Stratagene). The Human Array-Ready Oligo set (version 2.0) was purchased from Qiagen and spotted on Codelink slides (GE Healthcare) in a dust filtered and humidity controlled clean room. The microarrays contained 70-mer oligo-nucleotides representing 21.329 human genes and expressed sequence tags (ESTs), as well as 3871 additional spots for control purposes.We applied total RNA and cRNA quality control criteria in accordance with the Tumour Analysis Best Practices Working Group[16]. Gene expression in metastases showing recurrence within six months after resection was compared to metastases that did not show recurrence for more than two years by using ANOVA[17]. In a fixed effect analysis, sample, array and dye effects were modelled. P-values were determined by a permutation F2-test in which residuals were shuffled 5000 times globally. Genes with $p<0.05$ after family wise error correction were considered significant.

Mass-spectrometry analysis

Tissue homogenization

Frozen tumour tissue sections of five stage IV patients with short time to recurrence (<6 months) and five patients with prolonged time to recurrence (> 24 months) were used for mass-spectrometry analysis. All patients were selected from dataset 1. The frozen tumour tissue sections were cut into pieces of approximately 20 mg, after which they were solubilized in 800µl SDS sample buffer (containing 62.5 mm Tris-HCl, 2% w/v SDS, 10% v/v glycerol, and 0.0025% bromphenol blue, 100 mm DTT, pH 6.8) using a micro grinder. Denaturation was done by heating samples for 10 min at 100°C. All remaining insoluble parts were removed by centrifugation (15 min; 14.000 rpm).

Fractionation Using Gel Electrophoresis

Equal amounts of protein (50 µg) were separated on NuPAGE Novex Bis-Tris Mini Gels (Invitrogen). Gels were stained with Coomassie brilliant blue G-250 (Pierce, Rockford, IL), washed and each lane was sliced into ten bands using a band pattern to guide the slicing. The gel slicing and in-gel digestion was performed in a laminar flow under keratin-free conditions.

In-gel Digestion, NanoLC-MS/MS Analysis

In-gel digestion and NanoLC-MS/MS analysis was performed as described in van Houdt et al. (van Houdt et al., 2011))

Protein identification

MS/MS spectra were searched against IPI human 3.62 (83947 entries) using Sequest version 27, rev 12 (Thermo, San Jose, CA, USA). Cysteine carboxamidomethylation and methionine oxidation were treated as variable modifications. Peptides precursor ions were searched with a maximum

mass deviation of 10 ppm and fragment ions with a maximum mass deviation of 1 Da. Sequest output files were imported in Scaffold 2.06.1 (Proteome software, Portland, OR)and search results of the ten gel bands per biological sample were combined. A protein was considered identified when at least 2 unique peptides were identified in one of the samples. Peptides were identified with a PeptideProphet[18] probability score >95% and a ProteinProphet[19] probability score >99%. Proteins were (label-free) quantified by spectral counting[20, 21] i.e. the sum of all MS/MS spectra for each identified protein. For each biological sample the spectral counts for each protein were normalised on the sum of the counts for that sample and multiplied by the average of the sums across samples. Subsequently, the beta-binominal test was applied to detect significantly differential proteins between early and late recurrence samples.

Tissue Microarray Construction

Tissue Microarrays (TMAs) were constructed from stage II and III colon cancer samples as described previously[14, 22]. In summary, formalin fixed, paraffin embedded specimens of resected colon cancer tumours were used as donor blocks. Three 0.6-mm cores were taken from the centre of the tumour and three cores from the periphery of the tumour and transferred into recipient TMA paraffin blocks, resulting in six cores per tumour. The maximum amount of samples that were transferred to an single TMA was 264.

Immunohistochemistry

Formalin-fixed paraffin-embedded cores were deparaffinized with xylene and rehydrated in decreasing ethanol dilutions. Endogenous peroxidase activity was blocked with 3% hydrogen peroxide. Antigen retrieval was achieved by boiling slides in citrate buffer (pH6) for 20 minutes. Slides were then incubated (overnight 4°C) with the monoclonal anti-Maspin antibody (clone G167-70; Pharmingen, San Jose, CA, USA) at a 1:1000 dilution. For detection, goat anti mouse poly-HRP (Powervision, Immunologic, Immunovision Technologies, Brisbane, USA) was used. All slides were developed with diaminobenzidine (DAB). Slides were counterstained with filtered hematoxylin, dehydrated through a graded series of ethanol's, immersed in xylene and mounted.

Immunoreactivity for Maspin was assessed and scored by two independent investigators being blinded to clinical, pathological- or survival data. The presence of nuclear and cytoplasmic staining in the tumour cells was assessed separately in each sample and divided into high and low scores. The immunohistochemistry scoring system used is based on scoring systems used in previous studies[23, 24]. A combination of intensity (negative, 1+, 2+ or 3+) and percentage of stained cells was used to score each core biopsy. Intensity score of 2+ in more than 50% of cells or 3+ in more than 10% of cells, was considered high (figure 4). In case of discrepancies between the scoring by the two investigators, the slides were reviewed and a consensus was reached. For analytical purposes protein expression was divided into high and low scores combining cytoplasmic and nuclear scores (see table 4).

Western blotting

The homogenized tumour tissue from all five patients with short time to recurrence (< 6 months), which was used for mass-spec analysis, was used for western blot validation. Equal amounts of protein was run out on NuPAGE Novex Tris-Acetate Mini Gel (Invitrogen) and was analyzed by Western blotting using primary antibodies directed against Maspin (clone G167-70; Pharmingen, San Jose, CA, USA) and β-Actin (AC-15, Novus Biologicals, Littleton, CO) in combination with secondary antibody peroxidase-conjugated anti-mouse IgG (Dako, Glostrup, Denmark). For

detection of antibodies Amersham ECL Western Blotting Detection Reagent was used (GE Healthcare Life Sciences)

Follow-up and survival

All patients were subjected to routine follow-up. The follow-up data were updated by letters and telephone calls to referring physicians and general practitioners. The duration of the follow-up and the time between surgery and the detection of recurrence were obtained as well colorectal cancer specific survival.

Statistical analysis

Time to recurrence and colorectal cancer specific survival (CRC-specific survival) data were calculated from the day of surgery to the day of the first recurrence or the day of death caused by colorectal cancer. Median time to recurrence and CRC –specific survival were estimated by the Kaplan-Meier method. To determine the influence of possible risk factors on time to recurrence and CRC-specific survival a univariable cox regression analysis was performed. A multivariable cox proportional hazards model, containing the factors that displayed p-values less than 0.2 in univariable analysis, was used to determine the independent prognostic impact of all variables on time to recurrence and CRC-specific survival. Statistical significance was assumed for *p*-values less than 0.05. Statistical analyses were performed using SPSS for Windows version 15.0 (SPSS, Chicago, IL, USA).

RESULTS

Gene expression profiling identifies Maspin as a marker for recurrence in stage IV CRC

Forty-six patients from dataset 1 fulfilled the inclusion- and quality control criteria. To identify genes that are differentially expressed, patients with metastases showing early (< 6 months, n=17) and prolonged (> 24 months, n=13) time to recurrence were selected (table 1). Gene expression profiling of these 30 tumours revealed that fourteen genes were significantly differentially expressed between the two groups: *SERPINB5, THEM2, GDF15, LYPLA1, AMPD1, ARL6IP5, LAPTM4A, C13ORF3, COLEC11, FYTTD1, BNIP3, SMYD2, GTF3c3, ASAP2*. Of these genes 11 were up-regulated in the group with time to recurrence shorter than 6 months (table 2). SERPINB5, also known as Maspin, was the gene most up-regulated in patients with a short time to recurrence. Maspin expression was ~2.1 times higher in tumours of patients with a short time to recurrence *versus* tumours in patients with a prolonged time to recurrence (figure 2A; p=0.01).

The Kaplan-Meier survival curves of all 46 patients from dataset 1 (including the 30 patients used for gene expression profiling) (figure 2B) show that the 2 year recurrence-free survival probability of patients with Maspin-high tumours (> median (168,6)) is an estimated 0.10 (95% CI = 0.00-0.20) compared to 0.39 (95% CI = 0.18-0.60) in patients with Maspin-low tumors (< median (168,6) (cox regression analysis p=0.007 HR=2.65 95%CI=1.307-5.380). Multivariable analysis shows that Maspin is an independent predictor of early recurrence (p=0.02, HR=2.971, 95% CI=1.168- 7558) in our training set. Adjuvant treatment was the only other independent predictor of early recurrence in multivariable analysis (p=0.05, HR=0.329, 95%CI=0.109-0.994) (supplemental table 1).

This result was validated using an independent microarray dataset from a cohort of 53 patients with stage IV primary colorectal cancer[25, 26]. Two Kaplan-Meier graphs, generated by

the R2 microarray analysis and visualization platform (http//r2.amc.nl) show that high levels (>median(259,6)) of Maspin are significantly correlated with disease specific- (figure 2C; p=0.005) and overall survival (figure 2D; p=0.029) in primary stage IV CRC patients.

Table 1. Clinical and pathological characteristics of patients included in micro-array analysis

Variable	Characteristics	DFS < 6 months n=17	DFS > 24 months n=13	p-value
Sex				
	Male	10 (58.8%)	7 (53.8%)	0.785
	Female	7 (41.2%)	6 (46.2%)	
Age (years)				
	(Mean; Median; SD)	62.24; 65.00; 14.70	63.84; 64.00; 8.09	0.715
Tumor location primary				
	Right sided	5 (29.4%)	6 (46.2%)	0.636
	Left sided	6 (35.5%)	3 (23.1%)	
	Rectum	6 (35.5%)	4 (30.8%)	
Histological grade				
	Well	3 (17.6%)		
	Moderate	12 (70.6%)	12 (92.3%)	0.714
	Poor	2 (11.8%)	1 (7.7%)	
	Unknown			
Nodal stage				
	N0	8 (47.1%)	7 (53.8%)	0.713
	N1	9 (52.9%)	6 (46.2%)	
	Unknown			
Interval between primary and LM				
	Synchronous	8 (47.1%)	3 (23.1%)	0.184
	Metachronous	9 (52.9%)	10 (76.9%)	
Neoadjuvant chemotherapy				
	Yes	5 (29.4%)	2 (15.4%)	0.375
	No	12 (70.6%)	11 (84.6%)	
Adjuvant chemotherapy				
	Yes	16 (94.1%)	6 (53.8%)	**0.025***
	No	1 (5.9%)	7 (46.2%)	
Nr of metastases				
	(Mean; Median; SD)	2.41; 2.00; 1.77	1.54; 1.00; 0.88	0.131
Size liver metastases				
	(Mean; Median; SD)	5.18; 4.21; 3.37	4.25; 3.70; 2.52	0.408
Preoperative CEA				
	(Mean; Median; SD)	111.46; 54.28; 134.77	37.26; 33.30; 30.81	0.125

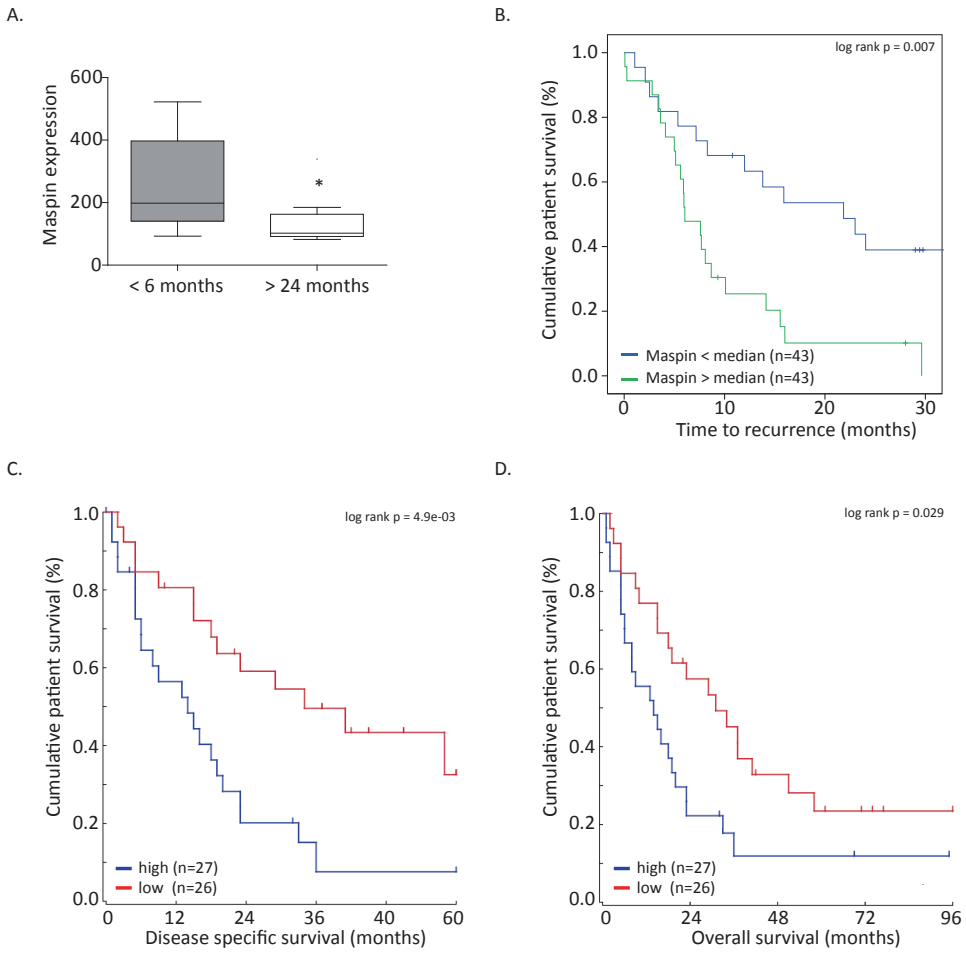

Figure 2. Microarray analysis of patients with short and prolonged time to recurrence identifies Maspin to be differentially expressed in stage IV CRC.

A – Median expression levels of Maspin in the early (<6 months, n=17) and prolonged (>24 months, n=13) time to recurrence groups (p=0.012).

B – Kaplan-Meier curves, of 46 patients in dataset 1, illustrating time to recurrence in stage IV CRC liver metastasis patients with high Maspin expression (> median) and low Maspin expression (< median) (p=0.005, log rank test). Median Maspin expression was used as a cut-off (168.6)

C – Kaplan-Meier curves illustrating time to recurrence in primary stage IV CRC patients with high Maspin expression (> median, n=27) and low Maspin expression (< median, n=26) using a previosuly published dataset (Smith et al., 2010)(p=0.005). Median Maspin expression was used as the cut-off value (259.6).

D – Kaplan-Meier curves illustrating overall survival in 53 primary stage IV CRC patients with high Maspin expression (> median) and low Maspin expression (< median) using Smith et al., 2010)(p=0.029). Median Maspin expression was used as the cut-off value (259.6).

Table 2. Differentially expressed genes found by micro-array analysis in early (<6 months) versus late (>24 months) recurrence groups.

Up-regulated genes in early recurrence group			
Gene	Description	Fold change	p-value
SERPINB5	Serpin B5	2.1	**0.0118**
COLEC11	Collectin-11 Precursor	1.4	0.0018
LAPTM4A	Lysosomal-associated transmembrane protein 4A	1.3	0.0000
C13orf3	Spindle and kinetochore-associated protein RAMA1	1.3	0.0016
LYPLAL1	Lysophospholipase-like protein 1	1.3	0.0000
GTF3C3	General transcription factor 3C polypeptide 3	1.3	0.0204
AMPD1	AMP deaminase 1	1.3	0.0000
ARL6IP5	PRA1 family protein 3	1.3	0.0000
SMYD2	SET and MYND domain-containing protein 2	1.2	0.0118
ASAP2	Arf-GAP with SH3 domain, ANK repeat and PH domain-containing protein 2	1.2	0.0356
FYTTD1	Forty-two-three domain-containing protein 1	1.2	0.0026
Down-regulated genes in early recurrence group			
Gene	Description	Fold change	p-value
THEM2	Thioesterase superfamily member 2	0.8	0.0000
BNIP3	BCL2/adenovirus E1B 19 kDa protein-interacting protein 3	0.7	0.0096
GDF15	Growth/differentiation factor 15 Precursor	0.6	0.0000

Mass-spectrometry analysis confirms Maspin as marker for early recurrence in stage IV CRC

In parallel to gene expression profiling we also analysed differentially expressed proteins in patients, from dataset 1, showing early (< 6 months) and prolonged (> 24 months) time to recurrence. To this end, mass-spectrometry analysis was performed on five tumours from each group (supplemental table 2). Protein-containing lysates of these tumour tissue samples were fractionated on an SDS-PAGE gel, followed by in-gel tryptic digestion (figure 3A). Analysis of the extracted peptides was performed by Nano-LC-MS/MS, followed by database searching. In total, 2097 unique proteins were identified in all patient samples. Forty-six proteins were present in significantly different amounts in the two groups, of which 26 were overrepresented and 20 were underrepresented in the tumours of patients with early recurrence (table 3). The sets of 14 genes and 46 proteins that showed a significant association with short or prolonged recurrence times contained only 1 overlapping factor: Maspin (figure 3B). Validation of the mass-spectrometry results by western blotting showed that the number of spectral counts detected by mass-spec analysis correlates very well with Maspin protein levels (figure 3C). These results demonstrate that Maspin is differentially expressed on both mRNA and protein level in stage IV CRC patients with early and late recurrence.

Table 3. Differentially expressed proteins (p<0,05) found by mass-spectrometry analysis in early (<6 months) versus late recurrence (>24 months) groups.

Up-regulated proteins in early recurrence group			
Protein	Description	Fold change	p-value
SERPINB5	Serpin peptidase inhibitor, clade B (ovalbumin), member 5	∞	0,01
RNASET2	Ribonuclease T2	∞	0,01
ICAM1	Intercellular adhesion molecule 1	∞	0,02
EIF2B1	Eukaryotic translation initiation factor 2B, subunit 1 alpha, 26kDa	∞	0,02
TPSAB1	Tryptase alpha/beta 1	∞	0,02
SF3A3	Splicing factor 3a, subunit 3, 60kDa	∞	0,05
OLFM4	Olfactomedin 4	31,9	0,05
IGFALS	Insulin-like growth factor binding protein, acid labile subunit	8,8	0,02
PTK7	PTK7 protein tyrosine kinase 7	8,3	0,02
LANCL1	LanC lantibiotic synthetase component C-like 1 (bacterial)	7,8	0,01
API5	Apoptosis inhibitor 5	5,8	0,05
XPOT	Exportin, tRNA (nuclear export receptor for tRNAs)	5,8	0,05
USP7	Ubiquitin specific peptidase 7 (herpes virus-associated)	5,3	0,04
ACSL3	Acyl-CoA synthetase long-chain family member 3	4,4	0,01
NUP155	Nucleoporin 155kDa	4	0,01
CLIC4	Chloride intracellular channel 4	3,9	0,01
KRT6B	Keratin 6B	3,6	0,04
MYL9	Myosin, light chain 9, regulatory	3,3	0,03
VARS	Valyl-tRNA synthetase	3,2	0
CYFIP1	Cytoplasmic FMR1 interacting protein 1	3,1	0,03
SYNE2	Spectrin repeat containing, nuclear envelope 2	2,8	0,05
NUDT21	Nudix (nucleoside diphosphate linked moiety X)-type motif 21	2,6	0,05
CKAP4	Cytoskeleton-associated protein 4	2,3	0,02
VIL1	Villin 1	2,2	0,04
HSD17B12	Hydroxysteroid (17-beta) dehydrogenase 12	2	0,05
YWHAQ	Tyrosine 3-monooxygenase	2	0,04
Down-regulated proteins in early recurrence group			
Protein		Fold change	p-value
PTTG1IP	Pituitary tumor-transforming 1 interacting protein	∞	0,011
DUT	Deoxyuridine triphosphatase	∞	0,013
CASP1	Caspase 1, apoptosis-related cysteine peptidase	∞	0,018
HSD17B4	Hydroxysteroid (17-beta) dehydrogenase 4	∞	0,024
VWF	von Willebrand factor	∞	0,024
RBM14	RNA binding motif protein 14	∞	0,026
LACTB2	lactamase, beta 2	∞	0,028
AMBP	Alpha-1-microglobulin/bikunin precursor	∞	0,042
ANKRD22	Ankyrin repeat domain 22	∞	0,046
ADCK3	AarF domain containing kinase 3	13,8	0,001
GYG1	Glycogenin 1	9,0	0,003
AKR1C3	Aldo-keto reductase family 1, member C3	6,2	0,053
PTGES2	Prostaglandin E synthase 2	5,4	0,053
SCCPDH	Saccharopine dehydrogenase (putative)	2,8	0,007
MRPL14	Mitochondrial ribosomal protein L14	2,7	0,011
CUL4A	Cullin 4A	2,7	0,051
SDCBP	Syndecan binding protein (syntenin)	2,6	0,029
CAST	Calpastatin	2,1	0,019
MCCC2	Methylcrotonoyl-CoA carboxylase 2 (beta)	1,9	0,004
HMCN1	Hemicentin 1	1,7	0,027

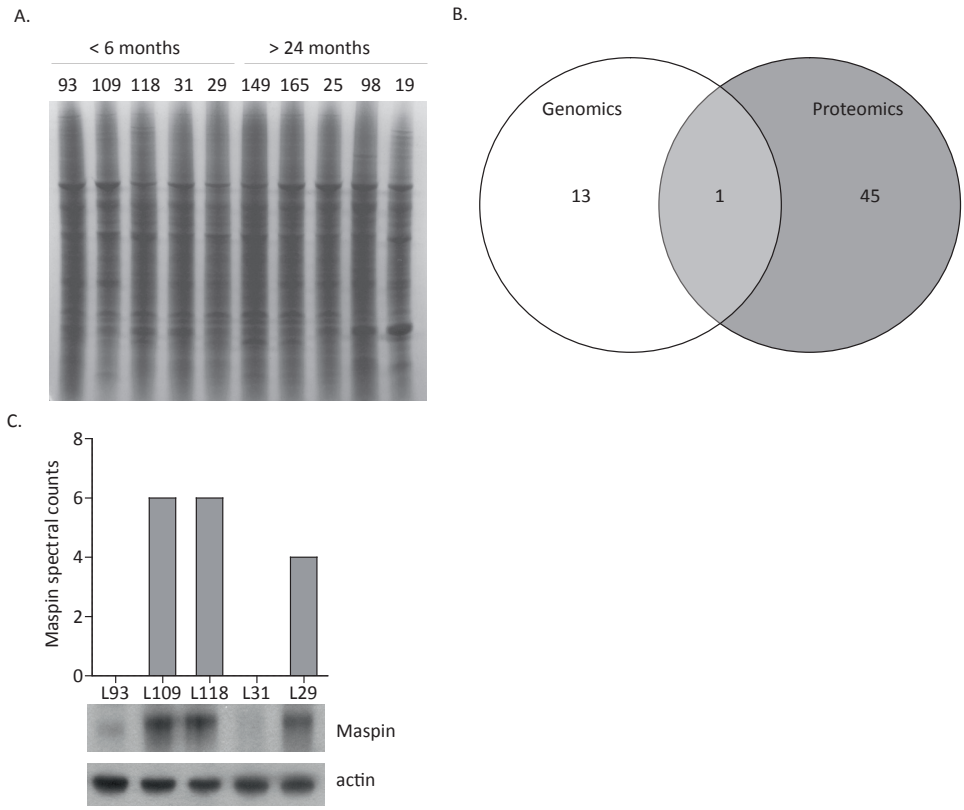

Figure 3. Mass-spectrometry based analysis of proteome differences between patients with early and prolonged time to recurrence in stage IV CRC.

A – Coomassie-stained protein gradient gel loaded with protein samples from tumours form patients with short (< 6 months) and prolonged (>24 months) time to recurrence. This gel was used for mass-spectrometry analysis.

B – Venn diagram showing overlap between differently expressed genes and proteins found by micro-array and mass-spectrometry analysis.

C – Western blot analysis of Maspin levels in patients with early time to recurrence (< 6 months) and the corresponding amount of spectral counts detected by mass-spectrometry analysis.

Tissue micro array analysis reveals that Maspin staining in the tumour centre is a stage specific marker in CRC

The above results indicate that Maspin could be a prognostic marker for early recurrence in stage IV CRC patients. This prompted us to assess whether this marker had a similar prognostic power in stage II and III CRC patients. To this end a total of 243 stage II and 166 stage III tumours on tissue microarrays containing FFPE tissue cores were stained with specific monoclonal Maspin antibody[23, 24, 27]. The presence of nuclear and cytoplasmic staining in both central tumour cores and peripheral tumour cores was assessed in each sample and divided in high and low scores. A high score was defined as an intensity score of 2+ in more than 50% of cells or 3+ in more than 10% of cells (table 4, figure 4).

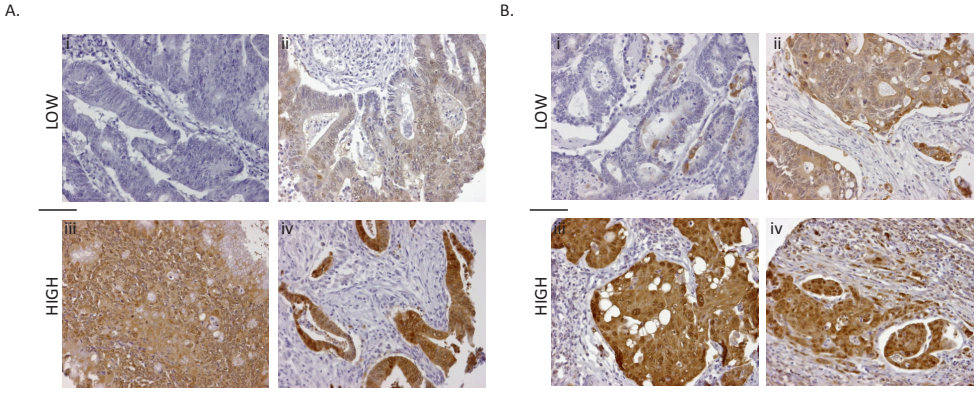

Figure 4. Representative immunohistochemical Maspin staining in colorectal cancer specimens.
A – Cytoplasmic immunoreactivity with Maspin. Upper panel representing low scores: negative (i) intensity 1+ in > 50% of cells (ii). Lower panel representing high scores: intensity 2+ (iii) and 3+ (iv) in > 50% of cells. B – Nuclear immunoreactivity of Maspin. Upper panel representing low scores: intensity 2+ in < 50% of cells (i/ii). Lower panel representing high scores: intensity 3+ in > 10% of cells (iii/iv).

Table 4. Immunohistochemical evaluation of nuclear and cytoplasmic staining in central and peripheral tumour cores.

Score	Intensity	Percentage of cells staining
High	3+	>10%
	2+	>50%
Low	3+	<10%
	2+	<50%
	1+	all
	negative	

Combined scoring groups		
Cytoplasmic **low**	AND	Nuclear **low**
Cytoplasmic **low**	AND	Nuclear **high**
Cytoplasmic **high**	AND	Nuclear **low**
Cytoplasmic **high**	AND	Nuclear **high**

In stage II CRC tumours (n=243), Maspin staining in the central tumour cores showed no significant differences in time-to-recurrence and CRC-specific survival times (table 5). Kaplan Meier curves of Maspin are depicted in figure 5 A, B. High Maspin expression was found to be correlated with a right-sided tumour location (p=0.001) (supplemental table 3).

In stage III CRC patients (n=166) Maspin staining in the central tumour cores was an independent predictor of time to recurrence and CRC-specific survival (table 6, figure 5 C,D). Patients with combined low cytoplasmic and nuclear staining score had estimated 2 year recurrence-free and CRC-specific survival probabilities of 0.74 (95% CI = 0.64-0.84) and 0.83 (0.74-0.92; log rank p= 0.011) respectively. Patients with a combined high cytoplasmic and nuclear score did markedly worse with estimated 2 year recurrence free and CRC specific survival probabilities of 0.42 (95% CI = 0.25-0.59) and 0.55 (0.38-0.72; log rank p=0.000) respectively. The low cytoplasmic and high nuclear group was left out of the analysis due to the low number of tumours in this group (n=4 in stage II, n=2 in stage III)

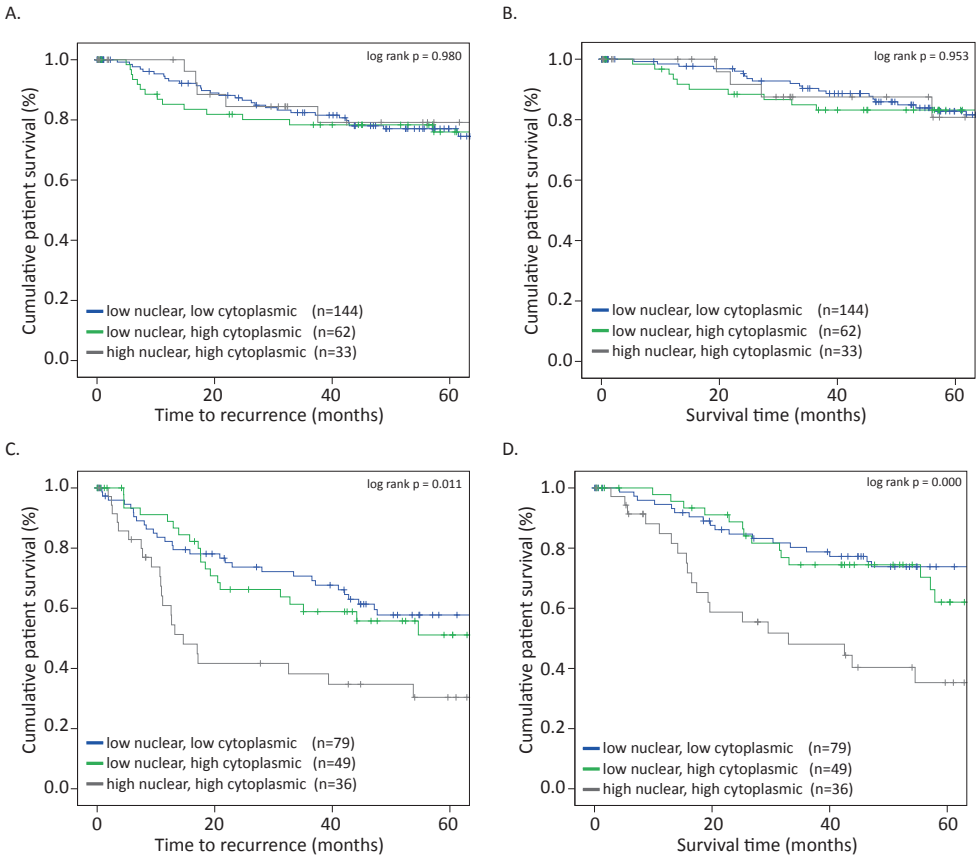

Figure 5. In stage III CRC high Maspin expression in central cores is correlated with early time to recurrence and colorectal specific death.

A – Kaplan-Meier curves illustrating the effects of different Maspin expression levels on time to recurrence in stage II CRC patients (p=0.98, log-rank test).

B – Kaplan-Meier curves illustrating the effect of different Maspin expression levels on colorectal specific survival in stage II CRC patients (p=0.95, log-rank test)

C – Kaplan-Meier curves illustrating the effects of different Maspin expression levels on time to recurrence in stage III CRC patients (p=0.011, log rank test).

D – Kaplan-Meier curves illustrating the effect of different Maspin expression levels on colorectal specific survival in stage III CRC patients (p=0.000, log-rank test)

*The low cytoplasmic and high nuclear group were left out of the analysis due to the low number of tumours in this group (n=4 in stage II, n=2 in stage III).

Table 5. Uni- and multivariate analysis of factors influencing disease-free survival in stage II CRC patients

Univariate analysis						
	Disease free survival			**Colorectal specific survival**		
Variable	**Hazard ratio**	**95%CI**	**p-value**	**Hazard ratio**	**95%CI**	**p-value**
Sex	0.854	0.498-1.464	0.566	0.803	0.434-1.484	0.483
Age (years)	1.008	0.984-1.032	0.535	1.021	0.991-1.051	0.169
Tumour size (mm)	0.990	0.975-1.006	0.215	0.996	0.979-1.013	0.605
Tumour location *(rightsided/left sided/rectum*	1.456	0.830-2.553	0.190	1.271	0.678-2.380	0.455
Nodal stage *(N0/N1/N2)*	n.a.			n.a.		
No. of lymph nodes retrieved	0.960	0.907-1.015	0.152	0.970	0.911-1.033	0.343
Histological grade *(well/moderate/poor)*	1.925	1.056-3.511	**0.033***	1.820	0.923-3.591	0.084
Mucinous differentiation *(present/absent)*	1.152	0.616-2.155	0.657	1.243	0.623-2.481	0.537
Ulceration *(present/absent)*	1.003	0.536-1.876	0.992	0.998	0.489-2.036	0.995
Angioinvasion *(present/absent)*	2.301	1.156-4.581	**0.018***	2.322	1.072-5.028	**0.033***
Adjuvant chemotherapy *(yes/no)*	1.289	0.943-1.762	0.112	1.259	0.869-1.768	0.184
Microsatelite stability status *(MSS/MSI)*	0.685	0.458-1.025	0.066	0.791	0.514-1.215	0.284
Central tumour cores						
Maspin staining						
Low nuclear, low cytoplasmic	1.015	0.733-1.405	0.930	0.937	0.639-1.375	0.740
Low nuclear, high cytoplasmic high nuclear, high cytoplasmic	0.792	0.282-2.224	0.658	0.999	0.307-3.255	0.999
Peripheral tumour cores						
Maspin staining						
Low nuclear, low cytoplasmic	0.987	0.694-1.404	0.943	0.717	0.440-1.168	0.201
Low nuclear, high cytoplasmic high nuclear, high cytoplasmic	1.291	0.359-4.643	0.696	2.074	0.396-10.859	**0.388**
Multivariable analysis						
	Disease free survival			**Colorectal specific survival**		
Variable	**Hazard ratio**	**95%CI**	**p-value**	**Hazard ratio**	**95%CI**	**p-value**
Histological grade	2.028	1.097-3.749	**0.024**	2.149	0.998-5.043	0.060
Angioinvasion	2.338	1.153-4.743	**0.019**	2.497	1.150-5.421	**0.021**
MMS-MSI	0.806	0.533-1.220	0.308			
Tumour location	1.146	0.636-2.064	0.650			
No. of lymph nodes retrieved	0.966	0.913-1.022	0.228			
Adjuvant chemotherapy	1.229	0.901-1.676	0.193	1.265	0.878-1.824	0.208
Age				1.021	0.989-1.053	0.201

Table 6. Uni- and multivariate analysis of factors influencing disease-free survival in stage III CRC patients

Univariate analysis						
	Disease free survival			**Colorectal specific survival**		
Variable	**Hazard ratio**	**95%CI**	**p-value**	**Hazard ratio**	**95%CI**	**p-value**
Sex	1.054	0.665-1.671	0.821	1.418	0.854-2.354	0.177
Age (years)	0.999	0.979-1.018	0.890	1.011	0.988-1.035	0.366
Tumor size (mm)	1.015	1.002-1.029	**0.021***	1.015	1.000-1.031	**0.048***
Tumor location *(rightsided/left sided/rectum)*	0.808	0.512-1.275	0.360	0.691	0.416-1.148	0.153
Nodal stage *(N0/N1/N2)*	2.110	1.328-3.353	**0.002***	2.262	1.355-3.777	**0.002***
No. of lymph nodes retrieved	0.989	0.942-1.038	0.651	0.992	0.940-1.047	0.765
Histological grade *(well/moderate/poor)*	0.673	0.412-1.099	0.113	0.643	0.367-1.127	0.123
Mucinous differentiation *(present/absent)*	1.093	0.628-1.902	0.752	1.131	0.612-2.092	0.694
Ulceration *(present/absent)*	0.807	0.463-1.404	0.447	0.560	0.320-1.007	0.053
Angioinvasion *(present/absent)*	3.226	2.029-5.130	**0.000***	3.107	1.860-5.189	**0.000***
Adjuvant chemotherapy *(yes/no)*	1.127	0.914-1.390	0.264	0.950	0.739-1.221	0.689
Microsatelite stability status *(MSS/MSI)*	1.025	0.713-1.472	0.895	0.365	0.523-1.269	0.365
Central tumour cores						
Maspin staining						
Low nuclear, low cytoplasmic	1.088	0.814-1.454	0.568	1.175	0.841-1.641	0.344
Low nuclear, high cytoplasmic high nuclear, high cytoplasmic	2.150	1.159-3.987	**0.009***	2.541	1.297-4.977	**0.007***
Peripheral tumour cores						
Maspin staining						
Low nuclear, low cytoplasmic	0.869	0.653-1.156	0.334	1.013	0.730-1.405	0.940
Low nuclear, high cytoplasmic high nuclear, high cytoplasmic	1.754	0.822-3.742	0.146	2.074	0.909-4.732	0.083
Multivariable analysis						
	Disease free survival			**Colorectal specific survival**		
	Hazard ratio	**95%CI**	**p-value**	**Hazard ratio**	**95%CI**	**p-value**
Diameter	1.014	1.001-1.027	**0.038**			
Angioinvasion	2.973	1.792-4.932	**0.000**	2.733	1.548-4.826	**0.001**
Combined Maspin staining (central tumor cores)	1.415	1.044-1.919	**0.025**	1.534	1.176-2.350	**0.005**
Histological grade	0.963	0.545-1.701	0.897	0.971	0.541-1.742	0.920
Tumor location				0.676	0.388-1.178	0.167
Nodal stage				1.525	0.843-2.758	0.163
Sex				1.165	0.662-2.051	0.597
Ulceration				0.571	0.305-1.068	0.079
Adjuvant				1.066	0.801-1.419	0.661

High Maspin expression in the central tumour cores was also associated with poor histological grade, mucinous differentiation and MSI-high status in stage III CRC patients (supplemental table 4). In multivariable analysis mucinous differentiation was the only independent factor associated with high Maspin expression.

Maspin staining in peripheral cores showed no correlation with time to recurrence or CRC-specific survival in stage II patients or stage III patients (table 5 and 6). The low cytoplasmic and high nuclear group was left out of the analysis due to the low number of tumours in this group (n=4 in stage II and n=2 in stage III)

We next validated these results using the microarray data from a cohort of 75 patients with stage II CRC and 78 patients with stage III CRC[25, 26]. Kaplan-Meier graphs, generated by the R2 microarray analysis and visualization platform (http//r2.amc.nl) show that high levels of Maspin (>median 486.2) are significantly (p=0.02) correlated with early recurrence in stage III but not in stage II CRC patients (figure 6).

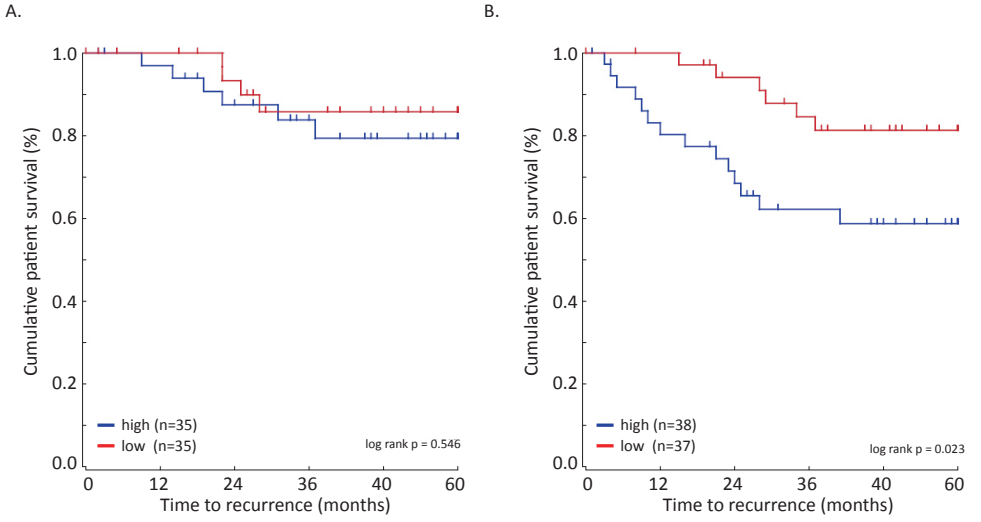

Figure 6. External validation, using the *SieberSmith* database, confirms that Maspin is a stage dependent prognostic marker.

A – Kaplan-Meier curves illustrating that high (> median) and low (< median) Maspin expression have no significant effect on time to recurrence in stage II CRC patients (n=70) (p=0.5). Median Maspin expression was used as the cut-off value (426.3).[25, 26]

B – Kaplan-Meier curves illustrating that stage III CRC patients (n=75) with high (> median) Maspin expression have significant shorter time to recurrence than patients with low (< median) Maspin expression (p=0.02). Median Maspin expression used as the cut-off value (486.2).[25, 26]

DISCUSSION

In this report we identified Maspin as a marker for early recurrence after surgery for colorectal liver metastases. Maspin is an prognostic factor for early recurrence in stage III and IV CRC patients, but not in stage II patients. Maspin is a member of the serine protease inhibitor (serpin) family. In breast cancer, Maspin acts as a tumour suppressor by inhibiting tumour cell motility, invasion and tumour growth[28]. In breast, ovarian and lung cancer Maspin expression is correlated with a relatively good prognosis[29, 30]. By contrast, studies in lung, breast, gastric and pancreatic cancer show that Maspin expression is associated with more aggressive disease[31-34]. The reasons for these discrepancies are presently unknown.

Mixed stage studies in CRC have failed to reach consensus whether Maspin is associated with good or poor prognosis[23, 35, 36]. A study in patients with only stage III disease has shown that high nuclear Maspin is significantly correlated with poor overall survival[24], which is in line with the results presented in this report. We used a combined nuclear and cytoplasmic expression score. The group with high cytoplasmic and high nuclear staining is associated with early recurrence. By contrast, the groups with low nuclear and either high or low cytoplasmic staining are associated with late recurrence. This suggests that high nuclear Maspin staining is the major variable determining the association with early recurrence. This is in line with earlier reports[24, 35]. In contrast to the results presented here, a previous study failed to detect a significant association of nuclear or cytoplasmic Maspin staining with outcome in a large cohort of stage III CRC patients[27]. Since all three studies made use of the same antibody, the different outcome of the study of Fung and colleagues may be related to the use of a different scoring system. The cutoffs used in this study, resulted in a very unevenly distributed number of samples per group, in which the vast majority (75%) of samples were allocated to one group. Moreover, this study did not take the intensity of the staining into account, while this has previously been associated with the amount of Maspin expression and clinical outcome[24]. However, when we apply the Fung scoring system to our own dataset, we still find that nuclear Maspin expression is associated with disease free and colorectal cancerspecific survival in stage III colorectal cancer patients (p=0.031 and p=0.001 data not shown). The same significant association between high levels of Maspin and early recurrence and colorectal-specific survival was seen when applying the Dietmeier et al scoring system (p=0.040 and p=0.019 data not shown)[24].

Tumours with high Maspin expression respond significantly better to adjuvant 5-FU chemotherapy in stage III CRC[24]. This trend was also observed in our study, although patient numbers were too low for this association to reach significance (data not shown). Maspin may therefore not only have value as a prognostic marker but possibly also as a marker for predicting response to adjuvant treatment in advanced stage CRC. Whether Maspin itself could be a drug target depends on whether it is causally involved in facilitating the metastatic process.

In this study, Maspin was highly up regulated using two different high-throughput screens suggestive of a key role in predicting time to recurrence after surgery of colorectalliver metastasis. To our knowledge this is the first study reporting a possible predictive role for Maspin in stage IV CRC. However, it must be noted that identification of Maspin and validation was performed in a relatively small cohort.

Experimental studies show that high Maspin expression is correlated with increased apoptosis resistance in CRC cells[37]. Furthermore, it has been shown that circulating tumour cells in peripheral blood of CRC patients express high levels of Maspin[38]. We did not find a difference in Maspin expression at the periphery of the tumour compared to the centre, however Bettstetter and

colleagues did find that Maspin expression levels were higher at the invasive tumour font when compared to the more central parts of CRC tumours[23]. This discrepancy can probably be explained by the fact that we scored peripheral cores containing mainly tumour bulk, but not necessarily cells invading the adjacent stroma, while Bettstetter et al, only scored Maspin expression in cell clusters detaching from the peripheral tumor bulk.

These results combined with the results of our study, demonstrating that high Maspin expression is associated with poor prognosis in CRC, that have metastasized to local lymph nodes or beyond, point to a potential role for Maspin in facilitating the metastatic process. Future work should therefore address whether (and how) high Maspin levels promote metastasis in advanced stage CRC.

REFERENCES

1. Siegel,R. *et al.* Cancer statistics, 2012. *CA Cancer J. Clin.* 62, 10-29 (2012).
2. Edge,S.B. & Compton,C.C. The American Joint Committee on Cancer: the 7th edition of the AJCC cancer staging manual and the future of TNM. *Ann. Surg. Oncol.* 17, 1471-1474 (2010).
3. O'Connell,J.B. *et al.* Colon cancer survival rates with the new American Joint Committee on Cancer sixth edition staging. *J. Natl. Cancer Inst.* 96, 1420-1425 (2004).
4. Kelley,R.K. *et al.* Personalized medicine and oncology practice guidelines: a case study of contemporary biomarkers in colorectal cancer. *J. Natl. Compr. Canc. Netw.* 9, 13-25 (2011).
5. Salazar,R. *et al.* Gene Expression Signature to Improve Prognosis Prediction of Stage II and III Colorectal Cancer. *J. Clin. Oncol.*(2010).
6. Webber,E.M. *et al.* Oncotype DX tumor gene expression profiling in stage II colon cancer. Application: prognostic, risk prediction. *PLoS. Curr.* 2, (2010).
7. Hanahan,D. & Weinberg,R.A. The hallmarks of cancer. *Cell* 100, 57-70 (2000).
8. Jones,S. *et al.* Comparative lesion sequencing provides insights into tumor evolution. *Proc. Natl. Acad. Sci. U. S. A* 105, 4283-4288 (2008).
9. Eberhard,J. *et al.* A cohort study of the prognostic and treatment predictive value of SATB2 expression in colorectal cancer. *Br. J. Cancer* 106, 931-938 (2012).
10. de Jong,M.C. *et al.* Rates and patterns of recurrence following curative intent surgery for colorectal liver metastasis: an international multi-institutional analysis of 1669 patients. *Ann. Surg.* 250, 440-448 (2009).
11. Fong,Y. *et al.* Clinical score for predicting recurrence after hepatic resection for metastatic colorectal cancer: analysis of 1001 consecutive cases. *Ann. Surg.* 230, 309-318 (1999).
12. Nordlinger,B. *et al.* Surgical resection of colorectal carcinoma metastases to the liver. A prognostic scoring system to improve case selection, based on 1568 patients. Association Francaise de Chirurgie. *Cancer* 77, 1254-1262 (1996).
13. Simmonds,P.C. *et al.* Surgical resection of hepatic metastases from colorectal cancer: a systematic review of published studies. *Br. J. Cancer* 94, 982-999 (2006).
14. Belt,E.J. *et al.* Loss of lamin A/C expression in stage II and III colon cancer is associated with disease recurrence. *Eur. J. Cancer* 47, 1837-1845 (2011).
15. Snoeren,N. *et al.* Exploring gene expression signatures for predicting disease free survival after resection of colorectal cancer liver metastases. *PLoS. One.* 7, e49442 (2012).
16. Tumour Analysis Best Practices Working Group. Expression profiling--best practices for data generation and interpretation in clinical trials. *Nat. Rev. Genet.* 5, 229-237 (2004).
17. Wu,H. *et al.* MAANOVA: A software package for the analysis of spotted cDNA microarray experiments. 2003. The Analysis of Gene Expression Data: Methods and Software.
18. Keller,A. *et al.* Empirical statistical model to estimate the accuracy of peptide identifications made by MS/MS and database search. *Anal. Chem.* 74, 5383-5392 (2002).
19. Nesvizhskii,A.I. *et al.* A statistical model for identifying proteins by tandem mass spectrometry. *Anal. Chem.* 75, 4646-4658 (2003).
20. Liu,H. *et al.* A model for random sampling and estimation of relative protein abundance in shotgun proteomics. *Anal. Chem.* 76, 4193-4201 (2004).
21. Pham,T.V. *et al.* On the beta-binomial model for analysis of spectral count data in label-free tandem mass spectrometry-based proteomics. *Bioinformatics.* 26, 363-369 (2010).
22. Simon,R. *et al.* Tissue microarrays. *Biotechniques* 36, 98-105 (2004).
23. Bettstetter,M. *et al.* Elevated nuclear maspin expression is associated with microsatellite instability and high tumour grade in colorectal cancer. *J. Pathol.* 205, 606-614 (2005).
24. Dietmaier,W. *et al.* Nuclear Maspin expression is associated with response to adjuvant 5-fluorouracil based chemotherapy in patients with stage III colon cancer. *Int. J. Cancer* 118, 2247-2254 (2006).
25. Jorissen,R.N. *et al.* Metastasis-Associated Gene Expression Changes Predict Poor Outcomes in Patients with Dukes Stage B and C Colorectal Cancer. *Clin. Cancer Res.* 15, 7642-7651 (2009).
26. Smith,J.J. *et al.* Experimentally derived metastasis gene expression profile predicts recurrence and death in patients with colon cancer. *Gastroenterology* 138, 958-968 (2010).
27. Fung,C.L. *et al.* Clinicopathological correlates and prognostic significance of maspin expression in 450 patients after potentially curative resection of node-positive colonic cancer. *Histopathology* 56, 319-330 (2010).

28. Zou,Z. *et al.* Maspin, a serpin with tumor-suppressing activity in human mammary epithelial cells. *Science* 263, 526-529 (1994).
29. Marioni,G. *et al.* Nuclear expression of maspin is associated with a lower recurrence rate and a longer disease-free interval after surgery for squamous cell carcinoma of the larynx. *Histopathology* 46, 576-582 (2005).
30. Zheng,H.C. *et al.* Cytoplasmic and nuclear maspin expression in lung carcinomas: an immunohistochemical study using tissue microarrays. *Appl. Immunohistochem. Mol. Morphol.* 16, 459-465 (2008).
31. Cao,D. *et al.* Prognostic significance of maspin in pancreatic ductal adenocarcinoma: tissue microarray analysis of 223 surgically resected cases. *Mod. Pathol.* 20, 570-578 (2007).
32. Umekita,Y. *et al.* Expression of maspin predicts poor prognosis in breast-cancer patients. *Int. J. Cancer* 100, 452-455 (2002).
33. Woenckhaus,M. *et al.* Nuclear and cytoplasmic Maspin expression in primary non-small cell lung cancer. *J. Clin. Pathol.* 60, 483-486 (2007).
34. Yu,M. *et al.* Paradoxical expression of maspin in gastric carcinomas: correlation with carcinogenesis and progression. *Hum. Pathol.* 38, 1248-1255 (2007).
35. Markl,B. *et al.* Shift from cytoplasmic to nuclear maspin expression correlates with shorter overall survival in node-negative colorectal cancer. *Hum. Pathol.* 41, 1024-1033 (2010).
36. Song,S.Y. *et al.* Expression of maspin in colon cancers: its relationship with p53 expression and microvessel density. *Dig. Dis. Sci.* 47, 1831-1835 (2002).
37. Payne,C.M. *et al.* Maspin is a deoxycholate-inducible, anti-apoptotic stress-response protein differentially expressed during colon carcinogenesis. *Clin. Exp. Gastroenterol.* 4, 239-253 (2011).
38. Findeisen,P. *et al.* Systematic identification and validation of candidate genes for detection of circulating tumor cells in peripheral blood specimens of colorectal cancer patients. *Int. J. Oncol.* 33, 1001-1010 (2008).

SUPPLEMENTAL TABLES

Supplemental table 1. Uni- and multivariate analysis of factors influencing disease-free survival in stage IV CRC patients

Univariate analysis			Disease Free survival		
Variable	**Characteristics**	**N=46**	**Hazard ratio**	**95%CI**	**p-value**
Sex					
	Male	31 (67.4%)	1.862	0.841-4.12	0.125
	Female	15 (32.6%)			
Age (years)					
	(Mean; Median; SD)	62.24; 65.00; 14.70	0.980	0.945-1.015	0.259
Tumor location primary					
	Right sided	16 (34.8%)	1.433	0.652-3.137	0.369
	Left sided	16 (34.8%)	0.832	0.368-1.877	0.657
	Rectum	14 (30.4%)			
Histological grade					
	Well	5 (10.7%)	0.950	0.561-1.611	0.850
	Moderate	36 (78.3%)	0.494	0.186-1.312	0.157
	Poor	5 (10.7%)			
	Unknown				
Nodal stage					
	N0	21 (45.7%)	1.113	0.575-2.156	0.751
	N1	25 (54.3%)			
Interval between primary and LM					
	Synchronous	17 (37.0%)	1.553	0.786-3.067	0.205
	Metachronous	29 (63.0%)			
Neoadjuvant chemotherapy					
	Yes	10 (21.7%)	1.537	0.715-3.302	0.271
	No	36 (78.3%)			
Adjuvant chemotherapy					
	Yes	13 (28.3%)	0.349	0.151-0.806	**0.014***
	No	33 (71.7%)			
Nr of metastases					
	(Mean; Median; SD)	2.13; 1.00; 1.73	1.150	0.958-1.380	0.135
Size liver metastases					
	(Mean; Median; SD)	4.93; 4.05; 3.19	1.034	0.938-1.139	0.503
Preoperative CEA					
	(Mean; Median; SD)	67.36; 31.00; 97.19	1.004	1.000-1.009	**0.038***
Fong score	≥ 3	12 (26.1%)	1.656	0.804-3.408	0.171
	< 3	34 (73.9%)			
Maspin gene expression	≥ median	23 (50%)	2.652	1.307-5.380	**0.007***
	< median	23 (50%)			

Multivariate analysis		Disease Free survival	
Variable	**Hazard ratio**	**95%CI**	**p-value**
Adjuvant chemotherapy	0.314	0.104-0.950	**0.040***
Maspin gene expression	2.741	1.119-6.712	**0.027***
Sex	0.644	0.278-1.489	0.303
Nr of metastases	0.983	0.777-1.242	0.884
Histological grade	1.465	0.816-2.630	0.201
Fong score	2.979	1.001-7.524	0.058
Cea pre-operative	1.002	0.997-1.007	0.450

Supplemental table 2. Clinical and pathological characteristics of patients included in mass-spec analysis

Variable	Characteristics	DFS < 6 months	DFS > 24 months
		n=5	n=5
Sex			
	Male	2	2
	Female	3	3
Age (years)			
	(Mean; Median; SD)	64.40; 63.00; 6.11	62.80; 64.40; 9.78
Tumor location primary			
	Right sided	3	3
	Left sided	1	2
	Rectum	1	1
Histological grade			
	Well	0	0
	Moderate	5	5
	Poor	0	0
Nodal stage			
	N0	2	2
	N1	3	3
	Unknown		
Interval between primary and LM			
	Synchronous (≤2 months)	1	3
	Metachronous (> 2months)	4	2
Neoadjuvant chemotherapy			
	Yes	1	1
	No	4	4
Adjuvant chemotherapy			
	Yes	0	3
	No	5	2
Nr of metastases			
	(Mean; Median; SD)	1.40; 1.00; 0.894	2.40; 3.00; 0.894
Size liver metastases			
	(Mean; Median; SD)	7.60; 5.5; 4.75	4.30; 4.20; 1.49
Preoperative CEA			
	(Mean; Median; SD)	256.32; 272.00; 1.58.17	21.67; 4.00; 30.89

Supplemental table 3. Patient- and tumour characteristics associated with central Maspin expression in stage II CRC patients

Variable	Characteristic	Low nuclear, Low cytoplasmic n=144	Low nuclear, high cytoplasmic n=62	High nuclear, high cytoplasmic n=33	p-value
Seks					
	Male	71 (49.3%)	33 (53.2%)	21 (63.3%)	0.229
	Female	73 (50.7%)	29 (46.8%)	12 (36.4%)	
Age (years)					
	(Mean; Median; SD)	71.61; 73.01; 11.63	71.91; 73,67; 12.32	76.53; 76.76; 8.04	0.856
Tumor size					
	(Mean:Median; SD)	4.43; 4.00; 22.06	3,90; 4.00; 2,17	3.82; 3.00; 1.81	0.686
Tumor location					
	right sided	50 (34.7%)	35 (56.5%)	19 (57.6%)	**0.001***
	left sided	72 (50.0%)	21 (33.8%)	11 (33.3%)	
	rectum	22 (15.3%)	6 (9.7%)	3 (9.1%)	
No. of lymph nodes retrieved					
	(Mean;Median; range; SD)	8.32; 7.00; (0-30); 5.25	7.39; 6,50; (0-23) 4.64	7.76; 7.00; (0-28); 5.21	0.447
Histological grade					
	Well	8 (5.6%)	7 (14,5%)	1 (3.0%)	0.756
	Moderate	122 (84.7%)	46 (74.2%)	29 (87.9%)	
	Poor	14 (9.7%)	9 (11.3%)	3 (9.1%)	
Mucinous differentiation					
	Yes	21 (14.6%)	21 (33.9%)	4 (12.1%)	0.086
	No	123 (85.4%)	41 (66.1%)	29 (87.9%)	
Ulceration					
	Present	111 (77.1%)	45 (72.7%)	22 (66.7%)	0.214
	Absent	33 (22.9%)	17 (27.3%)	11 (33.3%)	
Angioinvasion					
	Present	14 (9.7%)	8 (12,9%)	2 (6.1%)	0.955
	Absent	130 (90.3%)	54 (87.1%)	31 (93.9%)	
Adjuvant chemotherapy					
	Yes	18 (12.5%)	11 (17.7%)	2 (6.1%)	0.532
	No	122 (84.7%)	50 (80.6%)	30 (90.9%)	
	Other	4 (2.8%)	1 (1.6%)	1 (3.0%)	
Microsatelite stability status					
	MSS	96 (66.7%)	41 (66.1%)	22 (66.7%)	0.706
	MSI	21 (14.6%)	11 (17.7%)	6 (18.2%)	
	Unknown	27 (18.8%)	10 (16.1%)	5 (15.2%)	

Supplemental table 4. Patient- and tumour characteristics of factors associated with central Maspin expression in stage III CRC patients

Variable	Characteristic	Low nuclear, Low cytoplasmic	Low nuclear, High cytoplasmic	High nuclear, High cytoplasmic	p-value
		n=79	n=49	n=36	
Sex					
	Male	47 (59.5%)	31 (60.8%)	13 (36.1%)	0.061
	Female	32 (40.5%)	20 (39.2%)	23 (63.9%)	
Age (years)					
	(Mean; Median; SD)	70.30; 72.29; 11.90	70.79; 73.73; 11.18	72.51; 76.07; 12.84	0.528
Tumor size					
	(Mean;Median; SD)	4.16; 4.00; 21.86	4.13; 4.00;1.99	4.31; 3.75; 2.07	0.818
Tumor location					
	right sided	36 (45.6%)	21 (42.9%)	21 (58.3%)	0.380
	left sided	31 (39.2%)	16 (32.6%)	10 (27.8%)	
	Rectum	12 (15.2%)	12 (24.5%)	5 (13.9%)	
Nodal stage					
	N1	55 (69.6%)	36 (70.6%)	22 (61.1%)	0.480
	N2	24 (30.4%)	15 (29.4%)	14 (38.9%)	
No. of lymph nodes retrieved					
	(Mean; Median; range; SD)	9.32; 9.00; (1-19); 4.29	9.63; 8.00; (2-22); 4.85	9.89; 8.00; (2-25); 5.76	0.152
Histological grade					
	Well	2 (2.5%)	1 (2.0%)	2 (5.6%)	**0.031***
	Moderate	67 (84.8%)	40 (78.4%)	22 (61.1%)	
	Poor	10 (12.7%)	10 (19.6%)	12 (33.3%)	
Mucinous differentiation					
	Yes	11 (13.9%)	12 (23.5%)	13 (36.1%)	**0.008***
	No	68 (86.1%)	39 (76.5%)	23 (63.9%)	
Ulceration					
	Present	65 (82.3%)	40 (78.4%)	28 (77.8%)	0.518
	Absent	14 (17.7%)	11 (21.6%)	8 (22.2%)	
Angioinvasion					
	Present	27 (34.2%)	14 (27.5%)	17 (47.2%)	0.396
	Absent	52 (65.8%)	37 (72.5%)	19 (52.8%)	
Adjuvant chemotherapy					
	Yes	40 (50.7%)	25 (49.1%)	19 (52.8%)	0.974
	No	35 (44.3%)	20 (39.2%)	17 (47.2%)	
	other	4 (5.0%)	6 (11.8%)		
Microsatelite stability status					
	MSS	66 (83.5%)	39 (76.5%)	22 (61.1%)	**0.045***
	MSI	9 (11.4%)	8 (15.7%)	10 (27.8%)	
	Unknown	4 (5.1%)	4 (7.8%)	4 (11.1%)	

Supplemental table 5. Patient- and tumour characteristics associated with peripheral Maspin expression in stage II CRC patients

Variable	Characteristic	Low nuclear, Low cytoplasmic n=110	Low nuclear, high cytoplasmic n=55	High nuclear, high cytoplasmic n=12	p-value
Sex					
	Male	54 (49.1%)	32 (58.2%)	5 (41.7%)	0.408
	Female	56 (50.9%)	23 (41.8%)	7 (58.3%)	
Age (years)					
	(Mean; Median; SD)	70.98; 73.19; 12.99	73.85; 75.94; 10.43	72.56; 73.90; 12.31	0.559
Tumor size					
	(Mean:Median; SD)	4.52; 4.00; 2.93	3,90; 4.00; 2,17	3.54; 3.00; 1.48	0.838
Tumor location					
	Right sided	51 (46.4%)	18 (32.7%)	9 (75%)	0.755
	Left sided	44 (40%)	29 (52.7%)	2 (16.7%)	
	Rectum	15 (13.6%)	8 (15.5%)	1 (8.3%)	
No. of lymph nodes retrieved					
	(Mean;Median; range; SD)	7.58; 6.00; 4.51	7.09; 6.00; 4.62	10.75; 15.13; 6.89	0.261
Histological grade					
	Well	7 (6.4%)	4 (7.3%)	1 (8.3%)	0.960
	Moderate	88 (80%)	44 (80.%)	9 (75%)	
	Poor	15 (13.6%)	7 (12.7%)	2 (16.7%)	
Mucinous differentiation					
	Yes	25 (22.7%)	9 (16.4%)	4 (33.3%)	0.640
	No	85 (77.3%)	46 (83.6%)	8 (66.7%)	
Ulceration					
	Present	82 (74.5%)	37 (67.3%)	12 (100%)	0.214
	Absent	28 (25.5)	18 (32.7%)		
Angioinvasion					
	Present	10 (9.1%)	8 (14.5%)	2 (16.7%)	0.226
	Absent	100 (90.9%)	47 (85.5%)	10 (83.3%)	
Adjuvant chemotherapy					
	Yes	14 (12.7%)	19 (16.4%)	3 (75%)	0.541
	No	94 (85.5%)	44 (80%)	9 (25%)	
	Other	2 (3.6%)	2 (3.6%)		
Microsatelite stability status					
	MSS	70 (63.6%)	37 (67.3%)	6 (50%)	0.427
	MSI	18 (16.4%)	9 (16.4%)	5 (41.7%)	
	Unknown	22 (20%)	9 (16.4%)	1 (8.3%)	

Supplemental table 6. Patient- and tumour characteristics of factors associated with peripheral Maspin expression in stage III CRC patients

Variable	Characteristic	Low nuclear, Low cytoplasmic n=59	Low nuclear, High cytoplasmic n=55	High nuclear, High cytoplasmic n=20	p-value
Seks					
	Male	37 (62.7%)	29 (52.7%)	9 (45%)	0.141
	Female	22 (37.3%)	26 (47.3%)	11 (55%)	
Age (years)					
	(Mean; Median; SD)	71.25; 72.78; 11.44	68.51; 70.98; 12.99	72.49; 76.15; 10.75	0.858
Tumor size					
	(Mean;Median; SD)	4.38; 4.00; 1.94	3.83; 4.00; 1.32	5.39; 4.00; 3.64	0.864
Tumor location					
	Right sided	23 (39%)	29 (52.7%)	12 (60%)	0.057
	Left sided	20 (33.9%)	17 (30.9%)	7 (35%)	
	Rectum	16 (27.1%)	9 (16.4%)	1 (5%)	
Nodal stage					
	N1	45 (76.3%)	35 (63.6%)	10 (50%)	**0.019***
	N2	14 (23.7%)	20 (36.4%)	10 (50%)	
No. of lymph nodes retrieved					
	(Mean; Median; range; SD)	9.08; 8.00; 4.65	10.64; 11.00; 4.80	8.10; 8.00; 3.68	0.170
Histological grade					
	Well	1 (1.7%)	1 (1.8%)	1 (5.0 %)	0.265
	Moderate	50 (84.7%)	45 (81.8%)	12 (60.0%)	
	Poor	8 (13.6%)	9 (16.4%)	7 (35.0%)	
Mucinous differentiation					
	Yes	13 (22%)	9 (16.4%)	7 (35.0%)	0.644
	No	46 (78%)	46 (83.6%)	13 (65.0%)	
Ulceration					
	Present	51 (86.4%)	44 (80%)	17 (85%)	0.713
	Absent	8 (13.6%)	11 (20%)	3 (15%)	
Angioinvasion					
	Present	22 (37.3%)	16 (29.1%)	7 (35%)	0.526
	Absent	37 (62.7%)	39 (70.9%)	13 (65%)	
Adjuvant chemotherapy					
	Yes	30 (50.8%)	28 (50.9%)	9 (45.0%)	0.361
	No	26 (44.1%)	23 (41.8%)	10 (50%)	
	Other	3 (5.1%)	4 (7.2%)	1 (5.0%)	
Microsatelite stability status					
	MSS	47 (79.7%)	41 (74.5%)	14 (70.0%)	0.121
	MSI	6 (10.2%)	11 (20.0%)	5 (25%)	
	Unknown	6 (10.2%)	3 (5.5%)	1 (5.0%)	

9

GENERAL DISCUSSION

In this thesis different aspects of cancer stem cells in colorectal cancer are described. The main findings are summarized below and several important questions that remain unanswered or have been specifically raised by our work are discussed.

Therapy resistance in colon cancer stem cells

Several reports have shown that chemotherapy of colorectal tumors causes an enrichment of the cancer stem cell (CSC) population[1-3], possibly due to a relative resistance of CSCs to chemotherapy[4, 5]. These resistance mechanisms may include high expression levels of ABC transporters, active DNA repair capacity and high expression of anti-apoptotic factors. CSCs may have 'inherited' these mechanisms from normal stem cells[6]. By using the colonosphere culture system, described in **chapter 2**, we studied drug resistance in relation to the CSC phenotype. Colonosphere cultures are highly enriched in CSCs but also contain 15-30% spontaneously differentiated tumor cells which fail to form clones and tumors. Tumor-derived colonosphere cultures are currently one of the best in-vitro culture systems for human colorectal tumors. Large collections of colonosphere cultures can be used to correlate genetic alterations with mechanisms of drug resistance.

In **chapter 2** we show that the resistance of colonospheres to irinotecan is due to a remarkable collaboration between differentiated cells expressing the drug transporter ABCB1 and undifferentiated CSCs that do not express ABCB1 but provide clone-forming capacity. The ABCB1-expressing differentiated cells are localized at the outer rim of the colonospheres and prevent irinotecan to reach the drug-sensitive CSCs localized in the inner cell mass. Indeed, drug resistance is abrogated by combining irinotecan with valspodar (PSC-833), a second generation ABCB1- pump inhibitor. The described functional cooperation between differentiated tumor cells and CSCs in mediating drug resistance provides a novel paradigm for drug resistance. The selective expression of ABCB1 on differentiated cells was also observed in the normal intestine where expression was restricted to the lumen-facing top compartment of the intestinal crypts and undetectable in the crypt bottom where stem cells reside[7]. In addition, immunohistochemistry for ABCB1 on a tissue microarray containing 544 colorectal tumors of the CApecitabine, IRinotecan, and Oxaliplatin in advanced colorectal cancer (CAIRO-I) cohort showed that ABCB1 is exclusively expressed by lumen-forming differentiated tumor cells. Furthermore, there was a near-significant association between poor histological differentiation grade and lack of ABCB1 expression.

Early clinical studies in which ABC drug transporter inhibitors have been combined with chemotherapy to overcome resistance, so-called 'reversal trials', have mainly generated disappointing results. However, none of the clinical reversal trials involved irinotecan and none were performed in cohorts of colorectal cancer patients[8]. Therefore, the contribution of ABC transporters to primary and acquired resistance of colorectal tumors to irinotecan is not known. In addition, these early 'reversal trials' studied heterogeneous cancer patient groups. Importantly, it was not assessed whether the ABC transporter inhibitors actually increased drug retention in the tumors. Most trials involved patient groups that had progressed on previous chemotherapy regimens, and this may have caused ABC transporter-independent mechanisms of (multi-) drug resistance. Given all these issues, it is far too early to generally dismiss ABC transporter inhibition as a potentially effective strategy in achieving sensitization of specific tumor types to specific chemotherapeutic drugs, especially in the treatment of chemo-naïve patients[6, 9-11].

One approach to assess whether ABCB1 plays a role in irinotecan resistance in colorectal tumors in patients is to analyse tumor samples of irinotecan-treated patients and to assess whether ABCB1 transporter expression correlates with response to therapy. To do this we made use of tumor samples of the CAIRO-I study, in which patients in the first treatment arm received

irinotecan as a single drug in the second line. Preliminary data show that there is no significant difference in response to irinotecan treatment in tumors expressing high or low levels of ABCB1, or its relative ABCG2. A potential pitfall in the interpretation of this study is that all tumors had progressed on capecitabine treatment, which may have caused ABC transporter-independent mechanisms of (multi-) drug resistance.

Future studies should identify the relationship between genetic alterations and response to irinotecan in the presence or absence of ABC transporter inhibitors. The newly generated 'live biobank' of organoid cultures that is currently being generated in the UMCU provides an excellent platform for such a study. The results of such a study could be used for the design of a clinical study in which pre-selected patient groups are treated with irinotecan alone or in combination with a third generation ABCB1 inhibitor. Trials with first and second generation ABCB1 inhibitors often required chemotherapy under-dosing due to the fact that they target cytochrome P450, causing a pharmacokinetic interaction with chemotherapeutic drugs and higher toxicity[10]. The advantage of third generation ABCB1 inhibitors is that they are more specific and do not target cytochrome P450.

In **chapters 4 and 5** we have used an unbiased proteomics approach to further address the relationship between colorectal CSCs and drug resistance. To this end, we compared CSC-enriched colonosphere cultures and their isogenic stably differentiated progeny. In **chapter 4,** mass spectrometry of the proteome revealed that proteins governing cell survival are overrepresented in the colonosphere cultures. An altered expression of apoptosis regulators has been related to chemoresistance in several tumor types[12]. We have identified BIRC6, also known as Apollon or Bruce, as a key player in apoptosis resistance to platinum-containing chemotherapeutic drugs. BIRC6 is a member of the inhibitors of apoptosis proteins (IAPs) which prevent apoptosis, at least in part, by inhibiting caspase activation[13, 14]. In line with our result, it was recently demonstrated that IL4 stimulates expression of survivin (BIRC5) to protect colorectal CSCs against apoptosis[15, 16]. Although we did not identify BIRC5 as a CSC-enriched protein, it is possible that different tumors resist apoptotic stimuli by increasing the expression of distinct IAP family members. At present, no specific BIRC6 inhibitor has been developed. By contrast, other IAPs have been successfully targeted in preclinical and clinical studies by SMAC mimetics[17-19]. SMAC mimetics target several IAP members, but were not specifically tested for their ability to inhibit BIRC6. Based on our results we would recommend efforts to target BIRC6 for the treatment of colon CSCs. In addition, combined treatment of SMAC inhibitors with platinum based chemotherapy should be explored as an approach to eradicating colon CSCs on a large collection of patient derived colonospheres.

Factors secreted by cancer cells can also play an important role in the acquisition of drug resistance[20-22]. In **chapter 5**, we conducted a comparative secretome analysis of colonospheres and their isogenic differentiated progeny. In line with **chapter 4,** cell survival proteins were significantly enriched in the secretome of colonospheres. In addition, we found that cancer stem cells secrete high levels of drug-metabolizing enzymes, including aldehyde dehydrogenase 1 (ALDH1A1) and bleomycin hydrolase (BLMH). These enzymes cause extracellular detoxification of maphosphamide and bleomycin respectively. An important new concept that may be extracted from this study is that secretion of specific proteins from CSCs modulates drug responses in nearby tumor cells. Thus, CSCs not only possess multiple mechanisms that promote self-preservation, but may also preserve cells in their direct vicinity by secreting drug-detoxifying enzymes. This is reminiscent of the stem cell support function of Paneth cells in normal colon tissue[23]. Drug-detoxifying enzymes secreted by CSCs could provide survival signals to their own closely associated differentiated support cells and this may be essential for their own survival.

To what extent the mechanisms described above are operating within colorectal tumors during chemotherapy needs to be addressed in future experiments. In addition, it would be of great interest to study the secretome of the different cell populations after chemotherapy treatment. Identification and possible targeting of specific secreted drug-metabolizing enzymes, up-regulated after chemotherapy treatment, could be of added value in the treatment of patients with colorectal cancer. Again, the colonosphere and organoid culturing systems form ideal platforms for conducting such studies as they contain both CSCs and differentiated tumor cells.

Regulation of the colorectal cancer stem cell phenotype

In **chapters 6 and 7** we studied the effects of reactive oxygen species (ROS) and hypoxia on colonosphere cultures. In **chapter 6** we show that the H_2O_2-reducing enzyme glutathione peroxidase 2 (GPx2), is required for the survival of clonogenic tumor cells, but also for the generation of proliferating differentiated tumor mass and metastasis formation. Our results are in line with studies showing that tumor cells have to prevent excessive ROS accumulation as this may lead to cell death, cell cycle arrest and senescence[24]. In addition, it has also been shown that other ROS neutralizing enzymes (TIGAR, TR1 and Nrf2) have an important role in tumor initiation and progression by regulating the intracellular redox balance[25-27]. It may seem paradoxical that GPx2, which induces proliferation and differentiation, is essential for metastasis formation, as CSCs rather than differentiated cells are expected to carry metastatic capacity[2]. We envision that GPx2 is required for maintenance of CSC 'fitness' but also for the capacity of disseminated CSCs to generate proliferating differentiated tumor mass at the secondary site. Whether GPx2 also controls the complex dynamics of epithelial-to-mesenchymal and mesenchymal-to-epithelial transitions during the metastasis cascade[28, 29] remains to be elucidated.

Our in vitro en in vivo findings that GPx2 is essential for the generating of proliferating differentiated tumor mass and metastasis formation is supported by multiple large patient derived transcriptomics datasets, where a strong positive correlation between GPx2 expression, differentiation and proliferation was found. Interestingly, high GPx2 levels were only significantly correlated with metastasis formation within the aggressive CCS3 subtype of colon tumors[30, 31]. In fact, our metastasis experiments were conducted with the HT-29 colonosphere cultures which belongs to this CCS3 mesenchymal subgroup[30]. This result opens up therapeutic opportunities as the CCS3 subtype is relatively resistant to current systemic therapy[31]. The next step would therefore be to study how therapeutic elevation of ROS levels would affect chemotherapy resistance and metastasis formation by CCS3-type tumors. Therapeutically increasing ROS levels could be achieved by targeting the enzymatic activity of GPx or by ROS-generating agents, as iron-chelators, redox cyclers and/or Elesclomol. ROS-generating agents have been found to be effective in many cases, for example arsenic trioxide in acute promyelocytic leukemia[32, 33]. However, low clinical response and resistance to ROS-generating agents have also been reported[32, 34, 35], which may be due to the activation of antioxidant pathways such as that controlled by Nrf2[35, 36]. To maximally exploit ROS-mediated cell-death as a therapeutic strategy, drugs that induce ROS generation can be combined with compounds that suppress antioxidant pathways. This approach might be particularly useful in cancer cells that have become adapted to stress and resistant to anticancer agents. For example, the combination of a ROS-generating agent with an SOD inhibitor showed potent activity against primary chronic lymphocytic leukaemia cells[37]. Currently several exogenous ROS-generating agents and inhibitors of the antioxidant system are in clinical trials as single agents or in combination therapy[38]. Unfortunately, at present there is no drug available that specifically targets GPx2.

The results described in **chapter 6** identify GPx2 as a critical regulator of differentiation in colon tumors. Differentiation stimulation is seen as a potential therapeutic strategy to eliminate the cancer stem cell population[39]. Differentiation therapy could deplete the cancer stem cell population, and give rise to differentiated tumor mass with increased susceptibility to chemotherapy. Clinically effective differentiation therapy would need to be combined with chemotherapy in order to eradicate both cancer stem cell and differentiated cell populations within a tumor. Recently, such a study was performed in triple-negative breast cancer, where tumors were treated with a TGFβ inhibitor to induce differentiation, in combination with paclitaxel. This eradicated the rapidly proliferating differentiated tumor mass[40]. These results must be interpreted with caution as we show in our own results in **chapter 6** that the cancer stem cell pool is preserved after inducing differentiation by means of overexpressing GPx2. Therefore in-depth studies are required to establish whether or not differentiation therapy results in depletion of the cancer stem cell population before testing such compounds in clinical trials.

Microenvironmental cues can contribute to the installation of an aggressive phenotype[41]. An important feature of the tumor microenvironment is hypoxia[42]. Previous work by our group has demonstrated that micrometastases in the liver adopt a highly aggressive phenotype after liver injury induced by ischemia-reperfusion[43-45]. Accelerated tumor growth was exclusively observed in tissue areas that were characterized by hypoxia[45]. In **chapter 7**, we use colonosphere-initiated liver tumors, to show that liver surgery (ischemia-reperfusion injury) promotes the cancer stem cell phenotype and causes accelerated tumor outgrowth. To our knowledge, this is the first study demonstrating a causative link between surgery-induced hypoxia and acquisition of the cancer stem cell phenotype in vivo. The next step would be to design a clinical study in which the phenotype and growth behaviour of liver metastases is analysed before and after the first surgical procedure. Based on our results we suggest that minimizing surgery-induced hypoxia may help prevent aggressive local tumor recurrence. Hypoxia is also strongly associated with poor drug response. Possibly, this could be due to a hypoxia-induced cancer stem cell phenotype, as CSCs are generally considered to be relatively drug resistant[3, 46]. We have shown that after treating colonospheres with the hypoxia-activated pro-drug TPZ the cancer stem cell fraction is lowered and all clone-forming capacity is lost. TPZ inhibits topoisomerase II and strongly redcues aggressive tumor outgrowth in hypoxic tissue areas[47]. The results presented in **chapter 2** show that CSCs are sensitive to the topoisomerase I inhibiter irinotecan. Thus, CSCs may not be selectively resistant to the type of DNA damage resulting from topoisomerase inhibition. This is now being tested in a large panel of colonosphere cultures. This work forms a solid basis for the design of clinical trials in which (hypoxia-activated) topoisomerase inhibitors are tested as adjuvant therapy following partial liver resection or RFA ablation.

REFERENCES

1. Dylla,S.J. *et al.* Colorectal cancer stem cells are enriched in xenogeneic tumors ` following chemotherapy. *PLoS. One.* 3, e2428 (2008).
2. Pang,R. *et al.* A subpopulation of CD26+ cancer stem cells with metastatic capacity in human colorectal cancer. *Cell Stem Cell* 6, 603-615 (2010).
3. Todaro,M. *et al.* Colon cancer stem cells dictate tumor growth and resist cell death by production of interleukin-4. *Cell Stem Cell* 1, 389-402 (2007).
4. Dean,M. ABC transporters, drug resistance, and cancer stem cells. *J. Mammary. Gland. Biol. Neoplasia.* 14, 3-9 (2009).
5. Donnenberg,V.S. & Donnenberg,A.D. Multiple drug resistance in cancer revisited: the cancer stem cell hypothesis. *J. Clin. Pharmacol.* 45, 872-877 (2005).
6. Zhou,B.B. *et al.* Tumour-initiating cells: challenges and opportunities for anticancer drug discovery. *Nat. Rev. Drug Discov.* 8, 806-823 (2009).
7. Kosinski,C. *et al.* Gene expression patterns of human colon tops and basal crypts and BMP antagonists as intestinal stem cell niche factors. *Proc. Natl. Acad. Sci. U. S. A* 104, 15418-15423 (2007).
8. Coley,H.M. Overcoming multidrug resistance in cancer: clinical studies of p-glycoprotein inhibitors. *Methods Mol. Biol.* 596, 341-358 (2010).
9. Amiri-Kordestani,L. *et al.* Targeting MDR in breast and lung cancer: discriminating its potential importance from the failure of drug resistance reversal studies. *Drug Resist. Updat.* 15, 50-61 (2012).
10. Borst,P. Cancer drug pan-resistance: pumps, cancer stem cells, quiescence, epithelial to mesenchymal transition, blocked cell death pathways, persisters or what? *Open. Biol.* 2, 120066 (2012).
11. Robey,R.W. *et al.* ABC transporters: unvalidated therapeutic targets in cancer and the CNS. *Anticancer Agents Med. Chem.* 10, 625-633 (2010).
12. Johnstone,R.W. *et al.* Apoptosis: a link between cancer genetics and chemotherapy. *Cell* 108, 153-164 (2002).
13. Salvesen,G.S. & Duckett,C.S. IAP proteins: blocking the road to death's door. *Nat. Rev. Mol. Cell Biol.* 3, 401-410 (2002).
14. Deveraux,Q.L. *et al.* Endogenous inhibitors of caspases. *J. Clin. Immunol.* 19, 388-398 (1999).
15. Di Stefano,A.B. *et al.* Survivin is regulated by interleukin-4 in colon cancer stem cells. *J. Cell Physiol* 225, 555-561 (2010).
16. Signore,M. *et al.* Targeting apoptosis pathways in cancer stem cells. *Cancer Lett.* 332, 374-382 (2013).
17. Fulda,S. Targeting inhibitor of apoptosis proteins (IAPs) for cancer therapy. *Anticancer Agents Med. Chem.* 8, 533-539 (2008).
18. Gyrd-Hansen,M. & Meier,P. IAPs: from caspase inhibitors to modulators of NF-kappaB, inflammation and cancer. *Nat. Rev. Cancer* 10, 561-574 (2010).
19. Oost,T.K. *et al.* Discovery of potent antagonists of the antiapoptotic protein XIAP for the treatment of cancer. *J. Med. Chem.* 47, 4417-4426 (2004).
20. Arlt,A. *et al.* Autocrine production of interleukin 1beta confers constitutive nuclear factor kappaB activity and chemoresistance in pancreatic carcinoma cell lines. *Cancer Res.* 62, 910-916 (2002).
21. Conze,D. *et al.* Autocrine production of interleukin 6 causes multidrug resistance in breast cancer cells. *Cancer Res.* 61, 8851-8858 (2001).
22. Yao,L. *et al.*Discovery of IL-18 as a novel secreted protein contributing to doxorubicin resistance by comparative secretome analysis of MCF-7 and MCF-7/Dox. *PLoS. One.* 6, e24684 (2011).
23. Sato,T. *et al.* Paneth cells constitute the niche for Lgr5 stem cells in intestinal crypts. *Nature* 469, 415-418 (2011).
24. Hamanaka,R.B. & Chandel,N.S. Mitochondrial reactive oxygen species regulate cellular signaling and dictate biological outcomes. *Trends Biochem. Sci.* 35, 505-513 (2010).
25. Cheung,E.C. *et al.* TIGAR is required for efficient intestinal regeneration and tumorigenesis. *Dev. Cell* 25, 463-477 (2013).
26. DeNicola,G.M. *et al.* Oncogene-induced Nrf2 transcription promotes ROS detoxification and tumorigenesis. *Nature* 475, 106-109 (2011).
27. Yoo,M.H. *et al.* Thioredoxin reductase 1 deficiency reverses tumor phenotype and tumorigenicity of lung carcinoma cells. *J. Biol. Chem.* 281, 13005-13008 (2006).

28. Ocana,O.H. *et al.* Metastatic colonization requires the repression of the epithelial-mesenchymal transition inducer Prrx1. *Cancer Cell* 22, 709-724 (2012).
29. Tsai,J.H. *et al.* Spatiotemporal regulation of epithelial-mesenchymal transition is essential for squamous cell carcinoma metastasis. *Cancer Cell* 22, 725-736 (2012).
30. De Sousa E Melo *et al.* Poor-prognosis colon cancer is defined by a molecularly distinct subtype and develops from serrated precursor lesions. *Nat. Med.* 19, 614-618 (2013).
31. Sadanandam,A. *et al.* Reconciliation of classification systems defining molecular subtypes of colorectal cancer: interrelationships and clinical implications. *Cell Cycle* 13, 353-357 (2014).
32. Niu,C. *et al.* Studies on treatment of acute promyelocytic leukemia with arsenic trioxide: remission induction, follow-up, and molecular monitoring in 11 newly diagnosed and 47 relapsed acute promyelocytic leukemia patients. *Blood* 94, 3315-3324 (1999).
33. Soignet,S.L. *et al.* Complete remission after treatment of acute promyelocytic leukemia with arsenic trioxide. *N. Engl. J. Med.* 339, 1341-1348 (1998).
34. Attia,S. *et al.* A phase 2 consortium (P2C) trial of 3-aminopyridine-2-carboxaldehyde thiosemicarbazone (3-AP) for advanced adenocarcinoma of the pancreas. *Invest New Drugs* 26, 369-379 (2008).
35. Ramanathan,B. *et al.* Resistance to paclitaxel is proportional to cellular total antioxidant capacity. *Cancer Res.* 65, 8455-8460 (2005).
36. Hour,T.C. *et al.* Characterization of molecular events in a series of bladder urothelial carcinoma cell lines with progressive resistance to arsenic trioxide. *Anticancer Drugs* 15, 779-785 (2004).
37. Zhou,Y. *et al.* Free radical stress in chronic lymphocytic leukemia cells and its role in cellular sensitivity to ROS-generating anticancer agents. *Blood* 101, 4098-4104 (2003).
38. Trachootham,D. *et al.* Targeting cancer cells by ROS-mediated mechanisms: a radical therapeutic approach? *Nat. Rev. Drug Discov.* 8, 579-591 (2009).
39. Pattabiraman,D.R. & Weinberg,R.A. Tackling the cancer stem cells - what challenges do they pose? *Nat. Rev. Drug Discov.* 13, 497-512 (2014).
40. Bhola,N.E. *et al.* TGF-beta inhibition enhances chemotherapy action against triple-negative breast cancer. *J. Clin. Invest* 123, 1348-1358 (2013).
41. Friedl,P. & Alexander,S. Cancer invasion and the microenvironment: plasticity and reciprocity. *Cell* 147, 992-1009 (2011).
42. Vaupel,P. & Mayer,A. Hypoxia in cancer: significance and impact on clinical outcome. *Cancer Metastasis Rev.* 26, 225-239 (2007).
43. van der Bilt,J.D. *et al.* Ischemia/reperfusion accelerates the outgrowth of hepatic micrometastases in a highly standardized murine model. *Hepatology* 42, 165-175 (2005).
44. van der Bilt,J.D. *et al.* Selective portal clamping to minimize hepatic ischaemia-reperfusion damage and avoid accelerated outgrowth of experimental colorectal liver metastases. *Br. J. Surg.* 93, 1015-1022 (2006).
45. van der Bilt,J.D. *et al.* Perinecrotic hypoxia contributes to ischemia/reperfusion-accelerated outgrowth of colorectal micrometastases. *Am. J. Pathol.* 170, 1379-1388 (2007).
46. Dean,M., Fojo,T., & Bates,S. Tumour stem cells and drug resistance. *Nat. Rev. Cancer* 5, 275-284 (2005).
47. Govaert,K.M. *et al.* Effects of tirapazamine on experimental colorectal liver metastases after radiofrequency ablation. *Br. J. Surg.* 99, 567-575 (2012).

10

SUMMARY IN DUTCH

NEDERLANDSE SAMENVATTING

INTRODUCTIE

Ondanks het feit dat er de laatste decennia grote vorderingen zijn gemaakt in het kankeronderzoek komen er wereldwijd jaarlijks 15 miljoen kankerpatiënten bij. De helft van deze patiënten zal uiteindelijk aan deze ziekte overlijden. Darmkanker is na longkanker de voornaamste oorzaak van kanker gerelateerd overlijden. In Nederland wordt er jaarlijks bij meer dan 12.000 mensen darmkanker geconstateerd en zijn er jaarlijks bijna 5000 sterfgevallen. Patiënten overlijden aan de gevolgen van uitzaaiingen, meestal in de lever. Bij de behandeling van uitgezaaide darmkanker is het terugkeren van de tumor na een ogenschijnlijke effectieve therapie een groot probleem. Mogelijk biedt het kankerstamcelconcept hier uitkomst. Op dit moment is het kankerstamcelconcept één van de meest spraakmakende concepten binnen het oncologisch onderzoek. Dit concept gaat uit van het gegeven dat het overgrote deel van de tumorcellen in een (darm)tumor niet in staat is om nieuwe tumoren of uitzaaiingen te vormen. Dit is voorbehouden aan een kleine populatie 'kankerstamcellen' die de drijvende kracht zijn achter de ongecontroleerde tumorgroei. Het concept van de kankerstamcel als ultieme bron van tumorvorming en uitzaaiing heeft geleid tot de hypothese dat het doden van deze celpopulatie kan leiden tot genezing. Conventionele chemotherapie is gericht op het elimineren van de snel delende 'bulk' van de tumor en is niet zozeer gericht op de kankerstamcelpopulatie. Na chemotherapie keert de tumor dan ook vrijwel altijd weer terug. Omdat het opnieuw uitgroeien en uitzaaien van de tumor per definitie gedreven wordt door cellen met tumorvormend vermogen is het idee ontstaan dat kankerstamcellen van nature resistent zouden kunnen zijn tegen chemotherapeutica. Het is dan ook de verwachting dat het genezen van darmkankerpatiënten alleen mogelijk is als therapieën ontwikkeld worden die naast de tumormassa ook de kankerstamcelpopulatie succesvol kunnen doden. Het concept dat het doden van kankerstamcellen genezing zou kunnen geven, biedt veel hoop. Dit is alleen nog onvoldoende getoetst. In dit proefschrift staan kankerstamcellen centraal en gaan wij in op de therapieresistentie van kankerstamcellen en de effecten die vrije zuurstofradicalen en hypoxie (verminderde zuurstofspanning) hebben op de kankerstamcelpopulatie. Om dit en andere eigenschappen van kankerstamcellen te onderzoeken, hebben wij in het laboratorium een uniek model ontwikkeld om kankerstamcellen uit vers humaan tumormateriaal te isoleren en vervolgens te kweken. Na het isoleren groeien de kankerstamcellen uit tot 3D-tumorbolletjes (sferoïden) die verrijkt zijn voor kankerstamcellen met daaromheen een kleine percentage gedifferentieerde cellen (dochtercellen).

KANKERSTAMCELLEN EN THERAPIERESISTENTIE

In de eerste hoofdstukken van dit proefschrift wordt ingegaan op de therapieresistentie van kankerstamcellen (hoofdstukken 2 tot en met 5). In **hoofdstuk 2** laten wij zien dat een veel gebruikt chemotherapeuticum in de behandeling van darmkanker, irinotecan, juist heel goed in staat is om kankerstamcellen te elimineren. Echter, in de context van tumorweefsel worden de kankerstamcellen tegen irinotecan beschermd door hun dochtercellen (de meer gedifferentieerde cellen) die in staat zijn om irinotecan het tumorweefsel uit te pompen. Dit doen zij middels de ABCB1- drug efflux pomp die op het celmembraan aanwezig is. Het doden van kankerstamcellen in tumoren met irinotecan werkt hierdoor alleen als de pompfunctie van de dochtercellen gelijktijdig wordt geremd. Dit doen wij door humane tumoren in muizen met irinotecan in combinatie met een ABCB1 pompremmer te behandelen. Deze therapie leidt tot tumorreductie en celdood van

de kankerstamcelpopulatie. In dit hoofdstuk laten wij dus zien dat kankerstamcellen zelf niet resistent zijn tegen irinotecan, maar beschermd worden door de omliggende gedifferentieerde dochtercellen. Op dit moment krijgen kankerpatiënten irinotecan toegediend zonder deze aanvullende therapie. Nu wij een combinatietherapie hebben gevonden die de kankerstamcellen kan doden, zal de effectiviteit van deze nieuwe behandeling in de toekomst in zoveel mogelijk darmtumoren worden onderzocht.

In de **hoofdstukken 3, 4 en 5** gebruiken wij proteomics om beter inzicht te krijgen in de vraag welke signaleringcascades en eiwitten uniek zijn voor kankerstamcellen, om zodoende de biologie van de kankerstamcel beter te begrijpen en eventuele therapie 'targets' te identificeren. Proteomics is een analyse waarbij een overzicht van de expressie van alle eiwitten in een cel kan worden verkregen. Deze analyse geeft op zijn beurt weer een overzicht van de processen die binnen een cel actief of inactief zijn. In **hoofdstuk 3** geven wij een overzicht van recente ontwikkelingen binnen het proteomics veld en beschrijven wij hoe proteomics gebruikt kan worden bij het bestuderen van de biologie van een kankerstamcel. In **hoofdstuk 4** beschrijven wij de resultaten van een proteomics analyse waarin de eiwitexpressie van kankerstamcellen wordt vergeleken met de daaruit voortkomende gedifferentieerde dochtercellen. Uit deze analyse komt naar voren dat eiwitten die gerelateerd zijn aan de geprogrammeerde celdood, genaamd apoptose, hoog tot expressie komen binnen de kankerstamcelpopulatie. BIRC6, een anti-apoptose eiwit, is het eiwit dat het hoogst tot expressie komt binnen de kankerstamcelpopulatie. Vervolgens laten wij zien dat de aanwezigheid van BIRC6 binnen de kankerstamcel belangrijk is voor therapieresistente tegen apoptose inducerende chemotherapie. We suggereren in dit hoofdstuk dan ook dat BIRC6 een goede 'target' kan zijn om specifieke remmers voor te ontwikkelen, om de kankerstamcel-resistentie tegen apoptose inducerende chemotherapie op te heffen.

Naast het bestuderen van de eiwitten die zich in de cel bevinden, het proteome (zoals in hoofdstuk 4 beschreven), kunnen ook de gesecreteerde eiwitten (dit zijn de uitgescheiden eiwitten) worden bestudeerd. Het secretoom (alle gesecreteerde eiwitten) wordt verkregen door tumorcellen van het medium (de vloeistof waarin cellen gekweekt worden) te scheiden en vervolgens het medium middels proteomics te analyseren. Het secretoom vormt een goede afspiegeling van de processen die zich binnen een cel afspelen. Daarnaast kunnen gesecreteerde eiwitten ook een belangrijke rol spelen bij het afbreken en omzetten van geneesmiddelen, zoals chemotherapie. Hierdoor kunnen zij een rol van betekenis spelen in therapieresistentie van een tumorcel. In **hoofdstuk 5** laten wij zien dat het secretoom van kankerstamcellen in vergelijking tot de gedifferentieerde dochtercellen verrijkt is met eiwitten die belangrijk zijn voor de bescherming van de cel. Daarnaast hebben wij een aantal enzymen geïdentificeerd die in de extracellulaire ruimte (de ruimte buiten de cel) chemotherapeutica onschadelijk kunnen maken. Door het afbreken van chemotherapie in de extracellulaire ruimte beschermen zij niet alleen zichzelf, maar ook de omringende gedifferentieerde dochtercellen. Deze studie suggereert dat gesecreteerde enzymen naast intracellulaire (binnen de cel) enzymen een belangrijke rol spelen in de therapieresistentie van kankerstamcellen. Op basis van de resultaten beschreven in de bovenstaande hoofdstukken concluderen wij dat de kankerstamcellen niet voor alle chemotherapeutica resistent zijn, dat het mechanisme van therapieresistentie heel divers kan zijn afhankelijk van het type therapie dat gegeven wordt en dat gesecreteerde enzymen een belangrijke bijdrage leveren aan de therapieresistentie van kankerstamcellen.

HET EFFECT VAN VRIJE ZUURSTOFRADICALEN EN HYPOXIE OP KANKERSTAMCELLEN

In het tweede deel van het proefschrift (hoofdstukken 6 en 7) gaan wij in op de effecten die zuurstofradicalen (reactive oxygen species) en hypoxie (verlaagde zuurstofspanning) hebben op kankerstamcellen. Zuurstofradicalen of vrije radicalen zijn kortlevende, zeer reactieve deeltjes die gevormd worden in een cel door verschillende enzymen. Zuurstofradicalen kunnen veel schade aanrichten, omdat zij willekeurig chemische reacties aangaan met eiwitten, vetten en DNA, wat uiteindelijk kan leiden tot apoptose (celdood). Anderzijds zijn er ook aanwijzingen dat zuurstofradicalen juist van belang zijn voor het normaal functioneren van cellen. Welke uitwerking zuurstofradicalen zullen hebben op tumorcellen hangt sterk af van de concentratie en het tumortype. Tumorcellen kunnen zich beschermen tegen de schadelijke effecten van zuurstofradicalen met behulp van antioxidanten die zuurstofradicalen wegvangen en omzetten tot niet-reactieve stoffen. In **hoofdstuk 6** bestuderen wij welke effect glutathione peroxidase 2 (GPx2) (een belangrijk antioxidant) heeft op de groei, de metastasering en differentiatie van dikke darmtumoren. Wij laten zien dat GPx2 belangrijk is voor het beschermen van kankerstamcellen tegen celdood als cellen worden blootgesteld aan hoge concentraties zuurstofradicalen. Daarnaast bevordert GPx2 de tumorgroei en het metastaseren van dikke darmtumoren en is GPx2 essentieel voor het vormen van snel delende en gedifferentieerde cellen. Kortom, deze bovenstaande resultaten tonen aan dat de neutralisatie van zuurstofradicalen door de antioxidant GPx2 in dikke darmtumoren de groei, metastasering en differentiatie bevordert.

In **hoofdstuk 7** onderzoeken wij het effect van hypoxie, veroorzaakt door een chirurgische ingreep, op de kankerstamcelpopulatie. Hypoxie wordt gedefinieerd als een te lage zuurstofspanning voor de benodigde metabolische activiteiten van een cel. In de dagelijkse praktijk wordt vaak bij het reseceren van delen van de lever de bloedtoevoer naar de lever afgeklemd, om zo het bloedverlies te verminderen. Uit eerdere studies verricht door onze onderzoeksgroep is gebleken dat na het afklemmen en weer openzetten van de vaten naar de lever, grote delen van de resttumor en/of micrometastasen (uitzaaiingen die niet te zien zijn middels beeldvorming) hypoxisch zijn en dat deze gebieden worden gekenmerkt door een agressieve en versnelde groei van tumorcellen. Wij laten in dit hoofdstuk zien dat deze versnelde en agressieve groei het gevolg is van een snelle de-differentiatie van goed gedifferentieerde tumorcellen naar ongedifferentieerde kankerstamcellen met een hoog metastaserend vermogen. Verder laten wij zien dat de kankerstamcelpopulatie die ontstaat na blootstelling aan hypoxie gevoelig is voor een hypoxie-geactiveerde prodrug. Deze resultaten zijn klinisch relevant, omdat zij een verklaring zijn voor de agressieve uitgroei van micrometastasen die vaak na leverchirurgie ontstaan. Verder suggereert onze data dat patiënten na een leverresectie het best gebaat zijn bij een behandeling met een hypoxie-geactiveerde prodrug.

HET IDENTIFICEREN VAN GENEN EN EIWITTEN DIE GEASSOCIEERD ZIJN MET TUMORPROGRESSIE

In **hoofdstuk 8** verlaten wij de kankerstamcellen en richten wij ons op het identificeren van genen en eiwitten die belangrijk zijn voor het voorspellen van de prognose van patiënten met dikke darmkanker. Dit is klinisch van belang, omdat er patiënten zijn waarbij direct na de operatie de kanker terugkomt. Deze patiënten kunnen gebaat zijn bij aanvullende(chemotherapeutische)

behandelingen. Tegelijkertijd zijn er ook patiënten die na een operatie nog lang leven. Voor hen is aanvullende chemotherapie wellicht niet nodig. Voor dit onderzoek hebben wij gebruik gemaakt van genomics en proteomics, waarbij wij de relatieve expressieniveaus (activiteit) van duizenden genen en eiwitten in een tumor gelijktijdig kunnen bestuderen. Wij gebruiken deze techniek, omdat het (agressieve) gedrag van tumoren sterk samenhangt met de activiteit van genen en eiwitten. Voor dit onderzoek hebben wij tumoren geselecteerd van patiënten met dikke darmkanker met uitzaaiingen naar de lever die na een operatie de ziekte zeer snel terug hebben gekregen (binnen 6 maanden) en patiënten die na de operatie lang ziektevrij zijn gebleven (meer dan 2 jaar). Uit zowel de genomics- als proteomics analyse komen een aantal factoren naar voren die geassocieerd worden met een korte ziektevrije overleving. De enige factor die door beide analyses werd geïdentificeerd en geassocieerd kon worden met korte ziektevrije overleving was Maspin. Vervolgens is de expressie van Maspin onderzocht in patiënten met stadium II (geen uitzaaiing naar de lymfklieren) en stadium III (met uitzaaiing naar de lymfklieren) dikke darmtumoren. Hieruit kwam naar voren dat een hoge expressie van Maspin een sterk voorspellende waarde heeft voor patiënten met een stadium III tumor, maar niet voor patiënten met een stadium II tumor. Hieruit concluderen wij dat de rol van genen en/of eiwitten per stadia van de ziekte kan verschillen. Verder wijst het feit dat Maspin alleen van prognostische waarde is in darmtumoren die uitgezaaid zijn naar lokale lymfklieren en of de lever erop dat Maspin mogelijk een belangrijke rol speelt in het metastaseringsproces.

11

AUTHORS AND AFFILIATIONS
REVIEW COMMITTEE
DANKWOORD
LIST OF PUBLICATIONS
CURRICULUM VITAE AUCTORIS

AUTHORS AND AFFILIATIONS

University Medical Center Utrecht, The Netherlands
Department of Surgery
IHM Borel Rinkes, MD PhD
WJ van Houdt, MD PhD
KM Govaert, MD
EJA Steller, MD PhD
FJH Hoogwater, MD PhD
O Kranenburg, PhD
S Fatrai, PhD
J Laoukili, PhD
DAE Raats, BsC
A Verheem
N Snoeren, MD PhD
MW Nijkamp, MD PhD
ZJ Cheung, MD
MT de Bruijn, MD PhD
AM Prins, MD
R van Hillegersberg, MD PhD

Department of Oncogenomics
FC Holstege, PhD
MJ Koerkamp, Msc
SR van Hooff, Msc

Diakonessenhuis, The Netherlands
Department of Surgery
A Pronk, MD PhD

VU University Medical Center , The Netherlands
OncoProteomics Laboratory
CR Jimenez, PhD
TV Pham, PhD
SR Piersma, PhD
J Knol, PhD
SA Fratantoni, Msc

Department of Pathology
GA Meijer, MD PhD
RJ Fijneman, PhD
M de Wit, PhD
JA Goos, Msc

Department of Surgery
EJ Belt, MD PhD

Kennemer Gasthuis, The Netherlands
Department of Pathology
H Bril, MD PhD

Department of Surgery
HB Stockmann, MD PhD

German Institute of Human Nutrition Potsdam-Rehbruecke, Germany
Department Biochemistry of Micronutrients
AP Kipp, PhD
R Brigelius-Flohé, PhD

Hubrecht Institut-Royal Netherlands Academy of Arts and Sciences (KNAW) and University Medical Center Utrecht, The Netherlands
H Clevers, MD PhD
RG Vries, PhD

Academic Medical Center, University of Amsterdam, The Netherlands
Department of Oncogenomics
J Koster, PhD

REVIEW COMMITTEE

Prof. dr. P. J. van Diest
Professor of Pathology, University Medical Center Utrecht

Prof. dr. J.P. Medema
Professor of Experimental Oncology and Radiobiology, Academic Medical Center Amsterdam

Prof. dr. R.H. Medema
Professor of Experimental Oncology, University Medical Center Utrecht and Netherlands Cancer Institute

Prof. dr. M. Toner
Professor of Surgery and Bioengineering , Harvard Medical School (USA)

Prof. dr. R. Van Hillegersberg
Professor of Surgery, University Medical Center Utrecht

DANKWOORD

Dit proefschrift zou niet tot stand zijn gekomen zonder hulp van een heleboel mensen die bij mijn promotie betrokken zijn geweest. Langs deze weg wil ik deze mensen daarom graag bedanken.

Prof. dr. I.H.M. Borel Rinkes, beste Inne,
Ik had het voorrecht om als student binnen je onderzoeksgroep te mogen beginnen. Ik heb toen vaak vol verbijstering zitten kijken hoe jij tijdens besprekingen structuur en lijn in veelal toch wel warrige verhalen weet aan te brengen. Petje af hoe je als clinicus zo een succesvolle onderzoeksgroep weet op te zetten en samen met Onno begeleidt. Het was en is een eer om mijn onderzoek onder jouw begeleiding te mogen verrichten. Bedankt voor het vertrouwen dat je in mij hebt. Zo stond je direct achter mijn onderzoekstrip naar Mehmet in Boston. Ik heb de afgelopen jaren ontzettend veel van je mogen leren. Je bent een fantastische 'people's manager' en je enorme positieve instelling werkt stimulerend en haalt het beste in mij en in de onderzoeksgroep naar boven. Daarnaast kijk ik met veel plezier terug op onze reizen naar Philadelphia en Boston. Ik hoop de komende jaren in de kliniek nog veel van je te mogen leren.

Dr. O. Kranenburg, beste Onno,
Je bent met recht een (K)RAS optimist! Problemen komen niet in je woordenboek voor. Je denkt alleen in oplossingen. Kom ik je kamer weer binnen met een stapeltje resultaten waarvan ik denk dat ze direct de prullenbak in kunnen, geef jij er toch weer een positieve draai aan. Ik heb grote bewondering voor jouw gedrevenheid, betrokkenheid en enthousiasme om ons als jonge artsen in zo een korte tijd op te leiden tot onderzoekers. Zonder jouw hulp was dit proefschrift er zeker niet gekomen. Bedankt voor het vertrouwen dat je in mij hebt en je vastberadenheid om extra geld te regelen, zodat ik een jaar extra kon blijven. Naast het onderzoek heb ik je de afgelopen jaren ook op persoonlijk vlak beter leren kennen. Ik kijk dan ook met veel plezier terug naar onze trip naar Berlijn! Ik hoop in de toekomst nog veel met je samen te mogen werken.

Dr. C.R. Jimenez, beste Connie,
Zonder proteomics en jouw lab zou dit boekje er niet zijn geweest. Ik kan oprecht zeggen dat bijna ieder hoofdstuk van dit boekje gebaseerd is op een eiwit dat door een proteomicsscreen is geïdentificeerd. Jouw enthousiasme en welwillendheid om steeds opnieuw met ons in zee te gaan, was bewonderingswaardig. Ik heb genoten van de maanden die ik op je lab heb mogen doorbrengen. Bedankt voor al je hulp bij het tot stand komen van dit proefschrift, zonder alle 'runs' was de data er niet gekomen.

De leden van de promotiecommissie:
Prof. dr. P.J. van Diest, beste Paul,
Uren hebben wij achter de microscoop doorgebracht om de ABCB1 expressie te scoren. Je welwillendheid om altijd te helpen en je geduld en professionele aanpak zijn van grote waarde geweest. Bedankt voor je tijd en het kritisch beoordelen van mijn proefschrift als voorzitter van de beoordelingscommissie.

Prof. dr. M. Toner, dear Mehmet,
My stay at your lab really stands out as one of the highlights of my PhD program. It has been a privilege to work with you and your dedicated researchers of your institute. Thanks for all your

trust in letting me participate in such an important project, which resulted in a landmark paper. Thanks for coming all the way from Boston to take place in my thesis committee. It is highly appreciated. And who knows maybe we will meet again in Boston!

Prof. dr. R. van Hillegersberg, beste Richard,
Bedankt voor je betrokkenheid en support tijdens mijn onderzoek. Samen het tennistoernooi tijdens de chirurgen-cup winnen, was heel mooi! Bedankt voor je bijdrage aan de beoordelingscommissie. Ik zie ernaar uit nog veel van je te mogen leren in de kliniek en daag je uit voor een tennispotje.

Prof. dr. R.H. Medema, beste Rene,
Wat was het voor onze onderzoeksgroep een grote aderlating toen jouw onderzoeksgroep vertrok naar het AVL. Jouw waardevolle inbreng tijdens de werkbesprekingen en daarbuiten werden erg gemist. Ik ben dankbaar dat ik de eerste jaren van mijn onderzoekstijd van je heb mogen leren en heb kunnen zien hoe jij je onderzoeksgroep begeleidt en op hoog niveau invulling geeft aan de wetenschap. Ik waardeer het zeer dat je tijd hebt genomen om het proefschrift te beoordelen en in de beoordelingscommissie hebt willen plaatsnemen.

Prof. dr. J.P. Medema, beste Jan-Paul,
Vol verwondering heb ik gekeken naar de kankerstamcel papers die uit jou lab zijn voortgekomen. Ik kan met recht zeggen dat jullie het toonaangevende lab in Nederland zijn als het gaat om colorectale kankerstamcellen. Bedankt voor al de overlegmomenten, de tijd en de energie die je hebt gestoken in het kritisch lezen van onze manuscripten. Het is voor mij een grote eer dat je plaats hebt willen nemen in mijn beoordelingscommissie.

Dr. M.R. Vriens, beste Menno,
Bedankt voor je interesse in mijn onderzoek en je vertrouwen in mij als assistent in opleiding tot chirurg. De afgelopen tijd heb ik in de kliniek al veel van je mogen leren en ben ik je als begeleider erg gaan waarderen. Ik hoop in de toekomst nog meer van je te mogen leren.

Marielle Hoefakker en Romy Liesdek,
Bedankt voor al jullie hulp en ondersteuning. Jullie zijn echt onmisbaar voor ons.

Medewerkers van de biobank**, Natalie, Jan en Jan-Willem**, de snelheid en precisie waarmee jullie al het tumormateriaal verwerkten is van onschatbare waarde geweest. Bedankt voor jullie flexibiliteit en inzet. **Petra van der Groep**, bedankt voor al je hulp en adviezen bij het opzetten van immuunhistochemie. De samenwerking met jou is voor ons van grote waarde geweest.

Alle **stafleden** en **arts-assistenten** van de afdeling Heelkunde wil ik bedanken voor hun interesse in mijn onderzoek en vooral ook voor alle mooie momenten tijdens het werk en buiten het werk om.

Voorgangers bij de experimentele chirurgische oncologie, **Frederik Hoogwater, Maarten Nijkamp en Menno de Bruijn**, het was een voorrecht om met jullie te mogen werken. Veel van de resultaten hebben wij te danken aan jullie voorbereidend werk. Bedankt voor alle hulp, wijze adviezen en gezellige momenten. Jullie 'tips and tricks' zijn van grote waarde geweest. Ik zie ernaar uit binnenkort weer samen met jullie in de kliniek te mogen werken. **Nikol Snoeren**, we

hebben flink wat uren in het weekend achter de microscoop zitten zwoegen, maar het Maspin artikel is er gekomen! Je vrolijkheid, enthousiasme en humor maken het een genot om met je te werken. Bedankt voor je inzet, mede door jou is dit proefschrift er gekomen.

Het lab van de experimentele oncologie:
De Medema groep, jammer dat jullie Utrecht hebben verlaten. De inhoudelijke en luchtige gesprekken met jullie als echte wetenschappers in het kweeklab zijn van grote waarde geweest. **Rob Klompmaker** en **Livio Kleij**, bedankt voor al jullie hulp en technische ondersteuning.

De Voest, groep, inmiddels zijn jullie helaas ook vertrokken naar het AVL. **Prof. dr. E. Voest beste Emile,** je commentaar tijdens werkbesprekingen was scherp en 'to-the-point' en zijn daardoor een waardevolle toevoeging geweest. **Laura Hussen-Daenen, Jeanine Roodhart, Joost Vermaat, Sander Basten, Julia Houthuizen, Martijn Lolkema, Marco Koudijs, Ilse van Oosterom,** bedankt voor de prettige samenwerking, feedback en gezelligheid. **Judith Jans en Stefanie Kroeze,** van het urologie lab, bedankt voor de samenwerking.

De Derksen groep, Patrick Derksen, Ron Schackman, Miranda van Amersfoort, Eva Vlug, Robert van der Ven, bedankt voor jullie hulp en scherpzinnige commentaar. Collega's van de **Lens en Kops groep,** bedankt voor jullie gezelligheid op het lab.

Alle (oud) mede onderzoekers van de Heelkunde:
De vrienden van Isengard: **Charlotte van Kessel, Roy Verhage, Anne den Hartog, Emily Postma, Jakob Kist, Pieter van der Sluis, Stein van Esser, Eline van Hattum, Tjaakje Visser, Claire Pennenkamp, Jasper van Keulen.** Het was altijd gezellig om bij jullie langs te gaan, hoop nog met veel van jullie in de kliniek te mogen werken.

Promovendi chirurgie: **Okan Bastiaan, Marjolein Heeres, Dave Koole, Marin ter Aa, Sigrid de Meer, Pieter Leliefeld, Herman Zandvoort, Janesh Pillay, Claire Pennekamp, Peter Paul Wisman, Samira Fegrachi, Vincent Scholtes, Femke Maurits, Margriet Prins en Leonie Haverkamp.** Bedankt!

Mijn student-onderzoekers: **Anne Prins, Anne Rongen en Willem Berkovits,** bedankt voor jullie hulp en inzet.

VU Medisch Centrum, OncoProteomics Laboratory: **Sander Piersma, Jaco Knol, Thang Pham, Inge de Reus, Meike de Wit, Marc Warmoes, Silvina Fratantoni,** ik werd altijd met open armen ontvangen op jullie lab. Jullie kennis en enthousiasme over proteomics is erg aanstekelijk geweest. Bedankt voor al jullie hulp bij het opzetten en uitvoeren van mijn projecten. **Prof. dr. G.A. Meijer** en **Remond Fijneman**, van de afdeling Pathologie, bedankt voor jullie interesse en hulp bij het tot stand komen van het Maspin artikel.

Members of the Circulating Tumor Cell Center (Massachusetts General Hospital, Harvard Medical School, Boston, USA), thanks for making me feel at home, I really enjoyed my stay with you. **Daniel Haber, Shyamala Maheswaran, Shannon Stott, Elena Brachtel,** it has been a privilege working with you. Thank you for all your trust and support.

Robert Vries en Marc van de Wetering van het Clevers Lab, bedankt voor jullie hulp en adviezen bij onze kankerstamcelprojecten. Vooral de uren en gesprekken achter de FACS sorter zal ik niet snel vergeten.

Anna Kip and Jamila Laoukili, GPx2 partners! It has been great working with you. Your knowledge and skills have made the GPx2 project a success. Anna, the timing of your visits has been great.

Lutske Lodewijk en Kari Trumpi, mijn kamergenoten en 'the next generation' onderzoekers. Bedankt voor jullie gezelligheid binnen en buiten het lab. En ja, het komt allemaal uiteindelijk wel goed! Ik mis wel onze cola momenten! En wanneer worden de muizen weer bijgevuld? Ik zie ernaar uit met jullie in de kliniek samen te mogen werken.

Andre Verheem, bedankt voor al je hulp in het lab en in het GDL. Ik heb veel respect voor het feit dat je in deze fase van je carrière nog een switch hebt gemaakt naar het lab.

Andere lab-genoten van de Kranenburg-Borel Rinkes groep: **Szabolcs Fatrai, Jennifer Jongen, Thomas Vellinga, Susanne van Schelven, Tijana Borovski, Danielle Raats,** bedankt voor jullie hulp bij het uitvoeren van mijn werkzaamheden op het lab. Ik waardeer het enorm. Bedankt voor jullie adviezen en het delen van jullie ervaringen.

Klaas Govaert, wat is het toch jammer dat je er niet bij kunt zijn! Ik heb genoten van je oneindige energie en enthousiasme. En wat ben je toch altijd zo attent, daar kan ik nog veel van leren. Mooi dat wij nu weer directe collega's zijn.

Mijn paranimfen, Winan van Houdt en Ernst Steller:
Winan, onze wegen hebben elkaar voor het eerst ruim tien jaar geleden ín een verpleegtehuis gekruist. Ik heb je als receptioniste, arts-onderzoeker en arts-assistent mogen opvolgen. Zeer bijzonder hoe dit allemaal is gelopen. Vanaf dag één was en is er een klik en hebben wij veel moois met elkaar mogen meemaken. Bedankt voor je vriendschap. Ik heb de afgelopen jaren ontzettend veel van je mogen leren, zowel in het lab, de kliniek als privé. Het is een eer dat je mij als paranifm wilt ondersteunen.

Ernst, mijn onderzoeks- en tennismaat! Zij aan zij hebben wij mogen werken op het lab, jij aan CD95 en ik aan kankerstamcellen. En wat was het heerlijk om dan aan het eind van de dag onze frustraties op elkaar af te mogen vuren via een tennisbal. Je altijd kritische houding heeft mijn onderzoek verder geholpen. Ik zie ernaar uit dat we binnenkort samen kunnen gaan opereren! Bedankt dat je me als vriend en paranimf wilt ondersteunen.

Marish Oerlemans, trouwe vriend! Als geen ander weet jij hoe het is om een promotietraject te doorlopen. Je vriendschap is me ontzettend dierbaar. Dank je wel.

Lieve schoonfamilie, Jan & Coby, Marco & Eveliene (Aimeé, Féline en Xander), Christiaan & Anne-Margriet (Fleur en Thijmen), Robert-Jan & Inge (Sara), eindelijk is alles gepubliceerd, zijn de impact factors gehaald en heb ik weer tijd om met jullie een spelletje te doen! Wat bof ik met zo een (superieure) schoonfamilie. Bedankt voor jullie steun, interesse en gezelligheid.

Lieve Evan & Fleur, Anne-Wien & Bruce, Thandi & Struan en Martyn, ver weg, maar toch dichtbij! Bedankt voor jullie interesse en steun. Ik voel me zeer bevoorrecht om zo een leuke club (aangetrouwde) broers en zussen om mij heen te hebben. Ik zie ernaar uit iedereen volgend jaar maart weer te zien!

Lieve ouders, Ben en Lieneke, bedankt voor jullie opvoeding, wijsheid en onvoorwaardelijke steun en liefde. Zonder jullie had ik mij niet zo kunnen ontwikkelen. Pa, bedankt voor je interesse in mijn onderzoek en het aanhoren van mijn resultaten. Ik hoop dat wij snel met elkaar mogen gaan opereren. Jullie zijn geweldige ouders en een groot voorbeeld. Bedankt dat jullie speciaal voor deze gelegenheid over zijn gekomen uit Zuid-Afrika.

Lieve Benjamin, dit boekje staat vol met woorden, maar woorden schieten te kort om mijn liefde voor jou te beschrijven. Ik ben gek op je!

Mijn lieve Laura, eindelijk is het dan zover, het boekje is af! Dit zal ook voor jou een hele opluchting zijn, het heeft namelijk heel veel van jou gevraagd. Bedankt voor al je begrip en steun, zonder jou was het boekje er niet gekomen. Dit boek draag ik dan ook op aan jou en Benjamin! Je relativeringsvermogen, wijze adviezen gemend met de nodige humor hebben mij geholpen de juiste balans te vinden. Ik kan mij geen betere vrouw wensen. Ik hoop heel oud met je te worden!

LIST OF PUBLICATIONS

Emmink BL*, Laoukili J*, Kipp AP, Koster J, Govaert KM, Fatrai S, Verheem A, Steller EJA, Brigelius-Flohé R, Jimenez CR, Borel Rinkes IHM, Kranenburg O. GPx2 suppression of H2O2 stress links the formation of differentiated tumor mass to metastatic capacity in colorectal cancer.
Cancer Research. 2014 Sep; in press.

Gerlach JP, **Emmink BL**, Nojima H, Kranenburg O, Maurice MM. Wnt signalling induces accumulation of phosphorylated β-catenin 1 in two distinct 2 cytosolic complexes.
Submitted

Vellinga TT, Borovski T, de Boer VCJ, Fatrai S, van Schelven S, Trumpi K, Verheem A, Snoeren N, **Emmink BL**, Koster J, Borel Rinkes IHM, Kranenburg O. SIRT1/PGC1α dependent increase in oxidative phosphorylation supports chemotherapy resistance of colon cancer.
Submitted

Govaert KM, van Kessel CS, Steller EJ, **Emmink BL**, Molenaar IQ, Kranenburg O, van Hillegersberg R, Borel Rinkes IH. Recurrence location after resection of colorectal liver metastases influences prognosis.
Journal of Gastrointestinal Surgery 2014 May;18(5):952-60.

Govaert KM, **Emmink BL***, Nijkamp MW*, Cheung ZJ, Steller EJ, Fatrai S, de Bruijn MT, Kranenburg O, Borel Rinkes IHM. Hypoxia after liver surgery imposes an aggressive cancer stem cell phenotype on residual tumor cells.
Annals of Surgery 2014 Apr;259(4):750-9.

Emmink BL, Verheem A, van Houdt WJ, Steller EJ, Govaert KM, Pham TV, Piersma SR, Borel Rinkes IHM, Jimenez CR, Kranenburg O. The secretome of colon cancer stem cells contains drug-metabolizing enzymes.
Journal of Proteomics. 2013 Oct 8;91:84-96.

Emmink BL*, Snoeren N*, Koerkamp MJ, van Hooff SR, Goos JA, van Houdt WJ, de Wit M, Prins AM, Piersma SR, Pham TV, Belt EJ, Bril H, Stockmann HB, Meijer GA, van Hillegersberg R, Holstege FC, Jimenez CR, Fijneman RJ, Kranenburg OW, Rinkes IHM. Maspin is a marker for early recurrence in primary stage III and IV colorectal cancer.
British Journal of Cancer 2013 Sep 17;109(6):1636-47.

Ozkumur E, Shah AM, Ciciliano JC, **Emmink BL**, Miyamoto DT, Brachtel E, Yu M, Chen PI, Morgan B, Trautwein J, Kimura A, Sengupta S, Stott SL, Karabacak NM, Barber TA, Walsh JR, Smith K, Spuhler PS, Sullivan JP, Lee RJ, Ting DT, Luo X, Shaw AT, Bardia A, Sequist LV, Louis DN, Maheswaran S, Kapur R, Haber DA, Toner M. Inertial focusing for tumor antigen-dependent and -independent sorting of rare circulating tumor cells.
Science Translational Medicine. 2013 Apr 3;5(179):179ra47.

Steller EJ, Raats DA, Koster J, Rutten B, Govaert KM, **Emmink BL**, Snoeren N, van Hooff SR, Holstege FC, Maas C, Borel Rinkes IH, Kranenburg O. PDGFRB promotes liver metastasis formation of mesenchymal-like colorectal tumor cells.
Neoplasia 2013 Feb;15(2):204-17.

Emmink BL*, Kranenburg O*, Knol J, van Houdt WJ, Rinkes IHM, Jimenez CR. Proteomics in studying cancer stem cell biology.
Expert Review of Proteomics 2012 Jun;9(3):325-36.

Govaert KM, Nijkamp MW, **Emmink BL**, Steller EJ, Minchinton AI, Kranenburg O, Borel Rinkes IH. Effects of tirapazamine on experimental colorectal liver metastases after radiofrequency ablation.
British Journal of Cancer 2013 Apr;99(4):567-75.

Emmink BL*, Van Houdt WJ*, Pham TV, Piersma SR, Verheem A, Vries RG, Fratantoni SA, Pronk A, Clevers H, Borel Rinkes IH, Jimenez CR, Kranenburg O. Comparative proteomics of colon cancer stem cells and differentiated tumor cells identifies BIRC6 as a potential therapeutic target.
Molecular & Cellular Proteomics 2011 Dec;10(12):M111.011353.

Steller EJ, Ritsma L, Raats DA, Hoogwater FJ, **Emmink BL**, Govaert KM, Laoukili J, Rinkes IH, van Rheenen J, Kranenburg O. The death receptor CD95 activates the cofilin pathway to stimulate tumour cell invasion.
EMBO Reports 2011 Sep 1;12(9):931-7.

Raats DA, de Bruijn MT, Steller EJ, **Emmink BL**, Borel-Rinkes IH, Kranenburg O. Synergistic killing of colorectal cancer cells by oxaliplatin and ABT-737.
Cellular Oncology 2011 Aug;34(4):307-13.

Emmink BL*, Van Houdt WJ*, Vries RG, Hoogwater FJ, Govaert KM, Verheem A, Nijkamp MW, Steller EJ, Jimenez CR, Clevers H, Borel Rinkes IH, Kranenburg O. Differentiated human colorectal cancer cells protect tumor-initiating cells from irinotecan.
Gastroenterology 2011 Jul;141(1):269-78.

van Houdt WJ, Hoogwater FJ, de Bruijn MT, **Emmink BL**, Nijkamp MW, Raats DA, van der Groep P, van Diest P, Borel Rinkes IH, Kranenburg O. Oncogenic KRAS desensitizes colorectal tumor cells to epidermal growth factor receptor inhibition and activation.
Neoplasia 2010 Jun;12(6):443-52.

van Houdt WJ, de Bruijn MT, **Emmink BL**, Raats D, Hoogwater FJ, Borel Rinkes IH, Kranenburg O. Oncogenic K-ras activates p38 to maintain colorectal cancer cell proliferation during MEK inhibition.
Cellular Oncology 2010 Jan 1;32(4):245-57.

Hoogwater FJ, Nijkamp MW, Smakman N, Steller EJ, **Emmink BL,** Westendorp BF, Raats DA, Sprick MR, Schaefer U, Van Houdt WJ, De Bruijn MT, Schackmann RC, Derksen PW, Medema JP, Walczak H, Borel Rinkes IH, Kranenburg O. Oncogenic K-Ras turns death receptors into metastasis-promoting receptors in human and mouse colorectal cancer cells.
Gastroenterology. 2010 Jun;138(7):2357-67.

Emmink BL, Giles RH. Kankerstamcelonderzoek Deel 1: Conceptuele verschuivingen.
Oncocollectie: 1-2009

van Houdt WJ, Smakman N, van den Wollenberg DJ, **Emmink BL**, Veenendaal LM, van Diest PJ, Hoeben RC, Borel Rinkes IH, Kranenburg O. Transient infection of freshly isolated human colorectal tumor cells by reovirus T3D intermediate subviral particles.
Cancer Gene Therapy 2008 May;15(5):284-92.

** These authors contribute equally*

CURRICULUM VITAE

Benjamin Lucas Emmink was born on November 12th, 1981 in Utrecht, The Netherlands. At the age of two he and his family emigrated to South Africa. In 1999, he graduated from Outeniqua High School in George, South Africa. In 2000 he returned to the Netherlands. After successfully obtaining the required diploma's for medical school admission, he was admitted to medical school at Utrecht University in 2002. During his medical training he performed his surgical clinical rotation at the Provincial Hospital in George, South-Africa. As medical student he was involved in several research projects at the department of Surgical Oncology of the University Medical Center Utrecht and the OncoProteomics Laboratory of the VU University Medical Center Amsterdam. He obtained his medical degree in October 2008. When awarded a research grant from the Dutch Cancer Society he commenced a PhD program at the department of Surgical Oncology in November 2008 under supervision of prof. dr. I.H.M. Borel Rinkes and dr. O. Kranenburg. During his PhD program he collaborated closely with the OncoProteomics Laboratory of the VU University Medical Center Amsterdam, under supervision of dr. C.R. Jimenez. At the end of his PhD program he performed a research elective at the Circulating Tumor Cell Center, Massachusetts General Hospital and Harvard Medical School, Boston MA, under the supervision of prof. M. Toner. In June 2013 he started the residency program in general surgery under the auspices of dr. M.R. Vriens at the University Medical Center in Utrecht. The third, fourth and fifth year of his surgical training are scheduled at the St. Antonius Hospital Nieuwegein under the supervision of dr. P.M.N.Y.H. Go. For the sixth and final year of the program he will return to the University Medical Center in Utrecht. Benjamin Emmink is married and a proud father of a son.